Reconstruction of forest fires through chemical analysis of black carbon in ice cores from high-alpine glaciers

Inauguraldissertation
der Philosophisch-naturwissenschaftlichen Fakultät
der Universität Bern

vorgelegt von

Dimitri Osmont

aus Frankreich

Leiterin der Arbeit:

Prof. Dr. Margit Schwikowski

Departement für Chemie und Biochemie der Universität Bern

Reconstruction of forest fires through chemical analysis of black carbon in ice cores from high-alpine glaciers

Inauguraldissertation
der Philosophisch-naturwissenschaftlichen Fakultät
der Universität Bern

vorgelegt von

Dimitri Osmont

aus Frankreich

Leiterin der Arbeit:

Prof. Dr. Margit Schwikowski

Departement für Chemie und Biochemie der Universität Bern

Von der Philosophisch-naturwissenschaftlichen Fakultät angenommen.

Bern,   Der Dekan:

Prof. Dr. Z. Balogh

Contents

List of abbreviations

ALC	Annual Layer Counting
APD	Avalanche Photo-Detector
AQ	Aquadag
a.s.l.	Above sea level
BC	Black Carbon
BFHS	Broken Fire Hockey Stick
CG	Colle Gnifetti
CMIP	Coupled Model Intercomparison Project
DMA	Differential Mobility Analyzer
DWD	Deutscher Wetterdienst
eBC	Equivalent Black Carbon
EC	Elemental Carbon
ECM	Electrical Conductivity Measurements
ENSO	El Niño-Southern Oscillation
FAO	Food and Agriculture Organization
FELICS	Fast Electromechanical Lightweight Ice Coring System
FH	Fiescherhorn
GCD	Global Charcoal Database
GFS	Global Forescast System
GHG	Greenhouse Gas
HCO/HTM	Holocene Climatic Optimum/Holocene Thermal Maximum
HDF	Holtedahlfonna
IARC	International Agency for Research on Cancer
IC	Ion Chromatography
ICP-SFMS	Inductively Coupled Plasma-Sector Field Mass Spectrometry
IL	Illimani
INPE	Instituto Nacional de Pesquisas Espaciais (Brazil)
IPCC	Intergovernmental Panel on Climate Change
IR	Infrared
IRD	Institut de Recherche pour le Développement
ITCZ	Intertropical Convergence Zone
JFJ	Jungfraujoch
LALIA	Late Antique Little Ice Age
LF	Lomonosovfonna
LGM	Last Glacial Maximum
LIA	Little Ice Age
LOD	Limit of Detection
MAAP	Multiangle Absorption Photometer
MAC	Mass Absorption Coefficient
MADA	Monsoon Asia Drought Atlas
MEI	Multivariate ENSO Index
MODIS	Moderate Resolution Imaging Spectroradiometer
MSA	Methanesulfonate
MWP	Medieval Warm Period

NAO	North Atlantic Oscillation
NCDC	National Climatic Data Center
NH	Northern Hemisphere
NPI	Norwegian Polar Institute
nss	Non-sea-salt
OC	Organic Carbon
OECD	Organization for Economic Co-operation and Development
OWDA	Old World Drought Atlas
PAH	Polycyclic Aromatic Hydrocarbon
PC	Principal Component
PCA	Principal Component Analysis
PDSI	Palmer Drought Severity Index
PETG	Polyethylene Terephthalate-Glycol modified
Pg	Petagram (10^{15} g)
p-HBA	p-Hydroxybenzoic Acid
PMT	Photomultiplier Tube
PP	Polypropylene
PSI	Paul Scherrer Institut
rBC	Refractory Black Carbon
RCP	Representative Concentration Pathways
RWP	Roman Warm Period
(S)AOD	(Stratospheric) Aerosol Optical Depth
SASM	South America Summer Monsoon
SDTF	Seasonally Dry Tropical Forest
SP2	Single Particle Soot Photometer
TEM	Transmission Electron Microscope
ToE	Time of Emergence
VA	Vanillic Acid
VIIRS	Visible Infrared Imaging Radiometer Suite
VOC	Volatile Organic Compounds
VSMOW	Vienna Standard Mean Ocean Water
weq	Water equivalent
WS-CRDS	Wavelength Scanned-Cavity Ring Down Spectrometer
WSI	Water Stable Isotopes
YD	Younger Dryas

Summary

Wildfires are an important contributor to the global carbon budget. Complex relationships exist between fires, climate and humans as they are interconnected by an ensemble of feedbacks. Fires influence the climate by emitting greenhouse gases and aerosols and can have a significant influence on regional landscapes and vegetation cover. On the contrary, climate is a major driver of fire activity. Human societies have always made use of fire for their activities (cooking, heating, agriculture) but at the same time feared it and tried to control it. In the context of the current global warming, fires are expected to increase in duration, size and number in many regions of the world.

In order to accurately simulate future fire evolution, it is necessary to understand past mechanisms between fires, climate and humans and put them into the current context. For this purpose, paleoclimate archives are used to reconstruct paleofire activity. So far, most of the reconstructions have been derived from charcoal analyses from lake sediment cores. Worldwide compilations revealed a trend called the "broken fire hockey stick": while fire activity was following the trends of its main drivers, namely temperature and population density until 1870 AD, i.e. a decrease until 1750 AD and an strong increase until 1870 AD, a decoupling was observed since 1870 AD, as temperatures and population density kept on rising whereas fire activity dropped, possibly because of increasing anthropogenic pressure due to fire suppression and land-use changes.

However, this hypothesis remains controversial as charcoal records are characterized by a high dating uncertainty in their most recent part and can only provide information about local fire activity, meaning that they have to be compiled to extract a global signal. The initial charcoal compilation was strongly biased in number towards European and North American regions and neglected many regions with elevated current levels of biomass burning (Tropics, boreal Siberia).

Ice cores also have the potential to reconstruct paleofire activity. They present intrinsic advantages compared to lake-sediment charcoal records, such as a better controlled chronology and a much larger catchment area, from regional to continental scales. So far, few paleofire reconstructions have been performed by means of ice cores, most of them originating from polar regions. In these studies, a large variety of biomass burning proxies has been used: black carbon (BC), ammonium, light organic acids, molecular fire tracers (levoglucosan, vanillic acid, etc…), all of them having intrinsic advantages and limitations due to their different behaviors and sensitivities towards emission, transport, deposition and post-deposition processes..

This PhD thesis is part of the inter-disciplinary *PaleoFire* project, whose aim is to reconstruct paleofire history from high-mountain ice cores through a multi-proxy approach using refractory black carbon (rBC) and charcoal analyses combined with atmospheric modeling and remote sensing of fires, in order to test the "broken fire hockey stick" hypothesis.

Here, we focus on the rBC analysis in four high-mountain ice cores with well-controlled chronology: Lomonosovfonna in Svalbard, Illimani in the Bolivian Andes, Colle Gnifetti in the Swiss Alps and Tsambagarav in the Mongolian Altai. Those cores were processed and analyzed for rBC with a Single Particle Soot Photometer (SP2) allowing high-resolution measurements. Some of the cores were also analyzed for major ions and water stable isotopes.

In the Lomonosovfonna ice core, 800 years of rBC atmospheric variability could be reconstructed, showing a predominant anthropogenic contribution due to Eurasian fossil fuel emissions starting around 1860 AD. Two rBC maxima were reached, in the end of the 19th century and after the Second

World War. Declining rBC concentrations since the 1970s are in agreement with atmospheric concentrations in the Arctic, but contradict a previous study from another Svalbard ice core. Multiple evidence of disturbance of the record by summer melting was noted for periods with unexpectedly low rBC concentrations around 1885 AD or in the 1920–1930s. Before 1800 AD, the preindustrial rBC record, along with those from other biomass burning proxies, was used to reconstruct paleofire activity from boreal regions. Our multi-proxy approach showed that different trends could be found depending on the proxies, due to their different sensitivity towards emission, transport, deposition and post-deposition processes. rBC and ammonium displayed little variation in the preindustrial times while formate, vanillic acid and p-hydroxybenzoic acid experienced multi-decadal variations in line with other paleofire records from Northern Eurasia.

The Illimani ice core is the only one spanning the entire Holocene back to the last deglaciation 13000 years ago. A high correlation was observed between rBC and reconstructed temperature, suggesting that rBC acts as an indirect temperature proxy through biomass burning variations in the Amazon Basin, with enhanced concentrations during warm/dry periods such as the Holocene Climatic Optimum and the Medieval Warm Period and lower concentrations during cold/wet periods such as the last deglaciation or the Little Ice Age. Comparisons with other regional biomass burning records showed that the Illimani rBC record was able to efficiently capture past biomass burning trends and therefore forms the missing link between local lake-sediment charcoal records and remote Antarctic ice-core records. The increasing trend in rBC since 1730 AD seems to be related only to higher levels of biomass burning due to higher temperatures and more intensive deforestation and does not seem influenced by fossil fuel emissions.

The Colle Gnifetti rBC record allowed reconstructing one millennium of rBC atmospheric variations over Europe. Industrial emissions started to emerge from the natural background in the 1870s and therefore cannot be held responsible for the 19th-century glacier retreat in the Alps as around 80 % of it took place before that time. rBC emissions subsequently peaked in the first half of the 20th century and a close agreement with the neighboring elemental carbon (EC) record from Fiescherhorn ice core was observed, confirming the representativeness of our rBC record. In the preindustrial times, rBC and ammonium concentrations were lowered during cold periods associated with solar minima, suggesting reduced fire activity.

The Tsambagarav rBC record enabled to reconstruct 6000 years of fire dynamics in Central Asia. A much larger variability was observed in the oldest 1000 years of the core compared to the following 5000 years. The latitudinal position of the Intertropical Convergence Zone (ITCZ) was suggested to influence this variability. Greater variability was associated with a predominant Monsoon regime during the Holocene Climatic Optimum which then shifted to a more stable climate regime dominated by Westerlies towards the late Holocene. The rBC record also presented a clear minimum during the cold period of the Maunder solar minimum. Lastly, a clear impact of industrial pollution from the former Soviet Union was visible during the 20th century, particularly between 1960 and 1990.

As a result, three out of the four rBC ice-core records present a significant anthropogenic contribution in the last century and cannot be used to confirm or invalidate the "broken fire hockey stick" hypothesis. Nevertheless, the undisturbed Illimani record does not suggest a decline in fire activity in the 20th century. Moreover, none of the three charcoal records from Illimani, Colle Gnifetti and Tsambagarav produced in the framework of the *PaleoFire* project were able to confirm the existence of the "broken fire hockey stick". Such a trend may appear in global reconstructions, but does not reflect regional variations of biomass burning activity in at least Europe, tropical South America and Central Asia.

In addition to the absence of a "broken fire hockey stick" signal, three main conclusions can be drawn from the compilation of those four ice-core records. First, maximum rBC concentrations were observed during the Holocene Climatic Optimum (HCO), suggesting a much higher fire activity than in the present day. Second, the variability in rBC concentrations in the last 1000 years was clearly lower than during the HCO. Generally, slightly higher (lower) concentrations were recorded during the Medieval Warm Period (Little Ice Age). Third, anthropogenic emissions are clearly predominant in the most recent part of all the rBC records except Illimani. A significant anthropogenic contribution is evident in Lomonosovfonna since the 1860s, in Colle Gnifetti since the 1870s and in Tsambagarav for the time period 1960–1990 due to USSR industrial emissions.

Ice-core studies often focus only on paleofire trends but do not study transport and deposition processes in detail. For this purpose, specific case studies have to be considered. In this thesis, a snowpit study was conducted at Jungfraujoch, Swiss Alps, as part of a particular case study of rBC and charcoal deposition in a high-alpine snowpack following a massive biomass burning event (2017 Portuguese forest fires). This work, in combination with remote sensing of fires and atmospheric modelling, showed that biomass burning emissions could be reliably archived in the snowpack at a continental scale if transport and deposition conditions were favorable.

Further investigations have to be carried out to more accurately determine the footprint of the ice cores and the impact of transport and deposition processes, by including more case studies with a comprehensive analysis of satellite data. Discrepancies between the different biomass burning proxies also need to be extensively discussed, as well as the impact of melting on the rBC records, in order to be able to fully understand paleofire records extracted from ice cores.

1 Introduction

1.1 Ice cores as climate archives

1.1.1 Current climate change

In the last decades, climate change has become an issue of increasing concern. Climate, defined as the long-term and average evolution of weather parameters such as temperature, precipitation, atmospheric pressure, wind speed or humidity *(Cubash et al., 2013)*, has entered an unequivocal warming phase since the 1950s with unprecedented changes for the past millennia *(IPCC, 2013)*. The main reason for these changes originates from anthropogenic activities, which tend to modify the Earth radiative balance (i.e. the balance between incoming and outgoing energy in the Earth-atmosphere system, primarily controlled by solar radiation) due to the emission of greenhouse gases (GHGs) such as carbon dioxide (CO_2), methane (CH_4) or nitrous oxide (N_2O), and aerosol particles into the atmosphere. Evidence of fast and massive changes can be seen everywhere in our surrounding environment. Global Earth's surface temperature has been rising by 0.85 ± 0.2 °C over the time period 1880–2012. The frequency of extreme weather events (heat waves, droughts, heavy rain) has increased while cold spells became less frequent. The upper ocean also experienced a warming trend combined with an acidification induced by the growing absorption of atmospheric CO_2. Polar ice caps and mountain glaciers are retreating worldwide **(Fig. 1.1)** causing sea level rise (0.19 ± 0.02 m between 1901 and 2010). Sea ice and snow cover are shrinking in extent and duration *(IPCC, 2013)*.
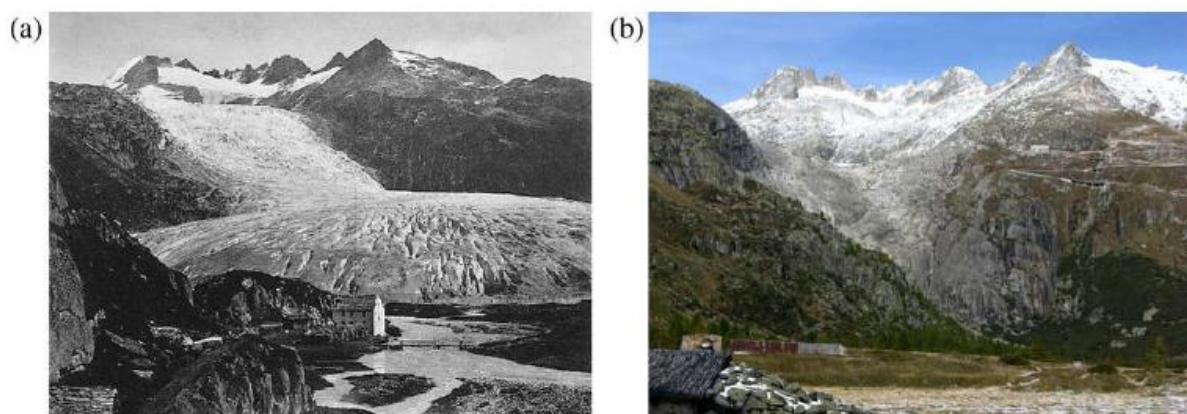
Fig. 1.1: Two pictures of Rhone glacier, Switzerland, in a) 1853 and b) 2008 *(Jouvet et al., 2009)*. The glacier receded 1.2 km between 1880 (start of the monitoring campaigns) and 2007 *(Jouvet et al., 2009)*. Glaciers are among the most spectacular indicators of current global warming.

Although the human influence on the current climate system is clear *(IPCC, 2013)*, many questions and processes remain unsolved or only partially understood as the climate system is characterized by a high level of complexity. Its different components, namely the atmosphere, cryosphere, hydrosphere, land surface and biosphere, are tightly interconnected through complex feedbacks. One of the major challenges concerns the ability to predict the future evolution of climate parameters in the context of global warming. For this purpose, model simulations are run with different scenarios based on potential future concentrations of GHGs in the atmosphere **(Fig. 1.2)**. For instance, in the worst case scenario, global temperatures in 2100 could be 4 °C higher than in preindustrial times, potentially leading to a range of adverse and severe consequences on the environment as well as on our societies.
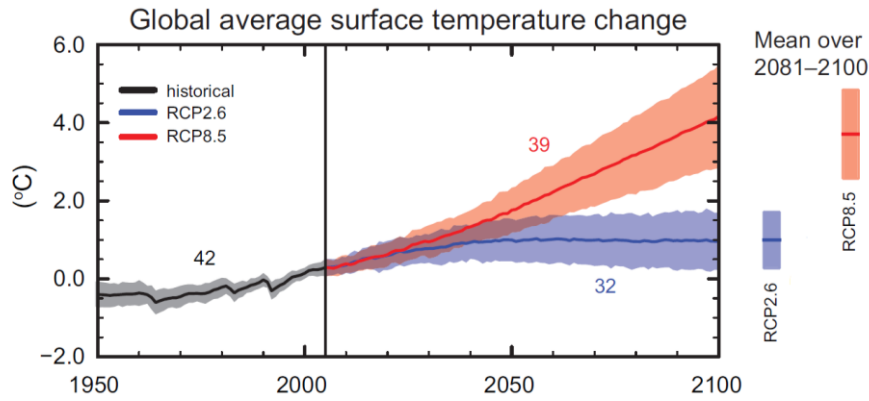
Fig. 1.2: Simulated future global average surface temperature change relative to 1986–2005 using the Coupled Model Intercomparison Project Phase 5 (CMIP5) model (adapted from *IPCC, 2013*). Four main scenarios of atmospheric GHG concentrations, called Representative Concentration Pathways (RCPs) are commonly used by the IPCC to describe four potential climate futures: RCP2.6, 4.5, 6.0 and 8.5, named after the additional radiative forcing (+2.6, +4.5, +6.0, and +8.5 W m^{-2}, respectively) they imply by the year 2100 compared to preindustrial values. In terms of GHG emissions, RCP2.6 means that the peak of GHG emissions is reached during the decade 2010–2020 and that emissions substantially decline thereafter. This is the only scenario enabling to stay below the +2 °C target defined by the Paris agreement. RCP4.5 (RCP6.0) corresponds to GHG emissions peaking around 2040 (2080) and then declining, respectively. RCP8.5 assumes that GHG emissions will keep on increasing at the same rate as present time (business-as-usual scenario).

As the input in climate models consists of real weather and climate data, there is a need for accurate data with broad coverage and high resolution at both spatial and temporal scales. In order to make reliable climate projections for the future, a comprehensive understanding of climate mechanisms has to be achieved. The best way to do so is to get access to information about past (and present) climate variability. Paleoclimatic data are then used to better constrain climate models, resulting in reduced uncertainties and a greater ability of the model to accurately simulate past and future climate evolution **(Fig. 1.3)**.
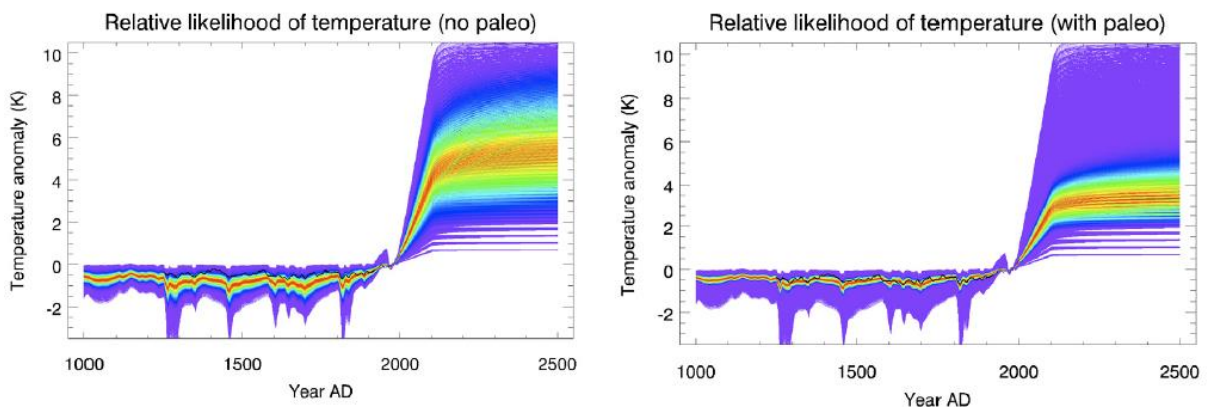
Fig 1.3: Relative likelihood of predicted temperature anomaly when the model (One-Box Energy Balance Model) is not constrained by paleoclimate reconstructions (left) versus when paleoclimate data are used to constrain the model (right). Red (blue) colors indicate higher (lower) likelihood, respectively. Figure adapted from *Yamazaki et al. (2009)*.

1.1.2 Paleoclimate archives

As reliable instrumental records of weather data did not start before 1850 AD at best, other tools have to be used to infer paleoclimate variations prior to that time. The analysis of natural and historical

archives can indirectly provide information related to past climate conditions. Natural paleoclimate archives include tree rings, sediment cores from lakes and oceans, ice cores from polar ice caps and high-altitude glaciers, corals, speleothems and boreholes, and can date back to millions of years for some of them. The basic principle is that climate conditions or atmospheric composition have affected their physical properties or chemical composition in such a way that this signal remained preserved in the material until the present day. Historical sources such as administrative documents, chronicles and paintings are also of great interest, but can only cover the last millennia, when human societies were developed enough to record this kind of information.

Paleoclimate archives enable us to put the recent climate change in the context of the natural variability over much longer timescales. They have shown that the Earth's climate was not uniform over time and experienced changes of greater magnitude than the current one. In addition, changes were not necessarily synchronous worldwide. For instance, three distinct phases can be observed in the Northern Hemisphere (NH) climate over the last millennium **(Fig. 1.4)**: in addition to the 20th century warming, a period of colder temperatures, called the Little Ice Age (LIA) occurred roughly between 1450 and 1850 AD *(Mann et al., 2009; Owens et al., 2017)*. Most of the Alpine glaciers were advancing at that time *(Lüthi, 2014)*, until the last maximum extent around 1850 AD *(Zumbühl et al., 2008)*, followed by a pronounced retreat which extended until present time *(Oerlemans, 2005)*. On the contrary, the period between 900 and 1250 AD, named Medieval Climate Anomaly (MCA) or Medieval Warm Period (MWP), was characterized by mild climate conditions *(Bradley et al., 2003; Lamb, 1965)* and reduced glacier extent *(Grove and Switur, 1994)*. Ice-core studies have shown that the MWP and LIA trends were also present in the Southern Hemisphere *(Arienzo et al., 2017; Kellerhals et al., 2010; Thompson et al., 1986)* and were therefore a global phenomenon whose intensity and duration varied regionally. Further back in the past, stable and warm conditions persisted over Europe at the apogee of the Roman Empire (around 300 BC to 200 AD) during the so-called Roman Warm Period (RWP, *Bianchi and McCave, 1999; Büntgen et al., 2011; McCormick et al., 2012)*. Evidence of the RWP was also found in a Central Asian ice core *(Herren, 2013)*. Climate variability increased from 250 to 600 AD, triggering important socioeconomic changes leading to the collapse of the Roman Empire and the Barbarian migrations in the context of a cold sixth century, the so-called Late Antique Little Ice Age (LALIA, *Büntgen et al., 2016)*.

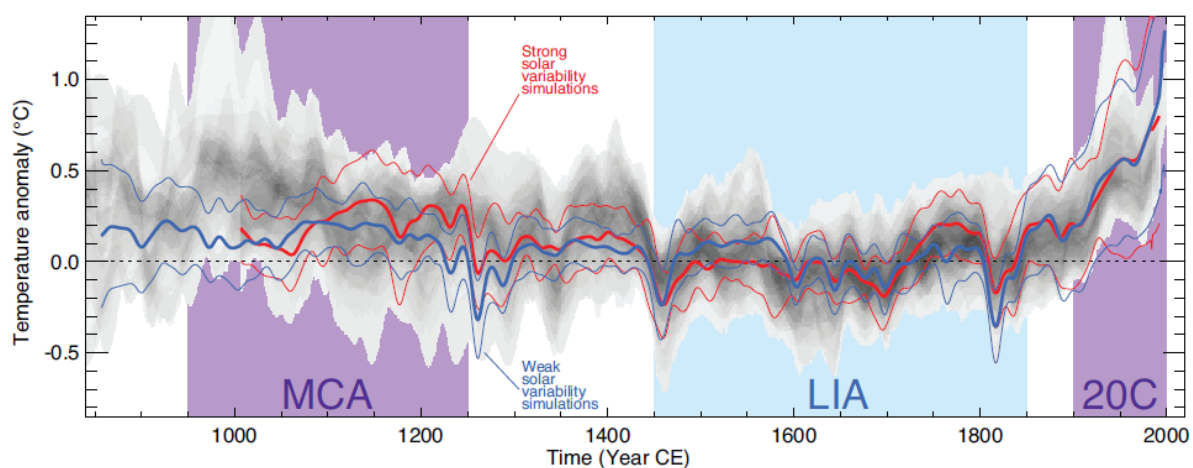**Fig. 1.4:** Reconstructed (grey) and simulated (blue/red according to solar variability simulations) Northern Hemisphere temperatures over the last millennium, highlighting the Medieval Climate Anomaly (MCA), the Little Ice Age (LIA) and the 20th century (20C). Data are anomalies relative to 1500–1850 AD mean temperatures smoothed with a 30-year filter *(Masson-Delmotte et al., 2013)*.

For longer timescales, a much larger climate variability can be observed. The NH glaciation starting around 3 million years ago *(Haug et al., 2005; Raymo, 1994)* initiated a period characterized by temperature oscillations of 4 to 6 °C at a global scale (more at the poles) between cold glacial periods and shorter but warm interglacials, with a periodicity of 41 kyr induced by a combination of orbital forcing parameters (eccentricity, obliquity and precession) influencing the Earth's radiative budget, as postulated by Milankovitch in 1941. 0.9 million years ago, periodicity changed to 100 kyr as evidenced by Antarctic ice-core records *(Petit et al., 1999; Schilt et al., 2010; Siegenthaler et al., 2005; Spahni et al., 2005)*. The reasons for the shift in oscillation periodicity and for 100 kyr-long cycles despite 41-kyr astronomic cycles remain partly unknown. The last glaciation began around 115 kyr ago and peaked 21 kyr ago during the so-called Last Glacial Maximum (LGM), which was followed by a progressive warming (last deglaciation) until the current interglacial period called the Holocene, which started 11700 years ago. Even if the Holocene is commonly perceived as a period with stable climatic conditions *(Johnsen et al., 1997)*, higher temperatures prevailed during the Holocene Climatic Optimum (HCO), also called Holocene Thermal Maximum (HTM), spanning roughly 9000–5000 years BP, before a return to colder conditions called sometimes "Neoglaciation" as many glaciers, which had disappeared during the HCO, started to reform *(Herren et al., 2013)*.

1.1.3 The ice core perspective

Glaciers are an important component of the Earth's surface as they cover around 10 % of it *(Vaughan et al., 2013)*. This encompasses the Antarctic ice sheet (8.2 % of the global land surface), the Greenland ice sheet (1.2 %) and thousands of mountain glaciers (0.5 %) which are mainly located in the Arctic, in the Alps, in the Himalayas and Central Asia, in the Andes, in Western North America and in Austral islands. Glaciers act as excellent indicators of climate variations as they usually expand (retreat) during cold (warm) periods, respectively. They are formed by the progressive accumulation and compaction of snow which does not melt in summer. As a consequence of this formation process, the snow becomes older and older with depth. Fresh snow contains a lot of trapped air and therefore has a low density (typically 0.1–0.2 g cm^{-3}). As the snow is progressively buried under more recent overlying snow, pressure increases in the underlying snow layers which start to undergo metamorphism. The interstitial air is gradually removed and the snow density increases as it is transformed into firn and finally ice (d = 0.9 g cm^{-3}), in which the remaining air is enclosed in bubbles.

During a snowfall event, atmospheric impurities such as aerosols and anthropogenic contaminants are scavenged by the snowflakes and archived in the snowpack. In addition to these wet deposition processes, dry deposition is also possible for some particles which can settle at the snow surface by gravity (e.g. mineral dust, pollens). Reactive atmospheric gases can also be transferred to the snowpack. Moreover, air bubbles trapped in the ice preserve samples of the past atmosphere. As a result of these processes, glaciers behave like powerful archives of past atmospheric composition, indirectly reflecting past climate variations. To get access to these precious archives, drilling expeditions are organized to polar ice sheets and mountain glaciers in order to retrieve ice cores, which are then melted and analyzed for a wide range of chemical compounds and physical properties, including:

- Water stable isotopes: the ratios of oxygen and hydrogen isotopes in the water molecules are affected by temperature and precipitation *(see section 3.4)*.
- Atmospheric trace gases: air bubbles trapped in glacier ice enable to directly access the composition of past atmosphere for trace gases such as CO_2, CH_4 and N_2O.

- Atmospheric aerosols: sea salt, mineral dust, biogenic and volcanic aerosols, anthropogenic contaminants (heavy metals, soot), pollen, DNA-fragments can be deposited on the snow surface and then archived in glacier ice.
- Melt features: these are transparent ice layers formed by the percolation and refreezing of liquid water. They affect the quality of the core but can also be used as an indirect proxy for temperature *(Okamoto et al., 2011; Winski et al., 2018)*.
- Density, from 0.1–0.2 g cm^{-3} for fresh snow to 0.9 g cm^{-3} for pure ice.
- Crystal size, axis orientation.

Ice-core study significantly contributed to the understanding of the past hundred thousand years of climate history. So far, ice cores from Greenland enabled to reconstruct up to 128 500 years of climate variability, back to the previous interglacial (Eemian), in the NEEM ice core. Deep drillings in Antarctica reached unprecedented ages of 420 000 years at Vostok, 720 000 years at Dome Fuji and 800 000 years at EPICA Dome C, the current record *(Jouzel, 2013)*. They provided invaluable records of past atmospheric trace gas composition over the last eight glacial/interglacial cycles **(Fig. 1.5)** showing common variations between CO_2, CH_4, N_2O and temperature and revealed that the current CO_2 concentration around 400 ppmv (parts per million by volume) had never been reached over the past 800 000 years *(Lüthi et al., 2008; Schilt et al., 2010)*. Explorations to find a site with more than one-million-year-old ice in chronological order so as to investigate the transition from 41 kyr to 100 kyr glacial/interglacial cycles are currently carried out in Antarctica *(Parrenin et al., 2017)*.
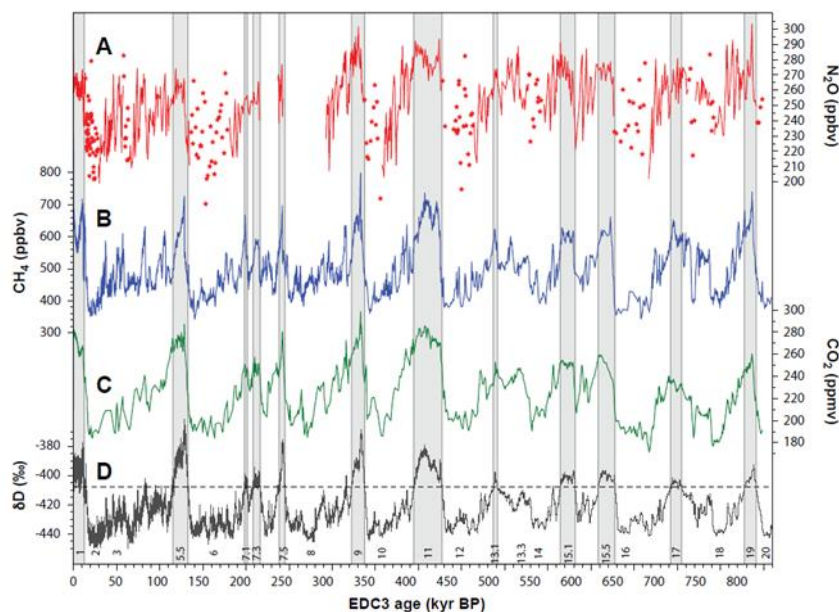
Fig. 1.5: a) N_2O, b) CH_4, c) CO_2 and d) δD (proxy for local temperature) records from the EPICA Dome C ice core spanning the last 800 000 years *(Schilt et al., 2010)*.

Compared to other paleoclimate archives, ice cores present the advantage of integrating emission sources over a larger area, from regional to continental scales (*Kehrwald et al., 2013a*, **Fig. 1.6**), and over relatively long timescales (see above) with often the possibility to achieve a high temporal resolution, especially in the upper part. According to the accumulation rate at the drill site, either long-term records with reduced resolution (low accumulation rate) or highly-resolved but shorter-term records (high accumulation rate, e.g. *Schwikowski et al., 1999*) can be obtained. On the other hand, ice cores possess intrinsic drawbacks. First, due to ice layer thinning with depth, dating is often challenging, particularly in the case of high-alpine ice cores where ice topography is more disturbed

due to steeper slopes, and has to be done by combining several methods *(see chapter 2)*. Second, an accurate source apportionment is difficult to perform as ice cores integrate atmospheric emissions over continental areas, which often prevents from resolving individual sources. Third, the chemical signal archived in the snowpack cannot be directly related to the intensity of the emission sources. Many processes can have an influence on the final record and have to be taken into account: transport pathways from the source to the ice-core site can fluctuate; the efficiency of the deposition at the ice-core site can vary according to climatic conditions; the accumulation rate can change over time; post-depositional processes such as melting *(Eichler et al., 2001; Osmont et al., 2018)*, sublimation *(Ginot et al., 2001)*, wind erosion *(Häberli et al., 1983)*, re-volatilization or diffusion in the snowpack in the case of volatile compounds such as carboxylic acids *(Legrand et al., 2016)*, can alter the chemical profile after deposition. Therefore, transfer functions have to be considered to convert the concentration in the ice into the original atmospheric concentration *(Schwikowski et al., 1998; Wolff et al., 1998)*.
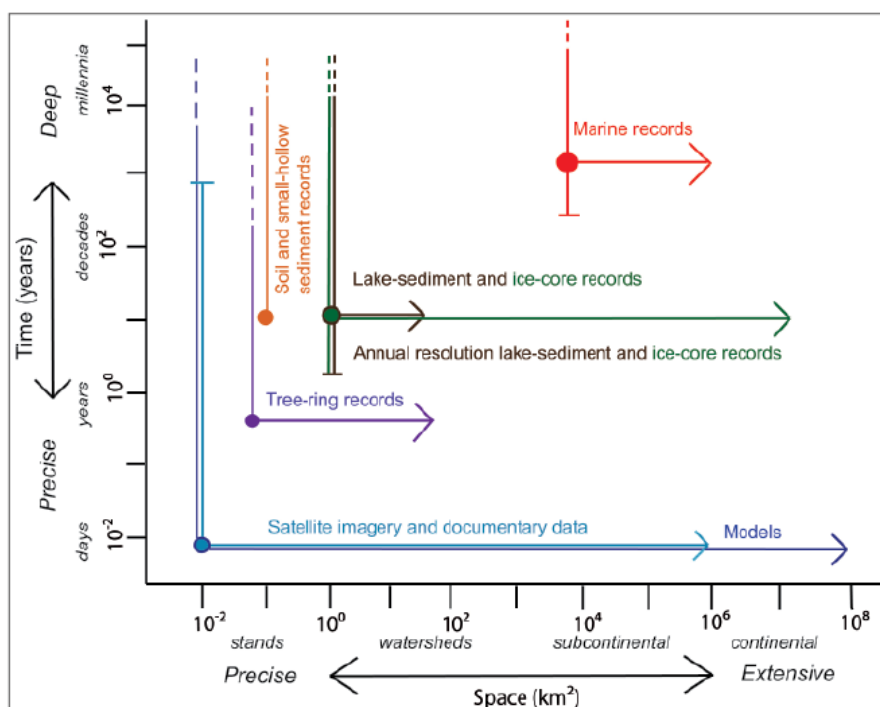
Fig. 1.6: Spatial and temporal resolution range for the main paleoclimate archives *(Kehrwald et al., 2013a)*.

1.2 Fires, climate and humans

1.2.1 Fires: the current situation

At the Earth's surface, wildfires are a natural phenomenon influencing vegetation cover over geological time spans and they substantially contribute to the global carbon budget. Nowadays, CO_2 emissions from fires (landscape fires and biomass burning) amount to 50 % of the CO_2 emissions produced by fossil fuel burning *(Bowman et al., 2009)*, which represents 2 to 4 Pg C yr^{-1} (e.g. 2.28 Pg C yr^{-1} for the year 2000 *(Ito and Penner, 2004)* or 3.1 Pg C yr^{-1} for the decade 2000–2010 *(van der Werf et al., 2013)*). Estimates of carbon emissions and burned areas vary significantly according to the studies due to the difficulty of obtaining accurate information, even if substantial progress has been achieved since the early 1980s when satellite measurements became available *(Keywood et al., 2011)*.

Depending on the studies, the annual burned area was comprised between 176 and 330 Mha (period 1997–2004, *Kloster et al., 2010*), or amounted to 313.9 Mha (year 2000, *Ito and Penner, 2004*), 343.7 Mha (average 1997–2004, *van der Werf et al., 2006*), 348 Mha (average 1997–2011, *Giglio et al., 2013*), or even reached 608 Mha (end of the 20th century, *Mouillot and Field, 2005*).

Despite this significant variability, the geographical distribution of fires is well documented **(Fig. 1.7)** and studies generally agree on it. Fires are rare in polar regions (> 70 °N and S) and totally absent in both cold and hot deserts. Their frequency increases towards the tropics, where it is maximal, and drops around the equator due to persistent humid conditions *(Mouillot and Field, 2005)*. In terms of both carbon emissions and annual burned area, Africa is the continent most affected by fires, representing 33 to 40 % of the global burned area, followed by South America (16 to 27 %, *Kloster et al., 2010*). Significant fire activity is also observed in Australia, South-East Asia, Central Asia, Central America, the USA, and in boreal forests, while burned area in Europe remains negligible compared to the other continents *(Mouillot and Field, 2005)*.
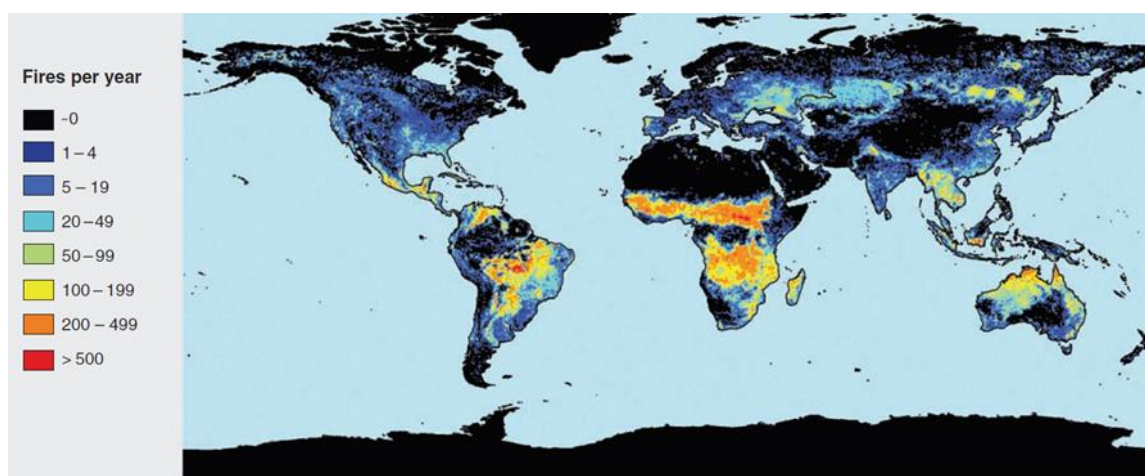
Fig. 1.7: Average number of fires observed by satellite per year per 1° grid cells *(Bowman et al., 2009)*.

Tropical savanna and grassland ecosystems are particularly prone to fires **(Fig. 1.8)**. They represent 86 % of the global burned area, mainly in Africa (55.7 %) and South America (16 %) *(Mouillot and Field, 2005)*. Forest fires account only for 11 % of the global burned area but are by far the dominant fire type in temperate and boreal regions *(Mouillot and Field, 2005)*. Peatland fires remain more anecdotic and are highly variable from year to year but can significantly contribute to global CO_2 emissions as they release a lot of CO_2 and carbon monoxide (CO) per unit of mass due to the high carbon content of peat. Peatland fires in 1997 in Indonesia were held responsible for carbon emissions equivalent to 13–40 % of the mean global carbon emissions from fossil fuel burning that year *(Page et al., 2002)*. Deforestation fires are located mainly in the tropics (Amazonia, equatorial Africa and South-East Asia) and have become an increasing concern since the second half of the 20th century. They are particularly problematic as they result in net carbon emissions *(van der Werf et al., 2010)* and tend to replace the existing vegetation by a more flammable one such as grasslands and shrublands *(Mouillot and Field, 2005)*. Lastly, fires are also used as an agricultural tool for slash-and-burn practices as well as for crop waste burning, especially in Asia *(van der Werf et al., 2010)*.

Savanna | woodland | deforestation | forest | agriculture | peat
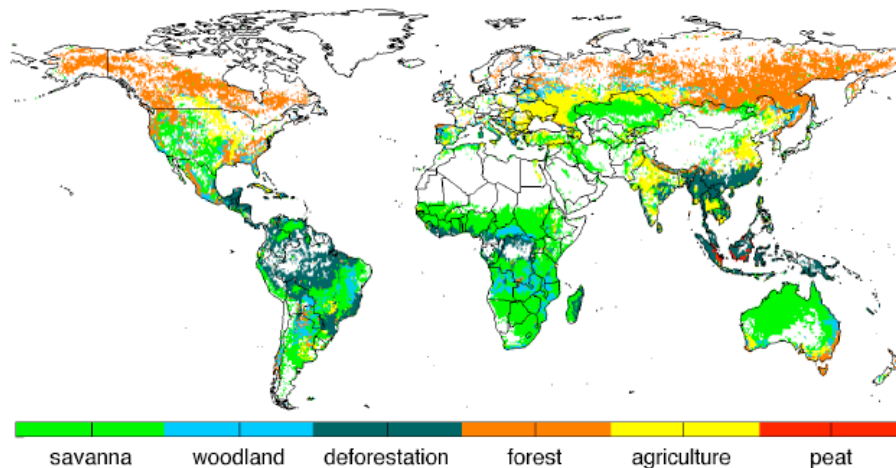
Fig. 1.8: Predominant fire type per 0.5° grid cell, based on C emissions *(van der Werf et al., 2010)*.

1.2.2 A complex relationship

Interactions between fires and climate are characterized by a certain level of complexity due to control and feedback mechanisms *(Keywood et al., 2011)*, further enhanced by the human impact on both fires and climate **(Fig. 1.9)**. Fires influence the climate by emitting GHGs (mainly CO_2 and CO) and aerosols *(Andreae and Merlet, 2001)*. Fire smoke contains significant amounts of carbonaceous substances such as black carbon (BC) and volatile organic compounds (VOCs). All these compounds can induce either a positive or a negative forcing on the Earth's radiative budget. On the other hand, for longer timescales, regional climatic conditions drive fire activity as they directly impact fuel type, quantity and quality. Even if it seems obvious that drier and warmer conditions tend to favor fire activity, linkages might be more complex in some regions. For instance, in areas where biomass growth is limited by moisture availability (arid regions), higher precipitation rates can enhance vegetation growth and therefore increase fuel loads available for the upcoming fire seasons *(Keywood et al., 2011; Marlon et al., 2013)*, provided that precipitation rates remain low enough so that it does not suppress fires *(Kehrwald et al., 2013b)*. Conversely, in more humid regions, an increase in precipitation will reduce fire activity *(Marlon et al., 2013)*. Prolonged droughts can also generate substantial amounts of highly flammable dead biomass which can easily cause severe fire episodes *(Eichler et al., 2011)*, if there is enough fuel to burn. In that respect, El Niño-Southern Oscillation (ENSO) processes are a key factor in controlling interannual fire variability in tropical regions *(Kloster et al., 2010)* due to their hydrological impacts on regional climate. For instance, the prominent El Niño year 1998 was accompanied by a peak in fire activity *(van der Werf et al., 2010)*. Climatic conditions also determine the dominant vegetation type of a region, which also influences fire activity as some species are more flammable than others. These differences in vegetation cover allow explaining why boreal North American forests experience intense flaming and crown fires while boreal Siberian forests are rather affected by ground and smoldering fires. In North America, black spruces and jack pines are flammable species which need fires to regenerate by dispersing seeds, whereas in Siberia, larches and Scots pines have evolved to resist fires but cannot survive if they burn *(Flannigan, 2015)*. Lastly, climatic conditions are directly responsible for fire ignition by lightning.

Since prehistoric times, humans and fires have always coexisted *(Bowman et al., 2011)*. Wildfires were often perceived as a threat to human societies, given the material damages and the economic and

life losses they induced. Recent dramatic fire events such as those in Russia in 2010 (54 fatalities), Portugal in 2017 (66 fatalities) and Greece in 2018 (96 fatalities) remind us of their dangerous aspects. Moreover, biomass burning plumes contain a whole range of adverse chemical compounds (ozone, CO, VOCs, soot) altering air quality and thus raising concern about health issues *(Keywood et al., 2011)*. On the other hand, human societies have been using fires as a tool for many purposes for ages. Apart from cooking and heating, the main use of fire was for agricultural purposes with the conversion of forests/shrublands into pastoral and agricultural lansdscapes, slash-and-burn techniques to increase soil fertility, crop waste burning, and also to limit fuel load in case natural fires happen *(Bowman et al., 2009, 2011)*. On the contrary, developed countries have initiated since the 19th century fire suppression policies to limit fire hazards *(Bowman et al., 2009; Keywood et al., 2011)*. However, an unexpected drawback of this strategy is the increase of the probability of catastrophic fire events due to fuel accumulation since managed forests experience a fire deficit, as observed in the Western USA in the last decades *(Keywood et al., 2011; Marlon et al., 2012)*.
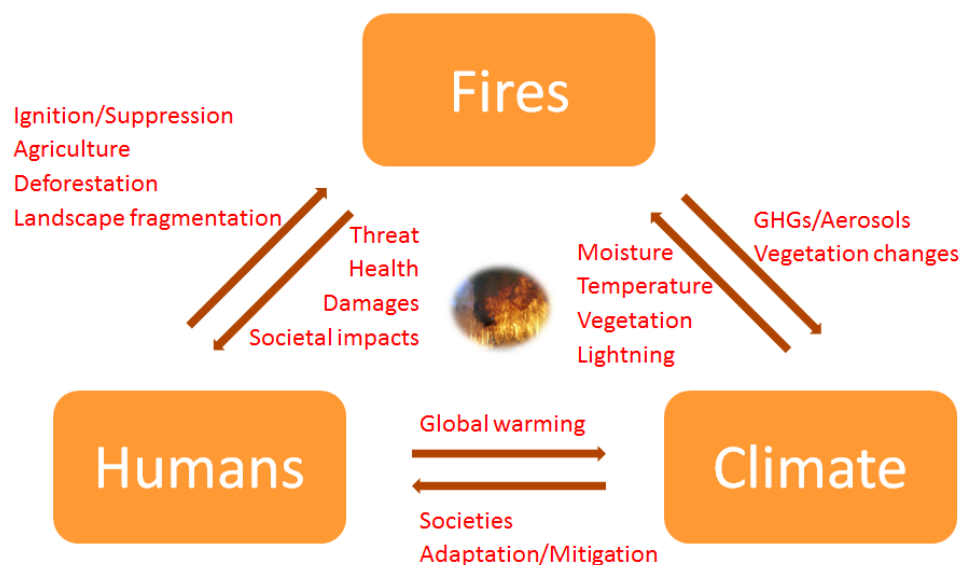
Fig. 1.9: Schematic diagram of the interactions between fires, climate and humans.

It thus results that 90 % of fire ignitions worldwide are intentional, for agricultural purposes, by negligence or arson *(Keywood et al., 2011)*, and that only in remote boreal regions do fires remain primarily driven by climate *(Mouillot and Field, 2005)*. In the context of global warming, fire activity is expected to increase in frequency, intensity, duration and extent in many regions of the world *(Bowman et al., 2011; Keywood et al., 2011)*. However, trends might differ between regions and remain unclear due to the complex mechanisms and feedbacks listed above.

1.2.3 Motivation: the "Broken Fire Hockey Stick" hypothesis

Since vegetation appeared around 420 million years ago, wildfires have always been part of the Earth history *(Bowman et al., 2009)*. To reconstruct past fire history, it is necessary to make use of paleoclimate archives as satellite monitoring of fires did not start before the 1980s and accurate biomass burning statistics were not available prior to the 20th century. So far, most of the paleofire reconstructions have been derived from charcoal profiles from sedimentary records. Charcoal is a specific by-product of wood burning and has been widely used as a proxy for fire activity (e.g. *Conedera et al., 2009; Tinner and Hu, 2003*). Macroscopic charcoal particles (> 100 μm) provide information about local fire history while microscopic charcoal particles recorded from pollen slides

(typically 10–100 μm) may be transported over long distances and therefore be useful to reconstruct regional fire trends *(Conedera et al., 2009; Marlon et al., 2016; Power et al., 2008)*.

Paleofire studies have shown that fire activity was low during the last glacial maximum and the last deglaciation, and increased towards the Holocene, suggesting temperature as the primary driver of fire activity, with a modulation by local changes in vegetation and fuel load *(Power et al., 2008)*. Large increases in fire activity were also observed during intervals of abrupt climate change *(Marlon et al., 2009)*. First increases in fire activity which can be partially related to the impacts of early human societies occurred between 3 and 2 ka *(Marlon et al., 2013)*. The Global Charcoal Database (GCD), a compilation of hundreds of sedimentary charcoal records worldwide **(Fig. 1.10, black line)**, revealed that fire activity declined from 1 to 1750 AD in line with the global decrease in temperature over this time period *(Marlon et al., 2008)* and despite rising population density, suggesting that climatic conditions were still driving fire activity during this period. Fire activity increased sharply between 1750 and 1870 AD, in a context of rising population density and global temperature following the end of the LIA. In addition to warmer temperatures, land-use changes (deforestation, land clearance) due to increasing human influences were mentioned as a possible cause. But after 1870 AD, fire activity dropped, despite rising temperatures and population density. Potential reasons are the implementation of fire suppression policies and landscape fragmentation due to intensive agriculture and grazing and road building, which prevented fires from spreading as they did in the past. This decoupling suggests that, in the last century, human influence on fires became more important than natural climate variability. It also indicates that biomass burning levels are maximal at intermediate levels of population density, as fires cannot spread in densely-populated areas *(Marlon et al., 2013)*. By analogy with the famous hockey-stick-shaped temperature curve and due to the recent decoupling between fire activity and its main drivers namely temperature and population density, this curve was thus called the **"broken" fire hockey stick (BFHS)**.
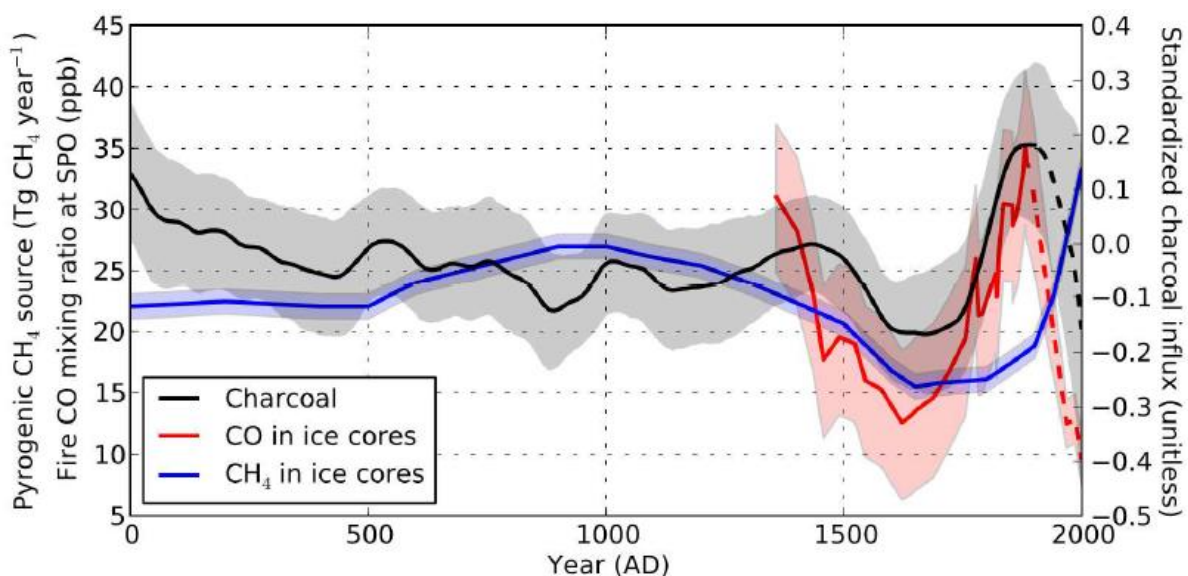
Fig. 1.10: Variability of biomass burning activity over the last two millennia based on a worldwide compilation of charcoal records *(Marlon et al., 2008)*, CO mixing ratios from fires using CO concentration measurements in an ice core from the South Pole *(Wang et al., 2010)*, and a similar approach but based on CH_4 *(Ferretti et al., 2005)*. The "broken" fire hockey stick is visible in the red and black curves, with a marked (though uncertain) decline of fire activity during the last decades, but not in the blue curve. Figure from *van der Werf et al., 2013*.

A similar trend was obtained for CO concentrations and isotopic ratios from Antarctic ice cores *(Wang et al., 2010)*. However, these trends were not supported by Antarctic CH_4 records *(Ferretti et al., 2005; Mischler et al., 2009)*. Moreover, the methods used possess intrinsic limitations and weaknesses. The dating of the upper part of sedimentary records, generally the last 250 years, *(W. Tinner, personal communication)* is highly uncertain due to the softness of the material. Similarly, CO measurements from the South Pole ice core ended in 1897 AD but were extended with firn measurements from other sites and modelling, resulting in greater uncertainties and unrealistic implications challenged by *van der Werf et al. (2013)*. Sedimentary charcoal records can only provide a local to regional fire reconstruction, which means that many records have to be compiled in order to draw continental-scale trends. This task carries additional uncertainties as analytical methods differ between the studies, leading to different charcoal size ranges and non-homogeneous units. Lastly, in the first versions of the GCD, European and North American regions were over-represented due to easier conditions of access, implying a bias in the global charcoal record towards fire history from these regions, where fire suppression had been intensively implemented since the end of the 19th century and which only represent less than 1 % of global current carbon emissions due to fires *(van der Werf et al., 2013)*. Such a decreasing trend in the 20th century is also inconsistent with exponentially increasing levels of deforestation observed in the tropics since the mid-20th century but would rather reflect trends from boreal and temperate forests where the burned area decreased between 1900 and the 1960s *(Mouillot and Field, 2005)*, highlighting again the methodological bias towards these regions.

The next GCD compilations therefore aimed at correcting this bias by including more charcoal records from other regions in order to obtain a better global representativeness. It resulted that the BFHS trend did not capture regional heterogeneity as some regions exhibited large increases in fire activity during the 20th century (Australia, parts of Europe, *Marlon et al., 2013*). As a consequence, the existence of the BFHS at a global scale remains uncertain. Ice cores could have the potential to improve our general understanding of past fire trends due to their much better controlled chronology and their much larger spatial representativeness. In this respect, ice-core records of biomass burning proxies could help solve important questions:

- Can the BFHS hypothesis be confirmed or invalidated by means of ice cores?
- Is this a global trend or just limited to some regions?
- What were the main drivers of fire activity through time?

1.3 Biomass burning proxies in ice cores

As explained before, wildfires can emit a wide range of chemical compounds to the atmosphere. They are then transported by atmospheric circulation and can be deposited at the snow surface where they will be archived and later extracted by ice-core drilling. We list below the main biomass burning proxies used in ice-core science, with a special focus on black carbon, and describe the current state of research in the field.

1.3.1 Black carbon

Black carbon (BC) refers to the main light-absorbing fraction of carbonaceous aerosols *(Gysel et al., 2011; Petzold et al., 2013)*. It is formed by the incomplete combustion of carbon-based fuels, namely biomass and fossil fuels, when the lack of oxygen prevents a total conversion of the fuel into CO_2 and water *(AMAP, 2011)*, which generates other compounds like soot, CO and Polycyclic Aromatic

Hydrocarbons (PAHs). BC is composed of aggregates of carbonaceous spherules of nanometric size **(Fig. 1.11a)** and is characterized by a unique set of properties *(Bond et al., 2013)*: it has a low chemical reactivity, resulting in insolubility in water and organic solvents, it is highly refractory, with a vaporization temperature around 4000 K, and it strongly absorbs visible light at all visible wavelengths (hence its black color). Per unit mass, BC is the strongest light-absorbing compound in the atmosphere *(Bond et al., 2013)*.

There is a lack of standardized definition for BC because it is not a single well-defined compound. Indeed, during combustion processes, carbonaceous aerosols are emitted in the form of a continuum of compounds *(Goldberg, 1985; Hedges et al., 2000)*. As temperature increases, combustion generates compounds with higher and higher carbon content and degrees of graphitization, from char, to charcoal, and finally soot **(Fig. 1.11b)**. Given this complexity, several analytical methods are applied to analyze BC. As they all make use of different BC properties, discrepancies in measured concentrations can reach up to 80 % *(Bond et al., 2013)*. Recently, a new terminology was introduced by *Petzold et al. (2013)* to clarify this situation and we will follow his recommendations here. Briefly, when referring to a specific analytical method, BC will be called:

- equivalent black carbon (eBC) when measured by light-absorbing techniques (filter measurements).
- refractory black carbon (rBC) when laser-induced incandescence methods are used *(this thesis)*.
- elemental carbon (EC) in the case of thermal-optical methods making the distinction between organic and elemental carbon (OC/EC).
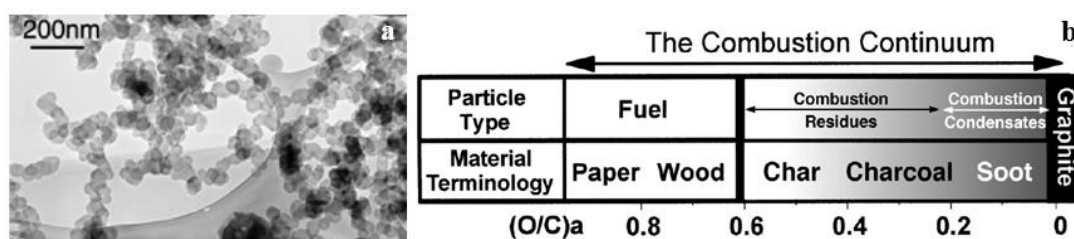
Fig 1.11: a) Transmission Electron Microscope (TEM) image of BC aggregates from smoke *(Bond et al., 2013)*. b) The BC combustion continuum *(Hedges et al., 2000)*.

BC can be emitted by a wide range of sources and therefore is not a specific proxy for biomass burning in ice cores. Current BC sources include *(Bond, 2007)*:

- Wildfires or "open" biomass burning (42 %).
- Residential biomass burning for heating/cooking (18 %).
- Emissions from traffic (24 %).
- Emissions from industry (10 %).
- Residential fossil fuel burning (6 %).

BC emissions, estimated by bottom-up inventories carrying substantial uncertainties, amounted to 7500 Gg yr^{-1} for the year 2000 *(Bond et al., 2013)*. Historical BC trends *(Bond et al., 2007)* show that Western countries were the main emitters until the mid-20th century. In the USA, BC emissions reached a peak around 1910 and started to decline as early as in the 1920s. In Western Europe, BC emissions plateaued in the early 20th century and decreased from the 1960s on. The main reason for reduced emissions was the implementation of cleaner technologies and stricter environmental

policies. Unfortunately, this decrease was largely compensated by a strong rise in emissions from developing countries, with China and India in the lead.

In recent years, BC has become a compound of increasing interest due to its deleterious impacts on both the climate and the human health. BC belongs to the fine particulate matter fraction. Due to its small size (nm range), particles can enter far into the human body, cross the lung membrane and end up in the blood circulation. Soot has been classified as carcinogenic to humans (group 1) by the International Agency for Research on Cancer (IARC). Regarding climate impacts, BC contributes to global warming as it strongly absorbs visible light. Total industrial-era BC climate forcing is estimated to be +1.1 ± 1 W m^{-2} *(Bond et al., 2013)*. According to some studies, BC could even be the second most important forcing agent after CO_2 *(Ramanathan and Carmichael, 2008)*. However, the current consensus is that BC anthropogenic forcing comes third, after CO_2 and CH_4 *(IPCC, 2013)*.
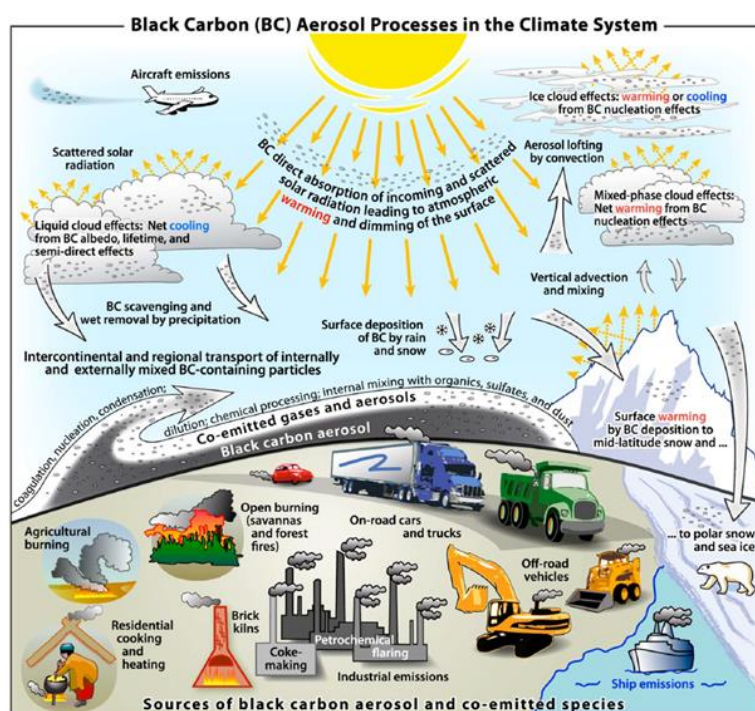
Fig. 1.12: BC impacts on the climate system *(Bond et al., 2013)*.

Three main effects of BC on climate **(Fig. 1.12)** can be distinguished *(AMAP et al., 2011; Bond et al., 2013)*:

- A direct radiative forcing: atmospheric BC aerosols directly absorb incoming and scattered solar radiation, leading to atmospheric warming and dimming at the surface.
- An indirect radiative forcing when BC gets deposited on snow and ice surfaces. As BC atmospheric lifetime is about one week *(Cape et al., 2012)*, BC particles can be transported over continental scales and be deposited in regions with snow cover. BC will therefore reduce the albedo of snow and can trigger or accelerate snow melting. Even if this forcing remains small at a global scale, it can strongly impact polar and high-mountain regions *(Hansen and Nazarenko, 2004)*.
- A modification of cloud properties, such as the number and size of cloud condensation nuclei. These mechanisms are currently poorly understood and their general impact remains unclear as they can induce either positive or negative forcing.

24

1.3.2 Other proxies

Numerous chemical compounds can be used as tracers for biomass burning emissions. Some of them are specifically produced by biomass burning while others can originate from different sources and are therefore non-specific tracers.

Specific biomass burning tracers include:

- **Charcoal:** it is a lightweight and black carbonaceous residue produced by wood combustion. There is a long tradition of charcoal analysis in sediment cores *(see section 1.2.3)*, but its analysis in ice cores has been initiated only recently *(Eichler et al., 2011; Hicks and Isaksson, 2006)*.
- A range of **organic tracers** stemming from the degradation of biopolymers *(Simoneit, 2002)*, recently introduced in ice-core science *(Gambaro et al., 2008; Grieman et al., 2015; Kehrwald et al., 2012)*. The most common ones are levoglucosan, produced by cellulose burning at temperatures higher than 300 °C *(Simoneit, 2002)* and vanillic (VA) and *p*-hydroxybenzoic (*p*-HBA) acids, predominantly emitted by conifer and grass burning, respectively *(Grieman et al., 2017; Grieman et al., 2018)*, whose structure is illustrated in **Fig. 1.13**. Other species include polysaccharides (galactosan, mannosan), syringic acid or dehydroabietic acid *(Rubino et al., 2016)*. However, little is known about their atmospheric lifetime and their degradation pathways since those compounds are sensitive to oxidation by OH radicals *(Hennigan et al., 2010; Hoffmann et al., 2010)*. They also seem affected by post-depositional processes in ice cores, such as melting *(Müller-Tautges et al., 2016)*.
- **Trace gases (CO and CH$_4$)** from Antarctic ice cores partially come from biomass burning. Their isotopic analysis can help disentangle their sources. Of particular interest are δ^{13}C-CH$_4$, δD-CH$_4$, δ^{13}C-CO and δ^{18}O-CO *(Ferretti et al., 2005; Rubino et al., 2016; Wang et al., 2010)*.
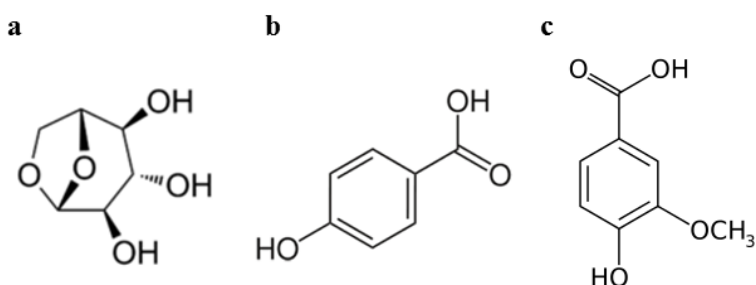
Fig. 1.13: Molecular structures of a) levoglucosan, b) *p*-hydroxybenzoic acid and c) vanillic acid.

In addition to BC, non-specific biomass burning proxies encompass:

- **EC/OC:** even if, like BC, they are also part of the carbonaceous fraction, they present the advantage of allowing source apportionment as subsequent ^{14}C analysis can be carried out on the two compounds, thus indicating the fraction of carbon originating from fossil fuel (no ^{14}C content) versus the fraction of biogenic carbon *(Jenk et al., 2007)*.
- **Major ions:** Ammonium (NH$_4^+$) is the compound of choice for reconstructing biomass burning history from polar ice cores *(Fischer et al., 2015; Legrand et al., 2016)*. Even if biogenic emissions drive background variations, they remain low compared to summer NH$_4^+$ peaks reflecting biomass burning events *(Legrand et al., 1992)*. Potassium (K$^+$) and nitrate (NO$_3^-$) have also been used but are generally not suitable as substantial non-biomass burning sources and post-depositional effects exist *(Legrand et al., 2016)*.

- **Light carboxylic acids:** within this group, formate ($HCOO^-$) is the only appropriate tracer as all the other ones (acetate (CH_3COO^-), oxalate ($C_2O_4^{2-}$) or glycolate ($C_2H_3O_3^-$)) are significantly affected by other sources and post-depositional processes due to the volatile character of their conjugate acid *(Legrand et al., 2016)*.

Each tracer possesses a set of intrinsic strengths and weaknesses due to its specificity, its sensitivity to fire emissions, post-depositional processes or contamination during chemical analysis. There is no "perfect" biomass burning tracer *per se*. Therefore, in the framework of the reconstruction of paleofires, it is suitable to combine several tracers in order to obtain a comprehensive overview of the situation. Nevertheless, limitations exist: even specific proxies cannot disentangle biomass burning emissions from wildfires and from energy-related sources (for cooking and heating). Similarly, a direct distinction between human-set fires and natural fires remains impossible *(Marlon et al., 2013)*.

1.3.3 State of the art in ice-core based fire reconstructions

Early studies in the 1990s, mainly in Greenland, aimed at identifying biomass burning proxies in snow and ice cores and suggested carboxylic acids and major ions (particularly NH_4^+ and $HCOO^-$) as suitable candidates *(Fuhrer et al., 1996; Legrand and DeAngelis, 1996; Meeker et al., 1997; Savarino and Legrand, 1998)*. Interesting case studies of biomass burning plumes transported to Greenland were also reported *(Dibb et al., 1996)*.

In addition to polar regions, high-mountain ice cores were also used to perform paleofire reconstruction. These ice cores brought complementary information to polar ice cores due to their greater proximity to source regions, making source attribution easier. They enabled to reconstruct regional to sub-continental fire histories and their connection to regional climate variations. NH_4^+ trends in the Mt Logan ice core (Canada) strongly differed from those from Greenland (20D, GISP2), suggesting different source regions, potentially Siberia *(Whitlow et al., 1994)*. A neighboring record from Eclipse ice field showed good agreement between NH_4^+, $C_2O_4^{2-}$ and K^+ peaks and forest fire history from Alaska and Yukon *(Yalcin et al., 2006)*. In the Belukha ice core (Siberian Altai), the NO_3^-, K^+ and charcoal records *(Eichler et al., 2011)* revealed an elevated fire activity around 1600–1680 AD following an extremely dry period (1540–1600 AD).

First BC (or more generally, carbonaceous compounds) measurements in ice cores were initiated by *Chýlek et al. (1992)* in the Dye-3 ice core (Greenland) and by *Lavanchy et al. (1999)* in the Colle Gnifetti ice core (Swiss Alps). *Chýlek et al. (1995)* already attributed BC peaks in the GISP2 ice core (Greenland) to biomass burning emissions. Those pioneering studies mainly relied on thermal-optical methods which were characterized by high uncertainties and poor repeatability due to the lack of standardized procedure, but were nevertheless able to document a 20th-century increase in BC due to anthropogenic emissions. After standardized protocols were introduced for EC and OC measurements *(Szidat et al., 2004)*, more accurate studies were carried out. *Jenk et al. (2006)* analyzed EC and OC in the Fiescherhorn ice core (Swiss Alps) and were able to do source apportionment by measuring the ^{14}C content of the EC and OC fractions. EC measurements were also performed on ice cores from Holtedahlfonna, Svalbard *(Ruppel et al., 2014)* and Col du Dôme, French Alps *(Legrand et al., 2007)*. However, the aforementioned studies did not really focus on biomass burning reconstruction and suffer from low resolution (several years per sample) due to the fact that EC and OC measurements by thermal-optical methods require hundreds of grams of ice per sample.

A breakthrough in the field of BC analysis in ice cores was achieved by the introduction of laser-induced incandescence methods using the Single Particle Soot Photometer (SP2) to quantify rBC, allowing high resolution (a few cm per sample or even continuous flow analysis techniques now) and

reproducible measurements, making the detection of single biomass burning events possible. The first study was carried out on the D4 ice core, Greenland *(McConnell et al., 2007)*. Numerous rBC records from polar and high-mountain ice-cores were subsequently published. The majority of them did not specifically focus on paleofire trends but provided a broad overview of past BC trends and sources, such as those from the Elbrus, Caucasus *(Lim et al., 2017)*, the East Rongbuk glacier, Himalayas *(Kaspari et al., 2011)*, Geladaindong, Tibet *(Jenkins et al., 2016)*, WAIS Divide (WD) and Law Dome, Antarctica *(Bisiaux et al., 2012)*, Devon Island, Canadian Arctic *(Zdanowicz et al., in review)*, the NEEM 2011-S1 ice core, Greenland *(Sigl et al. 2013)*. Most of these studies identified a clear increase in rBC since the beginning of the Industrial Revolution due to anthropogenic emissions. The time of this increase differed according to the location. It started earlier in Greenland (1880s) due to early North American emissions, later in the Caucasus (1940s), reflecting USSR and Eastern Europe emissions, and even more recently (1970s) in the Himalayas, in agreement with the recent economic development of Asian countries.

Some rBC ice-core studies focused further on biomass burning emissions and paleofire reconstruction. *McConnell et al. (2007)* used the difference between the rBC and the vanillic acid records to disentangle the fraction of rBC stemming from fossil fuel to that coming from biomass burning. Using the Summit 2010 ice core (Greenland), *Keegan et al. (2014)* estimated the impact of rBC originating from biomass burning on the surface melting of the Greenland ice sheet. *Wang et al. (2015)* analyzed rBC in the Muztagh Ata ice core (Eastern Pamirs) and used levoglucosan to disentangle rBC sources, revealing increased open fires in the 1940s and 1950s and enhanced anthropogenic contribution in the 1980s and 1990s. Using rBC in association with levoglucosan and NH_4^+, *Zennaro et al. (2014)* reconstructed two millennia of boreal fire activity derived from the NEEM ice core (Greenland), showing higher levels of biomass burning between 1000 and 1300 AD and lower levels between 700 and 900 AD, in line with NH temperature variations. By combining rBC records from WD and B40 (Antarctica), *Arienzo et al. (2017)* were able to reconstruct South American biomass burning variations through the entire Holocene. Higher concentrations were observed during the Holocene Climatic Optimum and lower concentrations during the Little Ice Age, in agreement with South American hydroclimate variations.

Organic tracer measurements in ice cores were more recently implemented. First publications dealt with levoglucosan analyses in Col du Dôme and Colle Gnifetti ice cores but values were below the limit of detection *(Legrand et al., 2007)*, and with vanillic acid in the D4 ice core *(McConnell et al., 2007)*. Advances in analytical techniques allowed analyses down to the pg g^{-1} (or parts per trillion, ppt) level. *Kawamura et al. (2012)* analyzed several organic tracers (levoglucosan, vanillic acid, dehydroabietic acid and *p*-hydroxybenzoic acid) in the Ushkovsky ice core (Kamchatka). Comparable peak occurrence was found between the four tracers but with different long-term trends due to their different vegetation sources. For instance, only dehydroabietic acid, related to conifer burning, showed an increasing trend in the 20th century. Several tracers were also compared in the Grenzgletscher ice core (Swiss Alps), and *p*-hydroxybenzoic acid was found to be the best organic fire tracer in this area as it exhibited a good correlation with regional burned area *(Müller-Tautges et al., 2016)*. As mentioned before, levoglucosan was also measured in the NEEM ice core *(Zennaro et al., 2014)*. Vanillic and *p*-hydroxybenzoic acids were also analyzed in ice cores from Akademii Nauk ice cap (Severnaya Zemlya archipelago, *Grieman et al., 2017*) and Lomonosovfonna (Svalbard, *Grieman et al., 2018*), to document past biomass burning variations in Northern Eurasia. Lastly, the vanillic acid record from TUNU ice core (Greenland, *Grieman et al., in review*) provides insight into past biomass burning emissions in North America and nicely reflects temperature variations, with higher values during the RWP and MWP and lower values during the LALIA and LIA.
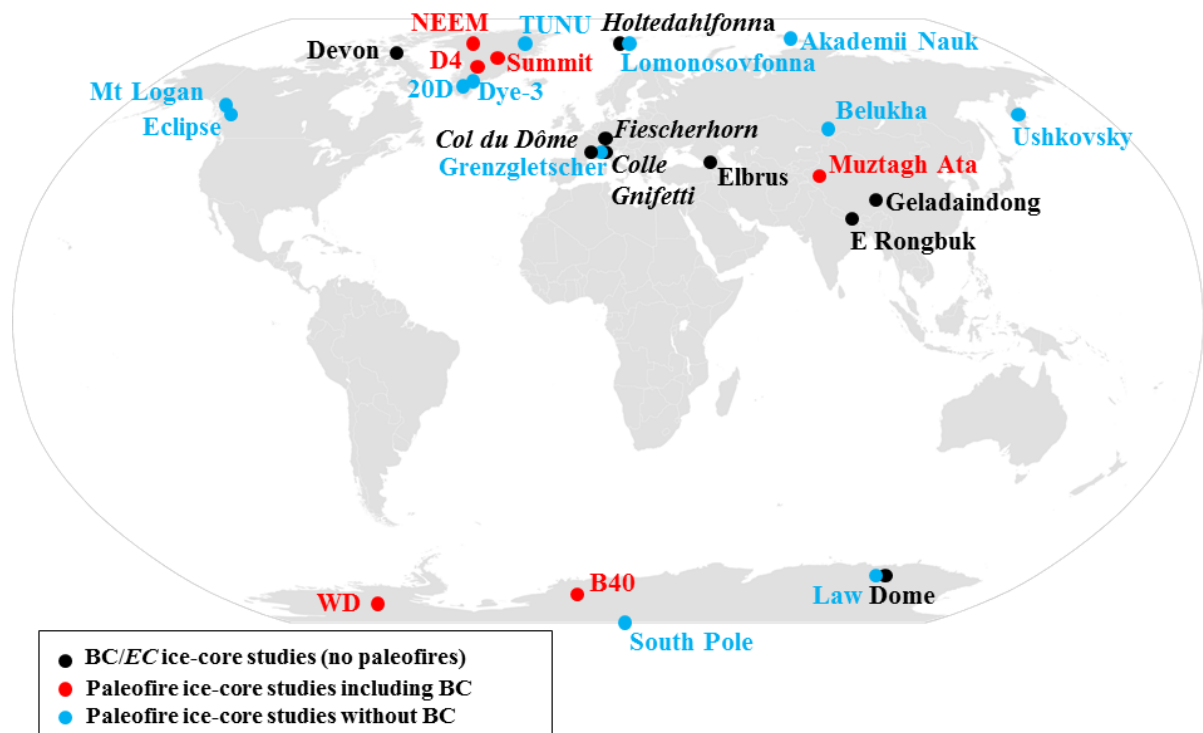
Fig. 1.14: Location of the ice-core sites of interest mentioned in chapter 1. For additional details, see *Rubino et al. (2015)* and *Legrand et al. (2016)*. The Summit site in Greenland encompasses several ice-core projects (GISP2, GRIP, GRIP 93, Eurocore).

1.4 Aim of the study: the *PaleoFire* project

This PhD thesis is part of the inter-disciplinary project called *PaleoFire*. The *PaleoFire* project aims at improving the understanding of the complex linkages between fires, climate and humans, in order to test the "broken" fire hockey stick hypothesis *(Marlon et al., 2008)*. *PaleoFire* is based on the analysis of biomass burning proxies, mainly charcoal and rBC, in four existing high-alpine ice cores from different regions with complementary climatic and human settings **(Fig. 1.15)**: the European Arctic (Lomonosovfonna), the tropical Andes (Illimani), the Mongolian Altai (Tsambagarav) and the Alps (Colle Gnifetti), presented in greater detail in chapter 2 of this thesis. Contrary to sedimentary charcoal records, these ice cores present the advantage of having good and controlled chronologies, especially after 1850 AD, allowing for accurately-dated high-resolution analyses, and are representative of much larger source regions, enabling to reconstruct regional to sub-continental paleofire trends.

Fig. 1.15: High-alpine ice cores used in the *PaleoFire* project.

PaleoFire consists of a collaboration between four different research groups **(Fig. 1.16)** in order to associate laboratory analyses with atmospheric modeling and remote sensing of fires. This is an innovative approach which allows linking accurate ice core data with their atmospheric footprint and with coinciding observations from satellites, resulting in proxy calibration. The four sub-group tasks are detailed below:

- rBC analyses in ice cores, in addition to ice-core extraction and sampling. In the framework of the project, a shallow firn core from Illimani and an ice core from Colle Gnifetti were extracted in 2015 to update the existing ice-core records. Two deep ice cores from Belukha glacier, Siberian Altai, were also retrieved in 2018 but will be used for future projects.
  (sub-group A ,this thesis, Paul Scherrer Institute, Laboratory of Environmental Chemistry)

- microscopic charcoal and pollen analyses in ice cores, in order to connect paleofire history with natural and human-induced vegetation changes.
  (sub-group B, University of Bern, Institute of Plant Sciences)

- atmospheric modeling of BC and charcoal, to put the ice-core data into a broad context and to quantify the atmospheric footprint of each of the ice cores.
  (sub-group C, ETH Zürich, Institute for Atmospheric and Climate Science)

- remote sensing of fires, to support modeling and backward trajectories. The accuracy of the different satellite products was assessed and 30-year time series of fires were compiled and compared to the ice-core records to allow for proxy calibration.
  (sub-group D, University of Bern, Institute of Geography)
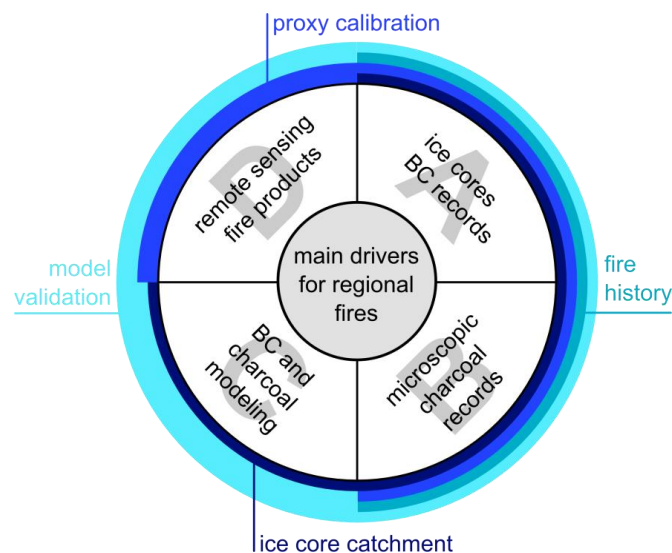
Fig 1.16: Schematic structure of the *PaleoFire* project (from *SNF Sinergia proposal PaleoFire, M. Schwikowski*).

References

AMAP: The Impact of Black Carbon on Arctic Climate, Quinn, P. K., Stohl, A., Arneth, A., Berntsen, T., Burkhart, J. F., Christensen, J., Flanner, M., Kupiainen, K., Lihavainen, H., Shepherd, M., Shevchenko, V., Skov, H., and Vestreng, V., Arctic Monitoring and Assessment Programme (AMAP), Oslo, Norway, 72 pp, 2011.

Andreae, M. O. and Merlet, P.: Emission of trace gases and aerosols from biomass burning, *Global Biogeochemical Cycles*, 15(4), 955–966, 2001.

Arienzo, M. M., McConnell, J. R., Murphy, L. N., Chellman, N., Das, S., Kipfstuhl, S., and Mulvaney, R.: Holocene black carbon in Antarctica paralleled Southern Hemisphere climate, *Journal of Geophysical Research: Atmospheres*, 122, 2017.

Bianchi, G. G. and McCave, N.: Holocene periodicity in North Atlantic climate and deep-ocean flow south of Iceland, *Nature*, 397, 515–517, 1999.

Bisiaux, M. M., Edwards, R., McConnell, J. R., Curran, M. A. J., Van Ommen, T. D., Smith, A. M., Neumann, T. A., Pasteris, D. R., Penner, J. E., and Taylor, K.: Changes in black carbon deposition to Antarctica from two high-resolution ice core records, AD 1850–2000, *Atmospheric Chemistry and Physics*, 12, 4107–4115, 2012.

Bond, T. C.: Testimony for the Hearing on Black Carbon and Climate Change, House Committee on Oversight and Government Reform, United States House of Representatives, The Honorable Henry A. Waxman, Chair, October 18, 2007.

Bond, T. C., Bhardwaj, E., Dong, R., Jogani, R., Jung, S. K., Roden, C., Streets, D. G., and Trautmann, N. M.: Historical emissions of black and organic carbon aerosol from energy-related combustion, 1850–2000, *Global Biogeochemical Cycles*, 21, 2007.

Bond, T. C., Doherty, S. J., Fahey, D. W., Forster, P. M., Berntsen, T., DeAngelo, B. J., Flanner, M. G., Ghan, S., Karcher, B., Koch, D., Kinne, S., Kondo, Y., Quinn, P. K., Sarofim, M. C., Schultz, M. G., Schulz, M., Venkataraman, C., Zhang, H., Zhang, S., Bellouin, N., Guttikunda, S. K., Hopke, P. K., Jacobson, M. Z., Kaiser, J. W., Klimont, Z., Lohmann, U., Schwarz, J. P., Shindell, D., Storelvmo, T., Warren, S. G., and Zender, C. S.:

Bounding the role of black carbon in the climate system: A scientific assessment, *Journal of Geophysical Research: Atmospheres*, 118, 5380–5552, 2013.

Bowman, D. M. J. S., Balch, J. K., Artaxo, P., Bond, W. J., Carlson, J. M., Cochrane, M. A., D'Antonio, C. M., DeFries, R. S., Doyle, J. C., Harrison, S. P., Johnston, F. H., Keeley, J. E., Krawchuk, M. A., Kull, C. A., Marston, J. B., Moritz, M. A., Prentice, I. C., Roos, C. I., Scott, A. C., Swetnam , T. W., van der Werf, G. R., and Pyne, S. J.: Fire in the Earth System, *Science*, 324(5926), 481–484, 2009.

Bowman, D. M. J. S., Balch, J. K., Artaxo, P., Bond, W. J., Cochrane, M. A., D'Antonio, C. M., DeFries, R. S., Johnston, F. H., Keeley, J. E., Krawchuk, M. A., Kull, C. A., Mack, M., Moritz, M. A., Pyne, S. J., Roos, C. I., Scott, A. C., Sodhi, N. S., and Swetnam, T. W.: The human dimension of fire regimes on Earth, *Journal of Biogeography*, 38(12), 2223–2236, 2011.

Bradley, R. S., Hughes, M. K., and Diaz, H. F.: Climate in Medieval time, *Science*, 302, 404–405, 2003.

Büntgen, U., Tegel, W., Nicolussi, K., McCormick, M., Frank, D., Trouet, V., Kaplan, J. O., Herzig, F., Heussner, K. U., Wanner, H., Luterbacher, J., and Esper, J.: 2500 years of European climate variability and human susceptibility, *Science*, 331, 578–582, 2011.

Büntgen, U., Myglan, V. S., Charpentier Ljungqvist, F., McCormick, M., Di Cosmo, N., Sigl, M., Jungclaus, J., Wagner, S., Krusic, P. J., Esper, J., Kaplan, J. O., de Vaan, M. A. C., Luterbacher, J., Wacker, L., Tegel, W., and Kirdyanov, A. V.: Cooling and societal change during the Late Antique Little Ice Age from 536 to around 660 AD, *Nature Geoscience*, 9, 231–236, 2016.

Cape, J. N., Coyle, M., and Dumitrean, P.: The atmospheric lifetime of black carbon, *Atmospheric Environment*, 59, 256–263, 2012.

Chýlek, P., Johnson, B., and Wu, H.: Black carbon concentration in Greenland Dye-3 ice core, *Geophysical Research Letters*, 19(19), 1951–1953, 1992.

Chýlek, P., Johnson, B., Damiano, P. A., Taylor, K. C., and Clement, P.: Biomass burning record and black carbon in the GISP2 ice core, *Geophysical Research Letters*, 22(2), 89–92, 1995.

Conedera, M., Tinner, W., Neff, C., Meurer, M., Dickens, A. F., and Krebs, P.: Reconstructing past fire regimes: methods, applications, and relevance to fire management and conservation, *Quaternary Science Reviews*, 28(5), 555–576, 2009.

Cubasch, U., Wuebbles, D., Chen, D., Facchini, M. C., Frame, D., Mahowald, N. and Winther, J.-G.: Introduction, in Climate Change 2013: The Physical Science Basis, Contribution of Working Group I to the Fifth Assessment Report of the Intergovernmental Panel on Climate Change, edited by T. F. Stocker, D. Qin, G.-K. Plattner, M. Tignor, S. K. Allen, J. Boschung, A. Nauels, Y. Xia, V. Bex, and P. M. Midgley, Cambridge University Press, Cambridge, United Kingdom and New York, NY, USA., 2013.

Dibb, J. E., Talbot, R. W., Whitlow, S. I., Shipham, M. C., Winterle, J., McConnell, J., and Bales, R.: Biomass burning signatures in the atmosphere and snow at Summit, Greenland: An event on 5 August 1994, *Atmospheric Environment*, 30(4), 553–561, 1996.

Eichler, A., Schwikowski, M., and Gäggeler, H. W.: Meltwater-induced relocation of chemical species in Alpine firn, *Tellus B*, 53, 192–203, 2001.

Eichler, A., Tinner, W., Brütsch, S., Olivier, S., Papina, T., and Schwikowski, M.: An ice-core based history of Siberian forest fires since AD 1250, *Quaternary Science Reviews*, 30, 1027–1034, 2011.

Ferretti, D., Miller, J., White, J., Etheridge, D., Lassey, K., Lowe, D., Meure, C., Dreier, M., Trudinger, C., van Ommen, T., and Langenfelds, R.: Unexpected changes to the global methane budget over the past 2000 years, *Science*, 309, 1714–1717, 2005.

Fischer, H., Schüpbach, S., Gfeller, G., Bigler, M., Rothlisberger, R., Erhardt, T., Stocker, T. F., Mulvaney, R., and Wolff, E.: Millennial changes in North American wildfire and soil activity over the last glacial cycle, *Nature Geoscience*, 8, 723–728, 2015.

Flannigan, M.: Fire evolution split by continent, *Nature Geoscience*, 8, 167–168, 2015.

Fuhrer, K., Neftel, A., Anklin, M., Staffelbach, T., and Legrand, M.: High-resolution ammonium ice core record covering a complete glacial-interglacial cycle, *Journal of Geophysical Research: Atmospheres*, 101, 4147–4164, 1996.

Gambaro, A., Zangrando, R., Gabrielli, P., Barbante, C., and Cescon, P.: Direct determination of levoglucosan at the picogram per milliliter level in Antarctic ice by high-performance liquid chromatography/electrospray ionization triple quadrupole mass spectrometry, *Analytical Chemistry*, 80(5), 1649–1655, 2008.

Giglio, L., Randerson, J. T., and van der Werf, G. R.: Analysis of daily, monthly, and annual burned area using the fourth-generation global fire emissions database (GFED4), *Journal of Geophysical Research: Biogeosciences*, 118(1), 317–328, 2013.

Ginot, P., Kull, C., Schwikowski, M., Schotterer, U., and Gäggeler, H. W.: Effects of postdepositional processes on snow composition of a subtropical glacier (Cerro Tapado, Chilean Andes), *Journal of Geophysical Research*, 106(D23), 32375–32386, 2001.

Goldberg, E. D.: Black Carbon in the Environment, Wiley, New York, USA, 1985.

Grieman, M., Greaves, J., and Saltzman, E.: A method for analysis of vanillic acid in polar ice cores, *Climate of the Past*, 11, 227–232, 2015.

Grieman, M. M., Aydin, M., Fritzsche, D., McConnell, J. R., Opel, T., Sigl, M., and Saltzman, E. S.: Aromatic acids in a Eurasian Arctic ice core: a 2600-year proxy record of biomass burning, *Climate of the Past*, 13, 395–410, 2017.

Grieman, M. M., Aydin, M., Isaksson, E., Schwikowski, M., and Saltzman, E. S.: Aromatic acids in an Arctic ice core from Svalbard: a proxy record of biomass burning, *Climate of the Past*, 14, 637–651, 2018.

Grieman, M. M., Aydin, M., McConnell, J. R., and Saltman, E. S.: Burning-derived vanillic acid in an Arctic ice core from Tunu, Northeastern Greenland, *Climate of the Past Discussions*, 2018, in review.

Grove, J. M. and Switsur, R.: Glacial geological evidence for the medieval warm period, *Climatic Change*, 26, 143–169, 1994.

Gysel, M., Laborde, M., Olfert, J. S., Subramanian, R., and Gröhn, A. J.: Effective density of Aquadag and fullerene soot black carbon reference materials used for SP2 calibration, *Atmospheric Measurement Techniques*, 4, 2851–2858, 2011.

Häberli, W., Schotterer, U., Wagenbach, D., Häberlischwitter, H., and Bortenschlager, S.: Accumulation Characteristics on a Cold, High-Alpine Firn Saddle from a Snow-Pit Study on Colle-Gnifetti, Monte-Rosa, Swiss Alps, *Journal of Glaciology*, 29, 260–271, 1983.

Hansen, J. and Nazarenko, L.: Soot climate forcing via snow and ice albedos, *PNAS*, 101, 423–428, 2004.

Haug, G. H., Ganopolski, A., Sigman, D. M., Rosell-Mele, A., Swann, G. E. A., Tiedemann, R., Jaccard, S. L., Bollmann, J., Maslin, M. A., Leng, M. J., and Eglin-ton, G.: North Pacific seasonality and the glaciation of North America 2.7 million years ago, *Nature*, 433(7028), 821–825, 2005.

Hedges, J. I., Eglinton, G., Hatcher, P. G., Kirchman, D. L., Arnosti, C., Derenne, S., Evershed, R. P., Kögel-Knabner, I., de Leeuw, J. W., Littke, R., Michaelis, W., and Rullkötter, J.: The molecularly-uncharacterized component of nonliving organic matter in natural environments, *Organic Geochemistry*, 31, 945–958, 2000.

Hennigan, C. J., Sullivan, A. P., Collett, J. L., and Robinson, A. L.: Levoglucosan stability in biomass burning particles exposed to hydroxyl radicals, *Geophysical Research Letters*, 37, L09806, 2010.

Herren, P.-A.: Ice core based climate reconstruction from the Mongolian Altai, PhD thesis, University of Bern, 2013.

Herren, P.-A., Eichler, A., Machguth, H., Papina, T., Tobler, L., Zapf, A., and Schwikowski, M.: The onset of Neoglaciation 6000 years ago in western Mongolia revealed by an ice core from the Tsambagarav mountain range, Quaternary Science Reviews, 69, 59–69, 2013.

Hicks, S. and Isaksson, E.: Assessing source areas of pollutants from studies of fly ash, charcoal and pollen from Svalbard snow and ice, *Journal of Geophysical Research*, 111, D02113, 2006.

Hoffmann, D., Tilgner, A., Iinuma, Y., and Herrmann, H.: Atmospheric stability of levoglucosan: a detailed laboratory and modeling study, *Environmental Science and Technology*, 44, 694–699, 2010.

IPCC: Climate Change 2013: The Physical Science Basis. Contribution of Working Group I to the Fifth Assessment Report of the Intergovernmental Panel on Climate Change [Stocker, T.F., D. Qin, G.-K. Plattner, M. Tignor, S.K. Allen, J. Boschung, A. Nauels, Y. Xia, V. Bex and P.M. Midgley (eds.)], Cambridge University Press, Cambridge, United Kingdom and New York, NY, USA, 1535 pp, 2013.

Ito, A. and Penner, J. E..: Global estimates of biomass burning emissions based on satellite imagery for the year 2000, *Journal of Geophysical Research*, 109, D14S05, 2004.

Jenk, T. M., Szidat, S., Schwikowski, M., Gäggeler, H. W., Brütsch, S., Wacker, L., Synal, H. A., and Saurer, M.: Radiocarbon analysis in an Alpine ice core: record of anthropogenic and biogenic contributions to carbonaceous aerosols in the past (1650-1940), *Atmospheric Chemistry and Physics*, 6, 5381–5390, 2006.

Jenk, T.M., Szidat, S., Schwikowski, M., Gäggeler, H. W., Wacker, L., Synal, H.-A., and Saurer, M.: Microgram level radiocarbon (14C) determination on carbonaceous particles in ice, *Nuclear Instruments and Methods in Physics Research B*, 259(1), 518–525, 2007.

Jenkins, M., Kaspari, S., Kang, S.-C., Grigholm, B., and Mayewski, P. A.: Tibetan Plateau Geladaindong black carbon ice core record (1843–1982): Recent increases due to higher emissions and lower snow accumulation, *Advances in Climate Change Research*, 7, 132–138, 2016.

Johnsen, S. J., Clausen, H. B., Dansgaard, W., Gundestrup, N. S., Hammer, C. U., Andersen, U., Andersen, K. K., Hvidberg, C. S., Dahl-Jensen, D., Steffensen, J. P., Shoji, H., Sveinbjörnsdóttir, Á. E., White, J., Jouzel, J., and Fisher, D.: The δ^{18}O record along the Greenland Ice Core Project deep ice core and the problem of possible Eemian climatic instability, *Journal of Geophysical Research*, 102 (C12), 26397–26410, 1997.

Jouvet, G., Huss, M., Blatter, H., Picasso, M., and Rappaz, J.: Numerical simulation of Rhônegletscher from 1874 to 2100, *Journal of Computational Physics*, 228, 6426–6439, 2009.

Jouzel, J.: A brief history of ice core science over the last 50 yr, *Climate of the Past*, 9, 2525–2547, 2013.

Kaspari, S. D., Schwikowski, M., Gysel, M., Flanner, M. G., Kang, S., Hou, S., and Mayewski, P. A.: Recent Increase in Black Carbon Concentrations from a Mt. Everest Ice Core Spanning 1860−2000 AD, *Geophysical Research Letters*, 38, 2011.

Kawamura, K., Izawa, Y., Mochida, M., and Shiraiwa, T.: Ice core records of biomass burning tracers (levoglucosan and dehydroabietic, vanillic and p-hydroxybenzoic acids) and total organic carbon for past 300 years in the Kamchatka Peninsula, Northeast Asia, *Geochimica et Cosmochimica Acta*, 99, 317–329, 2012.

Keegan, K. M., Albert, M. R., McConnell, J. R., and Baker, I.: Climate change and forest fires synergistically drive widespread melt events of the Greenland Ice Sheet, *PNAS*, 111, 7964–7967, 2014.

Kellerhals, T., Brütsch, S., Sigl, M., Knüsel, S., Gäggeler, H. W., and Schwikowski, M.: Ammonium concentration in ice cores: A new proxy for regional temperature reconstruction?, *Journal of Geophysical Research*, 115, D16123, 2010.

Kehrwald, N., Zangrando, R., Gabrielli, P., Jaffrezo, J.-L., Boutron, C., Barbante, C., and Gambaro, A.: Levoglucosan as a specific marker of fire events in Greenland snow, *Tellus B*, 64, 18169, 2012.

Kehrwald, N. M., Whitlock, C., Barbante, C., Brovkin, V., Daniau, A.-L., Kaplan, J. O., Marlon, J. R., Power, M. J., Thonicke, K., and van der Werf, G. R.: Fire research: linking past, present, and future data, *Eos*, 94(46), 421–423, 2013a.

Kehrwald, N., Zennaro, P., and Barbante, C.: Increasing fire activity in a warming climate? Ice core record insights from the present and the last interglacials, *PAGES news*, 21, 1, 16–17, 2013b.

Keywood, M., Kanakidou, M., Stohl, A., Dentener, F., Grassi, G., Meyer, C. P., Torseth, K., Edwards, D., Thompson, A. M., Lohmann, U., and Burrows, J.: Fire in the air: Biomass burning impacts in a changing climate, *Critical Reviews in Environmental Science and Technology*, 43(1), 40–83, 2011.

Kloster, S., Mahowald, N. M., Randerson, J. T., Thornton, P. E., Hoffman, F. M., Levis, S., Lawrence, P. J., Feddema, J. J., Oleson, K. W., and Lawrence, D. M.: Fire dynamics during the 20th century simulated by the Community Land Model, *Biogeosciences*, 7, 1877–1902, 2010.

Lamb, H. H.: The early medieval warm epoch and its sequel, *Palaeogeography, Palaeoclimatology, Palaeoecology*, 1, 13–37, 1965.

Lavanchy, V. M. H., Gäggeler, H. W., Schotterer, U., Schwikowski, M., and Baltensperger, U.: Historical record of carbonaceous particle concentrations from a European high-alpine glacier (Colle Gnifetti, Switzerland), *Journal of Geophysical Research: Atmospheres*, 104(D17), 21227–21236, 1999.

Legrand, M. and De Angelis, M.: Light carboxylic acids in Greenland ice: A record of past forest fires and vegetation emissions from the boreal zone, *Journal of Geophysical Research*, 101(D2), 4129–4145, 1996.

Legrand, M., De Angelis, M., Staffelbach, T., Neftel, A., and Stauffer, B.: Large perturbation of ammonium and organic-acids content in the Summit-Greenland ice core: Fingerprint from forest fires, *Geophysical Research Letters*, 19, 473–475, 1992.

Legrand, M., Preunkert, S., Schock, M., Cerqueira, M., Kasper-Giebl, A., Afonso, J., Pio, C., Gelencsér, A., and Dombrowski-Etchevers, I.: Major 20th century changes of carbonaceous aerosol components (EC, WinOC, DOC, HULIS, carboxylic acids, and cellulose) derived from Alpine ice cores, *Journal of Geophysical Research*, 112, D23S11, 2007.

Legrand, M., McConnell, J., Fischer, H., Wolff, E. W., Preunkert, S., Arienzo, M., Chellman, N., Leuenberger, D., Maselli, O., Place, P., Sigl, M., Schüpbach, S., and Flannigan, M.: Boreal fire records in Northern Hemisphere ice cores: a review, *Climate of the Past*, 12, 2033–2059, 2016.

Lim, S., Faïn, X., Ginot, P., Mikhalenko, V., Kutuzov, S., Paris, J.-D., Kozachek, A., and Laj, P.: Black carbon variability since preindustrial times in the eastern part of Europe reconstructed from Mt. Elbrus, Caucasus, ice cores, *Atmospheric Chemistry and Physics*, 17, 3489–3505, 2017.

Lüthi, D., Le Floch, M., Bereiter, B., Blunier, T., Barnola, J.-M., Siegenthaler, U., Raynaud, D., Jouzel, J., Fischer, H., Kawamura, K., and Stocker, T. F.: High-resolution carbon dioxide concentration record 650,000–800,000 years before present, *Nature*, 453, 379–382, 2008.

Lüthi, M. P.: Little Ice Age climate reconstruction from ensemble reanalysis of Alpine glacier fluctuations, *The Cryosphere*, 8, 639–650, 2014.

Mann, M. E., Zhang, Z., Rutherford, S., Bradley, R. S., Hughes, M. K., Shindell, D., Ammann, C., Faluvegi, G. and Ni, F.: Global signatures and dynamical origins of the Little Ice Age and Medieval Climate Anomaly, *Science*, 326(5957), 1256–1260, 2009.

Marlon, J., Bartlein, P., Carcaillet, C., Gavin, D. G., Harrison, S. P., Higuera, P. E., Joos, F., Power, M. J., and Prentice, C. I.: Climate and human influences on global biomass burning over the past two millennia, *Nature Geoscience*, 1, 697–701, 2008.

Marlon, J., Bartlein, P., Walsh, M. K., Harrison, S. P., Brown, K. J., Edwards, M. E., Higuera, P. E., Power, M. J., Anderson, R. S., Briles, C. E., Brunelle, A., Carcaillet, C., Daniels, M., Hu, F. S., Lavoie, M., Long, C. J., Minckley, T., Richard, P. J. H., Scott, A. C., Shafer, D. S., Tinner, W., Umbanhowar Jr, C. E., and Whitlock, C.:Wildfire responses to abrupt climate change in North America, *PNAS*, 106, 2519–2524, 2009.

Marlon, J. R., Bartlein, P. J., Gavin, D. G., Long, C. J., Anderson, R. S., Briles, C. E., Brown, K. J., Colombaroli, D., Hallett, D. J., Power, M. J., Scharf, E. A., and Walsh, M. K.: Long-term perspective on wildfires in the western USA, *PNAS*, 109(9), 3203–3204, 2012.

Marlon, J. R., Bartlein, P. J., Daniau, A.-L., Harrison, S. P., Maezumi, S. Y., Power, M. J., Tinner, W., and Vanniere, B.: Global biomass burning: a synthesis and review of Holocene paleofire records and their controls, *Quaternary Science Reviews*, 65, 5–25, 2013.

Marlon, J. R., Kelly, R., Daniau, A.-L., Vannière, B., Power, M. J., Bartlein, P., Higuera, P., Blarquez, O., Brewer, S., Brücher, T., Feurdean, A., Romera, G. G., Iglesias, V., Maezumi, S. Y., Magi, B., Courtney Mustaphi, C. J., and Zhihai, T.: Reconstructions of biomass burning from sediment–charcoal records to improve data–model comparisons, *Biogeosciences*, 13, 3225–3244, 2016.

Masson-Delmotte, V., Schulz, M., Abe-Ouchi, A., Beer, J., Ganopolski, A., Gonzalez Rouco, J. F., Jansen, E., Lambeck, K., Luterbacher, J., Naish, T., Osborn, T., Otto-Bliesner, B., Quinn, T., Ramesh, R., Rojas, M., Shao, X. and Timmermann, A.: Information from Paleoclimate Archives, edited by T. F. Stocker, D. Qin, G.-K., Plattner, M. Tignor, S. K. Allen, J. Boschung, A. Nauels, Y. Xia, V. Bex, and P. M. Midgley, Cambridge University Press, Cambridge, United Kingdom and New York, NY, USA., 2013.

McConnell, J. R., Edwards, R., Kok, G. L., Flanner, M. G., Zender, C. S., Saltzman, E. S., Banta, J. R., Pasteris, D. R., Carter, M. M., and Kahl, J. D. W.: 20th-century industrial black carbon emissions altered arctic climate forcing, *Science*, 317, 1381–1384, 2007.

McCormick, M., Büntgen, U., Cane, M. A., Cook, E. R., Harper, K., Huybers, P., Litt, T., Manning, S. W., Mayewski, P. A., More, A. F. M., Nicolussi, K., and Tegel, W.: Climate change during and after the Roman Empire: Reconstructing the past from scientific and historical evidence, *Journal of Interdisciplinary History*, 43, 169–220, 2012.

Meeker, L. D., Mayewski, P. A., Twickler, M. S., Whitlow, S. I., and Meese, D.: A 110,000-year history of change in continental biogenic emissions and related atmospheric circulation inferred from the Greenland Ice Sheet Project Ice Core, *Journal of Geophysical Research: Oceans*, 102(C12), 26489–26504, 1997.

Mischler, J. A., Sowers, T. A., Alley, R. B., Battle, M., Mc- Connell, J. R., Mitchell, L., Popp, T., Sofen, E., and Spencer, M. K.: Carbon and hydrogen isotopic composition of methane over the last 1000 years, *Global Biogeochemical Cycles*, 23, GB4024, 2009.

Mouillot, F. and Field, C.: Fire history and the global carbon budget: a $1° \times 1°$ fire history reconstruction for the 20th century, *Global Change Biology*, 11, 398–420, 2005.

Müller-Tautges, C., Eichler, A., Schwikowski, M., Pezzatti, G. B., Conedera, M., and Hoffmann, T.: Historic records of organic compounds from a high Alpine glacier: influences of biomass burning, anthropogenic emissions, and dust transport, *Atmospheric Chemistry and Physics*, 16, 1029–1043, 2016.

Oerlemans, J.: Extracting a climate signal from 169 glacier records, *Science*, 308, 675–677, 2005.

Okamoto, S., Fujita, K., Narita, H., Uetake, J., Takeuchi, N., Miyake, T., Nakazawa, F., Aizen, V. B., Nikitin, S. A., and Nakawo, M.: Reevaluation of the reconstruction of summer temperatures from melt features in Belukha ice cores, Siberian Altai, *Journal of Geophysical Research*, 116(D2), D02110, 2011.

Osmont, D., Wendl, I. A., Schmidely, L., Sigl, M., Vega, C. P., Isaksson, E., and Schwikowski, M.: An 800-year high-resolution black carbon ice core record from Lomonosovfonna, Svalbard, *Atmospheric Chemistry and Physics*, 18, 12777–12795, 2018.

Owens, M. J., Lockwood, M., Hawkins, E., Usoskin, I., Jones, G. S., Barnard, L., Schurer, A., and Fasullo, J.: The Maunder minimum and the Little Ice Age: an update from recent reconstructions and climate simulations, *Journal of Space Weather and Space Climate*, 7, A33, 2017.

Page, S. E., Siegert, F., Rieley, J. O., Boehm, H.-D. V., Jaya, A., and Limin, S.: The amount of carbon released from peat and forest fires in Indonesia during 1997, *Nature*, 420, 61–65, 2002.

Parrenin, F., Cavitte, M. G. P., Blankenship, D. D., Chapellaz, J., Fischer, H., Gagliardini, O., Masson-Delmotte, V., Passalacqua, O., Ritz, C., Roberts, J., Siegert, M. J., and Young, D. A.: Is there 1.5-million-year-old ice near Dome C, Antarctica?, *The Cryosphere*, 11, 2427–2437, 2017.

Petit, J. R, Jouzel, J., Raynaud, D., Barkov, N. I., Barnola, J.-M., Basile, I., Bender, M., Chapellaz, J., Davis, M., Delaygue, G., Delmotte, M., Kotlyakov, V. M., Legrand, M., Lipenkov, V. Y., Lorius, C., Pépin, L., Ritz, C., Saltzman, E., and Stievenard, M.: Climate and atmospheric history of the past 420,000 years from the Vostok ice core, Antarctica, *Nature*, 399, 429–436, 1999.

Petzold, A., Ogren, J. A., Fiebig, M., Laj, P., Li, S. M., Baltensperger, U., Holzer-Popp, T., Kinne, S., Pappalardo, G., Sugimoto, N., Wehrli, C., Wiedensohler, A., and Zhang, X. Y.: Recommendations for reporting "black carbon" measurements, *Atmospheric Chemistry and Physics*, 13, 8365–8379, 2013.

Power, M. J., Marlon, J., Ortiz, N., Bartlein, P. J., Harrison, S. P., Mayle, F. E., Ballouche, A., Bradshaw, R. H. W., Carcaillet, C., Cordova, C., Mooney, S., Moreno, P. I., Prentice, I. C., Thonicke, K., Tinner, W., Whitlock, C., Zhang, Y., Zhao, Y., Ali, A. A., Anderson, R. S., Beer, R., Behling, H., Briles, C., Brown, K. J., Brunelle, A., Bush, M., Camill, P., Chu, G. Q., Clark, J., Colombaroli, D., Connor, S., Daniau, A.-L., Daniels, M., Dodson, J., Doughty, E., Edwards, M. E., Finsinger, W., Foster, D., Frechette, J., Gaillard, M.-J., Gavin, D. G., Gobet, E., Haberle, S., Hallett, D. J., Higuera, P., Hope, G., Horn, S., Inoue, J., Kaltenrieder, P., Kennedy, L., Kong, Z. C., Larsen, C., Long, C. J., Lynch, J., Lynch, E. A., McGlone, M., Meeks, S., Mensing, S., Meyer, G., Minckley, T., Mohr, J., Nelson, D. M., New, J., Newnham, R., Noti, R., Oswald, W., Pierce, J., Richard, P. J. H., Rowe, C., Goñi, M. F. S., Shuman, B. N., Takahara, H., Toney, J., Turney, C., Urrego-Sanchez, D. H., Umbanhowar, C., Vandergoes, M., Vanniere, B., Vescovi, E., Walsh, M., Wang, X., Williams, N., Wilmshurst, J., and Zhang, J. H.: Changes in fire regimes since the Last Glacial Maximum: An assessment based on a global synthesis and analysis of charcoal data, *Climate Dynamics*, 30, 887–907, 2008.

Ramanathan, V. and Carmichael, G.: Global and regional climate changes due to black carbon, *Nature Geoscience*, 1, 221–227, 2008.

Raymo, M. E.: The initiation of Northern-Hemisphere glaciation, *Annual Review of Earth and Planetary Sciences*, 22, 353–383, 1994.

Rubino, M., D'Onofrio, A., Seki, O., and Bendle, J. A.: Ice-core records of biomass burning, *The Anthropocene Review*, 3, 140–162, 2016.

Ruppel, M. M., Isaksson, E., Ström, J., Beaudon, E., Svensson, J., Pedersen, C. A., and Korhola, A.: Increase in elemental carbon values between 1970 and 2004 observed in a 300-year ice core from Holtedahlfonna (Svalbard), *Atmospheric Chemistry and Physics*, 14, 11447–11460, 2014.

Savarino, J. and Legrand, M.: High northern latitude forest fires and vegetation emissions over the last millennium inferred from the chemistry of a central Greenland ice core, *Journal of Geophysical Research: Atmospheres*, 103(D7), 8267–8279, 1998.

Schilt, A., Baumgartner, M., Blunier, T., Schwander, J., Spahni, R., Fischer, H., and Stocker, T. F.: Glacial–interglacial and millennial-scale variations in the atmospheric nitrous oxide concentration during the last 800,000 years, *Quaternary Science Reviews*, 29(1–2), 182–192, 2010.

Schwikowski, M., Baltensperger, U., Gäggeler, H. W., and Poulida, O.: Scavenging of atmospheric constituents in mixed phase clouds at the high-alpine site Jungfraujoch part III: Quantification of the removal of chemical species by precipitating snow, *Atmospheric Environment*, 32(23), 4001–4010, 1998.

Schwikowski, M., Brütsch, S., Gäggeler, H. W., and Schotterer, U.: A high-resolution air chemistry record from an Alpine ice core: Fiescherhorn glacier, Swiss Alps, *Journal of Geophysical Research*, 104 (D11), 13709–13719, 1999.

Siegenthaler, U., Stocker, T. F., Monnin, E., Lüthi, D., Schwander, J., Stauffer, B., Raynaud, D., Barnola, J. M., Fischer, H., Masson-Delmotte, V., and Jouzel, J.: Stable carbon cycle-climate relationship during the late Pleistocene, *Science*, 310(5752), 1313–1317, 205.

Sigl, M., McConnell, J. R., Layman, L., Maselli, O., McGwire, K., Pasteris, D., Dahl-Jensen, D., Steffensen, J. P., Vinther, B., Edwards, R., Mulvaney, R., and Kipfstuhl, S.: A new bipolar ice core record of volcanism from WAIS Divide and NEEM and implications for climate forcing of the last 2000 years, *Journal of Geophysical Research: Atmospheres*, 118, 1151–1169, 2013.

Simoneit, B. R. T.: Biomass burning – a review of organic tracers for smoke from incomplete combustion, *Applied Geochemistry*, 17, 129–162, 2002.

Spahni, R., Chappellaz, J., Stocker, T. F., Loulergue, L., Hausammann, G., Kawamura, K., Fluckiger, J., Schwander, J., Raynaud, D., Masson-Delmotte, V., and Jouzel, J.: Atmospheric methane and nitrous oxide of the late Pleistocene from Antarctic ice cores, *Science*, 310(5752), 1317–1321, 2005.

Szidat, S., Jenk, T. M., Gäggeler, H. W., Synal, H.-A., Hajdas, I., Bonani, G., and Saurer, M.: THEODORE, a two-step heating system for the EC/OC determination of radiocarbon (14C) in the environment, *Nuclear Instruments and Methods in Physics Research B*, 223–224, 829–836, 2004.

Tinner, W. and Hu, F.S.: Size parameters, size-class distribution and area-number relationship of microscopic charcoal: relevance for fire reconstruction, *The Holocene*, 13(4), 499–505, 2003.

Thompson, L. G., Mosley-Thompson, E., Dansgaard, W., and Grootes, P. M.: The Little Ice Age as recorded in the stratigraphy of the Tropical Quelccaya ice cap, *Science*, 234 (4774), 361–364, 1986.

van der Werf, G. R., Randerson, J. T., Giglio, L., Collatz, G. J., Kasibhatla, P. S., and Arellano Jr, A. F.: Interannual variability in global biomass burning emissions from 1997 to 2004, *Atmospheric Chemistry and Physics*, 6(11), 3423–3441, 2006.

van der Werf, G. R., Randerson, J. T., Giglio, L., Collatz, G. J., Mu, M., Kasibhatla, P. S., Morton, D. C., DeFries, R. S., Jin, Y., and van Leeuwen, T. T.: Global fire emissions and the contribution of deforestation,

savanna, forest, agricultural, and peat fires (1997–2009), *Atmospheric Chemistry and Physics*, 10, 11707–11735, 2010.

van der Werf, G. R., Peters, W., van Leeuwen, T. T., and Giglio, L.: What could have caused preindustrial biomass burning emissions to exceed current rates?, *Climate of the Past*, 9(1), 289–306, 2013.

Vaughan, D.G., Comiso, J. C., Allison, I., Carrasco, J., Kaser, G., Kwok, R., Mote, P., Murray, T., Paul, F., Ren, J., Rignot, E., Solomina, O., Steffen, K., and Zhang, T.: Observations: Cryosphere. In: Climate Change 2013: The Physical Science Basis. Contribution of Working Group I to the Fifth Assessment Report of the Intergovernmental Panel on Climate Change [Stocker, T.F., D. Qin, G.-K. Plattner, M. Tignor, S.K. Allen, J. Boschung, A. Nauels, Y. Xia, V. Bex and P.M. Midgley (eds.)]. Cambridge University Press, Cambridge, United Kingdom and New York, NY, USA, 2013.

Wang, M., Xu, B., Kaspari, S. D., Gleixner, G., Schwab, V. F., Zhao, H., Wang, H., and Yao, P.: Century-long record of black carbon in an ice core from the Eastern Pamirs: Estimated contributions from biomass burning, *Atmospheric Environment*, 115, 79–88, 2015.

Wang, Z., Chappellaz, J., Park, K., and Mak, J. E.: Large variations in Southern Hemisphere biomass burning during the last 650 years, *Science*, 330, 1663–1666, 2010.

Whitlow, S., Mayewski, P., Dibb, J., Holdsworth, G., and Twickler, M.: An ice-core-based record of biomass burning in the Arctic and sub-Arctic, 1750-1980, *Tellus B*, 46(3), 234–242, 1994.

Winski, D., Osterberg, E., Kreutz, K., Wake, C., Ferris, D., Campbell, S., Baum, M., Bailey, A., Birkel, S., Introne, D., and Handley, M.: A 400-year ice core melt layer record of summertime warming in the Alaska Range, *Journal of Geophysical Research: Atmospheres*, 123, 3594–3611, 2018.

Wolff, E. W., Hall, J. S., Mulvaney, R., Pasteur, E. C., Wagenbach, D., and Legrand, M.: Relationship between chemistry of air, fresh snow and firn cores for aerosol species in coastal Antarctica, *Journal of Geophysical Research*, 103(D9), 11057–11070, 1998.

Yalcin, K., Wake, C. R., Kreutz, K. J., and Whitlow, S. I.: A 1000-yr record of forest fire activity from Eclipse Icefield, Yukon, Canada, *The Holocene*, 16(2), 200–209, 2006.

Yamazaki, Y. H., Allen, M. R., Huntingford, C., Frame, D. J., and Frank, D. C.: Refining future climate projections using uncertain climate data of the last millennium, paper presented at EGU General Assembly 2009, Vienna, 2009.

Zdanowicz, C. M., Proemse, B. C., Edwards, R., Feiteng, W., Hogan, C. M., and Kinnard, C.: Historical black carbon deposition in the Canadian High Arctic: A 190-year long ice-core record from Devon Island, *Atmospheric Chemistry and Physics Discussions*, 2017, in review.

Zennaro, P., Kehrwald, N., McConnell, J. R., Schüpbach, S., Maselli, O. J., Marlon, J., Vallelonga,P., Leuenberger, D., Zangrando, R., Spolaor, A., Borrotti, M., Barbaro, E., Gambaro, A., and Barbante, C.: Fire in ice: two millennia of boreal forest fire history from the Greenland NEEM ice core, *Climate of the Past*, 10, 1905–1924, 2014.

Zumbühl, H. J., Steiner, D., and Nussbaumer, S. U.: 19th century glacier representations and fluctuations in the central and western European Alps: An interdisciplinary approach, *Global Planetary Change*, 60, 42–57, 2008.

2 Ice cores investigated in this thesis

This chapter aims at presenting the four ice cores of the project in greater detail. For each ice core, we will start with a general description of the regional environment and climate. We will then focus on the drill site and the drilling, and explain how the dating was performed. We will conclude by mentioning the previous studies carried out on the ice core.

2.1 Lomonosovfonna, Svalbard

2.1.1 Regional settings

Svalbard is an archipelago located around 700 km north of Norway and administrated by this country **(Fig. 2.1)**. It lies in the Arctic Ocean from 74 to 81 °N and from 10 to 35 °E, at the southern edge of the permanent sea ice zone. Its area is of approximately 61200 km^2. It is composed of four main islands, the largest one being Spitsbergen (38000 km^2). Glaciers cover around 60 % of the area of the archipelago *(Hisdal, 1998)*. The landscape is characterized by fjords surrounded by steep mountain slopes covered with ice caps. Large valleys enable glaciers to flow down to the sea level. The highest peak, Newtontoppen, reaches 1717 m a.s.l.
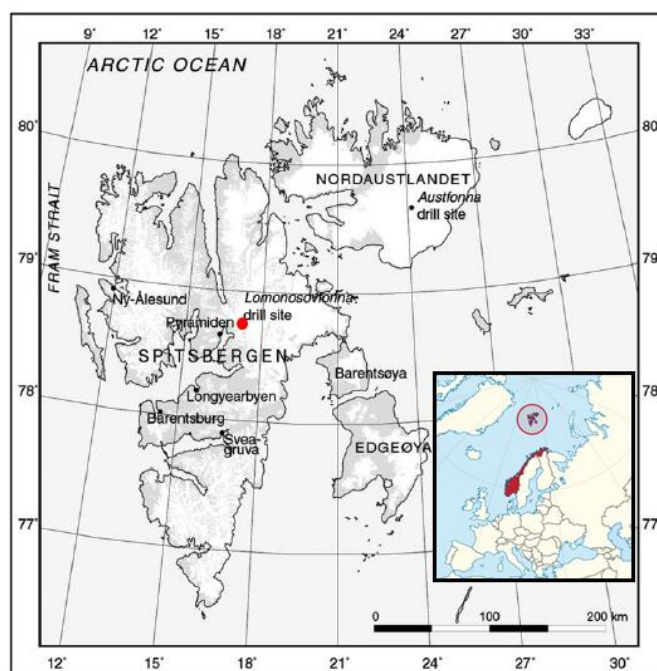
Fig. 2.1: Map of Svalbard with the overall situation (insert) and the location of the Lomonosovfonna drill site (red dot). Glaciated areas are shown in white. Adapted from *Isaksson et al. (2003)*.

Svalbard's climate **(Fig. 2.2)** is relatively mild with regard to its high latitude, especially in winter (average winter T at the sea level between −10 and −15 °C). This is due to the fact that the warm North Atlantic Water current, an extension of the Gulf Stream, extends up to Svalbard's south coast where it splits in two branches *(Hisdal, 1998; Isaksson et al., 2003, 2005)*. The climate in Svalbard is highly variable as the result of the influence of two different weather regimes. The high pressure area over Greenland and the Arctic Ocean brings stable cold and dry air masses from the northeast while the low pressure area over Iceland carries mid-latitude mild and humid air masses from the southwest *(Hisdal, 1998; Isaksson et al., 2003, 2005)*. This results in a temperature-moisture gradient from the

southwestern to the northeastern parts of the archipelago where the climate is more continental, with average temperatures around 5 °C lower *(Hisdal, 1998)*. The annual amount of precipitation also varies according to the location, with less than 500 mm on the west coasts and more than 1000 mm on the east coasts *(Hisdal, 1998)*. The driest season is generally spring and early summer *(Hisdal, 1998)*.
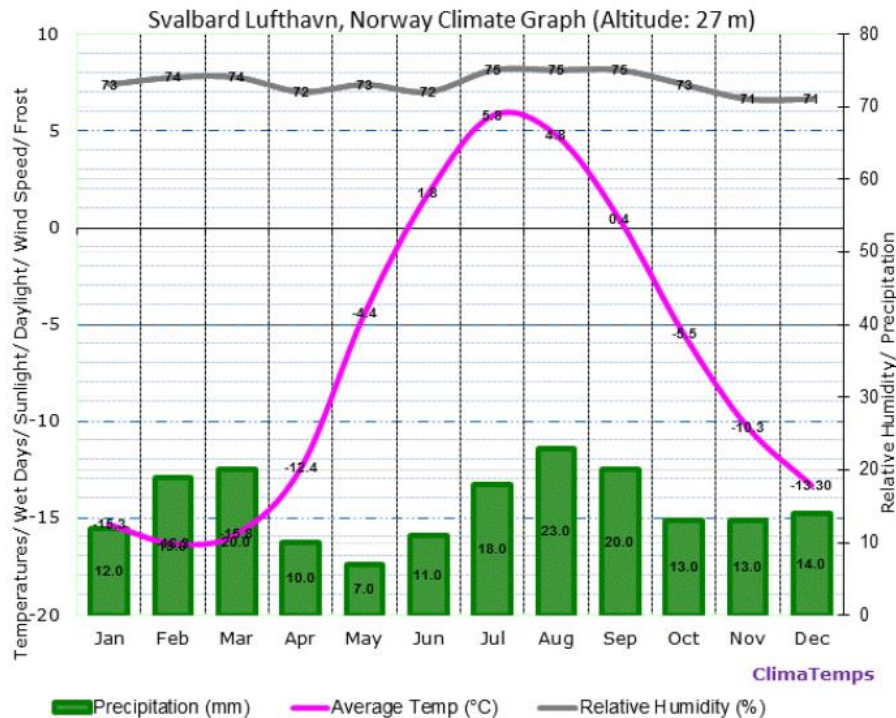
Fig 2.2: Climatic conditions at Svalbard airport, Longyearbyen (from *www.svalbard-aero.climatemps.com*).

2.1.2 Ice-core drilling

Due to its large glacier coverage and its interesting location within the Arctic, many ice-core studies have been carried out in Svalbard since the 1970s by Soviet and Japanese expeditions. Most of these ice cores were not extensively dated nor studied as only stratigraphy and some ions were analyzed (for a complete list of references, see *Wendl, 2014*). The influence of meltwater percolation was also investigated *(Koerner, 1997)* as this is a major concern for Svalbard ice cores due to positive summer temperatures. The first extensive studies were performed on the Lomonosovfonna 1997 (e.g. *Isaksson et al., 2001*) and Austfonna 1998 (e.g. *Watanabe et al., 2001*) ice cores.

Lomonosovfonna **(Fig. 2.1)** is one of the highest ice fields in Svalbard, reaching an elevation of 1250 m a.s.l. For this reason, it has been shown to be less influenced by melting than other drill sites such as Austfonna or Holtedahlfonna *(Beaudon et al., 2013; Pohjola et al., 2002)*, making it more appropriate for ice core drilling. The ice core used in the *PaleoFire* project is the Lomonosovfonna 2009 ice core (LF-09), drilled in March 2009 by a Norwegian-Swiss team on the eponymous ice field at 1202 m a.s.l. (78°49´24.4´´ N, 17°25´59.2´´ E). Using the Fast Electromechanical Lightweight Ice Coring System (FELICS, *Ginot et al., 2002a*), they could drill down to a depth of 149.5 m where the drill got stuck, and did not reach bedrock, whose depth is estimated to be around 200 m by radar surveys *(Petterson, unpublished data)*. The drill site is located 4.6 km south of the Lomonosovfonna 1997 drill site, which could not be revisited due to the opening of a large crevasse. Ice-core temperatures remained slightly negative, from −1.8 °C at 12 m to −2.2 °C at 42 m depth *(Wendl, 2014)*. The ice core was then shipped to the Paul Scherrer Institut (PSI), Switzerland, in a frozen state.

In addition to the deep LF-09 core, a shallow firn core (7.6 m long) was extracted in April 2011 (LF-11 core) around 110 m north and 20 m west of the LF-09 drill site by a team of scientists from the Norwegian Polar Institute (NPI) and the Uppsala University, Sweden, and brought to the NPI *(Vega et al., 2015)*.

2.1.3 Ice-core dating

The LF-09 dating **(Fig. 2.3)** is described in detail in *Wendl (2014)* and *Wendl et al. (2015)*. Briefly, the dating was performed by a combination of several methods to increase its accuracy. This includes:

- Annual layer counting (ALC) of Na^+ and $\delta^{18}O$ variations back to 1750 AD.
- Absolute dating based on ^{210}Pb decay by α-spectroscopy for the last century.
- Absolute dating with time markers: the 1963 tritium peak due to nuclear weapon testing and sulfate peaks produced by volcanic eruptions (Agung 1963/1964, Bezymianny 1956, Katmai 1912, Tambora 1815, Laki 1783, Hekla 1766, Kuwae 1458/1459 and Samalas 1257/1258).
- A two-parameter glacier flow model *(Thompson et al., 1998)* adjusted to fit the different reference horizons.
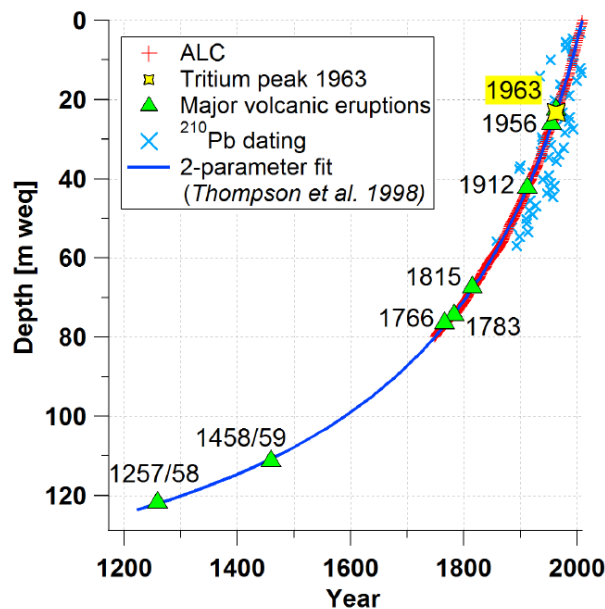
Fig 2.3: Depth-age relationship of the LF-09 ice core with the different methods applied *(Wendl et al., 2015)*.

Dating uncertainty was estimated to be:

- ±1 year in the vicinity of reference horizons.
- ±3 years between reference horizons down to 68 m water equivalent (weq, corrected for ice density) depth.
- ±3 years between 68 and 80 m weq depth (end of the annual layer counting).
- ±10 years below 80 m weq depth.

The accumulation rate in the LF-09 ice core was estimated to be 0.58 ± 0.13 m weq yr^{-1} *(Wendl et al., 2015)*.

The LF-11 core was dated by counting $\delta^{18}O$ variations and by assigning the minimum to the 1st of January of each year. The obtained timescale was adjusted by matching prominent ion peaks between

the LF-11 and LF-09 ice cores, leading to an accumulation rate of 0.49 m weq yr^{-1}. Further details are available in *Vega et al. (2015, 2016)*.

2.1.4 Previous studies

So far, two publications present results from the LF-09 ice core. Besides the dating methods, *Wendl et al. (2015)* discussed the nitrate, ammonium and methanesulfonate (MSA: $CH_3SO_3^-$) records and linked them to ocean productivity and biogenic emissions. The melt percent, based on the amount of ice lenses per year, and the sodium records are also displayed. *Grieman et al. (2018)* presented the VA and *p*-HBA records from the LF-09 ice core and connected them with northern Eurasian wildfires and changes in the North Atlantic Oscillation. In total, the available dataset for the LF-09 ice core encompasses the water stable isotope records (δ^{18}O and δD), the melt percent and 13 ionic records (Na^+, Mg^{2+}, Ca^{2+}, K^+, NH_4^+, Cl^-, SO_4^{2-}, NO_3^-, MSA, $HCOO^-$, CH_3COO^-, $C_2O_4^{2-}$ and F^-), for a total of 3997 samples cut at 3–4 cm resolution, and the VA and *p*-HBA records, obtained by merging 4 consecutive ionic samples into one sample, which produced a total of 997 samples.

Results from the LF-11 shallow core are included in two publications. *Vega et al. (2015)* discussed nitrate stable isotopes and major ions in snow and ice samples from four Svalbard sites, showing east-west zonal gradients suggesting the influence of different air masses. *Vega et al. (2016)* focused on ion relocation due to seasonal melting, revealing that nitrate was the most mobile within the snowpack. The available dataset for the LF-11 ice core comprises the δ^{18}O record and 10 ionic records (Na^+, Mg^{2+}, Ca^{2+}, K^+, NH_4^+, Cl^-, SO_4^{2-}, NO_3^-, Br^- and F^-), for a total of 155 samples cut a 4 cm resolution.

2.2 Illimani, Bolivian Andes

2.2.1 Regional settings

The Andes are the longest mountain range in the world (7000 km), and the highest one after the Himalayas. They stretch from north of Colombia to south of Chile and Argentina, and therefore encompass a wide range of climate and environments, from tropical to arid, temperate and cold (from north to south). The Bolivian Andes correspond to the fraction of the Andes located in Bolivia. Bolivia is composed of two distinct geographical regions **(Fig. 2.4)**: the Amazon Basin lowlands in the east of the country and the Altiplano, a high-elevation plateau (average altitude around 3500–4000 m a.s.l.) surrounded by two mountain ranges, the Western Cordillera (Sajama, 6542 m a.s.l.) which separates it from the Pacific Ocean, and the Eastern Cordillera (Illimani, 6462 m a.s.l.), which isolates it from the Amazon Basin. The (Bolivian) Andes host (20 %) 99 % of all tropical glaciers worldwide, respectively, which have retreated critically since the 1970s *(Rabatel et al., 2013)*.

The Bolivian Altiplano has a very specific climate due to the combination of tropical latitude with high altitude **(Fig. 2.5)**. It is characterized by a wet season during the slightly warmer austral summer (November to March) and a dry season during the austral winter (April-October). During the wet season, increased convection and moist air advection from the Amazon Basin and Gran Chaco region results in increased moisture influx from the East *(Garreaud et al., 2000; Vuille et al., 2000)*. As a consequence, 50 to 80 % of the annual precipitation occurs during the wet season *(Garreaud et al., 2003)*. During the dry season, the Intertropical Convergence Zone (ITCZ) is shifted northwards (over northern South America) generating stable and dry conditions over the Altiplano, sometimes

interrupted by snowfalls. Westerly winds prevail, restricting the Amazonian moisture influx to the eastern slopes of the Andes *(Vuille, 1999)*.
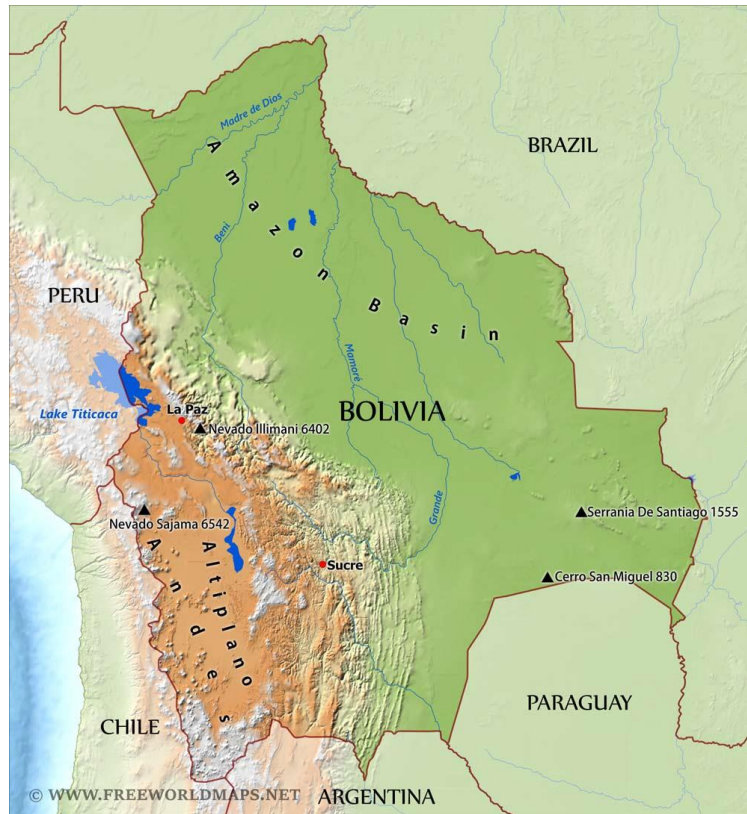
Fig. 2.4: Physical map of Bolivia including the location of Illimani (source: *www.freeworldmaps.net*).

The eastern origin of the moisture induces a dryness gradient over the Altiplano from east (annual precipitation > 700 mm) to west (annual precipitation between 200 and 400 mm) *(Garreaud et al., 2003)*. Internannual variability in precipitation is also controlled by El Niño-Southern Oscillation (ENSO). El Niño years are on average drier as moisture influx from the east is inhibited, while La Niña years are usually wetter *(Garreaud and Aceituno, 2001; Garreaud et al., 2003)*.
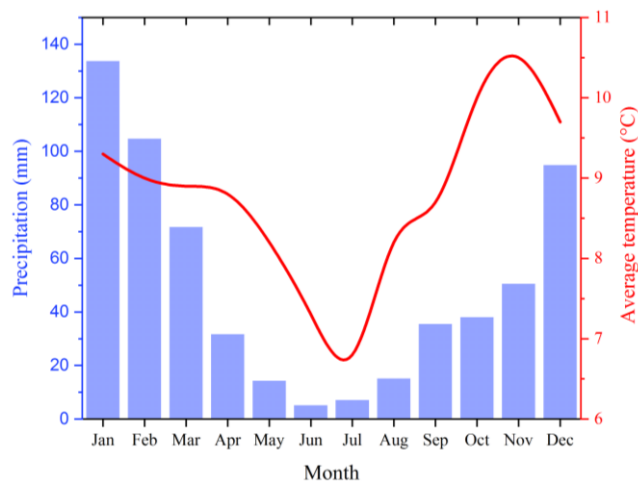
Fig. 2.5: Climate diagram for El Alto airport (near La Paz), 4058 m a.s.l. Data are averages over the time period 1961–1990, come from the Deutscher Wetterdienst (DWD), and are available at the following address: *https://www.dwd.de/DE/leistungen/klimadatenwelt/samerika/ah/bolivien/bolivien_node.html*

2.2.2 Ice-core drilling

In the Andes, first ice-core studies were conducted on Quelccaya ice cap, Peru, in 1983 *(Thompson et al., 1984, 1985, 1986)*. Other deep ice cores were drilled in 1993 on Huascarán, Peru *(Thompson et al., 1995)* and in 1997 on Sajama, Bolivia *(Thompson et al., 1998)*. These studies enabled to reconstruct past climate variations in South America back to the LGM and revealed that climate variations such as the LIA or MWP did not only occur in the NH *(Thompson et al., 1995, 2006)*. However, Andean ice cores possess intrinsic limitations due to uncertain dating *(Vimeux et al., 2009)*, strong sublimation processes for some sites *(Ginot et al., 2001)* and the complexity of the interpretation of stable isotopes records, not only linked with temperature but also with precipitation on a seasonal to inter-annual time scale *(Vimeux et al., 2009; Vuille et al., 2003; Vuille and Werner, 2005)*.

In June 1999, a joint French-Swiss team from IRD (Institut de Recherche pour le Développement) and PSI extracted two ice cores from Nevado Illimani **(Fig. 2.4)**, Bolivia, using the FELICS drill *(Ginot et al., 2002a)*. The drill site was located at 6300 m a.s.l. on a glacier saddle between the two summits of Pico Central and Pico Sur (16°39′ S, 67°47′ W). Both cores reached bedrock at 136.7 m depth (French core) and 138.7 m depth (Swiss core, *this thesis*). A good preservation of the chemical signal was suggested by the rare occurrence of melt layers and low borehole temperatures (max. −7 °C) indicative of a cold glacier *(Kellerhals et al., 2010a)*. As the Illimani site is located in the Eastern Cordillera, precipitation can also occur during the dry season, leading to a less pronounced seasonality with only 50 to 60 % of the annual precipitation falling during the wettest months (December to February) and a weaker impact of ENSO *(Garreaud et al., 2003; Vuille et al., 2000)*.

To update the Illimani 1999 ice core (IL-99), a shallow firn core (25.7 m long) was retrieved in June 2015 (IL-15) by a team of scientists from the PSI at the same location (16°38′58.57′′ S, 67°47′03.57′′ W) using a lightweight portable electromechanical drill, and was shipped frozen to PSI.

2.2.3 Ice-core dating

Dating of the IL-99 ice core was performed by a multi-parameter approach **(Fig. 2.6)** similar to the LF-09 ice core. The first 125 m of the core, back to 1200 ± 240 AD, were dated by *Knüsel et al. (2003)* using ALC based on electrical conductivity measurements (ECM), the 1964 AD tritium peak, independent ^{210}Pb dating for the most recent 100 years, ECM peaks indicative of volcanic eruptions (Pinatubo 1991, El Chichón 1982, Agung 1963, Krakatoa 1883, Tambora 1815 and the "unknown" (at that time) 1258, later identified as Samalas) and a model composed of a firn-densification model *(Herron and Langway, 1980)* in the upper part combined with a two-stage ice-flow model *(Dansgaard and Johnsen, 1969)* forced to fit the reference points.

Dating of the uppermost 59.2 m was refined to a seasonal resolution by *Knüsel et al. (2005)*. For this purpose, they used ALC of five seasonally-resolved compounds: ECM, Na^+, Ca^{2+}, $HCOO^-$ and the dust-related principal component (PC1 in *Knüsel et al., 2005*) obtained by Principal Component Analysis (PCA).

Kellerhals et al. (2010a) then revised the original dating. They performed ALC on the more regular NH_4^+ variations and extended it for six additional meters of the core. They reassigned the sulfate peak of the 1258 Samalas eruption from 99.9 to 90.2 m weq. They extended the dating to the bottom of the core by including ^{14}C dating of eight samples. Lastly, they used a 2-parameter model *(Thompson et al., 1990)* fitted to the time markers to obtain a continuous depth-age relationship, except between the last five ^{14}C dates where linear interpolation was used due to the very strong layer thinning. A

comprehensive description of the dating can be found in *Kellerhals (2008)*. The IL-99 ice core finally spans 1999 AD–13000 BP (i.e. the entire Holocene back to the last deglaciation), with an average accumulation rate of 0.58 m weq yr^{-1}. Dating uncertainty is assessed to be ±2 years in the vicinity of volcanic horizons, ±5 years for the time period 1800–1999 AD (ALC), ±20 years for between 1250 and 1800 AD (model), and ±110 years at the youngest ^{14}C age (1060–1280 BP, *Kellerhals et al., 2010a*).

The IL-99 French core (not used here), albeit shorter, was shown to cover the last 18000 years BP *(Ramirez et al., 2003)*. Different dating methods were applied. In addition to ALC by ECM and absolute time markers (tritium and sulfate peaks), dust microparticle counting and isotopic analyses (δ^{18}O and δD) were employed. Wiggle matching of the Illimani δD record to the Huascarán δ^{18}O record *(Thompson et al., 1995)* was used in the bottom part of the Illimani French core due to the strong resemblances between the two isotopic profiles.
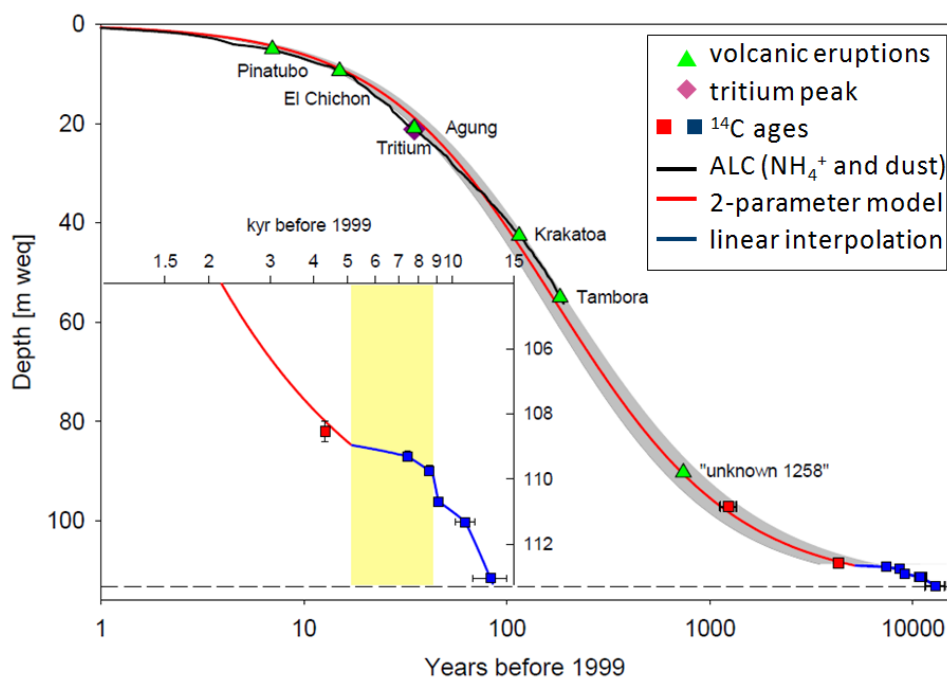
Fig. 2.6: Depth-age relationship in the IL-99 ice core (adapted from *Kellerhals, 2008*).

Dating of the IL-15 core was performed in the framework of this thesis using well-resolved seasonal variations of rBC and Ca^{2+} *(see Supplement of Chapter 5)*, attributing simultaneous minima of both compounds to first of January of each year. Linear interpolation was made between two adjacent minima, thus neglecting the seasonal pattern of precipitation. The timescale of the IL-15 core was adjusted by wiggle matching to the top part of the IL-99 core thanks to a 10 cm thick ice lens present in both records and corresponding to the warm year 1998 and to three characteristic peaks in the rBC profile for the years 1995–1996. The IL-15 ice core thus spans the time period 1995–2015, corresponding to a net accumulation rate of 0.72 m weq yr^{-1}.

2.2.4 Previous studies

First studies focused on the potential of the Illimani site to accurately record past climate variability. Shallow firn core analyses revealed a clear seasonality in the stable isotope signal and in the concentrations of chemical compounds as well as a minor impact of post-depositional sublimation at

the Illimani site *(Ginot et al., 2002b)*. Deposition processes were investigated in detail by *Bonnaveira (2004)*, who drew a similar conclusion to *Ginot et al. (2002b)* regarding post-depositional processes.

Dating of the IL-99 Swiss core was presented in *Knüsel et al. (2003)*. *Knüsel et al. (2005)* discussed the impact of ENSO on the ionic records, showing elevated dust concentrations during El Niño phases. *Kellerhals et al. (2010b)* suggested thallium as an appropriate volcanic eruption tracer. *Kellerhals et al. (2010a)* reconstructed temperatures of the last 1600 years based on the NH_4^+ record, interpreted as a proxy for biogenic emissions from the Amazon Basin. *Eichler et al. (2015)* focused on historical regional silver production and 20th-century leaded gasoline pollution. Lastly, *Eichler et al. (2017)* showed that extensive copper metallurgy in the Andes started 2700 years ago.

Dating of the IL-99 French core, including isotopic records, was presented in *Ramirez et al. (2003)*. *Correia et al. (2003)* focused on 20th-century trace element records in order to disentangle the contribution from dust and anthropogenic sources. *De Angelis et al. (2003)* discussed the volcanic eruptions recorded in the ice core. Finally, *Gay et al. (2014)* introduced an alternative statistical dating method based on the ion profiles.

The available dataset resulting from the previous studies on the IL-99 Swiss core is composed of 13 ionic records (Na^+, Mg^{2+}, Ca^{2+}, K^+, NH_4^+, Cl^-, SO_4^{2-}, NO_3^-, MSA, $HCOO^-$, CH_3COO^-, $C_2O_4^{2-}$ and F^-) for the entire core (4283 samples), 38 trace element records (^{7}Li, ^{23}Na, ^{24}Mg, ^{27}Al, ^{44}Ca, ^{45}Sc, ^{51}V, ^{52}Cr, ^{55}Mn, ^{56}Fe, ^{59}Co, ^{60}Ni, ^{63}Cu, ^{66}Zn, ^{85}Rb, ^{88}Sr, ^{90}Zr, ^{95}Mo, ^{109}Ag, ^{111}Cd, ^{121}Sb, ^{133}Cs, ^{138}Ba, ^{139}La, ^{140}Ce, ^{141}Pr, ^{146}Nd, ^{147}Sm, ^{153}Eu, ^{172}Yb, ^{182}W, ^{205}Tl, ^{206}Pb, ^{207}Pb, ^{208}Pb, ^{209}Bi, ^{232}Th and ^{238}U) for the entire core, except the first 4.3 m (snow), measured by Continuous Flow Analysis Inductively Coupled Plasma-Sector Field Mass Spectrometry (CFA-ICP-SFMS) allowing high resolution (around 1 cm, total of 11258 datapoints), and the δ^{18}O record for the bottommost 3 m spanning 4000–13000 years BP and presented in *Sigl et al. (2009)*.

2.3 Colle Gnifetti, Swiss Alps

2.3.1 Regional settings

The Alps are the main mountain range in Europe **(Fig. 2.7)**. They stretch from the Mediterranean Sea at the southwest to the Austrian plains at the northeast (roughly with the shape of a crescent from Genoa to Vienna) over more than 1000 km, with a width comprised between 100 and 400 km. They host the highest summits of Europe (Caucasus excepted), with the most elevated point, Mont Blanc, reaching 4809 m a.s.l. A wide range of environments and climatic conditions can be found over the Alps as they act as a climatic border between Western Europe (maritime climate), Northern Europe (continental climate) and Southern Europe (Mediterranean climate). The Alps contain around 5150 glaciers (with sizes > 0.02 km^2), covering a total area of 2910 km^2 *(Paul et al., 2011)*. However, most of them are not suitable for ice-core studies as they are temperate glaciers lying at too low elevations (< 3500–4000 m a.s.l.) and therefore affected by summer melting. Cold glaciers above 4000 m with a rather flat topography are required to accurately preserve paleoclimate information. Given these requirements, only a few sites are available for ice-core drilling: Col du Dôme (4250 m a.s.l.) in the Mont Blanc massif (France), Colle Gnifetti (4450 m a.s.l.) in the Monte Rosa massif (Switzerland), Fiescherhorn (3900 m a.s.l.) in the Bernese Oberland (Switzerland) and Mt. Ortles (3850 m a.s.l.) in the Italian Alps, recently investigated *(Gabrielli et al., 2016)*. The Alps are a highly valuable study site as ice-core research can be combined with a dense network of observational data (temperature,

precipitation, glacier lengths) sometimes spanning the last 250 years (e.g. *Böhm et al., 2010*), which is unique in the world.
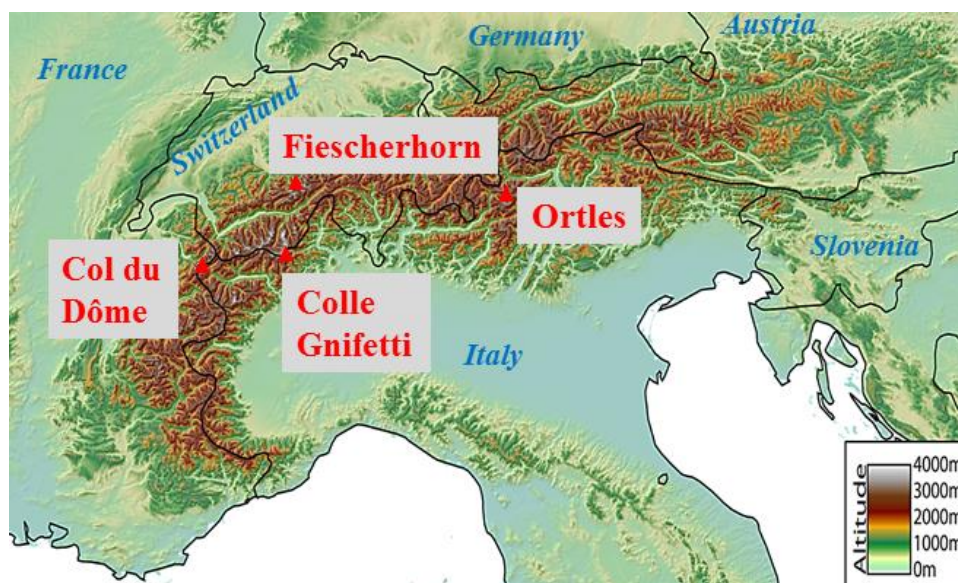
Fig. 2.7: Physical map of the Alps with the major ice-core sites in red (adapted from *https://fr.wikipedia.org/wiki/Géographie_des_Alpes*).

2.3.2 Ice-core drilling

The Colle Gnifetti (CG) site is located on a saddle at 4450 m a.s.l. (45°55′ N, 7°52′ E) on the Swiss-Italian border between the two summits of Zumsteinspitze (4562 m) and Signalkuppe/Punta Gnifetti (4553 m) in the Monte Rosa massif. Due to its topography, the CG site is characterized by strong wind erosion in winter leading to a summer-biased accumulation of snow *(Bohleber et al., 2013; Häberli et al., 1983; Oeschger, 1977; Schwikowski et al., 1999)*. The northeastern side of the saddle is composed of a 2000 m high steep ice cliff acting as a sink for snow but also bringing polluted air from the Po valley by convection of air masses in summer.

The CG site has a long history of ice-core drilling involving two different research groups, from the PSI/University of Bern and the University of Heidelberg. Ice cores were retrieved there in 1976, 1977, 1982 (4 cores), 1995 (2 cores), 2003 (2 cores, *this thesis*), 2005 (2 cores), 2008 (2 shallow firn cores), 2013 and 2015 (2 cores, *this thesis*). In our group, ice-core records of ammonium *(Döscher et al., 1996)*, carbonaceous aerosols *(Lavanchy et al., 1999; Thevenon et al., 2009)*, sulfate and nitrate *(Döscher et al., 1995; Schwikowski et al., 1999)*, organic pollutants *(Gabrieli et al., 2010; Kirchgeorg et al., 2013)* or trace elements *(Barbante et al., 2004; Gabrieli and Barbante, 2014; Gabrieli et al., 2011; Schwikowski et al., 2004)* have highlighted the strong impact of anthropogenic pollution on the European atmospheric composition during the last centuries. The research group from the University of Heidelberg mainly focused on mineral dust variability and temperature reconstruction based on water stable isotopes *(Bohleber et al., 2013, 2018; Wagenbach et al., 2012 and references therein)*.

In September 2003, a Swiss-Italian team extracted two deep cores from CG using the FELICS drill *(Ginot et al., 2002a)*. Both cores were drilled a few meters apart (45°55′50.4′′ N, 7°52′33.5′′ E) and reached bedrock at 81.9 m (CG03A core) and 81.1 m (CG03B core) depth. Borehole temperatures ranged between −12.5 and −13.5 °C, indicative of a cold glacier, and only 1 % of the ice core length was composed of ice lenses due to the refreezing of melt water, suggesting a good preservation of the

CG record and a minimal impact of melting on the chemical profiles *(Sigl, 2009)*. The two cores were shipped to PSI in frozen conditions.

In September 2015, a team from PSI came back to CG and extracted two ice cores 18 m northwest of the CG03 drill site (45°55′45.7′′ N, 7°52′30.5′′ E). The first core (CG15A) reached bedrock at 76 m depth while the second core (CG15B), drilled two meters apart, did only reach 47 m depth when drilling was stopped *(Sigl, 2015)*. Both cores were brought frozen to PSI. The upper 12 m of the CG15A ice core have been sampled in the framework of the *PaleoFire* project to update the CG03 records, while the remaining parts were kept for future studies.

2.3.3 Ice-core dating

The CG03A ice core has been dated using a multi-parameter approach **(Fig. 2.8)** described in detail in *Jenk et al.(2009)*, resulting in an accumulation rate of 0.45 m weq yr^{-1}. Dating methods encompass:

- ALC for the most recent 240 years, mostly based on NH_4^+ seasonal variations.
- Independent ^{210}Pb dating (not shown).
- The 1963 tritium peak.
- Sulfate peaks indicative of volcanic eruptions: Katmai 1912, Tambora 1815 and Laki 1783.
- Outstanding Saharan dust events identified by Ca^{2+} peaks: 1977, 1947, 1936, 1901 and 1863.
- A two-parameter model fitted to the time horizons *(Thompson et al., 1990)*.
- ^{14}C dating (9 samples) for the bottom part of the core. The age of the bottommost section of the core remains tentative as a large uncertainty was associated with the oldest ^{14}C age (15200 years BP). The CG03A ice core might contain remaining ice from the last glacial period (late Pleistocene), or at least ice older than 10 ka.
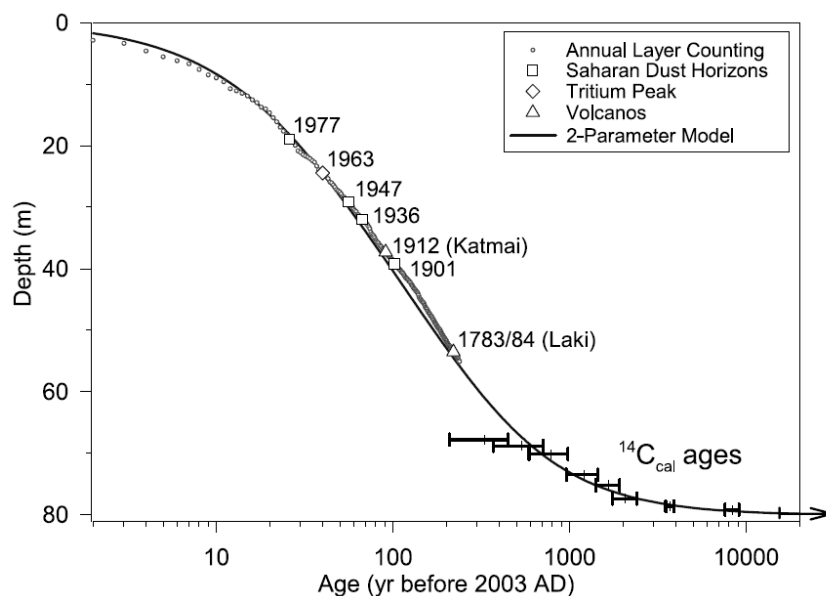
Fig. 2.8: Depth-age relationship in the CG03A ice core *(Jenk et al., 2009)*.

The CG03B ice core was sampled in the framework of this thesis down to 72.1 m depth. A full multi-parameter dating was not performed: the dating of the CG03B core was done against the chronology of the CG03A ice core owing to the very short distance between the CG03A and CG03B cores *(Sigl et al., 2018)*. The approach consisted in using the major ion records to align both cores. In total, 294 stratigraphic points (221 between 1741 and 2003 AD) such as Saharan dust events, the 1963 tritium

peak, volcanic eruptions or peaks with particular features were used to link both cores (**Table 2.1**, *Sigl et al., 2018*). Linear interpolation was employed to extend the dating between the tie-points. Differences in depth for the stratigraphic markers did not exceed 13 cm between the two cores *(Sigl et al., 2018)*, confirming the appropriateness of the method. Dating uncertainty was estimated to be ±1 year next to the reference horizons and ±5 years at most in the mid-19th century. This method led to a final time of 1039 AD at 72.1 m depth when sampling was stopped.

Table 2.1: Selected common age markers for the two CG03 ice cores *(Sigl et al., 2018).*

Type of Age Marker	Parameter	Year (AD)	CG03A Depth (m)	CG03B Depth (m)
SDE 1977	Ca^{2+}, Fe	1977	18.90	18.88
NWT	^3H	1963	24.45	n.a.
SDE 1947	Ca^{2+}, Fe	1947	29.23	29.32
SDE 1936	Ca^{2+}, Fe	1936	31.96	32.03
Katmai 1912	SO_4^{2-}, SO_4^{2-}/Ca^{2+}	1912	37.31	37.44
SDE 1901	Ca^{2+}, Fe	1901	39.20	39.28
SDE 1863	Ca^{2+}, Fe	1863	44.36	44.46
Tambora 1815	SO_4^{2-}, SO_4^{2-}/Ca^{2+}	1816	49.79	49.79
Laki 1783	SO_4^{2-}, SO_4^{2-}/Ca^{2+}	1783	53.50	53.42
Bedrock		-17000	80.18	81.14

SDE = Historic Saharan Dust Event (Wagenbach et al., 1996; Oeschger et al., 1977); NWT = Maximum of northern hemisphere nuclear weapon testing; n.a. not analyzed

The upper section of the CG15A ice core was dated by ALC of NH_4^+ and rBC profiles, attributing local minima to 1st of January of each year and using linear interpolation in between *(Sigl et al., 2018)*. Further adjustment was made by comparison with the CG08 and CG03B ice cores. The upper 12 m of the core thus span the time period 2001–2015 AD, with an average accumulation rate of 0.41 m weq yr^{-1}, very close to that of the CG03 cores.

2.3.4 Previous studies

Previous studies were only conducted on the CG03A ice core as the CG03B core was kept in reserve for future studies and started to be processed in the framework of the *PaleoFire* project. In addition to the dating, the CG03A ice core has been analyzed for mineral dust and BC by a thermal-optical method for the last millennium *(Thevenon et al., 2009)*, polycyclic aromatic hydrocarbons since 1700 AD (PAHs, *Gabrieli et al., 2010*), plutonium contamination from nuclear weapon testing *(Gabrieli et al., 2011)*, the isotopic composition of mineral dust to infer its origin (north-central and northwest part of the Saharan desert, *Thevenon et al., 2012*), and lead and uranium *(Gabrieli and Barbante, 2014)*.

2.4 Tsambagarav, Mongolian Altai

2.4.1 Regional settings

The Altai Mountains (**Fig. 2.9**) are a complex mountain system composed of several ranges located in northern Central Asia and spreading over four countries: Russia, Mongolia, China and Kazakhstan. Their highest point is Belukha Mountain (4506 m a.s.l.) at the border between Russia and Kazakhstan. All the ranges contain glaciated areas, in different extent, for a total of 1300 km^2, with approximately 500 km^2 in Mongolia *(Herren et al., 2013)*.
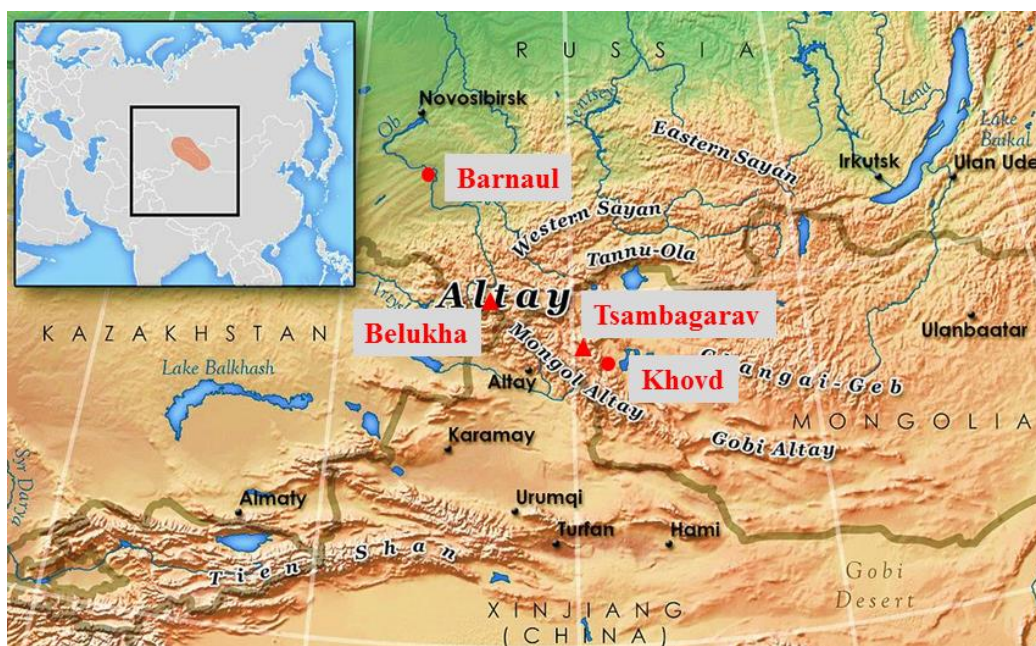
Fig. 2.9: Physical map of the Altai region with the sites of interest in red (adapted from *https://en.wikipedia.org/wiki/Altai_Mountains*).

The Altai region has the highest degree of continentality in the world as it is located very far from any ocean. It thus results in a pronounced continental climate **(Fig. 2.10)**, with very cold and dry winters under the influence of the Siberian High and relatively warm summers dominated by Westerlies *(Herren et al., 2013)*. Average temperature difference can reach up to 40 °C between winter and summer. Most of the precipitation occurs during summer months *(Herren et al., 2013)*. Regional differences in climate can be noted as the Altai acts as a barrier for humid air masses coming from the west. As a consequence, a strong precipitation gradient exists from the northwest (Russia Altai) to the southeast (Mongolian Altai), with a mean annual amount of precipitation decreasing from 800 mm to 200 mm. This directly impacts the regional vegetation and landscape. The northwestern side, in Russian Siberia, is covered with forests (taiga) and meadows at higher elevations while the southern side, in Mongolia, shows a semi-arid steppic landscape which progressively evolves into desertic conditions towards the southeast (Gobi desert).
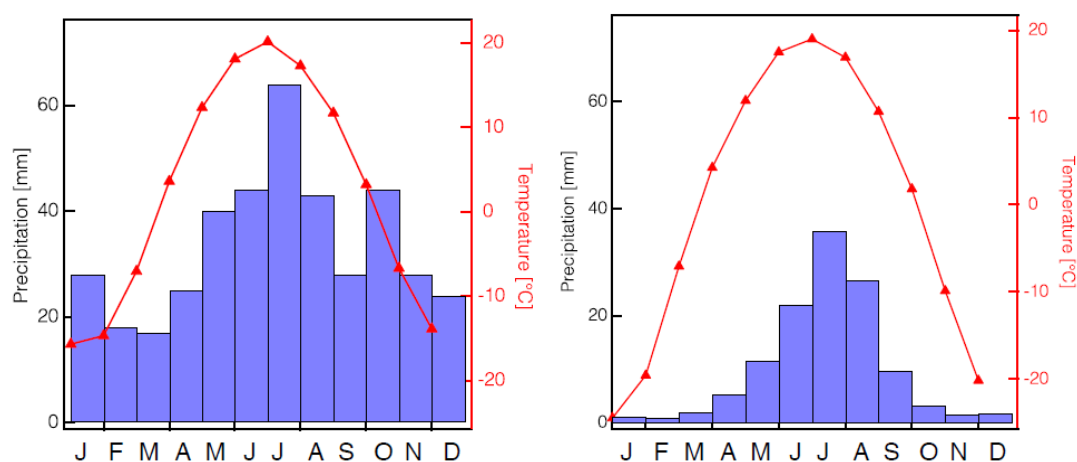
Fig. 2.10: Climate diagram from Barnaul, Russian Altai (left, 1850–2000 AD) and Khovd, Mongolian Altai, representative of the climatic conditions at Tsambagarav (right, 1959–2008) *(Herren, 2013)*.

2.4.2 Ice-core drilling

Due to the remoteness of the region, very few ice-core studies have been conducted in the past in the Altai. In Mongolia, a Chinese expedition retrieved a 40.2-m long ice core from the Tsambagarav range in 2008 but no results have been published so far. In the entire Altai, only two ice cores have been drilled at Belukha, in 2001 *(Olivier et al., 2003)* and 2003 *(Okamoto et al., 2011)*. In June–July 2009, a joint Russian-Swiss team conductedd a drilling campaign at the Tsambagarav range, western Mongolia *(Herren et al., 2013)*. A 72-m long ice core was extracted from the Khukh Nuru Uul ice cap (4130 m a.s.l., 48°39.338´ N, 90°50.826´ E), down to bedrock, using the FELICS drill *(Ginot et al., 2002a)*. In addition, a 52-m long parallel ice core was extracted, but bedrock was not reached due to time constraints. The ice cores were then shipped to PSI in frozen conditions.

2.4.3 Ice-core dating

Dating is described in detail in *Herren (2013)* and *Herren et al. (2013)*. A multi-parameter approach was also used (**Fig. 2.11**), including:

- ALC using the $\delta^{18}O$, Ca^{2+} and $HCOO^-$ profiles back to 1815 AD.
- The 1963 tritium peak.
- Sulfate peaks indicative of volcanic eruptions: Kharimkotan 1933, Katmai 1912, Shiveluch 1854 and Tambora 1815.
- Independent ^{210}Pb dating for the last 150 years.
- A simple glacier flow model for the upper 36 m weq *(Thompson et al., 1990)*.
- ^{14}C dating (10 samples) for the bottommost part of the core, below 36 m weq. A continuous timescale was generated by applying an exponential equation fitted to the different ^{14}C ages.

The Tsambagarav ice core spans the time period 4800 BC–2009 AD, with an estimated average accumulation rate of 0.33 m weq yr^{-1} for the period 1815–2009 AD *(Herren et al., 2013)*. Accumulation rates highly varied further back in the past, from 0.04 m weq yr^{-1} (preceding 4500 years) to 0.46 m weq yr^{-1} close to the bedrock *(Herren et al., 2013)*. The reliability of the depth-age relationship was confirmed by the independent ^{14}C dating of a fly found in the core at 65.78 m weq depth during the sampling for charcoal in 2016. The age of the fly was estimated to be 3442 ± 191 cal years BP while the age of the surrounding ice yielded 3495 ± 225 cal years BP *(Uglietti et al., 2016)*.

Dating uncertainties are the following *(Herren, 2013; Herren et al., 2013)*:

- ±1 year in the decade of an identified reference horizon.
- ±5 years for the section dated by ALC.
- ±10 years between 1250 and 1800 AD.
- ±75 years for the bottommost section (oldest 750 years of the core).
- ±150 years between the bottommost section and 1250 AD, during the period of reduced accumulation.
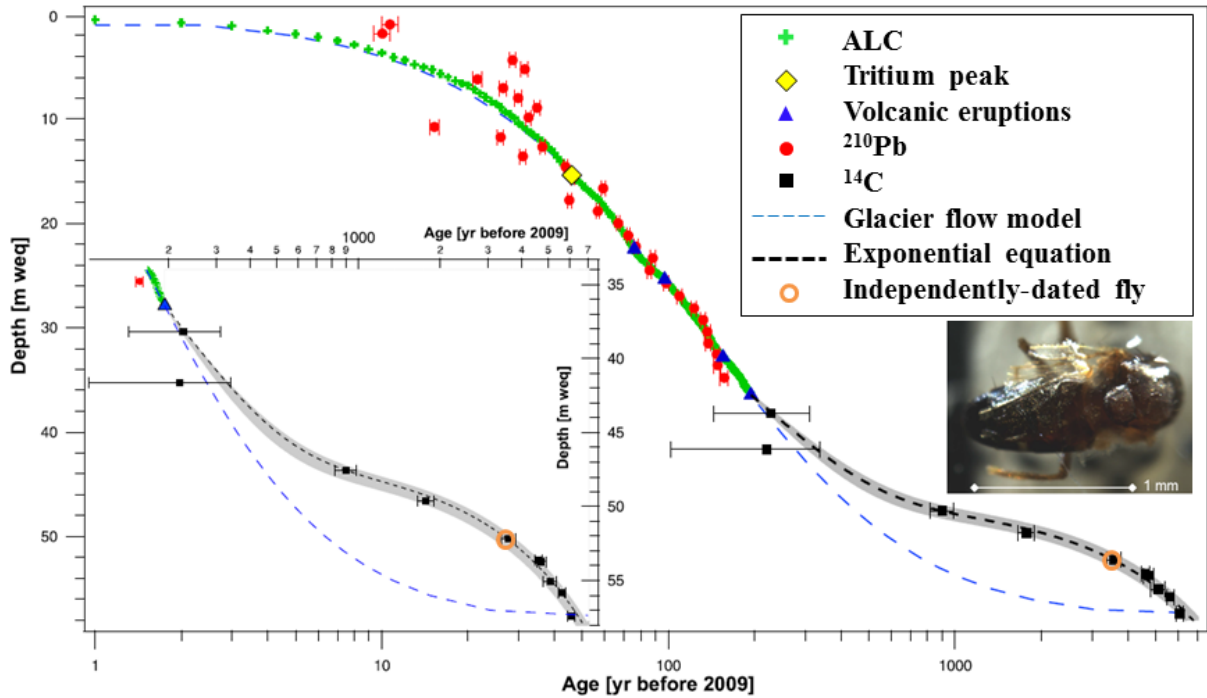
Fig 2.11: Depth-age relationship in the Tsambagarav ice core, with magnification of the lower 36 m in the insert and a picture of the fly *(photo by S. Brügger)*. Figure adapted from *Herren et al. (2013)*.

2.4.4 Previous studies

In addition to the dating methods, *Herren et al. (2013)* reconstructed the accumulation at Tsambagarav for the last 6000 years and concluded that ice-free conditions prevailed during the HCO at this site and that glaciers started to reform during the onset of the "Neoglaciation" around 6000 years ago. *Inceoglu et al. (2016)* presented the ^{10}Be record for the time period 1550–2009 AD in order to infer past solar activity.

The existing dataset for the Tsambagarav ice core comprises 13 ionic records (Na$^+$, Mg^{2+}, Ca^{2+}, K$^+$, NH$_4^+$, Cl$^-$, SO$_4^{2-}$, NO$_3^-$, MSA, HCOO$^-$, CH$_3$COO$^-$, C$_2$O$_4^{2-}$ and F$^-$) and the δ^{18}O record both spanning the entire core, for a total of 2944 samples.

2.5 Summary

Table 2.2: Summary of the main characteristics of the four ice-core sites of the *PaleoFire* project. Tentative values are given *in italic*.

Ice-core site	Main source regions	Specificities	Altitude (m a.s.l.)	Coring year	Bedrock reached	Length (m)	Time period	Accumulation (m weq yr^{-1})
Lomonosovfonna	Northern Eurasia	Summer melting	1202	2009	No	149.5	1222AD–2009AD	0.58
				2011	No	7.6	2004AD–2011AD	0.49
Illimani	Amazon Basin	ENSO Wet/dry season	6300	1999	Yes	138.7	11000BC–1999AD	0.58
				2015	No	25.7	1995AD–2015AD	0.72
Colle Gnifetti	Western/Central/Southern Europe (A, CH, D, F, I)	Winter wind erosion	4450	2003	Yes	81.1	*>8000BC*–2003AD	0.45
				2015	Yes	76.1	*>8000BC*–2015AD	*0.41*
Tsambagarav	Eastern Europe Central Asia Siberia	Summer accumulation	4130	2009	Yes	72	4800BC–2009AD	0.33

References

Barbante, C., Schwikowski, M., Döring, T., Gäggeler, H. W., Schotterer, U., Tobler, L., Van De Velde, K., Ferrari, C., Cozzi, G., Turetta, A., Rosman, K., Bolshov, M., Capodaglio, G., Cescon, P., and Boutron, C.: Historical record of European emissions of heavy metals to the atmosphere since the 1650s from Alpine snow/ice cores drilled near Monte Rosa, *Environmental Science and Technology*, 38, 4085–4090, 2004.

Beaudon, E., Moore, J. C., Martma, T., Pohjola, V. A., van de Wal, R. S. W., Kohler, J., and Isaksson, E.: Lomonosovfonna and Holtedahlfonna ice cores reveal east–west disparities of the Spitsbergen environment since AD 1700, *Journal of Glaciology*, 59, 1069–1083, 2013.

Bohleber, P., Wagenbach, D., Schöner, W., and Böhm, R.: To what extent do water isotope records from low accumulation Alpine ice cores reproduce instrumental temperature series?, *Tellus B*, 65, 17, 2013.

Bohleber, P., Erhardt, T., Spaulding, N., Hoffmann, H., Fischer, H., and Mayewski, P.: Temperature and mineral dust variability recorded in two low-accumulation Alpine ice cores over the last millennium, *Climate of the Past*, 14, 21–37, 2018.

Böhm, R., Jones, P. D., Hiebl, J., Frank, D., Brunetti, M., and Maugeri, M.: The early instrumental warm-bias: a solution for long central European temperature series 1760–2007, *Climatic Change*, 101, 41–67, 2010.

Bonnaveira, H.: Etude des phénomènes de dépôt et post-dépôt de la neige andine sur un site tropical d'altitude (Illimani-Bolivie-6340 m) en vue de l'interprétation d'une carotte de glace, PhD Thesis, Université Joseph Fourier, Grenoble, France, 2004.

Correia, A., Freydier, R., Delmas, R. J., Simões, J. C., Taupin, J.-D., Dupré, B., and Artaxo, P.: Trace elements in South America aerosol during 20th century inferred from a Nevado Illimani ice core, Eastern Bolivian Andes (6350ma.s.l.), *Atmospheric Chemistry and Physics*, 3, 2143–2177, 2003.

Dansgaard, W. and Johnsen, S. J.: A flow model and a time scale for the ice core from Camp Century, Greenland, *Journal of Glaciology*, 8(53), 215– 223, 1969.

De Angelis, M., Simões, J., Bonnaveira, H., Taupin J. D., and Delmas, R. J.: Volcanic eruptions recorded in the Illimani ice core (Bolivia): 1918–1998 and Tambora periods, *Atmospheric Chemistry and Physics*, 3, 1725–1741, 2003.

Döscher, A., Gäggeler, H. W., Schotterer, U., and Schwikowski, M.: A 130 year deposition record of sulfate, nitrate and chloride from a high-alpine glacier, *Water, Air, and Soil Pollution*, 85, 603–609, 1995.

Döscher, A., Gäggeler, H. W., Schotterer, U., and Schwikowski, M.: A historical record of ammonium concentrations from a glacier in the Alps, *Geophysical Research Letters*, 23, 2741–2744, 1996.

Eichler, A., Gramlich, G., Kellerhals, T., Tobler, L., and Schwikowski, M.: Pb pollution from leaded gasoline in South America in the context of a 2000-year metallurgical history, *Science Advances*, 1, e1400196, 2015.

Eichler, A., Gramlich, G., Kellerhals, T., Tobler, L., Rehren, Th., and Schwikowski, M.: Ice-core evidence of earliest extensive copper metallurgy in the Andes 2700 years ago, *Scientific Reports*, 7, 41855, 2017.

Gabrieli, J. and Barbante, C.: The Alps in the age of the Anthropocene: the impact of human activities on the cryosphere recorded in the Colle Gnifetti glacier, *Rendiconti Lincei Scienze Fisiche e Naturali*, 25, 71–83, 2014.

Gabrieli, J., Vallelonga, P., Cozzi, G., Gabrielli, P., Gambaro, A., Sigl, M., Decet, F., Schwikowski, M., Gaggeler, H., Boutron, C., Cescon, P., and Barbante, C.: Post 17th-Century Changes of European PAH Emissions Recorded in High-Altitude Alpine Snow and Ice, *Environmental Science and Technology*, 44, 3260–3266, 2010.

Gabrieli, J., Cozzi, G., Vallelonga, P., Schwikowski, M., Sigl, M., Eickenberg, J., Wacker, L., Boutron, C., Gaggeler, H., Cescon, P., and Barbante, C.: Contamination of Alpine snow and ice at Colle Gnifetti, Swiss/Italian Alps, from nuclear weapons tests, *Atmospheric Environment*, 45, 587–593, 2011.

Gabrielli, P., Barbante, C., Bertagna, G., Bertó, M., Binder, D., Carton, A., Carturan, L., Cazorzi, F., Cozzi, G., Dalla Fontana, G., Davis, M., De Blasi, F., Dinale, R., Dragà, G., Dreossi, G., Festi, D., Frezzotti, M., Gabrieli, J., Galos, S. P., Ginot, P., Heidenwolf, P., Jenk, T. M., Kehrwald, N., Kenny, D., Magand, O., Mair, V., Mikhalenko, V., Lin, P. N., Oeggl, K., Piffer, G., Rinaldi, M., Schotterer, U., Schwikowski, M., Seppi, R., Spolaor, A., Stenni, B., Tonidandel, D., Uglietti, C., Zagorodnov, V., Zanoner, T., and Zennaro, P.: Age of the Mt. Ortles ice cores, the Tyrolean Iceman and glaciation of the highest summit of South Tyrol since the Northern Hemisphere Climatic Optimum, *The Cryosphere*, 10, 2779–2797, 2016.

Garreaud, R. D.; Intraseasonal variability of moisture and rainfall over the South American Altiplano, *Monthly Weather Review*, 128(9), 3337–3346, 2000.

Garreaud, R. D. and Aceituno, P.: Interannual rainfall variability over the South American Altiplano, *Journal of Climate*, 14(12), 2779– 2789, 2001.

Garreaud, R., Vuille, M., and Clement, A. C.: The climate of the Altiplano: observed current conditions and mechanisms of past changes, *Palaeogeography, Palaeoclimatology, Palaeoecology*, 194, 5–22, 2003.

Gay, M., De Angelis, M., and Lacoume, J.-L.: Dating a tropical ice core by time–frequency analysis of ion concentration depth profiles, *Climate of the Past*, 10, 1659–1672, 2014.

Ginot, P., Kull, C., Schwikowski, M., Schotterer, U., and Gäggeler, H. W.: Effects of postdepositional processes on snow composition of a subtropical glacier (Cerro Tapado, Chilean Andes), *Journal of Geophysical Research*, 106(D23), 32375–32386, 2001.

Ginot, P., Stampfli, F., Stampfli, D., Schwikowski, M., and Gäggeler, H. W.: FELICS, a new ice core drilling system for high-altitude glaciers, *Memoirs of National Institute of Polar Research Special Issue*, 56, 38–48, 2002a.

Ginot, P., Schwikowski, M., Schotterer, U., Stichler, W., Gäggeler, H. W., Francou, B., Gallaire, R., and Pouyaud, B.: Potential for climate variability reconstruction from Andean glaciochemical records, *Annals of Glaciology*, 35, 443– 450, 2002b.

Grieman, M. M., Aydin, M., Isaksson, E., Schwikowski, M., and Saltzman, E. S.: Aromatic acids in an Arctic ice core from Svalbard: a proxy record of biomass burning, *Climate of the Past*, 14, 637–651, 2018.

Häberli, W., Schotterer, U., Wagenbach, D., Häberlischwitter, H., and Bortenschlager, S.: Accumulation Characteristics on a Cold, High-Alpine Firn Saddle from a Snow-Pit Study on Colle-Gnifetti, Monte-Rosa, Swiss Alps, *Journal of Glaciology*, 29, 260–271, 1983.

Herren, P.-A.: Ice core based climate reconstruction from the Mongolian Altai, PhD thesis, University of Bern, 2013.

Herren, P.-A., Eichler, A., Machguth, H., Papina, T., Tobler, L., Zapf, A., and Schwikowski, M.: The onset of Neoglaciation 6000 years ago in western Mongolia revealed by an ice core from the Tsambagarav mountain range, *Quaternary Science Reviews*, 69, 59–69, 2013.

Herron, M. M. and Langway Jr., C. C.: Firn densification: An empirical model, *Journal of Glaciology*, 25(93), 373–385, 1980.

Hisdal, V.: Svalbard: nature and history, Norsk Polarinstitutt, Oslo, Norway, 1998.

Inceoglu, F., Knudsen, M. F., Olsen, J., Karoff, C., Herren, P.-A., Schwikowski, M., Aldahan, A., and Possnert, G.: A continuous ice-core [10]Be record from Mongolian mid-latitudes: Influences of solar variability and local climate, *Earth and Planetary Science Letters*, 437, 47–56, 2016.

Isaksson, E., Pohjola, V., Jauhiainen, T., Moore, J., Pinglot, J. F., Vaikmae, R., van de Wal, R. S. W., Hagen, J. O., Ivask, J., Karlöf, L., Martma, T., Meijer, H. A. J., Mulvaney, R., Thomassen, M., and van den Broeke, M.: A new ice-core record from Lomonosovfonna, Svalbard: viewing the 1920–97 data in relation to present climate and environmental conditions, *Journal of Glaciology*, 47, 335–345, 2001.

Isaksson, E., Hermanson, M., Hicks, S., Igarashi, M., Kamiyama, K., Moore, J., Motoyama, H., Muir, D., Pohjola, V., Vaikmäe, R., van de Wal, R. S. W., and Watanabe, O.: Ice cores from Svalbard–useful archives of past climate and pollution history, *Physics and Chemistry of the Earth*, 28, 1217–1228, 2003.

Isaksson, E., Kohler, J., Pohjola, V., Moore, J., Igarashi, M., Karlöf, L., Martma, T., Meijer, H., Motoyama, H., Vaikmäe, R., and van de Wal, R. S. W.: Two ice-core δ^{18}O records from Svalbard illustrating climate and sea-ice variability over the last 400 years, *The Holocene*, 15(4), 501–509, 2005.

Jenk, T. M., Szidat, S., Bolius, D., Sigl, M., Gäggeler, H. W., Wacker, L., Ruff, M., Barbante, C., Boutron, C. F., and Schwikowski, M.: A novel radiocarbon dating technique applied to an ice core from the Alps indicating late Pleistocene ages, *Journal of Geophysical Research: Atmospheres*, 114, D14305, 2009.

Kellerhals, T.: Holocene climate fluctuations in tropical South America deduced from an Illimani ice core, PhD thesis, University of Bern, 2008.

Kellerhals, T., Brütsch, S., Sigl, M., Knüsel, S., Gäggeler, H. W., and Schwikowski, M.: Ammonium concentration in ice cores: A new proxy for regional temperature reconstruction?, *Journal of Geophysical Research*, 115, D16123, 2010a.

Kellerhals, T., Tobler, L., Brütsch, S., Sigl, M., Wacker, L., Gäggeler, H. W., and Schwikowski, M.: Thallium as a tracer for preindustrial volcanic eruptions in an ice core record from Illimani, Bolivia, *Environmental Science and Technology*, 44, 888–893, 2010b.

Kirchgeorg, T., Dreyer, A., Gabrieli, J., Kehrwald, N., Sigl, M., Schwikowski, M., Boutron, C., Gambaro, A., Barbante, C., and Ebinghaus, R.: Temporal variations of perfluoroalkyl substances and polybrominated diphenyl ethers in alpine snow, *Environmental Pollution*, 178, 367–374, 2013.

Knüsel, S., Ginot, P., Schotterer, U., Schwikowski, M., Gäggeler, H. W., Francou, B., Petit, J. R., Simões, J. C., and Taupin, J. D.: Dating of two nearby ice cores from the Illimani, Bolivia, *Journal of Geophysical Research*, 108(D6), 4181, 2003.

Knüsel, S., Brütsch, S., Henderson, K., Palmer, A. S., and Schwikowski, M.: ENSO signals of the 20th century in an ice core from Nevado Illimani, Bolivia, *Journal of Geophysical Research*, 110, D01102, 2005.

Koerner, R.: Some comments on climatic reconstructions from ice cores drilled in areas of high melt, *Journal of Glaciology*, 43(143), 90–97, 1997.

Lavanchy, V. M. H., Gäggeler, H. W., Schotterer, U., Schwikowski, M., and Baltensperger, U.: Historical record of carbonaceous particle concentrations from a European high-alpine glacier (Colle Gnifetti, Switzerland), *Journal of Geophysical Research: Atmospheres*, 104, 21227–21236, 1999.

Oeschger, H.: First results from Alpine core drilling projects, *Zeitschrift für Gletscherkunde und Glazialgeologie*, 13, 193–208, 1977.

Okamoto, S., Fujita, K., Narita, H., Uetake, J., Takeuchi, N., Miyake, T., Nakazawa, F., Aizen, V. B., Nikitin, S. A., and Nakawo, M.: Reevaluation of the reconstruction of summer temperatures from melt features in Belukha ice cores, Siberian Altai, *Journal of Geophysical Research*, 116(D2), D02110, 2011.

Olivier, S., Schwikowski, M., Brütsch, S., and Eyrikh, S.: Glaciochemical investigation of an ice core from Belukha glacier, Siberian Altai, *Geophysical Research Letters*, 30(19), 1–3, 2003.

Paul, F., Frey, H., and Le Bris, R.: A new glacier inventory for the European Alps from Landsat TM scenes of 2003: challenges and results, *Annals of Glaciology*, 52(59), 144–152, 2011.

Pohjola, V. A., Moore, J. C., Isaksson, E., Jauhiainen, T., Van de Wal, R. S. W., Martma, T., Meijer, H. A. J., and Vaikmäe, R.: Effect of periodic melting on geochemical and isotopic signals in an ice core from Lomonosovfonna, Svalbard, *Journal of Geophysical Research*, 107, 4036–4049, 2002.

Rabatel, A., Francou, B., Soruco, A., Gomez, J., Cáceres, B., Ceballos, J. L., Basantes, R., Vuille, M., Sicart, J.-E., Huggel, C., Scheel, M., Lejeune, Y., Arnaud, Y., Collet, M. ,Condom, T., Consoli, G., Favier, V., Jomelli, V., Galarraga, R., Ginot, P., Maisincho, L.,Mendoza, J., Ménégoz, M., Ramirez, E., Ribstein, P., Suarez, W.,

Villacis, M. and Wagnon, P.: Current state of glaciers in the tropical Andes: A multi-century perspective on glacier evolution and climate change, *The Cryosphere*, 7, 81–102, 2013.

Ramirez, E., Hoffmann, G., Taupin, J. D., Francou, B., Ribstein, P., Caillon, N., Ferron, F. A., Landais, A., Petit, J. R., Pouyaud, B., Schotterer, U., Simões, J. C., and Stievenard, M.: A new Andean deep ice core from Nevado Illimani (6350 m), Bolivia, *Earth and Planetary Science Letters*, 212, 337–350, 2003.

Schwikowski, M., Döscher, A., Gäggeler, H. W., and Schotterer, U.: Anthropogenic versus natural sources of atmospheric sulphate from an Alpine ice core, *Tellus B*, 51, 938–951, 1999.

Schwikowski, M., Barbante, C., Döring, T., Gäggeler, H. W., Boutron, C., Schotterer, U., Tobler, L., Van De Velde, K. V., Ferrari, C., Cozzi, G., Rosman, K., and Cescon, P.: Post-17th-century changes of European lead emissions recorded in high-altitude alpine snow and ice, *Environmental Science and Technology*, 38, 957–964, 2004.

Sigl, M.: Ice core based reconstruction of past climate conditions from Colle Gnifetti, Swiss Alps, PhD thesis, University of Bern, 2009.

Sigl, M.: a new deep ice core from Colle Gnifetti (4454 m asl), *PSI Annual report*, Laboratory of Environmental Chemistry, 2015.

Sigl, M., Jenk, T. M., Kellerhals, T., Szidat, S., Gäggeler, H. W., Wacker, L., Synal, H.-A., Boutron, C., Barbante, C., Gabrieli, J., and Schwikowski, M.: Instruments and Methods Towards radiocarbon dating of ice cores, *Journal of Glaciology*, 55, 985–996, 2009.

Sigl, M., Abram, N. J., Gabrieli, J., Jenk, T. M., Osmont, D., and Schwikowski, M.: 19th century glacier retreat in the Alps preceded the emergence of industrial black carbon deposition on high-alpine glaciers, *The Cryosphere*, 12, 3311–3331, 2018.

Thevenon, F., Anselmetti, F. S., Bernasconi, S. M., and Schwikowski, M.: Mineral dust and elemental black carbon records from an Alpine ice core (Colle Gnifetti glacier) over the last millennium, *Journal of Geophysical Research: Atmospheres*, 114, D17102, 2009.

Thevenon, F., Chiaradia, M., Adatte, T., Hueglin, C., and Poté, J.: Characterization ofModern and FossilMineral Dust Transported to High Altitude in theWestern Alps: Saharan Sources and Transport Patterns, *Advances in Meteorology*, 2012.

Thompson, L. G., Mosley-Thompson, E., and Arnao, B. M.: El Niño-Southern Oscillation events recorded in the stratigraphy of the tropical Quelccaya ice cap, Peru, *Science*, 226, 50–52, 1984.

Thompson, L. G., Mosley-Thompson, E., Bolzan, J. F., and Koci, B. R.: A 1500-year record of tropical precipitation in ice core from the Quelccaya ice cap, Peru, *Science*, 229, 971–973, 1985.

Thompson, L. G., Mosley-Thompson, E., Dansgaard, W., and Grootes, P. M.: The Little Ice Age as recorded in the stratigraphy of the tropical Quelccaya ice cap, *Science*, 234, 361–364, 1986.

Thompson, L. G., Mosley-Thompson, E., Davis, M. E., Bolzan, J. F., Dai, J., Klein, L., Gundestrup, N., Yao, T., Wu, X., and Xie, Z.: Glacial stage ice-core records from the subtropical Dunde Ice Cap, China, *Annals of Glaciology*, 14, 288–297, 1990.

Thompson, L. G., Mosley-Thompson, E., Davis, M. E., Lin, P.-N., Henderson, K. A., Cole-Dai, J., Bolzan, J. F., and Lui, K.-B.: Late glacial stage and Holocene tropical ice core records from Huascarán, Peru, *Science*, 269, 46–50, 1995.

Thompson, L. G., Davis, M. E., Mosley-Thompson, E., Sowers, T. A., Henderson, K. A., Zagorodnov, V. S., Lin, P.-N., Mikhalenko, V. N., Campen, R. K., Bolzan, J. F., Cole-Dai, J., and Francou, B.: A 25,000-year tropical climate history from Bolivian ice cores, *Science*, 282(5395), 1858–1864, 1998.

Thompson, L. G., Mosley-Thompson, E., Brecher, H. H., Davis, M. E., Leon, B., Les, D., Ping-Nan, L., Mashiotta, T. A., and Mountain, K. R.: Abrupt tropical climate change: past and present, *PNAS*, 103(28), 10536–10543, 2006.

Uglietti, C., Zapf, A., Jenk, T. M., Sigl, M., Szidat, S., Salazar, G., and Schwikowski, M.: Radiocarbon dating of glacier ice: overview, optimisation, validation and potential, *The Cryosphere*, 10, 3091–3105, 2016.

Vega, C. P., Björkman, M. P., Pohjola, V. A., Isaksson, E., Pettersson, R., Martma, T., Marca, A. D., and Kaiser, J.: Nitrate stable isotopes and major ions in snow and ice samples from four Svalbard sites, *Polar Research*, 34, 23246, 2015.

Vega, C. P., Pohjola, V. A., Beaudon, E., Claremar, B., van Pelt, W. J. J., Pettersson, R., Isaksson, E., Martma, T., Schwikowski, M., and Bøggild, C. E.: A synthetic ice core approach to estimate ion relocation in an ice field site experiencing periodical melt: a case study on Lomonosovfonna, Svalbard, *The Cryosphere*, 10, 961–976, 2016.

Vimeux, F., Ginot, P., Schwikowski, M., Vuille, M., Hoffmann, G., Thompson, L. G., and Schotterer, U.: Climate variability during the last 1000 years inferred from Andean ice cores: A review of methodology and recent results, *Palaeogeography, Palaeoclimatology, Palaeoecology*, 281, 229–241, 2009.

Vuille, M.: Atmospheric circulation over the Bolivian Altiplano during dry and wet periods and extreme phases of the Southern Oscillation, *International Journal of Climatology*, 19(14), 1579–1600, 1999.

Vuille, M., and Werner, M.: Stable isotopes in precipitation recording South American summer monsoon and ENSO variability: observations and model results, *Climate Dynamics*, 25, 401–413, 2005.

Vuille, M., Bradley, R. S., and Keimig, F.: Interannual climate variability in the Central Andes and its relation to tropical Pacific and Atlantic forcing, *Journal of Geophysical Research*, 105(D10), 12447–12460, 2000.

Vuille, M., Bradley, R. S., Healy, R., Werner, M., Hardy, D. R., Thompson, L. G., and Keimig, F.: Modeling δ18O in precipitation over the tropical Americas: Part II. Simulation of the stable isotope signal in Andean ice cores, *Journal of Geophysical Research*, 108(D6), 4175, 2003a.

Wagenbach, D., Bohleber, P., and Preunkert, S.: Cold alpine ice bodies revisited: What may we learn from their isotope and impurity content?, *Geografiska Annaler: Series A, Physical Geography*, 94, 245–263, 2012.

Watanabe, O., Motoyama, H., Igarashi, M., Kamiyama, K., Matoba, S., Goto-Azuma, K., Narita, H., and Kameda, H.: Studies on climatic and environmental changes during the last few hundred years using ice cores from various sites in Nordaustlandet, Svalbard, *Memoirs of National Institute of Polar Research Special Issue*, 54, 227–242, 2001.

Wendl, I. A.: High resolution records of black carbon and other aerosol constituents from the Lomonosovfonna 2009 ice core, PhD thesis, University of Bern, 2014.

Wendl, I. A., Eichler, A., Isaksson, E., Martma, T., and Schwikowski, M.: 800-year ice-core record of nitrogen deposition in Svalbard linked to ocean productivity and biogenic emissions, *Atmospheric Chemistry and Physics*, 15, 7287–7300, 2015.

3 Methods

In this chapter, the analytical methods employed in the course of this project are presented. Analyses for rBC, major ions and water stable isotopes were carried out. A particular focus will be made on rBC analyses as they constitute the core of the project.

3.1 Ice-core processing

3.1.1 General procedure

After the drilling, the 70 cm long ice-core sections are packed in polyethylene tubes and shipped to PSI in insulated boxes so that they remained frozen. Ice-core sections are processed in a −20 °C cold room following standardized procedures *(Eichler et al., 2000)* ensuring a high level of cleanliness to avoid contamination during the cutting. Each section is unpacked, weighed and measured (length and diameter, normally 8 cm) to calculate its average density. Pictures are taken and the stratigraphy is studied in detail. For this purpose, the sections are placed on a backlit bench. Features like ice lenses, breaks, colored layers and missing parts are noted. Core sections are then put on a Teflon coated tabletop and cut with a band saw. The snow dust is removed by brushing the table surface and both the table and the saw blade are regularly cleaned with acetone and ethanol to prevent contamination. Polyethylene gloves are worn during the entire process for the same reason. Outer parts of the core are used for analyses which are not sensitive to contamination (tritium, ^{210}Pb, charcoal) while samples for more sensitive analyses (ions, BC) are taken from the inner part of core, where process-induced contamination is less probable. The remaining parts of the core sections are then repacked in the same polyethylene tube and archived for future analyses.

The sample resolution is usually adjusted to take into account ice layer thinning with depth and is therefore decreasing from 8–10 cm in the firn section close to the surface to 2–3 cm at the bottom of the core. To assess the reproducibility of the entire analytical process, replicates samples are prepared from parallel ice-core sticks and follow the same process as the original samples. To control the level of cleanliness, procedural blanks are prepared by refreezing ultrapure water (Sartorius, ≥18.2 MΩ cm, with a 0.2 μm filter) in a plastic box and by cutting and analyzing the resulting ultrapure ice as normal samples, in order to eventually correct the final results for the contribution from the blanks.

3.1.2 Within the *PaleoFire* project

In the framework of the *PaleoFire* project, the ice cores mentioned in chapter 2 were sampled for rBC and charcoal. The cutting strategy for rBC *(this thesis)* and charcoal *(PhD thesis of Sandra Brugger, University of Bern)* varied from one ice core to the other as some of them had already been processed in the past (mainly Illimani and Tsambagarav) and others not, resulting in a wide variety of shapes depending on the ice-core sections, whose exhaustive description would be pointless. In some cases, rBC samples had already been prepared in 50 mL polypropylene (PP) vials (Semadeni AG, Switzerland) and cutting was not necessary. No charcoal samples had been prepared in the past with these ice cores so the sampling had to be done for every core. A minimal mass of 200–300 g of ice was required for charcoal and pollen counting, resulting in a much lower resolution for charcoal (2 samples per core section at the maximum) than for rBC. Charcoal samples were prepared in 1 L polyethylene terephthalate-glycol modified (PETG) jars (Semadeni AG, Switzerland). Charcoal and pollen analysis is extensively described in *Brugger et al. (2018)* and *Brugger et al. (in review)*. Below, we detail the cutting process for the different ice cores used in the project:

- The **LF-09 ice core** had already been sampled for rBC by PhD student Isabel Wendl. Two 1.9 x 1.9 cm sections were cut from the inner part of the core at 3–4 cm resolution and combined in one 50 mL PP vial. In total, 4046 samples were obtained for rBC analysis. Further information can be found in *Wendl (2014)*. Samples 907 to 1970 were analyzed by master student Loic Schmidely. 6 series of 20 replicates were also prepared. Preliminary analyses of charcoal and pollen revealed very low concentrations compared to the other cores of the project *(S. Brugger, personal communication)*. It was therefore decided that charcoal and pollen analyses in the LF-09 ice core were not a priority. So far, the LF-09 core has not been sampled for charcoal.
- The **LF-11 firn core** had already been sampled for rBC at the NPI (Norway) by PhD student Carmen Vega. 1.8 x 1.8 cm sections were cut at about 4 cm resolution, resulting in 155 samples (for details, see *Vega et al., 2015*).
- The topmost 33.15 m of the **IL-99 ice core** had already been sampled for rBC analysis at 10 cm resolution (316 samples in total, spanning 1966–1999 AD) by internship student Adam Hasenfratz. Sampling was then extended to the entire core at 3–4 cm resolution, yielding 2754 additional samples and 243 replicates from 12 ice-core sections. Some sections with poor ice-core quality (brittle ice) towards the bottom of the core could not be sampled at such resolution and were placed in 1 L plastic jars, roughly resulting in a 10–20 cm resolution. Another section with poor ice-core quality between 127.4 and 133 m depth spanning roughly 0–2000 BC was also resampled specifically at 3–7 cm resolution, resulting in 121 additional samples. From the rBC samples, a 1 mL aliquot was taken for water stable isotope measurements. Only 121 samples were prepared for charcoal and pollen out of the 206 ice-core sections, reflecting the lack of available material for many sections, as 2–3 sections had to be combined sometimes in the same 1 L jar.
- The **IL-15 firn core** was entirely sampled (and dated) in the framework of the *PaleoFire* project. This is the only core of the project with a smaller diameter (only 6 cm instead of 8 cm) because the drill used was a light and portable version of the FELICS *(Ginot et al., 2002)*. The IL-15 core was cut at 5–6 cm resolution following the cutting scheme in **Fig. 3.1**, producing a total of 487 rBC samples and one section with 13 replicates. Those samples were also analyzed for major ions and water stable isotopes. 21 samples were also prepared for charcoal analysis.
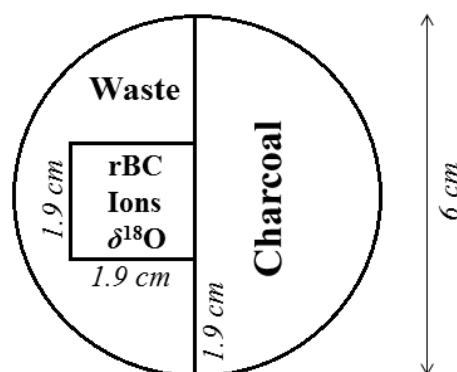

Fig. 3.1: Cutting scheme of the IL-15 ice core. Due to the small diameter and the low density of the material (snow/firn), the leftover part generally fell apart and could not be used.

- The **CG03B ice core** was entirely sampled (and dated) down to 72.1 m depth (year 1039 AD) following the cutting scheme presented in **Fig. 3.2**. The sampling resolution was lowered

from 5 cm at the surface to 2 cm close to the bottom. A total of 2276 samples was obtained for rBC and major ions, as well as 362 replicates from 19 ice-core sections. Similar to IL-99, some ice-core sections from the lower part of the core with poor ice quality were sampled at a lower resolution (around 10 cm). The sampling for charcoal produced 172 samples.

- The uppermost 11.9 m of the **CG15A ice core**, spanning 2001–2015 AD, were cut at 4–5 cm resolution following the same scheme as CG03B, yielding a total of 276 samples and one set of 14 replicates. 18 samples were prepared for charcoals (one per section).
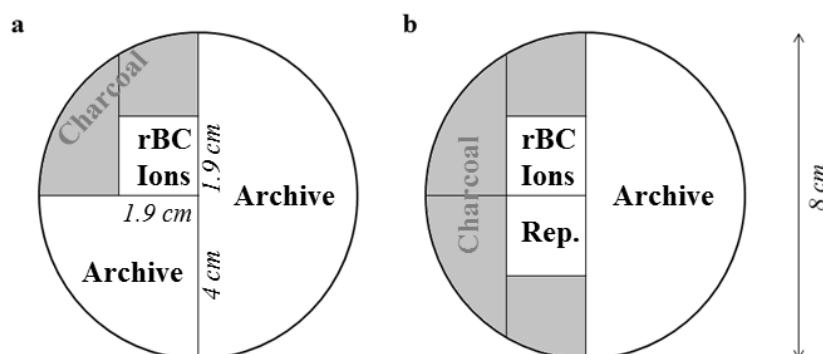
Fig. 3.2: Cutting scheme of the CG03B and CG15A ice cores, for sections with a) original samples only and b) original and replicate (Rep.) samples. In the case of CG15A, water stable isotopes were also measured from the same sample as rBC and ions *(see section 3.5).*

- The entire **Tsambagarav ice core** had already been sampled for rBC by PhD student Pierre-Alain Herren, at 2.5 cm resolution until 50.68 m depth where the resolution was increased to 2 cm, resulting in 2944 samples. Details about the sampling procedure can be found in *Herren (2013)*. Unfortunately, the first 1076 samples experienced melting and refreezing before the rBC analysis, which is a critical point for the quality of the analyses, leading to substantial but unquantifiable rBC losses *(see section 3.2.3)*. Therefore, the first 42 ice-core sections (the topmost 28.1 m, spanning 1945–2009 AD) had to be resampled. A lower resolution was chosen, from 7 cm at the surface until 4 cm at 28.1 m depth, resulting in 580 samples and 66 replicates from 4 different ice-core sections. In addition, 185 replicates were also prepared from 7 different sections belonging to the deepest 13 m of the core. Lastly, 261 samples were cut for charcoal analysis.

3.2 Black carbon analysis

3.2.1 The Single Particle Soot Photometer (SP2)

rBC samples were analyzed with a Single Particle Soot Photometer (SP2, Droplet Measurement Technologies, Inc., Longmont, CO, USA, *Schwarz et al., 2006*). The SP2 is based on the laser-induced incandescence principle *(Stephens et al., 2003)* and measures the mass concentration and size distribution of single rBC-containing aerosol particles. Its principle is the following **(Fig. 3.3)**: dry aerosol samples are drawn by a vacuum pump and injected as an air jet into the SP2 cavity. This air jet intersects a powerful (3 MW cm^{-2}) continuous Nd:YAG laser beam (λ = 1064 nm). Single rBC particles absorbs this radiation and are heated to their point of incandescence (around 3700–4300 K). As they vaporize, they emit intense visible thermal radiation (λ range: 350–800 nm) which is detected by two photomultiplier tubes (PMT). Optical filters are placed upstream to the PMTs so that the latter cover different ranges of wavelengths in order to improve their sensitivity, resulting in a broadband

detector (400–650 nm) and a narrowband detector (610–650 nm). In addition, two different electronic signal amplification gains (high and low) are possible for each PMT, thus generating a total of four different channels (Broad/Narrow Band High/Low Gain i.e. BBHG, BBLG, NBHG, NBLG). The SP2 can detect rBC particles with a mass-equivalent diameter ranging between 70 and 500 nm, which is equivalent to a mass range of 0.3–118 fg rBC per particle, assuming a rBC density of 1.8 g cm^{-3}. As the peak intensity of the incandescent light is proportional to the rBC mass in the particle *(Schwarz et al., 2006)*, direct quantification is possible after calibration with an appropriate standard.

Besides the PMTs, two avalanche photo-detectors (APD) are used to detect scattering of the incoming laser light at 1064 nm in order to measure particle size distribution in the range 200–400 nm which encompasses the accumulation mode of most particles *(SP2 operator manual, 2013)*. One of the APDs is sensitive to total particle scattering while the other one solely focuses on scattering by incandescent particles, which enables to focus on the amount of coating or the mixing state of rBC-containing particles. All the four detectors are placed on the same horizontal plan, separated by 90° angles.
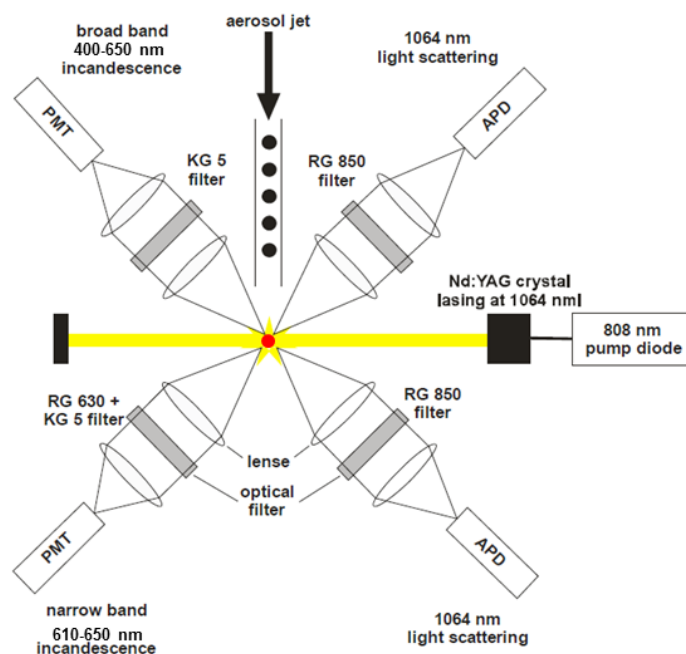
Fig 3.3: Schematic of the SP2 cavity (adapted from *Schläppi, 2010* and *Schwarz et al., 2006*).

Compared to other BC measurement techniques, the SP2 presents some interesting advantages. First, it is specific to BC particles since they are the only ones which can incandesce at such high temperatures due to their highly refractory properties *(Schwarz et al., 2006)*. As the PMTs can infer temperature based on the color of the radiation, it can clearly separate BC particles from other ones. Second, the SP2 is characterized by a high sensitivity as the limit of detection (LOD) is as low as 0.3 fg BC per particle or 10 ng m^{-3} *(SP2 operator manual, 2013)*. Third, it allows fast and direct quantification and therefore does not require a large amount of sample. This is particularly interesting for ice-core science, for which the available amount of material is usually low, as it only requires a few mL of sample, contrary to other techniques (optical, thermal-optical) consuming hundreds of grams of ice. Lastly, the SP2 detection is unaffected by particle coatings and morphology *(Cross et al., 2010; Laborde et al., 2012; Moteki and Kondo, 2007; Slowik et al., 2007)*. Only the presence of high concentrations of dust (typically 50 µg g^{-1}) can cause positive artifacts *(Schwarz et al., 2012)* but those concentrations were never met in our ice cores.

However, this technique also possesses intrinsic limitations. First, the SP2 is designed to solely analyze dry aerosols, making ice-core and snow analyses more complex *(see section 3.2.2)*. Second, the narrowness of the detection-size range (generally 70–500 nm, although it can be extended to 800 or even 1000 nm) hampers a correct quantification of large rBC particles, which can represent a significant part of the total mass, as they lead to the saturation of the detectors. This can be an important issue in snow and ice samples as they usually contain larger particles than atmospheric samples *(Schwarz et al., 2012)*. Third, as BC is not a well-defined compound with a fixed composition, finding an appropriate standard for calibration remains challenging, taking into account that different calibration curves are obtained depending on the standard *(Baumgardner et al., 2012)*. Ideally, standard materials should have the same physical properties (particle size distribution, refractive index, effective density) and chemical composition (elemental carbon content) as BC in the samples (which can also vary depending on the origin of the sample), so that they behave similarly in the SP2. It appears from previous studies that fullerene soot and Aquadag (AQ), a commercially available lubricant consisting of a colloidal dispersion of aggregates of irregular flakes of graphite in water, can serve as reference materials *(Gysel et al., 2011)*.

Here, the internal calibration of the SP2 was performed by measuring mass-selected fullerene soot from 0.1 to 100 fg, which corresponds to the usual size range of rBC particles found in the samples. Particle size (and hence mass) was selected by a Differential Mobility Analyzer (DMA). This calibration enables to associate a certain incandescence peak height with an absolute rBC mass and turned out to be very stable with time. Therefore, it was only performed once a year, after important maintenance tasks.

3.2.2 Setup for ice-core analysis

As the SP2 can only analyze dry aerosols, a previous aerosolization step is required for liquid samples (e.g. snow and ice-core samples once melted). A comprehensive description of the method development and validation can be found in *Wendl et al. (2014)* and *Lim et al. (2014)*. Briefly, an APEX-Q jet nebulizer (Elemental Scientific Inc., Omaha, NE, USA) was implemented upstream to the SP2 **(Fig. 3.4)**. Among several types of commercially available nebulizers, the APEX-Q was chosen because it was the only one for which the nebulization efficiency did not decrease for larger particle sizes *(Wendl et al., 2014)*. It consists of a self-aspiration nebulizer to aerosolize the liquid sample, followed by a glass cyclonic spray chamber heated to 100 °C to vaporize and remove water droplets, and by a Peltier-cooled (at 2 °C) multipass condenser, aiming to condense the remaining water vapor which is then eliminated by drain tubes thanks to a peristaltic pump. A dry rBC aerosol is therefore obtained at the outlet of the APEX-Q and directly injected into the SP2.

Self-aspiration of the sample in the nebulizer is caused by a flux of compressed air acting as a carrier gas. The liquid flow rate from the sample is primarily controlled by the flow rate of the carrier gas (1 L min^{-1}), the diameter of the capillary (0.25 mm), the length of the capillary (90 cm) and the geometry of the nebulizer (MicroFlow PFA-ST ES-2040), and used to lie between 0.25 and 0.30 mL min^{-1}. Maintaining a constant liquid flow rate ($\pm$ 10 %) is a crucial parameter for the accuracy of the measurements as variations in the liquid flow rate will directly impact the amount of rBC detected by the SP2 and will lead to misleading results. It is particularly important to ensure that the liquid flow rate does not change between the calibration and the sample measurements. However, as the liquid flow rate cannot be controlled, it has to be checked regularly (several times per day) and measurements are stopped in case of large variations. This check is done by analyzing a sample during a certain amount of time and by weighing it before and after the measurement, in order to calculate the loss of mass and therefore the resulting liquid flow rate. Furthermore, after measuring

hundreds of samples, the capillary and nebulizer usually tend to accumulate dust particles, resulting in a progressively decreasing liquid flow rate, and can even clog up, which implies a careful maintenance of the system.
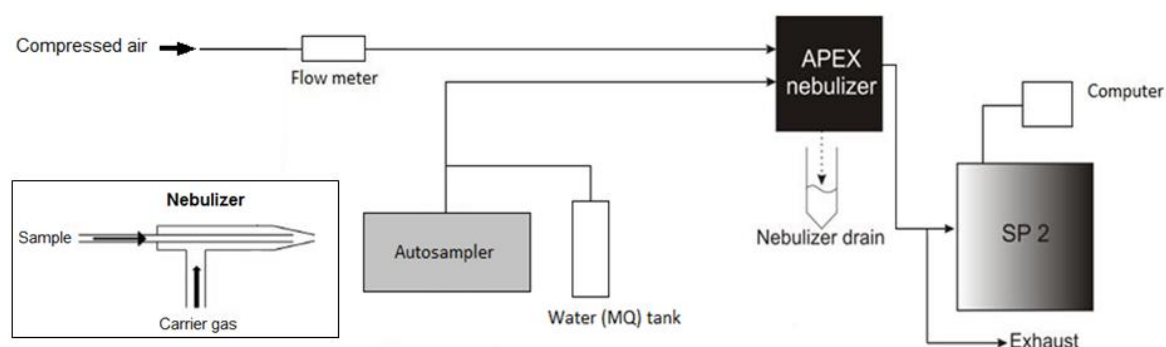
Fig. 3.4: Instrumental setup used at PSI for rBC analysis, with schematic of the nebulizer in the insert.

The use of such an aerosolization step increases the complexity of the system and induces losses of rBC particles during the process (imperfect nebulization, removal of rBC with the drain water, adsorption of rBC at the surface of the capillaries). Therefore, only a fraction of the rBC particles initially pumped from the sample will reach the SP2 inlet. This fraction corresponds to the aerosolization efficiency, whose accurate determination is not straightforward as it implies to monitor the amount of particles lost during the process. This efficiency was estimated by *Lim et al. (2014)* to be 75 ± 7 %. To take this efficiency into account, an additional calibration, called external calibration in contrast to the SP2 internal calibration, is performed. Aqueous BC standards of known concentration are prepared and measured in order to determine the response of the whole setup. A calibration curve ($R^2 > 0.999$) is created so that samples of unknown rBC concentration can thus be quantified. For the external calibration, AQ was the reference material used. 8 fresh AQ standards ranging from 0.1 to 100 ng g^{-1} were prepared twice a week by dilution in ultrapure water from a 2500 ng g^{-1} stock solution, and measured following the same procedure as ice-core samples *(see section 3.2.3)*.

3.2.3 Routine measurements

After cutting in the cold room, samples for rBC analysis were placed in 50 mL PP vials. These samples were then melted at room temperature or in a tepid water bath (faster) as both processes lead to similar results *(Lim et al., 2014)*. Samples were then sonicated for 25 min in a ultrasonic bath in order to break down possible agglomerates, and analyzed by the SP2 right after. At least 10000 rBC particles had to be counted to ensure a good statistical representativeness of the size distribution and reduce the impact of large rBC particles *(Schwarz et al., 2012)*. Those particles are rare but contain a significant fraction of the total rBC mass of the sample and can therefore shift the size distribution to larger values if not enough particles are recorded. Data processing was performed with the PSI SP2 Toolkit 4.110 developed by the Laboratory of Atmospheric Chemistry at PSI on the scientific data analysis software IGOR Pro. Further details are presented in the Appendix.

At room temperature in liquid samples, substantial decreases in rBC concentration have been documented, already after a couple of hours, possibly due to the fact that rBC particles can aggregate to sizes beyond the SP2 detection range or get adsorbed to the walls of the container, depending on the material *(Lim et al., 2014; Wendl et al., 2014)*. This implies that rBC samples have to be measured as soon as possible after melting. In cases when this was not possible, samples were stored in the

64

fridge at +2 °C. Refreezing and re-melting has to be avoided at all costs as it generates irreversible rBC losses, up to 45 ± 11 % *(Lim et al., 2014)* or 60 % *(Wendl et al., 2014)*. This number even increases in the case of multiple thaw-freeze-thaw cycles.

Maintenance of the system mainly consisted of rinsing the system with ultrapure water between each sample to lower the rBC background down to 0–1 particles cm^{-3}, cleaning the APEX-Q and the capillaries every day with 3 % nitric acid to dissolve dust particles and prevent clogging, monitoring the liquid flow as previously mentioned, and performing external calibrations with AQ standards twice a week. Consumable pieces such as nebulizers, capillaries or peristaltic pump rubbers were replaced when they were no longer able to allow stable enough liquid flow rates. The LOD of the method was estimated by measuring ultrapure water blanks 10 times and by calculating their average plus three times their standard deviation, which gave a value of 0.051 ng g^{-1} of rBC. Procedural blanks were also frequently measured and often returned values below the LOD (typically 0.01–0.02 ng g^{-1}), suggesting the absence of contamination from the analytical process.

The repeatability of the rBC detection, investigated by repeating several times the measurement of the same sample, turned out to be excellent, with a coefficient of variation (standard deviation / mean x 100) of 3.5 %, similar to the 3.9 % found by *Lim et al. (2014)*. Overall reproducibility, including uncertainties associated with the calibration and the nebulization efficiency, has been estimated to lie within 20 % *(Lim et al., 2014; Wendl et al., 2014)*. Replicate measurements of ice-core samples performed in the framework of this thesis also illustrate the good reproducibility of the method *(see results in respective chapters)*. However, by considering the total SP2 uncertainty with respect to the accuracy of the determination of rBC concentration in snow samples, uncertainties as high as 60 % can be reached *(Schwarz et al., 2012)*, mainly because of the limited detection size range of the SP2 towards large particles and the discrepancies between the different reference materials for calibration.

3.2.4 Optimization with autosampler

At the beginning of this project, an autosampler was installed (CETAC ASX-520, CETAC Technologies, Omaha, NE, USA) in order to speed up the measurements and improve their reproducibility *(Schmidely, 2015)*. However, the use of an autosampler is somewhat is contradiction with the fact that rBC samples have to be analyzed as soon as possible after melting. For this purpose, rBC losses over 24 hours were studied with 24 ice-core samples from LF, CG and Fiescherhorn, each sample being measured 5 to 14 times depending of its concentration. Similar rBC losses were observed for all samples, largely independent of the origin of the core, the rBC concentration or the dust content. Relative apparent losses were 41 ± 9 % after 24 h and 10 ± 6 % after 6 h *(Schmidely, 2015)*, which was therefore considered as the longest acceptable time for the samples to stay in the autosampler. As rBC losses were almost linear with time, a linear regression was performed on the entire set of samples, and reversed in order to be able to calculate the original rBC concentration at t_0, resulting in the following equation:

$$[rBC]_{\text{corrected}} = \frac{[rBC]_{\text{measured}}}{1 - 0.017\,t}$$

with $[rBC]_{\text{corrected}}$ the original rBC concentration at the initial time (t_0), i.e. the end of the sonication (ng g^{-1}), $[rBC]_{\text{measured}}$ the rBC concentration measured by the SP2 (ng g^{-1}), and t is the time in hours (h) elapsed since the end of the sonication.

Total rBC particle counting was kept at 10 000 counts as recommended *(Schwarz et al., 2012)*. However, two thresholds were implemented to avoid a too short (long) measurement time in the case

of samples with a very high (low) rBC concentration, respectively. A too short measurement time might not be representative of the real rBC concentration due to the presence of large particles and fluctuations of the system whereas a too long measurement time is critical as the entire sample can be consumed. The autosampler probe will then start to suck room air which blocks the self-aspiration process. Therefore, minimum (maximum) counting time was set to 1 min (30 min). Between each sample, the probe was rinsed with ultrapure water for 45 sec, which is a sufficient time for the rBC background to come back to 0–1 particle cm^{-3}. After rinsing, a waiting time of 1 min 45 sec was set before starting to record rBC particles, so that the background signal becomes stable. Stirring was not performed as its effects have been shown to be negligible *(Schwarz et al., 2012)*.
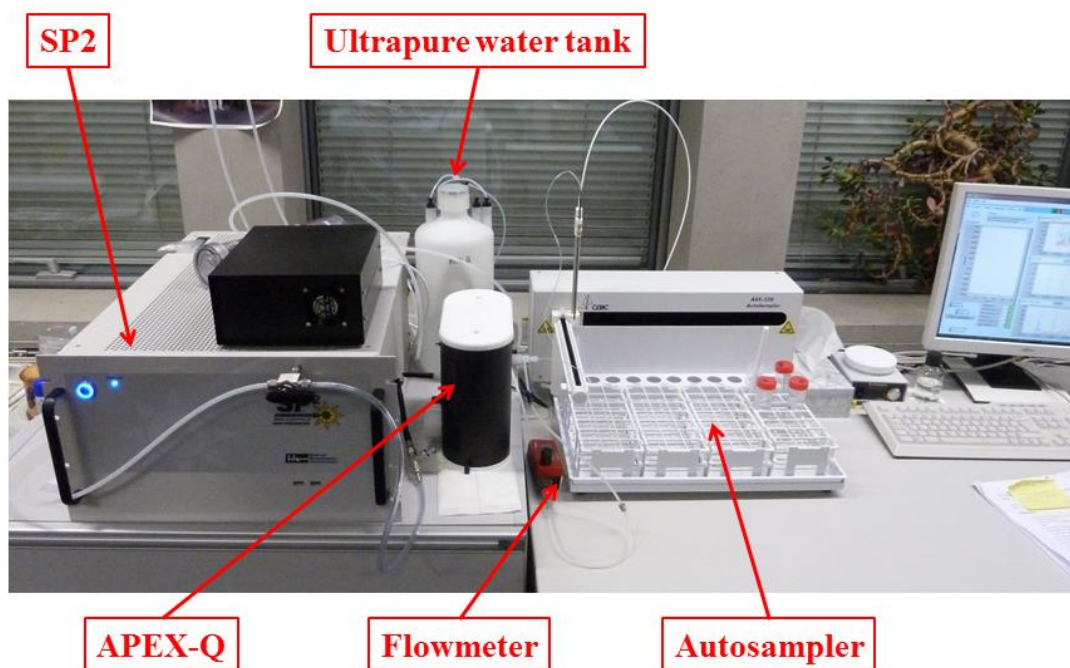
Fig 3.5: Photograph of the SP2 setup at PSI.

3.3 Major ion analysis

Following rBC analysis, the remaining samples were analyzed for water soluble major ions in order to reconstruct past air composition and pollution. 13 ions were measured, including 5 cations (ammonium NH_4^+, calcium Ca^{2+}, magnesium Mg^{2+}, potassium K^+ and sodium Na^+,) and 8 anions (acetate CH_3COO^-, chloride Cl^-, fluoride F^-, formate $HCOO^-$, methanesulfonate (MSA) $CH_3SO_3^-$, nitrate NO_3^-, oxalate $C_2O_4^{2-}$ and sulfate SO_4^{2-}). Major ion analyses were carried out by ion chromatography (IC). In this technique, the sample is eluted through a column filled with an ion-exchange resin in which the ions are separated based on their different affinity to the ion exchanger. The device used in this project was the Metrohm 850 Professional IC (Metrohm AG, Herisau, Switzerland) combined with an autosampler (858 Professional Sample Processor) and an 872 Extension Module. Different analytical methods, whose main parameters are given in **Table 3.1**, were applied to cations and anions. For each batch of measurements, external calibrations were made with standards of known concentrations prepared by dilution of in-house reference solutions of 10 µg g^{-1}. LODs for each species are presented in **Table 3.2**.

Table 3.1: Main parameters used for major ion analysis.

Component	Cations	Anions
Eluent	2.8 mM HNO_3	A: 1.5 mM Na_2CO_3 / 0.3 mM $NaHCO_3$ B: 8 mM Na_2CO_3 / 1.7 mM $NaHCO_3$
Flow rate	1 mL min^{-1}	0.9 mL min^{-1}
Loop	500 μL	500 μL
Separation column	Metrosep C4	Metrosep A Supp 10
Guard column	-	Metrosep A Supp 5
Suppression	-	0.05 M H_2SO_4 + 12 g oxalic acid
Detection	Conductivity	Conductivity

Table 3.2: Limits of detection (LOD) of the different ions for the method used at PSI.

Cations	LOD (ng g^{-1})	Anions	LOD (ng g^{-1})
NH_4^+	0.3	CH_3COO^-	0.7
Ca^{2+}	0.9	Cl^-	0.6
Mg^{2+}	0.4	F^-	0.1
K^+	0.8	$HCOO^-$	0.8
Na^+	0.4	MSA	0.5
		NO_3^-	0.6
		$C_2O_4^{2-}$	0.8
		SO_4^{2-}	1.0

3.4 Water stable isotope analysis

Isotopes are atoms of a particular chemical element differing in the number of neutrons. Stable isotopes exclude the radioactive ones which can be transformed by nuclear decay. For the hydrogen atom (1 proton), two different stable isotopes exist: with no neutron ($_1^1H$) or with 1 neutron ($_1^2H$ or D, deuterium). In the case of the oxygen atom (8 protons), the three stable isotopes are $_8^{16}O$ (the most abundant by far), $_8^{17}O$ and $_8^{18}O$. For a molecule of water ($^1H_2^{16}O$ in its most common form), different combinations, called isotopologues, are possible depending on the respective O and H isotopes contained, $H_2^{18}O$ or $HD^{16}O$ being the most common ones.

Interestingly, the relative proportions of the different water isotopologues (e.g. $^{18}O/^{16}O$ or D/H) can vary during water phase changes such as evaporation or condensation due to their different vapor pressures. The lighter (heavier) isotopologues have a higher (lower) vapor pressure. The lighter isotopologues therefore evaporate more rapidly. On the contrary, the heaviest ones condensate first. This leads to a temperature-dependent isotopic fractionation during the different stages of the water cycle *(Araguás-Araguás et al., 2000)*. As snow precipitation is able to preserve this information, water stable isotope measurements in ice cores can be used as proxies for past temperature variations.

In paleoclimate sciences, ($^{18}O/^{16}O$) and (D/H) isotopic ratios are commonly expressed as a relative deviation from the isotopic ratio of an international standard (Vienna Standard Mean Ocean Water, VSMOW), and reported as $\delta^{18}O$ and δD (‰), respectively. They are calculated as follows:

$$\delta^{18}O\,[‰] = \frac{\left(\frac{^{18}O}{^{16}O}\right)_{sample} - \left(\frac{^{18}O}{^{16}O}\right)_{VSMOW}}{\left(\frac{^{18}O}{^{16}O}\right)_{VSMOW}} \times 1000$$

$$\delta D\,[‰] = \frac{\left(\frac{D}{H}\right)_{sample} - \left(\frac{D}{H}\right)_{VSMOW}}{\left(\frac{D}{H}\right)_{VSMOW}} \times 1000$$

In the framework of the *PaleoFire* project, some of the ice cores were measured for water stable isotopes. For this purpose, 1 mL aliquots of the samples used for rBC/IC analyses were taken after melting and prior to sonication. In that case, samples were imperatively melted at room temperature (not in a warm bath) in order to avoid partial evaporation and condensation which can affect the isotopic ratios. Samples were then analyzed for $\delta^{18}O$ and δD with a wavelength-scanned cavity ring down spectrometer (WS-CRDS, Picarro L2130-i, Picarro Inc., Santa Clara, CA, USA). This device relies on the Beer-Lambert law and infrared (IR) spectroscopy. The Beer-Lambert law asserts that light intensity travelling through a medium decreases exponentially due to absorption by the medium. IR spectroscopy is the technique of choice here because the main vibration modes of water molecules are in the IR wavelength range, so IR light can be easily absorbed by water molecules. In brief, the WS-CRDS principle is the following: the water sample is evaporated in a cavity surrounded by mirrors with very high reflectivity in order to increase the mean path length of photons up to kilometers. An infrared laser beam is sent through the cavity, reflects multiple times on the mirrors until reaching a steady state. Once reached, the laser is switched off and the light starts to decay. This decay is measured by a photo-detector and depends on the sample isotopic composition. Additional details about the method can be found in *Mariani (2013)* and *Wendl (2014)*.

3.5 Summary of the analytical work

Table 3.3: Summary of the analytical work carried out in the framework of the *PaleoFire* project (IC: ion chromatography, WSI: water stable isotopes).

Ice-core site	Drilling year	rBC sampling	rBC resolution	Replicates[1]	Chemical analyses[2]	Charcoal samples
Lomonosovfonna	2009	Previously done *(4046 samples)*	3–4 cm	120 (6 sections)	rBC	Not done
	2011	Previously done *(155 samples)*	4 cm	No	rBC	Not done
Illimani	1999	Upper 33.15 m (1966–1999 AD) previously done *(316 samples)* Rest of the core *(2754 samples)* Resampling section 0–2000 BC *(121 samples)*	10 cm 3–4 cm 3–7 cm	No 243 (12 sections) No	rBC + IC + WSI rBC + WSI rBC + IC + WSI	121 (entire core)
	2015	Entire core *(487 samples)*	5–6 cm	13 (1 section)	rBC + IC + WSI	21 (entire core)
Colle Gnifetti	2003	Upper 72.1 m (1039–2002 AD) *(2276 samples)*	2–5 cm	362 (19 sections)	rBC + IC	172 (upper 72.1 m)
	2015	Upper 11.9 m (2001–2015 AD) *(276 samples)*	4–5 cm	14 (1 section)	rBC + IC + WSI	18 (upper 11.9 m)
Tsambagarav	2009	Previously done *(2944 samples, but samples 1–1076 refrozen)* Resampling upper 28.1 m (1945–2009 AD) *(580 samples)*	2–2.5 cm 4–7 cm	185 (7 sections) 66 (4 sections)	rBC rBC + IC	261 (upper 69.6 m)

---

[1] Replicates for rBC analysis have not been cut in previous works and were therefore all prepared in the framework of the *PaleoFire* project.

[2] IC measurements were performed on the same samples as rBC, following rBC analysis. For WSI measurements, a 1 mL aliquot was taken after melting of the rBC samples, prior to rBC analysis.

References

Araguás-Araguás, L., Froehlich, K., and Rozanski, K.: Deuterium and oxygen-18 isotope composition of precipitation and atmospheric moisture, Hydrological Processes, 14(8), 1341–1355, 2000.

Baumgardner, D., Popovicheva, O., Allan, J., Bernardoni, V., Cao, J., Cavalli, F., Cozic, J., Diapouli, E., Eleftheriadis, K., Genberg, P. J., Gonzalez, C., Gysel, M., John, A., Kirchstetter, T.W., Kuhlbusch, T. A. J., Laborde, M., Lack, D., Müller, T., Niessner, R., Petzold, A., Piazzalunga, A., Putaud, J. P., Schwarz, J., Sheridan, P., Subramanian, R., Swietlicki, E., Valli, G., Vecchi, R., and Viana, M.: Soot reference materials for instrument calibration and intercomparisons: a workshop summary with recommendations, *Atmospheric Measurement Techniques*, 5, 1869–1887, 2012.

Brugger, S. O., Gobet, E., Schanz, F. R., Heiri, O., Schwörer, C., Sigl, M., Schwikowski, M., and Tinner, W.: A quantitative comparison of microfossil extraction methods from ice cores, *Journal of Glaciology*, 64(245), 432–442, 2018.

Brugger, S. O., Gobet, E., Sigl, M., Osmont, D., Papina, T., Rudaya, N., Schwikowski, M., and Tinner, W.: Ice records provide new insights into climatic vulnerability of Central Asian forest and steppe communities, *Global and Planetary Change*, 2018, in review.

Cross, E. S., Onasch, T. B., Ahern, A., Wrobel, W., Slowik, J. G., Olfert, J., Lack, D. A., Massoli, P., Cappa, C. D., Schwarz, J. P., Spackman, J. R., Fahey, D. W., Sedlacek, A., Trimborn, A., Jayne, J. T., Freedman, A.,Williams, L. R., Ng, N. L., Mazzoleni, C., Dubey, M., Brem, B., Kok, G., Subramanian, R., Freitag, S., Clarke, A., Thornhill, D., Marr, L. C., Kolb, C. E., Worsnop, D. R., and Davidovits, P.: Soot particle studies – instrument intercomparison – project overview, *Aerosol Science and Technology*, 44, 592–611, 2010.

Eichler, A., Schwikowski, M., Gäggeler, H. W., Furrer, V., Synal, H.-A., Beer, J., Saurer, M., and Funk, M.: Glaciochemical dating of an ice core from upper Grenzgletscher (4200m a.s.l.), *Journal of Glaciology*, 46, 507–515, 2000.

Ginot, P., Stampfli, F., Stampfli, D., Schwikowski, M., and Gäggeler, H. W.: FELICS, a new ice core drilling system for high-altitude glaciers, *Memoirs of National Institute of Polar Research Special Issue*, 56, 38–48, 2002.

Gysel, M., Laborde, M., Olfert, J. S., Subramanian, R., and Gröhn, A. J.: Effective density of Aquadag and fullerene soot black carbon reference materials used for SP2 calibration, *Atmospheric Measurement Techniques*, 4, 2851–2858, 2011.

Herren, P.-A.: Ice core based climate reconstruction from the Mongolian Altai, PhD thesis, University of Bern, 2013.

Laborde, M., Mertes, P., Zieger, P., Dommen, J., Baltensperger, U., and Gysel, M.: Sensitivity of the Single Particle Soot Photometer to different black carbon types, *Atmospheric Measurement Techniques*, 5, 1031–1043, 2012.

Lim, S., Faïn, X., Zanatta, M., Cozic, J., Jaffrezo, J.-L., Ginot, P., and Laj, P.: Refractory black carbon mass concentrations in snow and ice: method evaluation and inter-comparison with elemental carbon measurement, *Atmospheric Measurement Techniques*, 7, 3307–3324, 2014.

Mariani, I.: Water stable isotopes in Alpine ice cores as proxies for temperature and atmospheric circulation, PhD thesis, University of Bern, 2013.

Moteki, N. and Kondo, Y.: Effects of mixing state on black carbon measurements by laser-induced incandescence, *Aerosol Science and Technology*, 41, 398–417, 2007.

Schläppi, M.: Accumulation rates and chemical composition of precipitation derived from Pío XI ice core, Southern Patagonia Icefield, PhD thesis, University of Bern, 2010.

Schmidely, L.: A 250-years black carbon record spanning the industrial era from the Lomo09 ice core, Svalbard, Master thesis, University of Bern, 2015.

Schwarz, J. P., Gao, R. S., Fahey, D. W., Thomson, D. S., Watts, L. A., Wilson, J. C., Reeves, J. M., Darbeheshti, M., Baumgardner, D. G., Kok, G. L., Chung, S. H., Schulz, M., Hendricks, J., Lauer, A., Kärcher, B., Slowik, J. G., Rosenlof, K. H., Thompson, T. L., Langford, A. O., Loewenstein, M., and Aikin, K. C.: Single-particle measurements of midlatitude black carbon and light-scattering aerosols from the boundary layer to the lower stratosphere, *Journal of Geophysical Research*, 111, D16207, 2006.

Schwarz, J. P., Doherty, S. J., Li, F., Ruggiero, S. T., Tanner, C. E., Perring, A. E., Gao, R. S., and Fahey, D. W.: Assessing Single Particle Soot Photometer and Integrating Sphere/Integrating Sandwich Spectrophotometer measurement techniques for quantifying black carbon concentration in snow, *Atmospheric Measurement Techniques*, 5, 2581–2592, 2012.

Single Particle Soot Photometer (SP2): Operator Manual, Droplet Measurement Technologies, Inc., Boulder, CO, USA, 2013.

Slowik, J. G., Cross, E. S., Han, J. H., Davidovits, P., Onasch, T. B., Jayne, J. T., Williams, L. R., Canagaratna, M. R., Worsnop, D. R., Chakrabarty, R. K., Moosmüller, H., Arnott, W. P., Schwarz, J. P., Gao, R.-S., Fahey, D. W., Kok, G. L., and Petzold, A.: An inter-comparison of instruments measuring black carbon content of soot particles, *Aerosol Science and Technology*, 41, 295–314, 2007.

Stephens, M., Turner, N., and Sandberg, J.: Particle identification by laser-induced incandescence in a solid-state laser cavity, *Applied Optics*, 42(19), 3726–3736, 2003.

Vega, C. P., Björkman, M. P., Pohjola, V. A., Isaksson, E., Pettersson, R., Martma, T., Marca, A. D., and Kaiser, J.: Nitrate stable isotopes and major ions in snow and ice samples from four Svalbard sites, *Polar Research*, 34, 23246, 2015.

Wendl, I. A.: High resolution records of black carbon and other aerosol constituents from the Lomonosovfonna 2009 ice core, PhD thesis, University of Bern, 2014.

Wendl, I. A., Menking, J. A., Färber, R., Gysel, M., Kaspari, S. D., Laborde, M. J. G., and Schwikowski, M.: Optimized method for black carbon analysis in ice and snow using the Single Particle Soot Photometer, *Atmospheric Measurement Techniques*, 7, 2667–2681, 2014.

4 An 800-year high-resolution black carbon ice core record from Lomonosovfonna, Svalbard

Dimitri Osmont[1,2,3], Isabel A. Wendl[1,2,3], Loïc Schmidely[2,4], Michael Sigl[1,2], Carmen P. Vega[5,a], Elisabeth Isaksson[6], Margit Schwikowski[1,2,3]

[1]Laboratory of Environmental Chemistry, Paul Scherrer Institut, 5232 Villigen, Switzerland
[2]Oeschger Centre for Climate Change Research, University of Bern, 3012 Bern, Switzerland
[3]Department of Chemistry and Biochemistry, University of Bern, 3012 Bern, Switzerland
[4]Climate and Environmental Physics, University of Bern, 3012 Bern, Switzerland
[5]Department of Earth Sciences, Uppsala University, 752 36 Uppsala, Sweden
[6]Norwegian Polar Institute, Fram Centre, 9296 Tromsø, Norway
[a]now at: School of Physics and Centre for Geophysical Research, University of Costa Rica, 11501-2060, San José, Costa Rica

Correspondence to: Margit Schwikowski (margit.schwikowski@psi.ch)

Abstract

Produced by the incomplete combustion of fossil fuel and biomass, black carbon (BC) contributes to Arctic warming by reducing snow albedo and thus triggering a snow-albedo feedback leading to increased snowmelt. Therefore, it is of high importance to assess past BC emissions to better understand and constrain their role. However, only a few long-term BC records are available from the Arctic, mainly originating from Greenland ice cores. Here, we present the first long-term and high-resolution refractory black carbon (rBC) record from Svalbard, derived from the analysis of two ice cores drilled at the Lomonosovfonna ice field in 2009 (LF-09) and 2011 (LF-11) and covering 800 years of atmospheric emissions. Our results show that rBC concentrations strongly increased from 1860 on due to anthropogenic emissions and reached two maxima, at the end of the 19th century and in the middle of the 20th century. No increase in rBC concentrations during the last decades was observed, which is corroborated by atmospheric measurements elsewhere in the Arctic but contradicts a previous study from another ice core from Svalbard. While melting may affect BC concentrations during periods of high temperatures, rBC concentrations remain well preserved prior to the 20th century due to lower temperatures inducing little melt. Therefore, the preindustrial rBC record (before 1800), along with ammonium (NH_4^+), formate ($HCOO^-$) and specific organic markers (vanillic acid, VA, and *p*-hydroxybenzoic acid, *p*-HBA), was used as a proxy for biomass burning. Despite numerous single events, no long-term trend was observed over the time period 1222–1800 for rBC and NH_4^+. In contrast, formate, VA, and *p*-HBA experience multi-decadal peaks reflecting periods of enhanced biomass burning. Most of the background variations and single peak events are corroborated by other ice core records from Greenland and Siberia. We suggest that the paleofire record from the LF ice core primarily reflects biomass burning episodes from northern Eurasia, induced by decadal-scale climatic variations.

4.1 Introduction

In the last decades, the Arctic region has experienced the strongest surface air temperature increases globally, referred to as the Arctic amplification *(Serreze and Barry, 2011)*, leading to a range of

severe consequences for glaciers, sea ice, wildlife, and local human societies and partially explained by strong snow and sea ice feedbacks implying surface albedo changes. Black carbon (BC) is one of the substances involved in this process. BC consists of aggregates of carbonaceous spherules produced in the form of aerosols by the incomplete combustion of fossil fuel and biomass. BC does not refer to a single well-defined compound because carbonaceous aerosols are emitted in the form of a continuum of compounds with different physical and chemical properties *(Goldberg, 1985)*, leading to a complex terminology depending on the method used for its quantification. Here we follow the recommendations given by *Petzold et al. (2013)* and will use the term rBC (refractory black carbon) when referring to our measurements carried out with the laser-induced incandescence method. BC possesses some unique properties: it is highly refractory, strongly absorbs visible light and has a very low chemical reactivity *(AMAP, 2011a; Bond et al., 2013)*. Its strong absorptive ability impacts the Earth radiative budget and contributes to global warming via three main effects: a direct radiative forcing by sunlight absorption in the atmosphere, a modification of cloud properties whose mechanisms remain poorly understood, and a snow and ice forcing when BC is deposited on those surfaces, thus lowering their albedo and triggering melting *(Bond et al., 2013, Hansen and Nazarenko, 2004)*. This latter effect is of great importance in the Arctic because most of the surface is permanently covered with snow and ice and BC concentrations in snow normally peak in spring, due to the Arctic haze phenomenon *(Quinn et al., 2007; Shaw, 1995)*, when daylight hours increase considerably and mean surface air temperatures rise *(Flanner et al., 2007)*. BC could be the second largest contributor to global warming after carbon dioxide *(Ramanathan and Carmichael, 2008)*. However, given its short atmospheric lifetime from days to weeks, BC impacts can be considerably lowered when mitigation strategies are implemented *(Bond et al., 2013)*.

Current global BC emissions are dominated by anthropogenic sources including industry, energy production, diesel engines and residential biofuel uses. While Western countries were responsible for most of the BC emissions until the mid-20th century, emerging economies in Asia are currently the major contributors *(Bond et al., 2007, 2013)*. Conversely, before the beginning of the Industrial Revolution, biomass burning sources were largely predominant *(Bond et al., 2013)*, encompassing wildfires and wood burning for heating, cooking and agricultural purposes. These general trends have been confirmed by recent ice core records from Greenland *(Keegan et al., 2014; McConnell et al., 2007; Sigl et al., 2013)*, the Himalayas *(Jenkins et al., 2016; Kaspari et al., 2011)*, the Caucasus *(Lim et al., 2017)* and the Alps *(Jenk et al., 2006)*. However, detailed source attribution remains difficult because every record is the synthesis of a wide range of BC emission sources, transport, deposition and post-deposition processes. Therefore, more ice core records are needed to achieve a finer spatial and temporal representativeness of BC in the Arctic, which can be used to better constrain climate–aerosol model simulations *(Bauer et al., 2013; Lee et al., 2013)*.

The Svalbard archipelago, located 700 km north of mainland Norway, is of great interest within the Arctic because it is subject to air masses originating from different sources compared to Greenland **(Fig. 4.1)**. While it is commonly assumed that North America is the dominant source region of air masses reaching Greenland *(Fuhrer et al., 1996; Legrand et al., 2016; Shindell et al., 2008)*, an attribution supported by ammonium *(Fischer et al., 2015)* and BC records *(McConnell et al., 2007)* from Greenland ice cores, atmospheric and ice core data from Svalbard rather reflect emissions from Eurasia *(Eleftheriadis et al., 2009; Goto-Azuma and Koerner, 2001; Tunved et al., 2013)*. *Hirdman et al. (2010a)* showed that northern Eurasia is the dominating source of the BC detected at Zeppelin station in Ny-Ålesund **(Fig. 4.1a)** over the entire year, with an influence from Siberian boreal forest fires in summer. Therefore BC data from Svalbard are useful to better disentangle the sources of Arctic BC. Several snow studies have already been conducted in Svalbard in order to assess the BC

impact on surface albedo *(Clarke and Noone, 1985; Doherty et al., 2010; Forsström et al., 2009, 2013)* and the contribution from local BC sources such as coal mining *(Aamaas et al., 2011)* **(Table 4.1)**. Atmospheric BC concentrations at Zeppelin station show a decreasing trend in the most recent years *(Eleftheriadis et al., 2009; Hirdman et al., 2010b)*, confirmed elsewhere in the Arctic *(Dutkiewicz et al., 2014; Gong et al., 2010; Sharma et al., 2004)*. However, only one long-term ice core record, drilled at Holtedahlfonna (HDF) **(Fig. 4.1a)**, is available from Svalbard, based on the analysis of elemental carbon (EC), a proxy for BC obtained by thermal-optical measurements *(Ruppel et al., 2014)*. Like the Greenland BC records, the record from HDF shows anthropogenic BC emissions starting in the second half of the 19th century and peaking around 1910. A recent and unexpected EC increase is also visible from 1970 onwards, contradicting atmospheric data and remaining partially unexplained *(Ruppel et al., 2014)*. Several hypotheses have been discussed, such as increased flaring emissions from Siberia *(Stohl et al., 2013)* or changes in BC scavenging efficiencies due to higher temperatures. However, in a more recent study on a shallow firn core from the same ice field, no comparable recent increase could be detected *(Ruppel et al., 2017)*.

Like other low elevation sites in the Arctic, Svalbard glaciers experience recurrent summer melting, which can alter the ice core records due to water percolation through the snowpack, leading to relocation of chemical compounds or even runoff in the warmest years. *Pohjola et al. (2002)* and *Vega et al. (2016)* concluded that most of the atmospheric signal was preserved at an annual, or in the worst cases, at a biannual resolution in the Lomonosovfonna 1997 (LF-97) and 2009 (LF-09) ice cores. *Moore et al. (2005)* also confirmed that chemical stratigraphy remained preserved despite high melt ratios. More recently, the impact of melting on the HDF ice core was assumed to be low compared to the EC deposition signal *(Ruppel et al., 2014, 2017)*. Similar findings were postulated for the Lomonosovfonna 2009 (LF-09) ice core in which melting impact was negligible on ionic species at a decadal resolution *(Wendl et al., 2015)*. However, it can become an issue when dealing with high-resolution records: *Kekonen et al. (2005)* found percolation lengths of up to 8 years for the warmest periods and half of the variance of the chemical dataset at those sites can be explained by post-depositional effects *(Beaudon et al., 2013)*.

Other covarying proxies can also be used to help disentangle the BC origin. Non-sea salt sulfate (nss-SO_4^{2-}) and nitrate (NO_3^-) are well-known tracers of anthropogenic pollution reaching Svalbard during the 20th century. These ions originate from increased SO_2 and NO_x emissions from Eurasia *(Goto-Azuma and Koerner, 2001; Matoba et al., 2002; Wendl et al., 2015)*. Nitrate stable isotopes (δ^{15}N-NO_3^-) measured in Svalbard ice cores have been used to apportion NO_x sources associated with forest fires and anthropogenic activity *(Vega et al., 2015a)*. Ammonium (NH_4^+) has been widely used in polar ice cores to reconstruct past biomass burning activity *(Fischer et al., 2015; Legrand et al., 2016)*. Formate ($HCOO^-$) is another appropriate proxy, despite post-depositional effects *(Legrand et al., 2016)*. Specific organic tracers of biomass burning such as vanillic acid (VA), levoglucosan or *p*-hydroxybenzoic acid (*p*-HBA) have also been recently introduced *(Grieman et al., 2015, 2017, 2018; Kawamura et al., 2012; Kehrwald et al., 2012; McConnell et al., 2007; Zennaro et al., 2014)*. In Arctic ice cores, while VA is rather associated with conifer and deciduous boreal tree burning, *p*-HBA is thought to be predominantly emitted by tundra grass and peat burning *(Grieman et al., 2018)*. However, little is known about their potential degradation in the atmosphere and their sensitivity to post-depositional processes, and their stability in the atmosphere has been recently questioned *(Hennigan et al., 2010; Hoffmann et al., 2010)*.

Here we present the first long-term and high-resolution rBC record from Svalbard, obtained by Single Particle Soot Photometer (SP2) analysis of two ice cores drilled on the Lomonosovfonna ice field in 2009 (LF-09) and 2011 (LF-11), further referred to as LF when both records are combined. After

focusing on the anthropogenic imprint and its source attribution since the mid-19th century, we will discuss the impact of snowmelt on the record during the 20th century and finally we will reconstruct paleofire trends by using the preindustrial rBC record along with other biomass burning proxies.

4.2 Methods

4.2.1 Drilling site and ice core characteristics

Lomonosovfonna is one of the highest ice fields in Svalbard **(Fig. 4.1)**, reaching 1250 m a.s.l. in its accumulation area *(Isaksson et al., 2001)*. For this reason, it is less affected by summer melting and meltwater percolation than other low-elevation glacier sites in Svalbard *(Gordiyenko et al., 1981; Pohjola et al., 2002)*, making it suitable for ice core studies. Therefore this site has already been regularly studied in the past. Two deep ice cores were retrieved in 1976 and 1982 by pioneering Soviet expeditions, mainly for stratigraphic purposes *(Gordiyenko et al., 1981; Zagorodnov et al., 1984)*. The first extensive study that retrieved both physical and chemical records from the ice was conducted on a deep ice core drilled in 1997 by an international team *(Isaksson et al., 2001)*.

In March 2009, using the Fast Electromechanical Lightweight Ice Coring System (FELICS) *(Ginot et al., 2002)*, a Norwegian–Swedish–Swiss team drilled a 149.5 m long ice core on Lomonosovfonna at 1202 m a.s.l. (78°49´24.4´´ N, 17°25´59.2´´ E), 4.6 km south of the 1997 drilling site, which could not be accessed due to the opening of a large crevasse. Bedrock at about 200 m of depth was not reached during the drilling. Further details about the drilling and the meteorological setting can be found in *Wendl et al. (2015)*. This ice core was then shipped frozen to the Paul Scherrer Institute (PSI) in Switzerland. In addition to the LF-09 ice core, a 7.6 m shallow firn core was retrieved in April 2011 ~110 m to the north and ~20 m to the west of the LF-09 site by a team from the Uppsala University and processed at the Norwegian Polar Institute (NPI) in Tromsø *(Vega et al., 2015b)*.
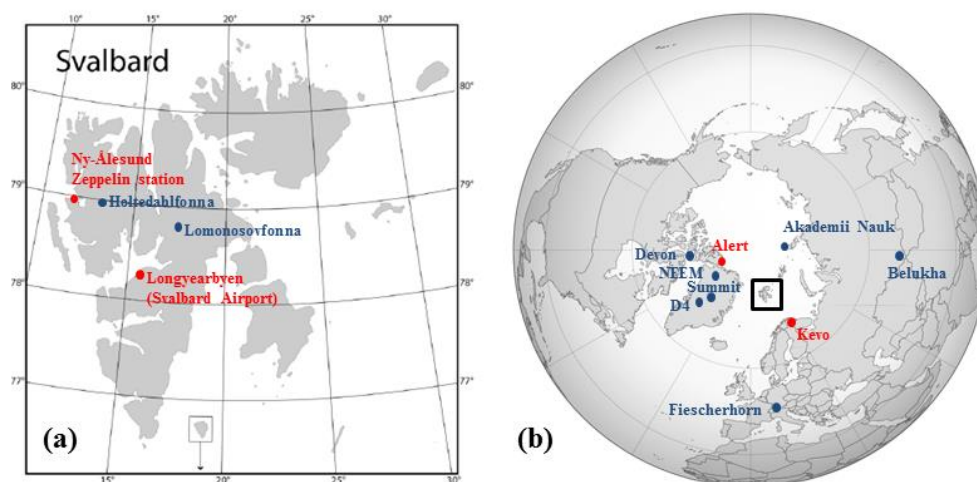
Fig. 4.1: a) Map of Svalbard with the location of the sites of interest (adapted from *Wendl et al., 2015*). b) Map with the other sites of interest mentioned in this study. Ice core sites are in blue and atmospheric measurement stations in red.

4.2.2 Sampling, chemical analyses and dating

The LF-09 ice core was processed in a −20 °C cold room at PSI following well-established procedures *(Eichler et al., 2000)*. In total, 3997 samples were cut at 3–4 cm resolution, which

corresponds to about monthly resolution at the top of the core to annual resolution at the bottom. The dating was performed using a multi-parameter approach including annual layer counting of the $\delta^{18}O$ and Na^+ signals back to 1750, ^{210}Pb decay, a two-parameter fit and absolute reference horizons such as volcanic eruptions (sulfate peaks) and the well-documented 1963 tritium peak *(Wendl et al., 2015)*. The LF-09 ice core thus spans the time period from 1222 to 2009, with an average accumulation rate of 0.58 ± 0.13 m yr^{-1} of water equivalent (weq). The dating uncertainty was assessed to be ± 1 year in the vicinity of the reference horizons and ± 3 years in between up to 68 m weq of depth, ± 3 years in both cases between 68 and 80 m weq, and ± 10 years below 80 m weq *(Wendl et al., 2015)*. *Wendl et al. (2015)* also determined the annual melt percent by calculating the relative thickness of the melt features (i.e. ice lenses) for each year. For rBC analysis, two parallel samples from the inner part of the core were combined in a 50 mL polypropylene vial. When the two samples were too long to fit in a single vial, the cutting resolution was increased, overall resulting in 4046 samples. As the first 110 samples had been melted and refrozen prior to analysis, leading to potential rBC losses *(Wendl et al., 2014)*, they were not considered in this study. Thus, the 2005–2009 time period is not covered by the LF-09 rBC record. In addition, VA and *p*-HBA were analyzed in the whole LF-09 ice core by *Grieman et al. (2018)*.

The LF-11 ice core was cut at 4 cm resolution following clean protocols, resulting in a total of 155 samples *(Vega et al., 2015b)*. The dating was performed by counting $\delta^{18}O$ annual cycles using the winter minimum as a reference and by matching prominent ion peaks with those from the LF-09 ice core *(Vega et al., 2015b, 2016)*. The LF-11 core thus spans the time period from 2004 to 2011, with an average accumulation rate of 0.49 m weq yr^{-1}.

4.2.3 rBC analysis

The entire LF-09 core and the LF-11 core were analyzed for rBC at PSI in several campaigns between 2012 and 2016 and in April–May 2016, respectively, following the procedure established by *Wendl et al. (2014)* for liquid samples and further evaluated by *Lim et al. (2014)*. Discrete rBC samples were melted at room temperature, sonicated in a ultrasonic bath for 25 min, and immediately analyzed by using a SP2 (Droplet Measurement Technologies, USA) *(Schwarz et al., 2006; Stephens et al., 2003)* coupled with a jet nebulizer (APEX-Q, Elemental Scientific Inc., USA). External calibrations from 0.1 to 50 ng g^{-1} (R^2 > 0.999) were usually performed twice a week by preparing eight fresh dilutions from a rBC standard (Aquadag®, Acheson Industries, Inc., USA) *(Gysel et al., 2011; Wendl et al., 2014)*. Before and after every day of measurements, the APEX-Q and the upstream capillaries were rinsed for 10 min with a solution of 3 % nitric acid prepared with ultrapure water (Sartorius, ≥18.2 MΩ cm, with a 0.2 μm filter). The liquid flow rate of the APEX-Q was monitored several times per day to avoid changes in the nebulizing efficiency, which can impact the rBC detection. When the flow rate was not steady (i.e. presented fluctuations larger than ± 10 %), the measurements were stopped. The instrumental blank was checked between every sample by rinsing the setup with ultrapure water until the rBC signal returned to the baseline value of 0–1 particle cm^{-3}. The limit of detection (LOD) was estimated by measuring ultrapure water blanks 10 times and by calculating their average plus 3 times their standard deviation, leading to a value of 0.051 ng g^{-1} of rBC. The procedure blank was controlled by analyzing frozen ultrapure water treated in the same way as ice core samples. Its value was always below the LOD (typically 0.01 ng g^{-1} of rBC), which confirms the adequate cleanliness level of the analytical procedure. In addition, six series of 20 replicate samples were cut from parallel ice core sticks and were analyzed **(Fig. 4.2a)**, showing a high level of reproducibility between original and replicate samples (r = 0.73, p < 0.001, n = 120, and averaged relative error for the 120 samples: 23 %).

Only the first 900 LF-09 samples were manually analyzed. Then a CETAC ASX-520 autosampler (CETAC Technologies, USA) was implemented in order to speed up the measurements and improve their reproducibility. Total rBC particle counting was kept to 10 000 as recommended (Schwarz et al., 2012), the limiting condition being a measuring time between 1 and 30 min. The autosampler probe was rinsed with ultrapure water for 45 sec between each sample and the waiting time in each vial before data acquisition was set to 1 min 45 sec, which turned out to be sufficient for the background signal to become stable. However, some difficulties arose from the fact that rBC concentrations tend to decrease with time due to particles sticking to the walls and agglomerating beyond the SP2 detection range, which implies that rBC samples have to be measured as fast as possible after sonication *(Lim et al., 2014; Wendl et al., 2014)*. We therefore studied the rBC degradation with time by using 24 ice core samples from Lomonosovfonna and the Swiss Alps (Colle Gnifetti and Fiescherhorn ice cores). Each sample was measured between 5 and 14 times (depending on the concentration) over 24 hours. They all showed a similar decreasing trend, largely independent of the ice core site, the rBC or dust concentrations. On average, the relative apparent rBC loss was 41 ± 9 % after 24 hours, and 10 ± 6 % after 6 hours, which was thus defined as the maximum waiting time considered as acceptable. To take this decrease into account, a linear regression was performed and a systematic correction as a function of time was implemented as follows:

$$[rBC]_{\text{corrected}} = \frac{[rBC]_{\text{measured}}}{1 - 0.017\,t}$$

where $[rBC]_{\text{corrected}}$ is the original rBC concentration at the initial time (t_0), i.e., the end of the sonication (ng g^{-1}), $[rBC]_{\text{measured}}$ is the rBC concentration measured by the SP2 (ng g^{-1}), and t is the time in hours (h) elapsed since the end of the sonication.

4.2.4 BC emission inventories

Historical BC emission inventories reconstructing past emissions and atmospheric loading are used to compare the LF rBC record with estimated trends in anthropogenic BC produced by fossil fuel and biomass combustion in order to carry out source apportionment. Here, we use the BC emission inventory from *Bond et al. (2007)* available at 5-year resolution, between 1850 and 2000, for countries or areas identified as potential BC source regions: Canada, the USA, OECD Europe, eastern Europe, and the former USSR. This inventory includes emissions from fossil fuel and biofuel combustion, but does not include open burning such as wildfires, which contribute to a substantial part of the Arctic BC burden in summer *(Stohl, 2006)*.

4.2.5 Paleofire detection

Our approach to detect years with increased forest fire activity in the LF-09 ice core follows the methodology proposed by *Fischer et al. (2015)*, which basically uses an outlier detection approach. From the annual averages, 31-year moving medians were created. For each year, the residues between the median and average were calculated. Median absolute deviations were obtained by averaging the residues over the whole LF-09 time period for specific fire proxies (VA, *p*-HBA) or proxies showing little anthropogenic influence (formate), and between 1222 and 1800 for proxies influenced by anthropogenic emissions (rBC, ammonium). Then a fire threshold was defined as the median plus 3 times the median absolute deviation, in such a way that this threshold takes background variations into account, which is of prime importance in the case of nonspecific proxies having other sources than biomass burning, such as biogenic emissions in the case of formate *(Legrand and De Angelis, 1996)* and ammonium *(Eichler et al., 2009; Fischer et al., 2015; Kellerhals et al., 2010)*. Every annual average above this threshold can thus be considered a year with significant biomass burning

emissions, and finally the centennial frequency of such episodes was obtained. As peaks can be smeared out over several years because of layer thinning with depth and post-depositional processes, a correction for neighboring outliers was implemented: a proxy signal exceeding the detection threshold over several consecutive years was considered to be a single episode and counted only once. As VA and p-HBA were available at lower resolution than the other species *(Grieman et al., 2018)*, annual resolution was sometimes not achieved in the deepest part of the ice core and therefore missing year values were obtained by linear interpolation between the adjacent years.

4.3 Results and discussion

4.3.1 High-resolution rBC record

Here we present the long-term and high-resolution rBC record from Svalbard derived from the combination of the LF-09 and LF-11 ice cores spanning the time periods 1222–2004 and 2004–2011, respectively **(Fig. 4.2a)**. In the LF-09 ice core, rBC concentrations are generally low with a range between the LOD (i.e., 0.051 ng g^{-1}) up to 39.0 ng g^{-1} in 1980, an average of 1.2 ± 2.3 ng g^{-1} (uncertainties are given as ± 1σ unless otherwise stated) and a median of 0.6 ng g^{-1}. Nominal sub-annual resolution was achieved for the entire time period, with a monthly resolution back to about 1930. Such a high resolution enables us to disentangle seasonal variations in the rBC ice core signal. Ice core rBC concentrations in Greenland *(McConnell et al., 2007)* as well as atmospheric BC concentrations at the Zeppelin station *(Eleftheriadis et al., 2009)* show a clear seasonal cycle with higher BC values in winter–early spring due to the Arctic haze phenomenon *(Shaw et al., 1995)*. However, despite a fine resolution and contrary to other parameters such as δ^{18}O or Na$^+$ concentration, a clear seasonality of rBC in the LF-09 core, i.e. with winter maxima (Arctic Haze) and some summer peaks (biomass burning) *(Hirdman et al., 2010a; Stohl, 2006)* was not observed on a regular basis, probably due to summer snowmelt affecting the rBC signal *(see section 4.3.3)*.

The rBC concentrations in the LF-11 ice core are comparable to preindustrial values (before 1800) measured in the LF-09 ice core, with an average of 0.5 ± 0.4 ng g^{-1}, a median of 0.3 ng g^{-1} and a range from LOD to 2.4 ng g^{-1}. This does not seem to be related to spatial variability as the two records show similar rBC concentrations in the overlapping year 2004 **(Fig. 4.2b)** but is related to an overall decreasing trend in BC emissions in the source regions. An analogous clear drop was also observed in the HDF EC concentrations *(Ruppel et al., 2017)* in a recent shallow core spanning 2005–2015 **(Table 4.1)** compared to the original HDF ice core covering 1700–2004 *(Ruppel et al., 2014)*. The very low rBC concentrations in the LF-11 core compared to the EC concentrations around local sources of contamination in Svalbard such as settlements and mining activities with values higher than 1000 ng g^{-1} for some samples *(Aamaas et al., 2011)* underlines that rBC contribution from local anthropogenic sources to the LF drill site appears to be minimal, at least for the most recent years.
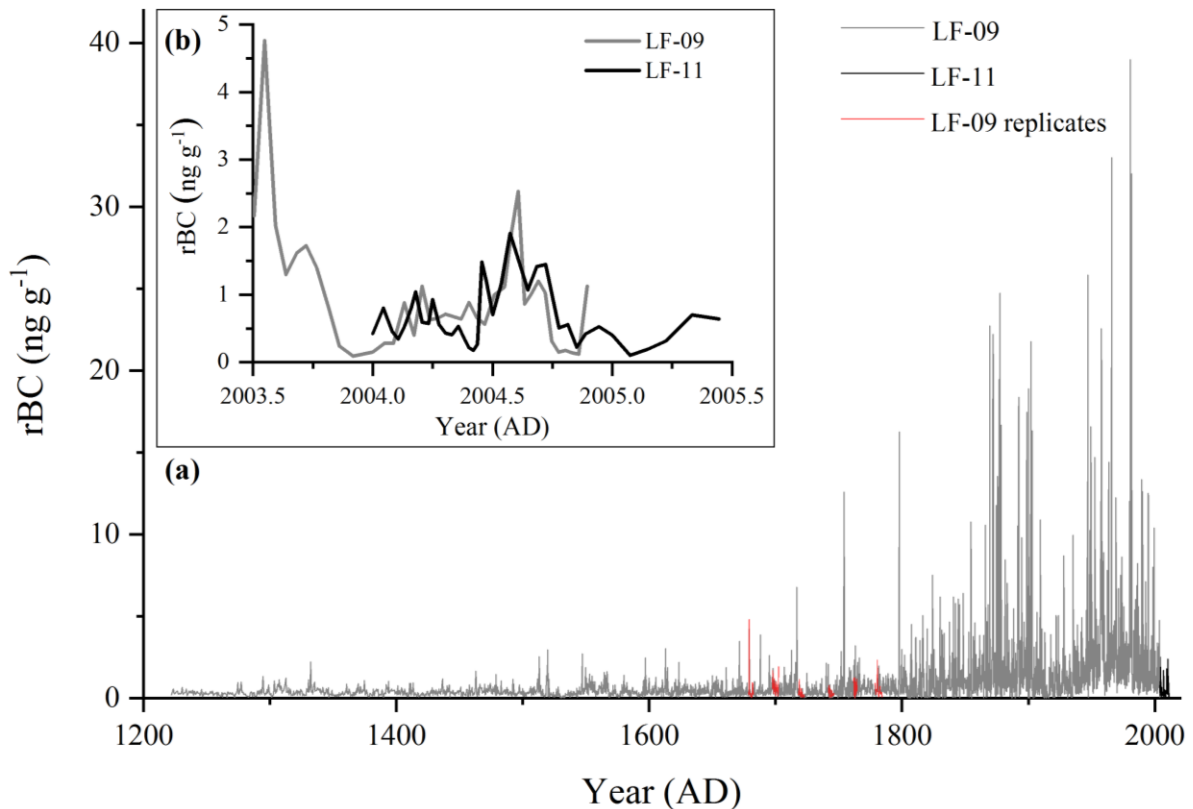
Fig. 4.2: rBC raw data from the LF-09 and LF-11 cores, a) combined for the entire records, spanning 1222–2011 and including the replicate measurements and b) showing the overlap between the two ice cores for the year 2004.

LF rBC concentrations are very similar to those observed in Greenland and Canadian Arctic ice cores obtained by SP2 analyses *(Keegan et al., 2014; McConnell et al., 2007; Sigl et al., 2013; Zdanowicz et al., in review)* **(Table 4.1)**. However, EC concentrations in Svalbard snow *(Aamaas et al., 2011; Doherty et al., 2010; Forsström et al., 2009, 2013)* as well as in the HDF and Fiescherhorn ice cores *(Jenk et al., 2006; Ruppel et al., 2014, 2017)* are 1 order of magnitude higher than rBC concentrations in the topmost part of the LF core. This can be mainly explained by the different analytical methods employed, which do not measure the same fraction of the carbonaceous compounds, as discussed by *Ruppel et al. (2014)*. Whereas the SP2 does not detect rBC particles larger than 500 nm, the optical and thermal-optical methods include a filtration step in which the smallest fraction of EC particles is generally lost. *Lim et al. (2014)* reported significant variations in the EC/rBC ratios in snow and ice, ranging from 0.5 to 3.4 according to the sample origin. Furthermore, in the aforementioned studies, most of the EC snow samples from Svalbard were collected in winter–spring, when EC concentrations in fresh snow are higher due to the Arctic haze and have not yet experienced summer melting of the snowpack, contrary to the LF ice core samples.

Table 4.1: rBC or EC concentrations (italic) from different ice core and snow studies in the Arctic and in Europe.

Site	Reference	Method	Sample type	Time period	rBC or *EC concentrations* (ng g⁻¹) Average (if specified, median) ± 1σ and time range in ( )
Svalbard					
Various	Clarke & Noone, 1985	Optical	Snow	1983	*30.9 (median: 33.5) ± 16.0*
Lomonosovfonna	Forsström et al., 2009	Thermal-optical	Snow	Spring 2007	*18.8 (median: 6.6) ± 29.4*
Ny-Ålesund	Doherty et al., 2010	Optical	Snow	2007, 2009	*13 (median) ± 9*
Ny-Ålesund	Aamaas et al., 2011	Thermal-optical	Snow	Winter 2008	*6.6 ± 4.3*
Various	Forsström et al., 2013	Thermal-optical	Snow	2007–2009	*11.4-13.8 (medians)*
Holtedahlfonna	Ruppel et al., 2014	Thermal-optical	Ice core	1700–2004	*23 (<1850) – 36 (1850–1950) – 45 (>1950)*
	Ruppel et al., 2017	Thermal-optical	Ice core	2005–2015	*10.4*
Lomonosovfonna	This study	SP2	Ice core	1222–2004	0.5 (<1850), 1.9 (1851–1950), 2.9 (>1951)[a]
		SP2	Ice core	2004–2011	0.5 (median: 0.3) ± 0.4
Greenland					
D4	McConnell et al., 2007	SP2	Ice core	1788–2002	1.7 (<1850) – 4 (1851–1951) – 2.3 (>1952)[a]
NEEM 2011-S1	Sigl et al., 2013	SP2	Ice core	78–1997	2.9 (<1850) – 4.9 (1851–1951) – 3.0 (>1952)[a]
Summit 2010	Keegan et al., 2014	SP2	Ice core	1742–2010	1.0 (<1850) – 2.2 (1851–1951) – 1.1 (>1952)[a]
Canadian Arctic					
Devon Island	Zdanowicz et al., in review	SP2	Ice core	1810–1990	1.5 ± 3.2 (whole record) – 3.6 (1910–1920)
Swiss Alps					
Fiescherhorn	Jenk et al., 2006; Gabbi et al., 2015	Thermal-optical	Ice core	1660–2002	*15 (<1850) – 26 (1850–1950) – 20 (>1950)*

[a]: calculated from annual averages

4.3.2 Anthropogenic rBC signal in the Lomonosovfonna ice cores

4.3.2.1 rBC long-term trends

In **Fig. 4.3a** rBC annual averages and 11-year moving averages are presented to document long-term trends in the LF ice core record. The most striking feature is the increase in rBC concentrations and variability from 1800 on that we attribute to rising anthropogenic BC emissions. Before 1800, annual rBC concentrations were low, with an average of 0.4 ± 0.3 ng g⁻¹ for the time period 1222–1799. Only small decadal variations without a significant long-term trend were observed. We therefore consider the time period before 1800 to be representative of preindustrial atmospheric conditions. A few years displayed rBC peaks *(see section 4.3.4)* probably originating from atmospheric deposition from biomass burning plumes reaching the Arctic, as *McConnell et al. (2007)* and *Zennaro et al. (2014)* described for Northern Greenland, but annual rBC values did not exceed 4.7 ng g⁻¹ (maximum in 1797). A clear minimum occurred between 1520 and 1540 with annual values lower than 0.2 ng g⁻¹. The time period 1800–1859 showed a steady slow increase in the 11-year moving average, at an average rate of 0.009 ng g⁻¹ yr⁻¹, and a larger variability, with an average of 1.0 ± 0.7 ng g⁻¹. From 1860 on rBC concentrations and variability dramatically increased, reaching two maxima around 1870 and 1895, before concentrations started declining. rBC averages were 2.3 ± 1.7 ng g⁻¹ for the period 1860–1909, which represents about a 6-fold increase compared to the pre-1800 concentrations. This period was then followed by low concentrations and reduced variability between 1910 and 1939, with an average of 1.0 ± 0.3 ng g⁻¹. Another strong increase occurred after 1940 and the highest long-term rBC concentrations of the record were reached in the 1950s and 1960s (average for the time period 1940–1969: 3.2 ± 2.4 ng g⁻¹). Concentrations started to decline in the 1970s. This downward trend

was briefly interrupted by high concentrations registered for the years 1980–1981 and then resumed until the present time (average for the time period 1970–2010: 2.3 ± 2.3 ng g^{-1}).

To account for potential biases due to changes in accumulation rates, annual rBC fluxes were calculated by multiplying annual rBC concentrations by annual snow accumulation (**Fig. 4.3b**). Trends in the rBC flux and concentration records are almost the same (except that the highest fluxes were recorded in the 1870s), implying that accumulation has low variability and little impact on rBC long-term trends. Consequently, fluxes will not be considered in the remaining part of the study.
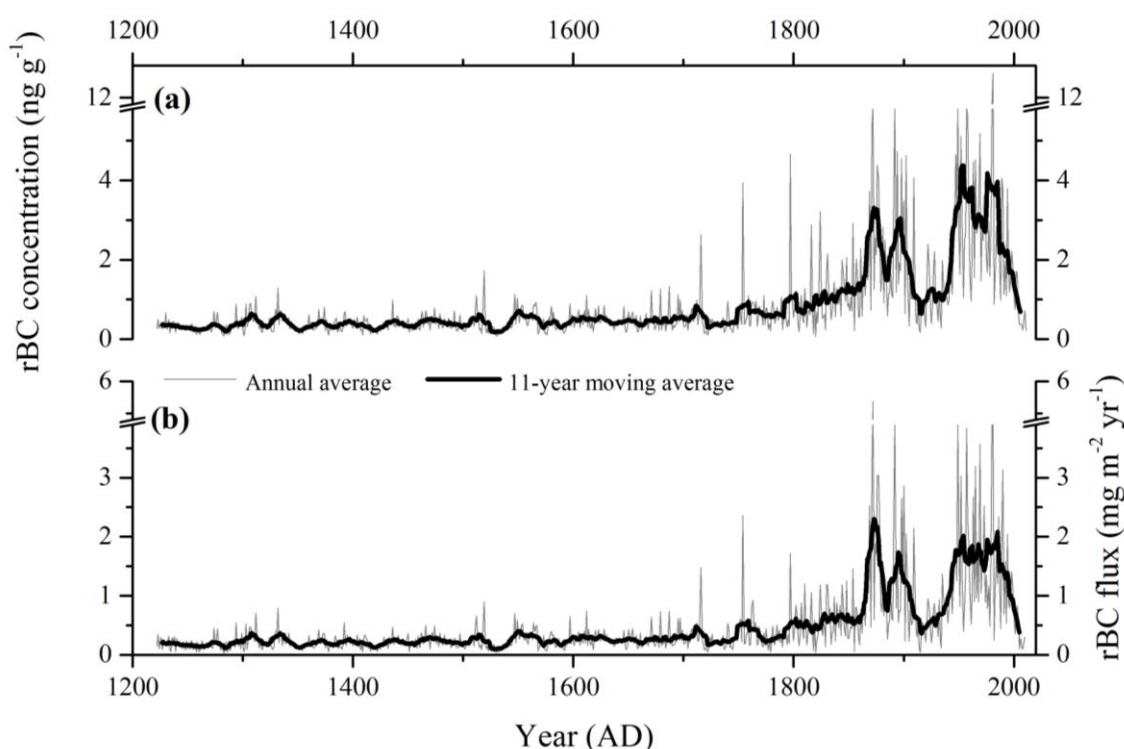

Fig. 4.3: The rBC long-term trends from the combined LF-09 and LF-11 cores, expressed as a) rBC concentrations and b) rBC fluxes.

We attribute an anthropogenic origin to the higher rBC concentrations after 1860, supported by a significant correlation (at the 0.05 confidence level) between rBC and other proxies for anthropogenic emissions in the LF-09 core, namely NO_3^- (**Fig. 4.4b**), non-sea-salt SO_4^{2-} (**Fig. 4.4c**), and, to a lesser extent, NH_4^+ (**Fig. 4.4d**). *Wendl et al. (2015)* argued that the trends in NO_3^- and NH_4^+ concentrations in the LF-09 core with a broad maximum between 1940 and 1980, followed by a significant decrease, indicate a strong anthropogenic influence during the 20th century related to NO_x and NH_3 emissions from sources located in Eurasia. Moreover, an increase in SO_4^{2-} concentrations, already starting at the end of the 19th century and caused by anthropogenic fossil fuel emissions, was observed in all the ice cores recently drilled in Svalbard *(Beaudon et al., 2013; Goto-Azuma & Koerner, 2001; Kekonen et al., 2005)*. Here we use non-sea-salt SO_4^{2-} to remove the substantial contribution of sea salt (about 40 % in the LF-09 ice core) to the total sulfate budget. This is performed using the following equation *(Wendl, 2014)*:

$$[nssSO_4^{2-}] = [SO_4^{2-}] - 0.12 \times [Na^+] \qquad [\text{µeq L}^{-1}]$$

As seen in **Fig. 4.4**, the broad peak between 1940 and 1980, the decline in concentrations after 1980, and the low concentrations observed in the 1920s and 1930s are present for all the species. The double

peak at the end of the 19th century is also visible, mainly for non-sea-salt SO_4^{2-}, but to a much smaller extent compared to the high rBC concentrations at that time. We argue that this difference can be partially explained by invoking melting as those compounds exhibit different sensitivities to snowmelt and water percolation *(see section 4.3.3)*, NO_3^- and SO_4^{2-} being the most mobile ions, whereas NH_4^+ remains unaffected *(Pohjola et al., 2002)*.
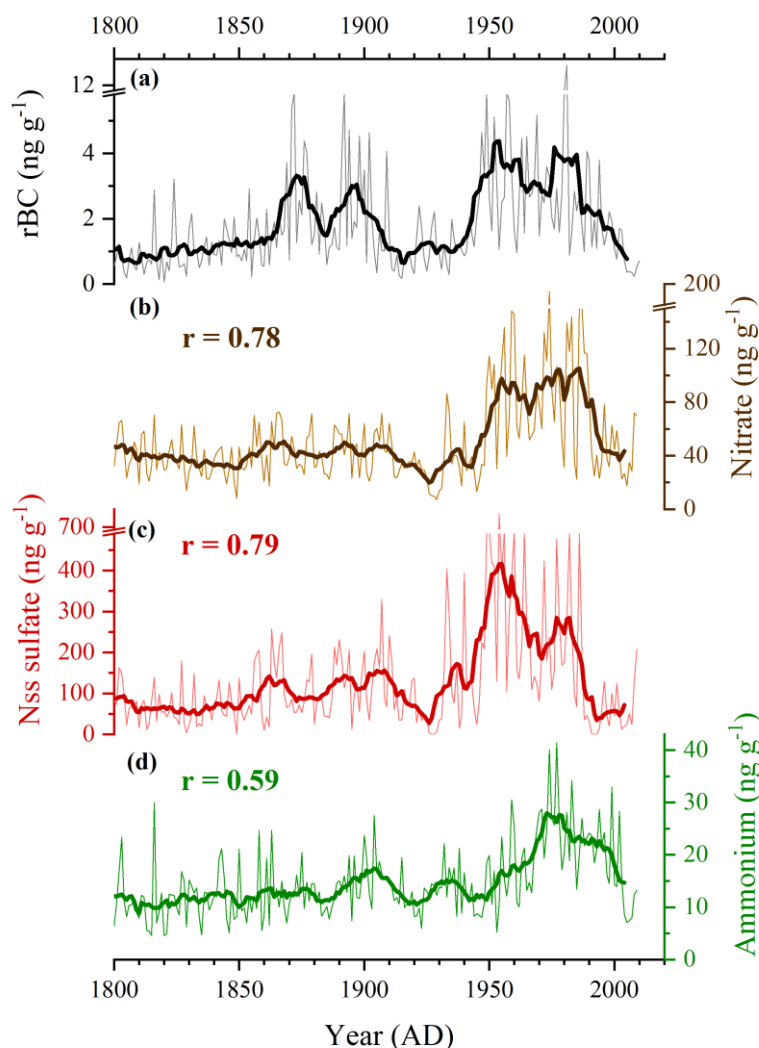
Fig. 4.4: a) rBC, b) nitrate, c) non-sea-salt sulfate, and d) ammonium records from 1800 on. The rBC record is combined for LF-09 and LF-11 spanning 1800–2010 while the other records only show LF-09 data spanning 1800–2009 *(Wendl et al., 2015)*. Thin lines represent annual averages. Bold lines are 11-year moving averages and are associated with Pearson correlation coefficients (r-values) between the respective ion records and the rBC record.

4.3.2.2 Source apportionment of the anthropogenic rBC

In order to interpret the anthropogenic rBC trend in the LF ice core and assess the source regions of anthropogenic rBC, we compare the LF record to other ice core rBC records and emission inventories. All rBC ice core records from Greenland show a similar broad concentration maximum (**Fig. 4.5b to 4.5d**) with values strongly increasing after 1880, peaking around 1910, followed by a clear decline close to preindustrial levels reached after the 1950s *(Keegan et al., 2014; McConnell et al., 2007; Sigl*

et al., 2013). These records are widely interpreted as proxies for North American BC emissions and they closely follow the main trends in emission inventories for this region (**Fig. 4.5g**, *Bond et al., 2007*). Atmospheric back-trajectory studies corroborated that North America is the dominant source of BC deposited in Greenland *(Shindell et al., 2008)*. For Svalbard, the rBC record is notably different with two maxima and contrasting timing. The rBC concentrations sharply increased already from 1860 onwards and peak values were also reached earlier, whereas they were low during times (1920–1940) when rBC concentrations in Greenland were strongly enhanced. The most striking difference is the second maximum observed after 1940 in the LF core which does not appear in any ice core from Greenland. We argue that this discrepancy is in part related to different source areas of air masses reaching Svalbard and Greenland. Air mass back-trajectory analysis obtained with the Lagrangian HYSPLIT model showed that Siberia followed by northern Europe were the dominant source regions for the LF site, while North America was only occasionally the origin of air masses reaching the site *(Grieman et al., 2018)*. Contributions from Siberia were higher in spring and fall, whereas European sources dominated in summer. Contrary to the HDF EC record (**Fig. 4.5e**, *Ruppel et al., 2014*), we do not observe any recent increase in rBC which would support their hypotheses of increased BC scavenging efficiency due to higher air temperatures or stronger flaring emissions from Russia. On the contrary, rBC concentrations in the LF record started declining in the 1970s and further decreased from the end of the 1980s until rBC levels were comparable to preindustrial values. Compared to the highest 1950–1970 rBC concentration average of 3.3 ng g^{-1}, the average decline over the time period 1970–2010 is 0.05 ng g^{-1} yr^{-1} (obtained by linear regression of the rBC annual averages from 1970 to 2010 without considering the exceptionally high values in 1980 and 1981), corresponding to a decrease of 1.5 % yr^{-1}. This is in agreement with the decreasing trend in atmospheric rBC burden observed everywhere in the Arctic over the last decades. *Eleftheriadis et al. (2009)* noted a BC decrease of 9.5 ng m^{-3} per decade at Zeppelin station, while *Sharma et al. (2004)* observed a 55 % BC decrease in Alert (**Fig. 4.1b**) between 1989 and 2002, mainly attributed to a dramatic drop in BC emissions after the USSR dissolved. A longer BC time series from Kevo, Finland, confirmed this declining rate, with a decrease of 1.8 % yr^{-1} for the period 1970–2010 *(Dutkiewicz et al., 2014)*, similar to our results. The authors mostly attributed this decrease to emission reductions and noted a poor correlation between BC concentrations and emissions inventories. Despite their common Svalbard origin, similarities between the HDF and LF records are not obvious. The LF and HDF records are less dissimilar than the LF and Greenland records as they do not show a uniform decline since the 1910s maximum but a second increase from the 1930s to 1960s in HDF and 1940s to 1970s in LF. The differences between both records might arise from the different analytical methods employed to quantify BC and from local differences in transport, deposition and melting effects. *Beaudon et al. (2013)* showed that the HDF ice core was more affected by melting, with outstanding melting features after 1970, than the LF ice core during the 20th century. In addition, the LF site is more frequently located above the thermal inversion layer in winter, in contrast to the HDF site, thus being more exposed to long-range pollution from the free troposphere *(Beaudon et al., 2013)*.
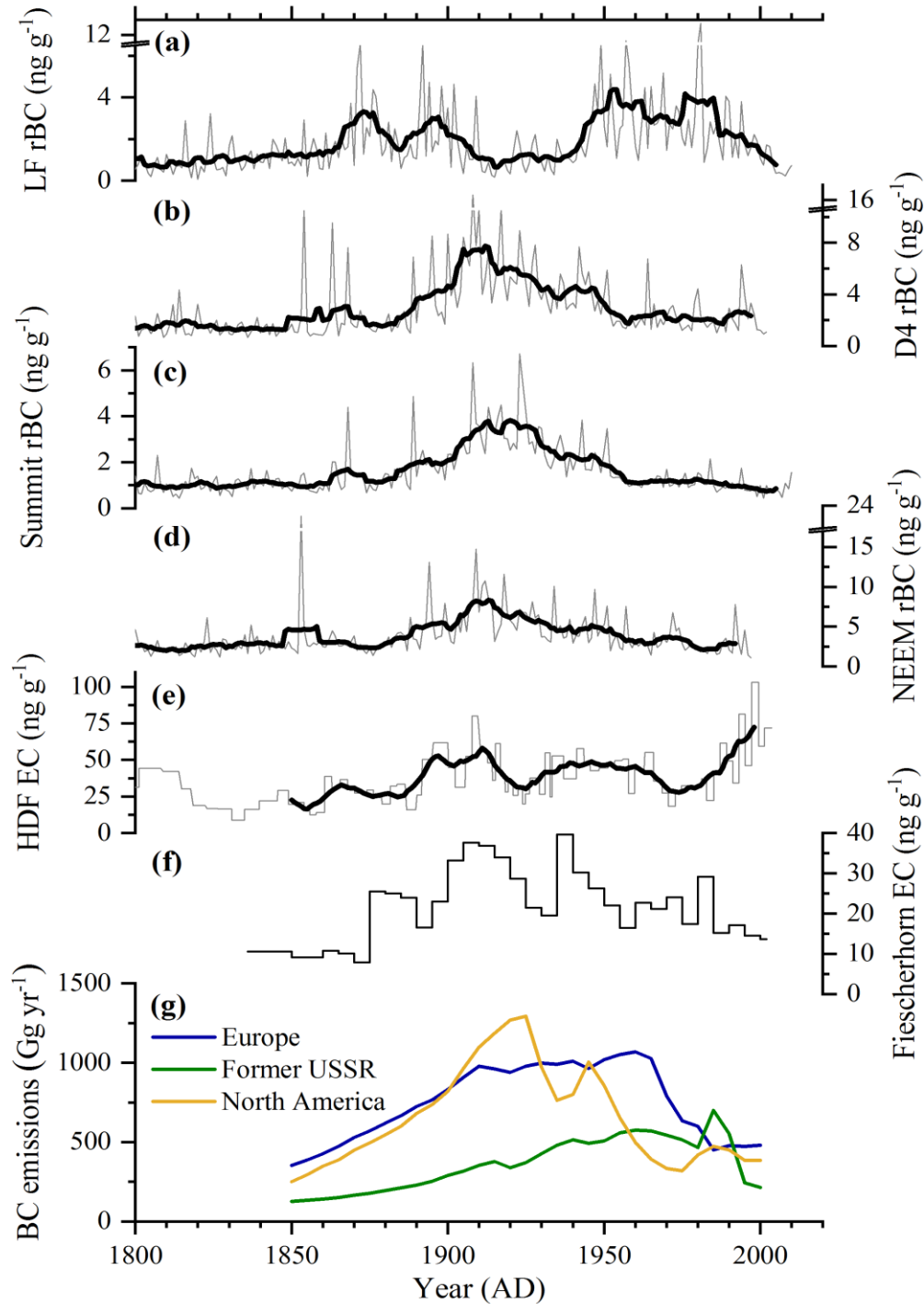
Fig. 4.5: Comparison of a) Lomonosovfonna rBC concentrations to other ice core records from 1800 on, namely rBC from b) D4, Greenland *(McConnell et al., 2007)*, c) Summit 2010, Greenland *(Keegan et al., 2014)*, and d) NEEM 2011-S1 *(Sigl et al., 2013)*, Greenland; e) EC from Holtedahlfonna, Svalbard *(Ruppel et al., 2014)*, and f) Fiescherhorn, Swiss Alps *(Gabbi et al., 2015; Jenk et al., 2006)*; and g) BC emission inventories (5 year averages) for Europe, North America, and the former USSR *(Bond et al., 2007)*. Europe represents the sum of OECD Europe and eastern Europe and North America the sum of Canada and the USA. Thin lines represent annual averages except for Holtedahlfonna (raw data) and Fiescherhorn (5 year averages) due to lower resolution. Bold lines are 11-year moving averages (in the case of Holtedahlfonna, they are calculated from a two-year resolution approximately). Note the different y-axis scales.

We therefore postulate that a clear anthropogenic signal is present in the LF record from 1860 on (**Fig. 4.5a**) due to the start of the Industrial Revolution in Europe. This period of extensive coal burning would be responsible for the double peak observed at the end of the 19th century in the rBC record. The second peak period starting around 1940 would reflect the Eurasian economic growth after World War II and the extensive use of coal and oil for industry, transport and energy production. The decline starting in the 1970s is consistent with emission inventories showing decreasing BC emissions for Europe due to the implementation of cleaner technologies and stricter environmental policies, and, from the 1990s on, for the former Soviet Union due to the collapse of the USSR and the subsequent economic crisis. However, some features of the LF rBC record remain unexpected. First, the sharp increase around 1860 is surprising since a smoother trend is observed at other Arctic sites (e.g., Greenland, HDF), in emission inventories and also in other anthropogenic proxies such as sulfate and nitrate from Arctic ice cores. The increase in rBC also occurs slightly earlier than in Greenland ice cores (1880s, **Fig. 4.5b to 4.5d**, *Keegan et al., 2014; McConnell et al., 2007; Sigl et al., 2013*) and an ice core from the Swiss Alps (1870s, **Fig. 4.5f**, *Jenk et al., 2006*). This earlier increase in rBC concentrations observed in the LF record supports our hypothesis that European BC emissions, probably from the early industrialized British Empire, might have dominated the LF-09 rBC record at that time. Indeed, the Industrial Revolution began in the second half of the 18th century in England *(Deane, 1965)* and spread to western Europe by 1850 *(Spielvogel, 2010)*. In the LF core, the first increase in rBC background concentrations appeared around 1800. In the HDF ice core, stronger acidity from 1850 on was attributed to the Industrial Revolution *(Beaudon et al., 2013)*. Local sources of contamination from coal mining in Svalbard can be excluded because the first industrial mines did not open until around 1900 *(Catford, 2002; Hisdal, 1998)*. Second, our record displays two local minima around 1885 and between 1910 and 1940, which cannot be explained only by lower emissions as reflected by emission inventories *(Bond et al., 2007)*. The economic crisis in the 1920s and 1930s might have contributed to these lower values, as also seen in the Fiescherhorn ice core, but it is unlikely to cause such a long and clear drop in rBC concentrations, as it started earlier and showed low rBC values similar to early 19th century levels. In addition, to our knowledge, no anthropogenic cause can explain the 1885 concentration drop. Interestingly, lower values are also found in the HDF EC record in the 1880s and 1920s, but the minima are less noticeable *(Ruppel et al., 2014)*. As discussed in the next section, we suggest that post-depositional effects induced by summer melting are mostly responsible for these features.

4.3.3 Influence of snow melting during the 20th century

Hitherto, it remains unclear what happens to BC when melting occurs at the surface of the snowpack. BC can be enriched at the surface due to its low solubility in water or it can be eluted with the meltwater and percolate downward through the snowpack. When the water refreezes further down, forming an ice lens, BC is trapped. If melting is considerable, runoff can occur, leading to a net loss of BC. *Doherty and al. (2013)* showed that BC particles tend to be retained at the snow surface when melting occurs, and that only 10–30 % of the BC is eluted with meltwater through the snowpack. However, *Xu et al. (2012)* observed that BC concentrations were higher not only at the surface but also in firn, at the bottom part of the snowpack, due to BC percolation and enrichment on top of superimposed ice, hindering further penetration of meltwater, while the intermediate snowpack zone was depleted in BC. Moreover, fresh snow displayed higher BC concentrations compared to snow experiencing summer melting. If BC concentrations are high, percolation can even be the dominant process *(Conway et al., 1996)*.

In **Fig. 4.6** a qualitative assessment of the melting impact on the LF-09 record is made. Quantitative values cannot be obtained, especially as runoff might have occurred. In addition to the annual melt

percent **(Fig. 4.6b)** calculated by *Wendl et al. (2015)*, we use the melt index **(Fig. 4.6c)** defined as $\log([Na^+]/[Mg^{2+}])$ by *Iizuka et al. (2002)* to quantify the impact of summer melting in Svalbard as sodium and magnesium have different washout efficiencies *(Beaudon et al., 2013; Grinsted et al., 2006)*, a higher value being indicative of a stronger melting. The highest values for both the annual melt percent and melt index are found in the 20th century, in agreement with temperature reconstructions from the Arctic *(McKay et al., 2014)* and the water stable isotope records from both LF-09 *(Wendl, 2014)* and LF-97 cores *(Divine et al., 2011)* showing a slight downward trend until the second half of the 19th century followed by an abrupt rise in the 20th century. Prior to 1850, colder temperatures, a lower melt index (average 1222–1850: 0.64) and melt percent (average 1222–1850: 28 %), and simultaneous peak occurrence for species with different sensitivity to elution (e.g., NH_4^+ and rBC) all suggest a reduced impact of melting and a better preservation of the original concentration.

The melt index shows two periods of enhanced melting in the LF-09 ice core, from the 1910s to 1930s and in the 1980s–1990s. The first one is associated with the well-known early 20th century pan-Arctic warming *(Bengtsson et al., 2004)*, also clearly visible in the temperature series from Svalbard Airport in Longyearbyen (**Fig. 4.6d**, *Nordli et al., 2014*), while the second one is explained by the current global warming trend *(AMAP, 2011b; IPCC, 2013)*. The existence of local algae in the LF-97 core only between 1900 and 1940 *(Hicks and Isaksson, 2006)* underlines the fact that wet surface snow was present at that time at the drill site, another clear indication of summer melting. In contrast, the annual melt percent displays the highest values around 1905 and some local maxima around 1955 and in the 1980s. Our hypothesis is that the strong 1920s melting peak was responsible for extensive water percolation through the snowpack, leading to the formation of ice lenses and producing the melt percent peak around 1905. This would correspond to a percolation length of over 15 years, which strongly exceeds the up to 8 years postulated by *Kekonen et al. (2005)*. A nonnegligible fraction of the rBC particles might have been eluted with the meltwater. Another substantial fraction might have been lost by runoff, which could explain the rBC minima from the 1910s to 1930s. Regarding the melt index peak in the 1980s and 1990s, as no clear increase can be seen in the annual melt percent record in the previous years, percolation must have been overwhelmed by surface runoff responsible for rBC losses. The dramatic decline of the melt percent since the 1990s also confirms the dominant contribution from runoff over percolation due to increasingly warm temperatures. *Kekonen et al. (2005)* also noted ion losses due to runoff since the 1990s in the LF-97 ice core. Nevertheless, we suggest that the decreasing trend in rBC since the 1970s is not only an artefact due to melting issues but is primarily driven by reductions in source emissions as confirmed by atmospheric measurements throughout the Arctic.

The case of the 1885 rBC minimum is more puzzling as there is no evidence of strong melting either in the melt index or in the annual melt percent record, which could indicate that losses happened only by runoff. Melting occurrence is supported by red layers typical of algae growing only in the presence of liquid water in LF-09 ice core sections around 1879–1881 and 1883–1885. Interestingly, *Keegan et al. (2014)* described a widespread melting event in Greenland associated with a prominent ice layer corresponding to the year 1889, which would lie within our dating uncertainties.

Furthermore, we cannot fully exclude that the apparent loss of rBC due to melting is an artefact of the SP2 analytical method. Losses of rBC from samples which were melted and refrozen in laboratory tests can reach 45 ± 11 % *(Lim et al., 2014)* or even up to 60 % for a single thaw–freeze–thaw cycle prior to analyses *(Wendl et al., 2014)*. One possible explanation is the agglomeration of rBC particles to larger sizes during the refreezing process, beyond the SP2 detection range *(Wendl et al., 2014)*. It is

unclear if such processes similarly occur during melting and refreezing of a snowpack, which would make the use of SP2-based methods less suited for ice cores experiencing strong summer melting.
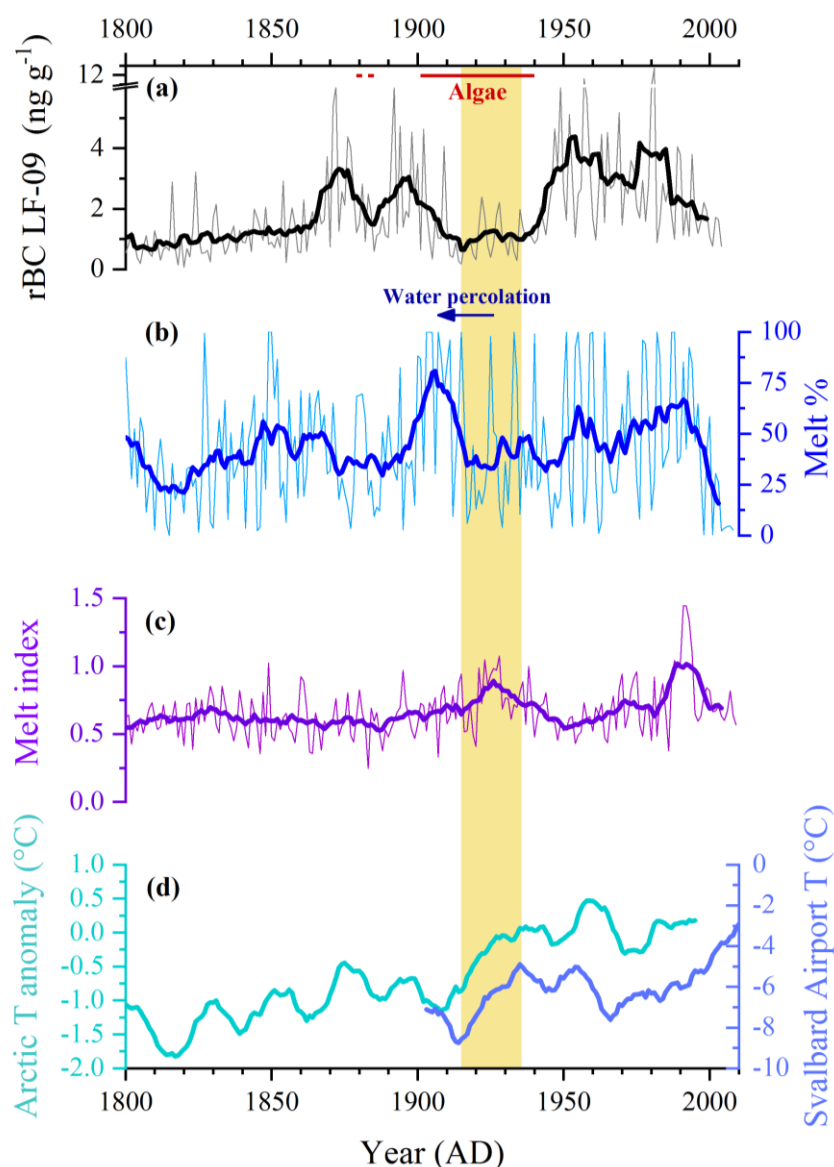

Fig. 4.6: Influence of melting on the LF-09 rBC record since 1800. Comparison of a) LF-09 rBC concentrations with b) LF-09 melt percent *(Wendl et al., 2015)*, c) LF-09 melt index calculated as log([Na$^+$]/[Mg^{2+}]), d) temperature anomalies from the whole Arctic *(McKay et al., 2014)*, and the temperature record from Svalbard Airport, Longyearbyen *(Nordli et al., 2014)*. Thin lines are annual averages and bold lines 11-year moving averages. The yellow bar represents the time period of the early 20th century Arctic warming responsible for enhanced melting in the LF-09 ice core. Time periods with algae, either in the LF-97 *(Hicks and Isaksson, 2006)* or LF-09 records, are represented by a red line.

4.3.4 Paleofire reconstruction

Even if the impact of summer melting and anthropogenic emissions hampered the use of rBC as a biomass burning proxy since the beginning of the Industrial Revolution, it is still possible to reconstruct past biomass burning trends in the preindustrial times (before 1800). This part of the record has a limited melting effect due to low air temperatures and presumably no anthropogenic input. In this period every rBC peak is assumed to correspond to a biomass burning episode whose emissions were transported to and deposited at the drilling site. Natural rBC emissions (wildfires) may

also have contributed to the rBC record since the beginning of the Industrial Revolution but their signature is largely masked by the anthropogenic signal. For instance, the highest rBC concentrations of the record in 1980 and 1981 could be linked with strong biomass burning seasons in Canada (4.8 and 6.1 Mha, respectively; *Stocks et al., 2003*) potentially related to the ammonium spikes noted in Greenland ice cores *(Legrand et al., 2016)*. The clear rBC peak visible in the LF record in summer 1994 could reflect the high fire activity in Canada for the year 1994, when 6.1 Mha burned *(Stocks et al., 2003)*. *Dibb et al. (1996)* documented the advection of a biomass burning plume from the Hudson Bay lowlands, Canada, to Greenland on August 5th 1994, suggested to be responsible for an increase in NH_4^+, K^+ and light carboxylic acid concentrations in the snowpack. Although northern Eurasia is assumed to be the main source of rBC in the LF record, those events reveal that advection of forest fire plumes from North America could possibly reach Svalbard under favorable conditions.

To identify common variability among the chemical species in the LF ice core and isolate biomass burning proxies, we performed a principal component analysis (PCA) **(Table 4.2)**. We used normalized annual averages and restricted our analysis to the preindustrial period (1222–1859) as many compounds (e.g., sulfate, rBC, ammonium, and nitrate) are influenced by anthropogenic activities. Four principal components (PCs) were retrieved. PC1 has high loadings of sodium, magnesium, potassium, calcium, nitrate, sulfate, chloride, and methanesulfonate, representing 52 % of the total variance and can be explained by mineral dust and marine sources *(Wendl et al., 2015)*. PC2 isolates light carboxylic acids (formate, acetate, and oxalate), accounting for 19 % of the total variance. These compounds are well-known proxies for biomass burning in Greenland ice cores, especially formate *(Legrand and De Angelis, 1996; Legrand et al., 2016)*. PC3 contains high loadings of rBC and ammonium, contributing to 15 % of the total variance and forming another group of biomass burning proxies. It is interesting to note that the preindustrial LF rBC record shows the highest correlation coefficient with ammonium independent of the resolution (significant at the 0.01 level). Most of the rBC peaks correspond to ammonium peaks (see below), reflecting a similar sensitivity to biomass burning emissions, transport, and deposition. We therefore suggest that ammonium is not only a proxy for Eurasian biogenic emissions as stated by *Wendl et al. (2015)* but also reflects a contribution from biomass burning, with biogenic emissions driving background variations while sharp peak events areg associated with forest fires. Lastly, PC4 shows high loadings of specific organic markers of biomass burning (VA and *p*-HBA) and explains around 13 % of the total variance. The fact that biomass burning proxies are split into three different groups highlights their different behaviors towards the processes driving biomass burning emissions, transport, deposition to and conservation within the snowpack, thus advocating for a multi-proxy reconstruction. These discrepancies can arise from the nature of the fire event (flaming or smoldering), the kind of vegetation burnt (grass, conifers, deciduous trees), or the sensitivity towards water percolation induced by summer melting. For instance, BC is preferentially emitted by flaming fires whereas smoldering fires are dominant in boreal regions *(Legrand et al., 2016)*. VA is mainly produced by incomplete combustion of conifers while *p*-HBA is dominant for grass burning *(Simoneit, 2002)*. Contrary to the other proxies used in this study, secondary production of formate from formaldehyde and numerous volatile organic compounds including alkenes is possible when the fire plume ages (see Fig. 1 in the review from *Legrand et al. (2016)*). Formate, like other light carboxylic acids, can also undergo post-depositional effects such as revolatilization and diffusion in the snowpack *(De Angelis and Legrand, 1995)*. Ammonium is almost not affected by summer melting and remains well preserved in the snowpack *(Pohjola et al., 2002)* while VA and *p*-HBA have been shown to be fully eluted by meltwater in an ice core from the Swiss Alps *(Müller-Tautges et al., 2016)*.

Table 4.2: Results of the principal component analysis (PCA) for the LF-09 preindustrial record (1222–1859) after VARIMAX rotation. Data are log-transformed annual averages. Values above 0.5 are in bold. MSA = methanesulfonate ($CH_3SO_3^-$).

	PC1	PC2	PC3	PC4
Sodium	**0.94**	-0.04	-0.08	-0.03
Potassium	**0.92**	0.08	-0.01	0.02
Magnesium	**0.91**	0.11	0.12	-0.12
Calcium	**0.63**	0.28	0.14	-0.12
Chloride	**0.95**	-0.06	-0.04	-0.06
Nitrate	**0.63**	0.36	0.48	-0.17
Sulfate	**0.86**	0.22	0.22	-0.13
MSA	**0.71**	0.28	0.30	-0.18
Acetate	0.08	**0.72**	-0.09	0.15
Formate	0.05	**0.87**	0.05	0.17
Oxalate	0.45	**0.59**	0.33	0.09
rBC	-0.09	-0.18	**0.83**	0.01
Ammonium	0.32	0.30	**0.66**	0.01
VA	-0.09	0.14	-0.14	**0.82**
p-HBA	-0.15	0.19	0.15	**0.80**
Variance explained (%)	52.2	19.3	15.1	13.3

These discrepancies are also reflected in the diverging long-term trends. rBC **(Fig. 4.7a)** and ammonium **(Fig. 4.7b)** display a relatively flat background over the preindustrial time period, meaning that they do not indicate any significant change in biogenic emissions and biomass burning. Only slight increases in background concentrations are visible around 1370 and 1545 for ammonium and around 1290–1340, 1470, 1545–1565, and after 1750 (possibly already influenced by anthropogenic emissions) for rBC. Conversely, formate, VA, and *p*-HBA **(Fig. 4.7c to 4.7e)** show more pronounced long-term variations. Elevated VA concentrations before 1400 (especially around 1250–1280 and 1360–1390) and three multi-decadal peaks in *p*-HBA around 1250–1280, 1520–1570, and 1610–1640 were attributed by *Grieman et al. (2018)* to North Atlantic Oscillation (NAO) changes, a positive mode implying a decrease in precipitation over Europe and central Asia believed responsible for enhanced biomass burning. The LF formate record displays the closest similarities with the *p*-HBA record. Three multi-decadal periods of elevated concentrations are also visible around 1260–1280, 1480–1560, and 1620–1650, superimposed on a general decreasing trend in background concentrations throughout the Little Ice Age, as observed for the VA and *p*-HBA *(Grieman et al., 2018)*, coinciding with a decrease in temperature deduced from the LF $\delta^{18}O$ record until 1880 *(Divine et al., 2011)*. The timing of elevated background concentrations is in agreement with other ice-core-based studies of biomass burning from Siberia *(Eichler et al., 2011; Grieman et al., 2017)*, thus supporting the attribution of northern Eurasia as a major source region for the LF site. *Eichler et al. (2011)* found prominent peaks in nitrate, potassium, and charcoal in the Belukha ice core, Siberian Altai, between 1600 and 1680 induced by the strongest regional forest fire episodes of the last 750 years following extremely dry conditions in central Asia around 1540–1600 responsible for dry dead wood accumulation. In the Akademii Nauk ice core, Siberian Arctic, *Grieman et al. (2017)* reported higher concentrations of VA and *p*-HBA for the time periods 1460–1660 and 1460–1540, respectively. Conversely, paleofire trends from the LF core notably differ from Greenland paleofire reconstructions that record low fire activity between 1600 and 1800 *(Legrand et al., 2016)*.
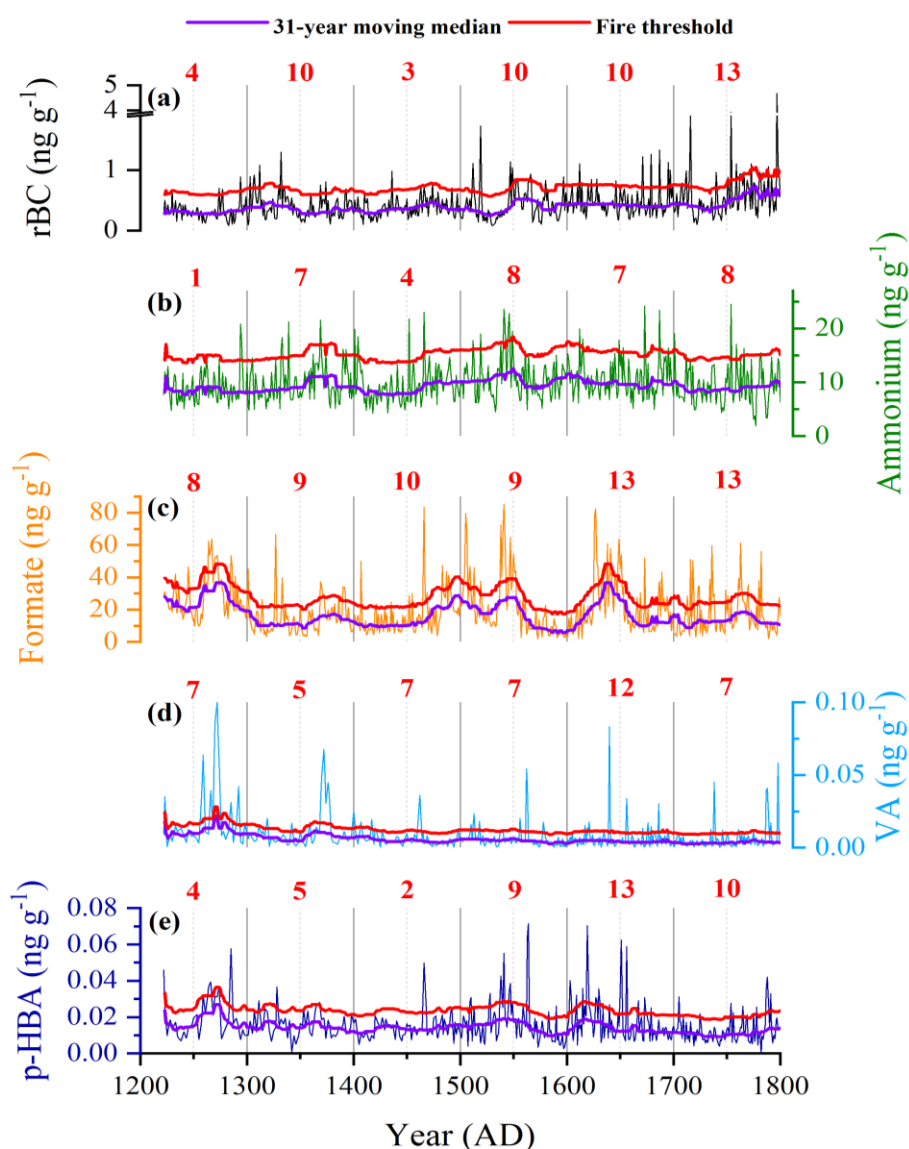
Fig. 4.7: Paleofire trends in the LF-09 ice core using a) rBC, b) ammonium, c) formate, d) vanillic acid (VA), and e) *p*-hydroxybenzoic acid (*p*-HBA) along with 31-year moving medians and the associated fire threshold. Thin lines are annual averages. Red numbers above the respective plots represent the number of years above the fire threshold per century, corrected for neighboring outliers. Ammonium and formate data are from *Wendl et al. (2015)* while VA and *p*-HBA data are from *Grieman et al. (2018)*.

The frequency counting of forest fire episodes enables to focus on episodic biomass burning plumes reaching Svalbard and can provide complementary information in addition to long-term variations. For rBC and ammonium, the centennial frequency of biomass burning episodes did not show a systematic trend throughout the Little Ice Age but showed fewer biomass burning episodes in the 13th and 15th centuries, and more in the 18th century, despite colder temperatures, though for the latter a contribution of early anthropogenic emissions cannot be fully excluded. The VA, *p*-HBA, and formate records provide complementary information as increases in the frequency are concomitant with increases in background concentrations, meaning that fire episodes are not just stochastic events but are associated with longer-term regional climate variations. This is the case in the 17th century for all of the three species and also in the 13th century for VA. **Table 4.3** shows the number of peaks matching (within ±1 year due to the different sampling) among the different proxies, associated with

the percentage it represents in relation to the total number of peaks for each proxy. The best agreement is obtained between rBC and ammonium, with 21 peaks matching, which corresponds to 60 % (42 %) of the total number of ammonium (rBC) peaks. However, substantial dating uncertainties *(Wendl et al., 2015)* have to be considered in the bottom part of the LF-09 ice core, preventing us from assigning a specific biomass burning episode to every single peak.

Table 4.3: Number of peaks matching within ±1 year among the different fire proxies (in bold) for the time period 1222–1800. Italic numbers below give the percentage of matching peaks in relation to the total number of peaks for each proxy.

	rBC	Ammonium	Formate	VA	*p*-HBA
rBC	-				
Ammonium	**21** *42 % rBC* *60 % ammonium*	-			
Formate	**19** *38 % rBC* *31 % formate*	**19** *54 % ammonium* *31 % formate*	-		
VA	**17** *34 % rBC* *38 % VA*	**10** *29 % ammonium* *22 % VA*	**21** *34 % formate* *47 % VA*	-	
p-HBA	**16** *32 % rBC* *37 % p-HBA*	**12** *34 % ammonium* *28 % p-HBA*	**17** *27 % formate* *40 % p-HBA*	**16** *36 % VA* *37 % p-HBA*	-

Interestingly, severe droughts were reported over central Europe in 1540 *(Wetter et al., 2014)* and over northern central Europe between 1437 and 1473 *(Cook et al., 2015)*. The case of the 1797 peak in the rBC and VA records is also remarkable as outstanding values in various biomass burning proxies were detected in several ice cores from Greenland during the last decade of the 18th century. In the NEEM ice core, rBC and levoglucosan were greatly enhanced between 1787 and 1791 *(Sigl et al., 2013; Zennaro et al., 2014)*, while a very strong peak was visible in 1794 in the D4 ice core *(McConnell et al., 2007)* and in 1799 in the Summit 2010 ice core *(Keegan et al., 2014)*. Ammonium records from the ice cores mentioned above all showed peak values in the same decade *(Legrand et al., 2016)*, supporting the fact that this period of enhanced biomass burning could originate from the same decadal-scale climatic event. Severe drought conditions prevailed in central Asia during this decade due to South Asian monsoon failure *(Cook et al., 2010)*. According to the dust proxy records from the Dasuopu ice core (Tibet), this decade experienced the driest conditions of the last millennium for this part of the globe *(Thompson et al., 2000)*. In the Altai region, 9 out of 10 years between 1783 and 1792 belonged to the 10 % of the coldest years of the time period 1200–1850, while the following summers between 1793 and 1811 were clearly warmer *(Büntgen et al., 2016)*. Those cold and dry conditions likely promoted dry dead wood accumulation, which then facilitated fire spread when temperatures rose later in the 1790s, a situation in agreement with the findings from *Eichler et al. (2011)*. In **Fig. 4.8** an exhaustive comparison is made between enhanced background concentration periods and peak years versus summer temperature anomalies and drought reconstructions from two regions of northern Eurasia for which datasets are available, namely northern Europe *(Cook et al., 2015; Esper et al., 2014)* and the Altai *(Büntgen et al., 2016; Cook et al., 2010)*. It appears that biomass burning episodes frequently occurred in concert with decadal-scale summer temperature increases. Conversely, the link with moisture variations seems less consistent as

conditions were either drier or wetter than average depending on the period, suggesting that summer temperature is the controlling factor for biomass burning activity in these regions. While dry conditions can lead to dead fuel accumulation *(Eichler et al., 2011)*, wet conditions promote biomass productivity, especially for grasslands *(Pederson et al., 2014)*. Both of these different mechanisms can enhance fire severity in the context of decadal-scale temperature increases.
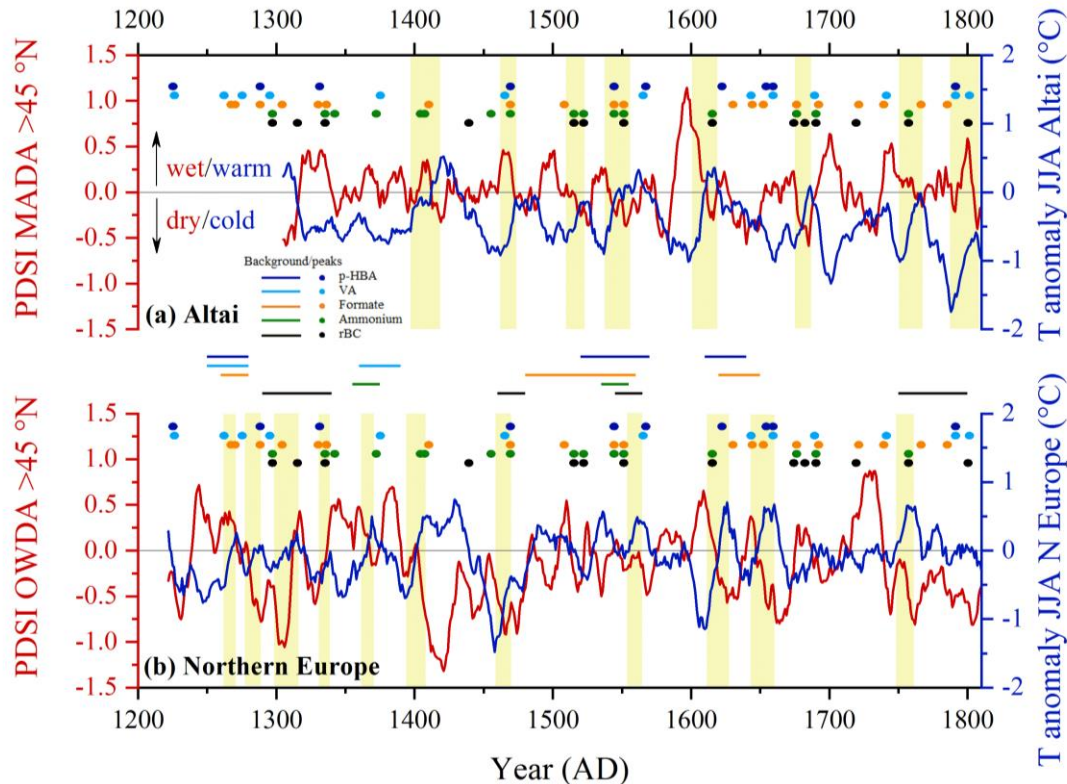

Fig. 4.8: Summer temperature (JJA) anomalies and drought (PDSI: Palmer drought severity index) reconstructions along with periods of enhanced biomass burning (colored lines between the two panels) and fire peaks (colored dots) in the LF ice core, a) for the Altai region: temperature record from *Büntgen et al. (2016)* and drought record from the Monsoon Asia Drought Atlas (MADA, selected area: 45–57.5 °N and 60–135 °E, *Cook et al., 2010*) and b) for Northern Europe: temperature record from *Esper et al. (2014)* and drought record from the Old World Drought Atlas (OWDA, selected area: 45–71 °N and 12 °W–45 °E, *Cook et al., 2015*). Yellow bars represent periods of increasing JJA temperatures associated with biomass burning peaks.

4.4 Conclusions

Refractory black carbon (rBC) was analyzed in two ice cores from the Lomonosovfonna ice field, Svalbard, spanning 1222–2011. Long-term trends were discussed and compared to other ice core records and climate proxies in order to assess the representativeness of the rBC signal archived in the LF ice core in terms of anthropogenic and biomass burning inputs. Our results show that a clear anthropogenic imprint is present since the beginning of the Industrial Revolution, thus hindering the identification of natural biomass burning trends in the most recent 2 centuries. Concentrations of rBC we attributed to predominantly industrial emissions show two maxima, at the end of the 19th century and in the middle of the 20th century. This profile differs from those observed in Greenland ice cores and we suggest that Eurasian emissions account for most of the rBC deposition in the LF ice core in contrast to Greenland where North American emission sources appear more important. Contrary to

the Holtedahlfonna EC record, LF rBC concentrations decreased in the last 40 years, in agreement with atmospheric measurements throughout the Arctic. However, during the warm climate regime over most of the 20th century, parts of the record experienced high levels of melting, which potentially disturbed the preservation of the rBC signal due to percolation and runoff. We thus advocate for a careful interpretation of the trends, especially for the time period with low concentrations between 1910 and 1940, which could be an artefact resulting from the early 20th century Arctic warming.

Before the 19th century, as both the melting and the anthropogenic influence are shown to be low, the LF rBC record can be used to reconstruct past biomass burning trends. No obvious long-term variability is evident in both the rBC and ammonium records. Formate, VA, and *p*-HBA records, however, exhibit a more pronounced decadal-to-centennial-scale variability with a decreasing long-term trend throughout the Little Ice Age interrupted by several multi-decadal periods of enhanced biomass burning activity, the most remarkable one occurring in the 17th century. Those periods, as well as some single peak events such as the one around 1790, coincide in time with other reconstructed periods of increased fire activity from ice cores in Siberia and Greenland. We suggest that the paleofire record from the LF ice core primarily reflects biomass burning episodes from northern Eurasia, induced by decadal-scale summer temperature increases. Our study highlights the need of a multi-proxy reconstruction in order to efficiently capture past changes in biomass burning as each proxy possesses its own behavior and sensitivity towards emission, transport, degradation in the atmosphere, deposition, and post-depositional processes. Such reconstructions are of prime importance to gain a better understanding of the complex linkages between fires, climate, and human activities as future biomass burning trends under a warmer climate remain largely unknown.

Data availability

After acceptance of the paper, rBC data will be available at the US National Oceanic and Atmospheric Administration (NOAA) data center for paleoclimate (ice core sites) at the following address: http://www.ncdc.noaa.gov/data-access/paleoclimatology-data/datasets/ice-core.

Author contribution

D.O. performed SP2 measurements, analyzed the data and wrote the paper. I.A.W. cut the LF-09 ice core, performed the dating and designed the analytical method. L.S. optimized the method and performed SP2 analyses. Mi.S helped with the data interpretation. C.P.V. processed and dated the LF-11 ice core. E.I. organized the field campaigns in Svalbard. Ma.S designed and led the project, organized and conducted ice core drilling and led the manuscript writing.

Competing interests

The authors declare that they have no conflict of interest.

Acknowledgements

References

Aamaas, B., Bøggild, C. E., Stordal, F., Berntsen, T., Holmén, K., and Ström, J.: Elemental carbon deposition to Svalbard snow from Norwegian settlements and long-range transport, *Tellus B*, 63(3), 340–351, 2011a.

AMAP: The Impact of Black Carbon on Arctic Climate, Quinn, P. K., Stohl, A., Arneth, A., Berntsen, T., Burkhart, J. F., Christensen, J., Flanner, M., Kupiainen, K., Lihavainen, H., Shepherd, M., Shevchenko, V., Skov, H., and Vestreng, V., Arctic Monitoring and Assessment Programme (AMAP), Oslo, Norway, 72 pp, 2011a.

AMAP: Snow, Water, Ice and Permafrost in the Arctic (SWIPA): Climate Change and the Cryosphere, Arctic Monitoring and Assessment Programme (AMAP), Oslo, Norway, xii + 538 pp, 2011b.

Bauer, S. E., Bausch, A., Nazarenko, L., Tsigaridis, K., Xu, B. Q., Edwards, R., Bisiaux, M., and McConnell, J.: Historical and future black carbon deposition on the three ice caps: Ice core measurements and model simulations from 1850 to 2100, *Journal of Geophysical Research: Atmospheres*, 118, 7948–7961, 2013.

Beaudon, E., Moore, J. C., Martma, T., Pohjola, V. A., van de Wal, R. S. W., Kohler, J., and Isaksson, E.: Lomonosovfonna and Holtedahlfonna ice cores reveal east–west disparities of the Spitsbergen environment since AD 1700, *Journal of Glaciology*, 59, 1069–1083, 2013.

Bengtsson, L., Semenov, V. A., and Johannessen, O. M.: The Early Twentieth-Century Warming in the Arctic - A Possible Mechanism, *Journal of Climate*, 17, 4045–4057, 2004.

Bond, T. C., Bhardwaj, E., Dong, R., Jogani, R., Jung, S. K., Roden, C., Streets, D. G., and Trautmann, N. M.: Historical emissions of black and organic carbon aerosol from energy-related combustion, 1850–2000, *Global Biogeochemical Cycles*, 21, 2007.

Bond, T. C., Doherty, S. J., Fahey, D. W., Forster, P. M., Berntsen, T., DeAngelo, B. J., Flanner, M. G., Ghan, S., Karcher, B., Koch, D., Kinne, S., Kondo, Y., Quinn, P. K., Sarofim, M. C., Schultz, M. G., Schulz, M., Venkataraman, C., Zhang, H., Zhang, S., Bellouin, N., Guttikunda, S. K., Hopke, P. K., Jacobson, M. Z., Kaiser, J. W., Klimont, Z., Lohmann, U., Schwarz, J. P., Shindell, D., Storelvmo, T., Warren, S. G., and Zender, C. S.: Bounding the role of black carbon in the climate system: A scientific assessment, *Journal of Geophysical Research: Atmospheres*, 118, 5380–5552, 2013.

Büntgen, U., Myglan, V. S., Charpentier Ljungqvist, F., McCormick, M., Di Cosmo, N., Sigl, M., Jungclaus, J., Wagner, S., Krusic, P. J., Esper, J., Kaplan, J. O., de Vaan, M. A. C., Luterbacher, J., Wacker, L., Tegel, W., and Kirdyanov, A. V.: Cooling and societal change during the Late Antique Little Ice Age from 536 to around 660 AD, *Nature Geoscience*, 9, 231–236, 2016.

Catford, K.: The Industrial Archaeology of Spitsbergen, *Industrial Archaeology Reviews*, 24(1), 23–36, 2002.

Clarke, A. D. and Noone, K. J.: Soot in the Arctic snowpack: a cause for perturbations in radiative transfer, *Atmospheric Environment*, 19, 2045–2053, 1985.

Conway, H., Gades, A., and Raymond, C. F.: Albedo of dirty snow during conditions of melt, *Water Resources Research*, 32, 1713–1718, 1996.

Cook, E. R., Anchukaitis, K. J., Buckley, B. M., D'Arrigo, R. D., Jacoby, G. C., and Wright, W. E.: Asian Monsoon Failure and Megadrought During the Last Millenium, *Science*, 328, 486–489, 2010.

Cook, E. R., Seager, R., Kushnir, Y., Briffa, K. R., Büntgen, U., Frank, D., Krusic, P. J., Tegel, W., van der Schrier, G., Andreu-Hayles, L., Baillie, M., Baittinger, C., Bleicher, N., Bonde, N., Brown, D., Carrer, M., Cooper, R., Čufar, K., Dittmar, C., Esper, J., Griggs, C., Gunnarson, B., Günther, B., Gutierrez, E., Haneca, K., Helama, S., Herzig, F., Heussner, K.-U., Hofmann, J., Janda, P., Kontic, R., Köse, N., Kyncl, T., Levanič, T., Linderholm, H., Manning, S., Melvin, T. M., Miles, D., Neuwirth, B., Nicolussi, K., Nola, P., Panayotov, M., Popa, I., Rothe, A., Seftigen, K., Seim, A., Svarva, H., Svoboda, M., Thun, T., Timonen, M., Touchan, R., Trotsiuk, V., Trouet, V., Walder, F., Ważny, T., Wilson, R.,and Zang, C.: Old World megadroughts and pluvials during the Common Era, *Science Advances*, 1, e1500561, 2015.

Deane, P.: The first industrial revolution, Cambridge University Press, Cambridge, UK, 1965.

De Angelis, M. and Legrand, M.: Preliminary investigations of post depositional effects on HCl, HNO3, and organic acids in polar firn, in Ice Core Studies of Global Biogeochemical Cycles, edited by R.J. Delmas, NATO ASI Series I, 30, 336–381, 1995.

Dibb, J. E., Talbot, R. W., Whitlow, S. I., Shipham, M. C., Winterle, J., McConnell, J., and Bales, R.: Biomass burning signatures in the atmosphere and snow at Summit, Greenland: An event on 5 August 1994, *Atmospheric Environment*, 30(4), 553–561, 1996.

Divine, D., Isaksson, E., Martma, T., Meijer, H. A. J., Moore, J., Pohjola, V., van de Wal, R. S. W., and Godtliebsen, F.: Thousand years of winter surface air temperature variations in Svalbard and northern Norway reconstructed from ice core data, *Polar Research*, 30, 7379, 2011.

Doherty, S. J., Warren, S. G., Grenfell, T. C., Clarke, A. D., and Brandt, R. E.: Light-absorbing impurities in Arctic snow, *Atmospheric Chemistry and Physics*, 10, 11647–11680, 2010.

Doherty, S. J., Grenfell, T. C., Forsström, S., Hegg, D. L., Brandt, R. E., and Warren, S. G.: Observed vertical redistribution of black carbon and other insoluble light-absorbing particles in melting snow, *Journal of Geophysical Research: Atmospheres*, 118, 5553–5569, 2013.

Dutkiewicz, V. A., DeJulio, A. M., Ahmed, T., Laing, J., Hopke, P. K., Skeie, R. B., Viisanen, Y., Paatero, J., and Husain, L.: Forty-seven years of weekly atmospheric black carbon measurements in the Finnish Arctic: Decrease in black carbon with declining emissions, *Journal of Geophysical Research: Atmospheres*, 119, 7667–7683, 2014.

Eichler, A., Schwikowski, M., Gäggeler, H. W., Furrer, V., Synal, H.-A., Beer, J., Saurer, M., and Funk, M.: Glaciochemical dating of an ice core from upper Grenzgletscher (4200m a.s.l.), *Journal of Glaciology*, 46, 507–515, 2000.

Eichler, A., Brütsch, S., Olivier, S., Papina, T., and Schwikowski, M.: A 750 year ice core record of past biogenic emissions from Siberian boreal forests, *Geophysical Research Letters*, 36, L18813, 2009.

Eichler, A., Tinner, W., Brütsch, S., Olivier, S., Papina, T., and Schwikowski, M.: An ice-core based history of Siberian forest fires since AD 1250, *Quaternary Science Reviews*, 30, 1027–1034, 2011.

Eleftheriadis, K., Vratolis, S., and Nyeki, S.: Aerosol black carbon in the European Arctic: Measurements at Zeppelin station, Ny Ålesund, Svalbard from 1998–2007, *Geophysical Research Letters*, 36, L02809, 2009.

Esper, J., Düthorn, E., Krusic, P. J., Timonen, M., and Büntgen, U.: Northern European summer temperature variations over the Common Era from integrated tree-rings density records, *Journal of Quaternary Science*, 29(5), 487–494, 2014.

Fischer, H., Schüpbach, S., Gfeller, G., Bigler, M., Rothlisberger, R., Erhardt, T., Stocker, T. F., Mulvaney, R., and Wolff, E.: Millennial changes in North American wildfire and soil activity over the last glacial cycle, *Nature Geoscience*, 8, 723–728, 2015.

Flanner, M. G., Zender, C. S., Randerson, J. T., and Rasch, P. J.: Present-day climate forcing and response from black carbon in snow, *Journal of Geophysical Research: Atmospheres*, 112, 2007.

Forsström, S., Ström, J., Pedersen, C. A., Isaksson, E., and Gerland, S.: Elemental carbon distribution in Svalbard snow, *Journal of Geophysical Research: Atmospheres*, 114(D19), 2009.

Forsström, S., Isaksson, E., Skeie, R. B., Ström, J., Pedersen, C. A., Hudson, S. R., Berntsen, T. K., Lihavainen, H., Godtliebsen, F., and Gerland, S.: Elemental carbon measurements in European Arctic snow packs, *Journal of Geophysical Research: Atmospheres*, 118, 1–14, 2013.

Fuhrer, K., Neftel, A., Anklin, M., Staffelbach, T., and Legrand, M.: High-resolution ammonium ice core record covering a complete glacial-interglacial cycle, *Journal of Geophysical Research: Atmospheres*, 101, 4147–4164, 1996.

Gabbi, J., Huss, M., Bauder, A., Cao, F., and Schwikowski, M.: The impact of Saharan dust and black carbon on albedo and long-term mass balance of an Alpine glacier, *The Cryosphere*, 9, 1385–1400, 2015.

Ginot, P., Stampfli, F., Stampfli, D., Schwikowski, M., and Gäggeler, H. W.: FELICS, a new ice core drilling system for high-altitude glaciers, *Memoirs of National Institute of Polar Research Special Issue*, 56, 38–48, 2002.

Goldberg, E. D.: Black Carbon in the Environment, Wiley, New York, USA, 1985.

Gong, S. L., Zhao, T. L., Sharma, S., Toom-Sauntry, D., Lavoué, D., Zhang, X. B., Leaitch, W. R., and Barrie, L. A.: Identification of trends and interannual variability of sulfate and black carbon in the Canadian high Arctic: 1981–2007, *Journal of Geophysical Research*, 115, D07305, 2010.

Gordiyenko, F. G., Kotlyakov, V. M., Punning, Y.-K. M., and Vairmäe, R.: Study of a 200-m core from the Lomonosov ice plateau on Spitsbergen and the paleoclimatic implications, *Polar Geography and Geology*, 5, 242–251, 1981.

Goto-Azuma, K. and Koerner, R. M.: Ice core studies of anthropogenic sulfate and nitrate trends in the Arctic, *Journal of Geophysical Research*, 106, 4959–4969, 2001.

Grieman, M., Greaves, J., and Saltzman, E.: A method for analysis of vanillic acid in polar ice cores, *Climate of the Past*, 11, 227–232, 2015.

Grieman, M. M., Aydin, M., Fritzsche, D., McConnell, J. R., Opel, T., Sigl, M., and Saltzman, E. S.: Aromatic acids in a Eurasian Arctic ice core: a 2600-year proxy record of biomass burning, *Climate of the Past*, 13, 395–410, 2017.

Grieman, M. M., Aydin, M., Isaksson, E., Schwikowski, M., and Saltzman, E. S.: Aromatic acids in an Arctic ice core from Svalbard: a proxy record of biomass burning, *Climate of the Past*, 14, 637–651, 2018.

Grinsted, A., Moore, J. C., Pohjola, V., Martma, T., and Isaksson, E.: Svalbard summer melting, continentality, and sea ice extent from the Lomonosovfonna ice core, *Journal of Geophysical Research*, 111, D07110, 2006.

Gysel, M., Laborde, M., Olfert, J. S., Subramanian, R., and Gröhn, A. J.: Effective density of Aquadag and fullerene soot black carbon reference materials used for SP2 calibration, *Atmospheric Measurement Techniques*, 4, 2851–2858, 2011.

Hansen, J. and Nazarenko, L.: Soot climate forcing via snow and ice albedos, *PNAS*, 101, 423–428, 2004.

Hennigan, C. J., Sullivan, A. P., Collett, J. L., and Robinson, A. L.: Levoglucosan stability in biomass burning particles exposed to hydroxyl radicals, *Geophysical Research Letters*, 37, L09806, 2010.

Hicks, S. and Isaksson, E.: Assessing source areas of pollutants from studies of fly ash, charcoal and pollen from Svalbard snow and ice, *Journal of Geophysical Research*, 111, D02113, 2006.

Hirdman, D., Sodemann, H., Eckhardt, S., Burkhart, J. F., Jefferson, A., Mefford, T., Quinn, P. K., Sharma, S., Ström, J., and Stohl, A.: Source identification of short-lived air pollutants in the Arctic using statistical analysis of measurement data and particle dispersion model output, *Atmospheric Chemistry and Physics*, 10, 669–693, 2010a.

Hirdman, D., Burkhart, J. F., Sodemann, H., Eckhardt, S., Jefferson, A., Quinn, P. K., Sharma, S., Ström, J., and Stohl, A.: Long-term trends of black carbon and sulfate aerosol in the Arctic: changes in atmospheric transport and source region emissions, *Atmospheric Chemistry and Physics*, 10, 9351–9368, 2010b.

Hisdal, V.: Svalbard: nature and history, Norsk Polarinstitutt, Oslo, Norway, 1998.

Hoffmann, D., Tilgner, A., Iinuma, Y., and Herrmann, H.: Atmospheric stability of levoglucosan: a detailed laboratory and modeling study, *Environmental Science and Technology*, 44, 694–699, 2010.

Iizuka, Y., Igarashi, M., Kamiyama, K., Motoyama, H., and Watanabe, O.: Ratios of Mg2+/Na+ in snowpack and an ice core at Austfonna ice cap, Svalbard, as an indicator of seasonal melting, *Journal of Glaciology*, 48, 452–460, 2002.

IPCC: Climate Change 2013: The Physical Science Basis. Contribution of Working Group I to the Fifth Assessment Report of the Intergovernmental Panel on Climate Change [Stocker, T.F., Qin, D., Plattner, G.-K., Tignor, M., Allen, S. K., Boschung, J., Nauels, A., Xia, Y., Bex, V., and Midgley, P. M. (eds.)], Cambridge University Press, Cambridge, United Kingdom and New York, NY, USA, 1535 pp, 2013.

Isaksson, E., Pohjola, V., Jauhiainen, T., Moore, J., Pinglot, J. F., Vaikmae, R., van de Wal, R. S. W., Hagen, J. O., Ivask, J., Karlöf, L., Martma, T., Meijer, H. A. J., Mulvaney, R., Thomassen, M., and van den Broeke, M.: A new ice-core record from Lomonosovfonna, Svalbard: viewing the 1920–97 data in relation to present climate and environmental conditions, *Journal of Glaciology*, 47, 335–345, 2001.

Jenk, T. M., Szidat, S., Schwikowski, M., Gaggeler, H. W., Brutsch, S., Wacker, L., Synal, H. A., and Saurer, M.: Radiocarbon analysis in an Alpine ice core: record of anthropogenic and biogenic contributions to carbonaceous aerosols in the past (1650–1940), *Atmospheric Chemistry and Physics*, 6, 5381-5390, 2006.

Jenkins, M., Kaspari, S., Kang, S.-C., Grigholm, B., and Mayewski, P. A.: Tibetan Plateau Geladaindong black carbon ice core record (1843–1982): Recent increases due to higher emissions and lower snow accumulation, *Advances in Climate Change Research*, 7, 132–138, 2016.

Kaspari, S. D., Schwikowski, M., Gysel, M., Flanner, M. G., Kang, S., Hou, S., and Mayewski, P. A.: Recent Increase in Black Carbon Concentrations from a Mt. Everest Ice Core Spanning 1860–2000 AD, *Geophysical Research Letters*, 38, 2011.

Kawamura, K., Izawa, Y., Mochida, M., and Shiraiwa, T.: Ice core records of biomass burning tracers (levoglucosan and dehydroabietic, vanillic and p-hydroxybenzoic acids) and total organic carbon for past 300 years in the Kamchatka Peninsula, Northeast Asia, *Geochimica et Cosmochimica Acta*, 99, 317–329, 2012.

Keegan, K. M., Albert, M. R., McConnell, J. R., and Baker, I.: Climate change and forest fires synergistically drive widespread melt events of the Greenland Ice Sheet, *PNAS*, 111, 7964–7967, 2014.

Kehrwald, N., Zangrando, R., Gabrielli, P., Jaffrezo, J.-L., Boutron, C., Barbante, C., and Gambaro, A.: Levoglucosan as a specific marker of fire events in Greenland snow, *Tellus B*, 64, 18196–18204, 2012.

Kekonen, T., Moore, J., Perämäki, P., Mulvaney, R., Isaksson, E., Pohjola, V., and van de Wal, R. S. W.: The 800 year long ion record from the Lomonosovfonna (Svalbard) ice core, *Journal of Geophysical Research*, 110, D07304, 2005.

Kellerhals, T., Brütsch, S., Sigl, M., Knüsel, S., Gäggeler, H. W., and Schwikowski, M.: Ammonium concentration in ice cores: A new proxy for regional temperature reconstruction?, *Journal of Geophysical Research*, 115, D16123, 2010.

Lee, Y. H., Lamarque, J. F., Flanner, M. G., Jiao, C., Shindell, D. T., Berntsen, T., Bisiaux, M. M., Cao, J., Collins, W. J., Curran, M., Edwards, R., Faluvegi, G., Ghan, S., Horowitz, L. W., McConnell, J. R., Ming, J., Myhre, G., Nagashima, T., Naik, V., Rumbold, S. T., Skeie, R. B., Sudo, K., Takemura, T., Thevenon, F., Xu, B., and Yoon, J. H.: Evaluation of preindustrial to present-day black carbon and its albedo forcing from Atmospheric Chemistry and Climate Model Intercomparison Project (ACCMIP), *Atmospheric Chemistry and Physics*, 13, 2607–2634, 2013.

Legrand, M. and De Angelis, M.: Light carboxylic acids in Greenland ice: A record of past forest fires and vegetation emissions from the boreal zone, *Journal of Geophysical Research*, 101(D2), 4129–4145, 1996.

Legrand, M., McConnell, J., Fischer, H., Wolff, E. W., Preunkert, S., Arienzo, M., Chellman, N., Leuenberger, D., Maselli, O., Place, P., Sigl, M., Schüpbach, S., and Flannigan, M.: Boreal fire records in Northern Hemisphere ice cores: a review, *Climate of the Past*, 12, 2033–2059, 2016.

Lim, S., Faïn, X., Zanatta, M., Cozic, J., Jaffrezo, J.-L., Ginot, P. and Laj, P.: Refractory black carbon mass concentrations in snow and ice: method evaluation and inter-comparison with elemental carbon measurement, *Atmospheric Measurement Techniques*, 7, 3307–3324, 2014.

Lim, S., Faïn, X., Ginot, P., Mikhalenko, V., Kutuzov, S., Paris, J.-D., Kozachek, A., and Laj, P.: Black carbon variability since preindustrial times in the eastern part of Europe reconstructed from Mt. Elbrus, Caucasus, ice cores, *Atmospheric Chemistry and Physics*, 17, 3489–3505, 2017.

Matoba, S., Narita, H., Motoyama, H., Kamiyama, K., and Watanabe, O.: Ice core chemistry of Vestfonna ice cap in Svalbard, Norway, *Journal of Geophysical Research*, 107(D23), 4721–4727, 2002.

McConnell, J. R., Edwards, R., Kok, G. L., Flanner, M. G., Zender, C. S., Saltzman, E. S., Banta, J. R., Pasteris, D. R., Carter, M. M., and Kahl, J. D. W.: 20th-century industrial black carbon emissions altered arctic climate forcing, *Science*, 317, 1381–1384, 2007.

McKay, N. P., and Kaufman, D. S.: An extended Arctic proxy temperature database for the past 2,000 years, *Scientific Data*, 1:140026, 2014.

Moore, J. C., Grinsted, A., Kekonen, T., and Pohjola, V.: Separation of melting and environmental signals in an ice core with seasonal melt, *Geophysical Research Letters*, 32, L10501, 2005.

Müller-Tautges, C., Eichler, A., Schwikowski, M., Pezzati, G. B., Conedera, M., and Hoffmann, T.: Historic records of organic compounds from a high Alpine glacier: influences of biomass burning, anthropogenic emissions, and dust transport, *Atmospheric Chemistry and Physics*, 16, 1029–1043, 2016.

Nordli, Ø., Przybylak, R., Ogilvie, A. E. J., and Isaksen, K.: Long-term temperature trends and variability on Spitsbergen: the extended Svalbard Airport temperature series, 1898–2012, *Polar Research*, 33, 21349, 2014.

Pederson, N., Hessl, A. E., Baatarbileg, N., Anchukaitis, K. J., and Di Cosmo, N.: Pluvials, droughts, the Mongol empire, and modern Mongolia, *PNAS*, 111(12), 4375–4379, 2014.

Petzold, A., Ogren, J. A., Fiebig, M., Laj, P., Li, S. M., Baltensperger, U., Holzer-Popp, T., Kinne, S., Pappalardo, G., Sugimoto, N., Wehrli, C., Wiedensohler, A., and Zhang, X. Y.: Recommendations for reporting "black carbon" measurements, *Atmospheric Chemistry and Physics*, 13, 8365–8379, 2013.

Pohjola, V. A., Moore, J. C., Isaksson, E., Jauhiainen, T., Van de Wal, R. S. W., Martma, T., Meijer, H. A. J., and Vaikmäe, R.: Effect of periodic melting on geochemical and isotopic signals in an ice core from Lomonosovfonna, Svalbard, *Journal of Geophysical Research*, 107, 4036–4049, 2002.

Quinn, P. K., Shaw, G., Andrews, E., Dutton, E. G., Ruoho-Airola, T., and Gong, S. L.: Arctic Haze: current trends and knowledge gaps, *Tellus B*, 59B, 99–114, 2007.

Ramanathan, V. and Carmichael, G.: Global and regional climate changes due to black carbon, *Nature Geoscience*, 1, 221–227, 2008.

Ruppel, M. M., Isaksson, E., Ström, J., Beaudon, E., Svensson, J., Pedersen, C. A., and Korhola, A.: Increase in elemental carbon values between 1970 and 2004 observed in a 300-year ice core from Holtedahlfonna (Svalbard), *Atmospheric Chemistry and Physics*, 14, 11447–11460, 2014.

Ruppel, M. M., Soares, J., Gallet, J.-C., Isaksson, E., Martma, T., Svensson, J., Kohler, J., Pedersen, C. A., Manninen, S., Korhola, A., and Ström, J.: Do contemporary (1980–2015) emissions determine the elemental carbon deposition trend at Holtedahlfonna glacier, Svalbard?, *Atmospheric Chemistry and Physics*, 17, 12779–12795, 2017.

Schwarz, J. P., Gao, R. S., Fahey, D. W., Thomson, D. S., Watts, L. A., Wilson, J. C., Reeves, J. M., Darbeheshti, M., Baumgardner, D. G., Kok, G. L., Chung, S. H., Schulz, M., Hendricks, J., Lauer, A., Karcher, B., Slowik, J. G., Rosenlof, K. H., Thompson, T. L., Langford, A. O., Loewenstein, M., and Aikin, K. C.: Single-particle measurements of midlatitude black carbon and light-scattering aerosols from the boundary layer to the lower stratosphere, *Journal of Geophysical Research*, 111, D16207, 2006.

Schwarz, J. P., Doherty, S. J., Li, F., Ruggiero, S. T., Tanner, C. E., Perring, A. E., Gao, R. S. and Fahey, D. W.: Assessing Single Particle Soot Photometer and Integrating Sphere/Integrating Sandwich Spectrophotometer measurement techniques for quantifying black carbon concentration in snow, *Atmospheric Measurement Techniques*, 5, 2581–2592, 2012.

Serreze, M. C. and Barry, R. G.: Processes and impacts of Arctic amplification: A research synthesis, *Global Planetary Change*, 77, 85–96, 2011.

Sharma, S., Lavoué, D., Cachier, H., Barrie, L. A., and Gong, S. L.: Long-term trends of the black carbon concentrations in the Canadian Arctic, *Journal of Geophysical Research: Atmospheres*, 109, D15203, 2004.

Shaw, G. E.: The Arctic Haze Phenomenon, *Bulletin of the American Meteorological Society*, 76, 2403–2413, 1995.

Shindell, D. T., Chin, N., Dentener, F., Doherty, R. M., Faluvegi, G., Fiore, A. M., Hess, P., Koch, D. M., MacKenzie, I. A., Sanderson, M. G., Schultz, M. G., Schulz, M., Stevenson, D. S., Teich, H., Textor, C., Wild, O., Bergman, D. J., Bey, I., Bian, H., Cuvelier, C., Duncan, B. N., Folberth, G., Horowitz, L. W., Jonson, J., Kaminski, J. W., Marmer, E., Park, R., Pringle, K. J., Szopa, S., Takemura, T., Zeng, G., Keating, T.J., and Zuber, A.: A multi-model assessment of pollution transport to the Arctic, *Atmospheric Chemistry and Physics*, 8, 5353–5372, 2008.

Sigl, M., McConnell, J. R., Layman, L., Maselli, O., McGwire, K., Pasteris, D., Dahl-Jensen, D., Steffensen, J. P., Vinther, B., Edwards, R., Mulvaney, R., and Kipfstuhl, S.: A new bipolar ice core record of volcanism from

WAIS Divide and NEEM and implications for climate forcing of the last 2000 years, *Journal of Geophysical Research: Atmospheres*, 118, 1151–1169, 2013.

Simoneit, B. R. T.: Biomass burning – a review of organic tracers for smoke from incomplete combustion, *Applied Geochemistry*, 17, 129–162, 2002.

Spielvogel, J. J.: Western Civilization: A Brief History, Seventh Edition, Wadsworth, Cengage Learning, Boston, USA, 732 pp, 2010.

Stephens, M., Turner, N., and Sandberg, J.: Particle identification by laser-induced incandescence in a solid-state laser cavity, *Applied Optics*, 42, 3726–3736, 2003.

Stocks, B. J., Mason, J. A., Todd, J. B., Bosch, E. M., Wotton, B. M., Amiro, B. D., Flannigan, M. D., Hirsch, K. G., Logan, K. A., Martell, D. L., and Skinner, W. R.: Large forest fires in Canada, 1959–1997, *Journal of Geophysical Research*, 108(D1), 8149, 2003.

Stohl, A.: Characteristics of atmospheric transport into the Arctic troposphere, *Journal of Geophysical Research*, 111, D11306, 2006.

Stohl, A., Klimont, Z., Eckhardt, S., Kupiainen, K., Shevchenko, V. P., Kopeikin, V. M., and Novigatsky, A. N.: Black carbon in the Arctic: the underestimated role of gas flaring and residential combustion emissions, *Atmospheric Chemistry and Physics*, 13, 8833–8855, 2013.

Thompson, L. G., Yao, T., Mosley-Thompson, E., Davis, M. E., Henderson, K. A., and Lin, P.-N.: A high-resolution millennial record of the South Asian Monsoon from Himalayan ice cores, *Science*, 289, 1916–1919, 2000.

Tunved, P., Ström, J., and Krejci, R.: Arctic aerosol life cycle: linking aerosol size distributions observed between 2000 and 2010 with air mass transport and precipitation at Zeppelin station, Ny-Ålesund, Svalbard, *Atmospheric Chemistry and Physics*, 13, 3643–3660, 2013.

Vega, C. P., Pohjola, V. A., Samyn, D., Pettersson, R., Isaksson, E., Björkman, M. P., Martma, T., Marca, A., and Kaiser, J.: First ice core records of NO3− stable isotopes from Lomonosovfonna, Svalbard, *Journal of Geophysical Research: Atmospheres*, 120, 313–330, 2015a.

Vega, C. P., Björkman, M. P., Pohjola, V. A., Isaksson, E., Pettersson, R., Martma, T., Marca, A. D., and Kaiser, J.: Nitrate stable isotopes and major ions in snow and ice samples from four Svalbard sites, *Polar Research*, 34, 23246, 2015b.

Vega, C. P., Pohjola, V. A., Beaudon, E., Claremar, B., van Pelt, W. J. J., Pettersson, R., Isaksson, E., Martma, T., Schwikowski, M., and Bøggild, C. E.: A synthetic ice core approach to estimate ion relocation in an ice field site experiencing periodical melt: a case study on Lomonosovfonna, Svalbard, *The Cryosphere*, 10, 961–976, 2016.

Wendl, I. A.: High resolution records of black carbon and other aerosol constituents from the Lomonosovfonna 2009 ice core, PhD thesis, University of Bern, 2014.

Wendl, I. A., Menking, J. A., Färber, R., Gysel, M., Kaspari, S. D., Laborde, M. J. G., and Schwikowski, M.: Optimized method for black carbon analysis in ice and snow using the Single Particle Soot Photometer, *Atmospheric Measurement Techniques*, 7, 2667–2681, 2014.

Wendl, I. A., Eichler, A., Isaksson, E., Martma, T., and Schwikowski, M.: 800-year ice-core record of nitrogen deposition in Svalbard linked to ocean productivity and biogenic emissions, *Atmospheric Chemistry and Physics*, 15, 7287–7300, 2015.

Wetter, O., Pfister, C., Werner, J. P., Zorita, E., Wagner, S., Seneviratne, S. I., Herget, J., Grünewald, U., Luterbacher, J., Alcoforado, M.-J., Barriendos, M., Bieber, U., Brázdil, R., Burmeister, K. H., Camenisch, C., Contino, A., Dobrovolný, P., Glaser, R., Himmelsbach, I., Kiss, A., Kotyza, O., Labbé, T., Limanówka, D., Litzenburger, L., Nordl, Ø., Pribyl, K., Retsö, D., Riemann, D., Rohr, C., Siegfried, W., Söderberg, J., and Spring, J.-L.: The year-long unprecedented European heat and drought of 1540 – a worst case, *Climatic Change*, 125, 349–363, 2014.

Xu, B., Cao, J., Joswiak, D. R., Liu, X., Zhao, H., and He, J.: Post-depositional enrichment of black soot in snow-pack and accelerated melting of Tibetan glaciers, *Environmental Research Letters*, 7, 014022, 2012.

Zagorodnov, V. S., Samoylov, O. Y., Raykovskiy, Y. V., Tarusov, A. V., Kuznetsov, M. N., and Sazonov, A. V.: Glubinnoye stroyeniye lednikovogo plato Lomonosova na o. Zap. Shpitsbergen [Depth structure of the Lomonosov ice plateau, Spitsbergen], *Mater. Glyatsiol. Issled.*, 50, 119–126, 1984.

Zdanowicz, C. M., Proemse, B. C., Edwards, R., Feiteng, W., Hogan, C. M., and Kinnard, C.: Historical black carbon deposition in the Canadian High Arctic: A 190-year long ice-core record from Devon Island, *Atmospheric Chemistry and Physics Discussions*, 2017, in review.

Zennaro, P., Kehrwald, N., McConnell, J. R., Schüpbach, S., Maselli, O. J., Marlon, J., Vallelonga,P., Leuenberger, D., Zangrando, R., Spolaor, A., Borrotti, M., Barbaro, E., Gambaro, A., and Barbante, C.: Fire in ice: two millennia of boreal forest fire history from the Greenland NEEM ice core, *Climate of the Past*, 10, 1905–1924, 2014.

5 A Holocene black carbon ice-core record of biomass burning in the Amazon Basin from Illimani, Bolivia

Dimitri Osmont[1,2,3], Michael Sigl[1,2], Anja Eichler[1,2], Theo M. Jenk[1,2], Margit Schwikowski[1,2,3]

[1]Laboratory of Environmental Chemistry, Paul Scherrer Institut, 5232 Villigen, Switzerland
[2]Oeschger Centre for Climate Change Research, University of Bern, 3012 Bern, Switzerland
[3]Department of Chemistry and Biochemistry, University of Bern, 3012 Bern, Switzerland

Correspondence to: Margit Schwikowski (margit.schwikowski@psi.ch)

Abstract

The Amazon Basin is one of the major contributors to global biomass burning emissions. However, regional paleofire trends remain partially unknown. Due to their proximity to the Amazon Basin, Andean ice cores are suitable to reconstruct paleofire trends in South America and improve our understanding of the complex linkages between fires, climate and humans. Here we present the first refractory black carbon (rBC) ice-core record from the Andes as a proxy for biomass burning emissions in the Amazon Basin, derived from an ice core drilled at 6300 m a.s.l. from Illimani glacier in the Bolivian Andes and spanning the entire Holocene back to the last deglaciation 13000 years ago. The Illimani rBC record displays a strong seasonality with low values during the wet season and high values during the dry season due to the combination of enhanced biomass burning emissions in the Amazon Basin and less precipitation at the Illimani site. Significant positive (negative) correlations were found with reanalyzed temperature (precipitation) data, respectively, for regions in Eastern Bolivia and Western Brazil characterized by a substantial fire activity. rBC long-term trends indirectly reflect regional climatic variations through changing biomass burning emissions as they show higher (lower) concentrations during warm/dry (cold/wet) periods, respectively, thus confirming that most of the Holocene Northern Hemisphere climate variations, such as the Younger Dryas, the 8.2 ka event, the Holocene Climatic Optimum, the Medieval Warm Period or the Little Ice Age, occurred as well in tropical South America. Highest rBC concentrations of the entire record occurred during the Holocene Climatic Optimum 7000–3000 BC, suggesting that this outstanding warm and dry period caused an exceptional biomass burning activity, unprecedented in the context of the past 13000 years. Recent rBC levels, rising since 1730 AD in the context of increasing temperatures and deforestation, are similar to those of the Medieval Warm Period. No decrease was observed in the 20th century, in contradiction with the global picture ("broken fire hockey stick" hypothesis).

5.1 Introduction

Fires play a major role in the global carbon cycle by emitting aerosols and greenhouse gases. Current global CO_2 emissions due to biomass burning represent ~50 % of those originating from fossil fuel combustion *(Bowman et al., 2009)*. The mean annual burned area worldwide amounts to 348 Mha for the time period 1997–2011 *(Giglio et al., 2013)*. South America is, after Africa, the second most affected region by biomass burning, accounting for 16 to 27 % of the global annual burned area between 1997 and 2004 *(Kloster et al., 2010; Schultz et al., 2008)*, leading to carbon emissions ranging from ~300 to 900 TgC yr^{-1} *(Kloster et al., 2010; Schultz et al., 2008)*. Biomass burning

102

mainly occurs in Southern Hemisphere South America, representing 13.6 % of the global annual carbon emissions from biomass burning *(van der Werf et al., 2010)*, with Brazil and Bolivia being the two countries most affected, accounting for 60 % and 10 % of active fire observations, respectively *(Chen et al., 2013)*. Savannas (cerrados) and seasonally dry tropical forests (SDTFs) located at the southern edge of the Amazon Basin are prone to extensive fires during the dry season between June and October, when many fires are ignited for land clearance purposes for agriculture and grazing *(Mouillot and Field, 2005; Power et al., 2016)*. Savanna burned area over South America remained fairly stable over the 20th century *(Mouillot and Field, 2005; Schultz et al., 2008)*. However, this trend masks regional discrepancies: while burning decreased along the Brazilian coast, it has strongly increased in the western part due to deforestation *(Mouillot and Field, 2005)*. On the contrary, tropical rain forests centered further north in the Amazon Basin rarely burn naturally due to persistent moist conditions and limited dry lightning *(Bowman et al., 2011; Cochrane, 2003)*, but since the 1960s they have experienced intensive deforestation fires at their southern edge, known as the "arc of deforestation" *(Cochrane et al., 1999)*. Southern Hemisphere South America accounted for 37 % of all deforestation fires worldwide over the time period 2001–2009 *(van der Werf et al., 2010)*. However, the contribution from deforestation fires to the total number of fires observed in South America seems to have decreased since 2005, particularly in Brazil due to stricter environmental policies, while fire activity significantly increased in Bolivia *(Chen et al., 2013)*. A similar observation was made by *van Marle et al. (2017a)*, who reported a strong increase in deforestation fires in the 1990s followed by a general decline since the 2000s.

For the time period before the start of satellite measurements (1980s), the lack of accurate data from the Amazon Basin hinders a detailed reconstruction of fire history. Historical reconstructions based on fire statistics, land-use practices and vegetation type and history have shown a dramatic increase of fires in the forested parts of South America over the last century *(Mouillot and Field, 2005)* as burning was almost absent from the Amazon Basin before the 1960s. So far, charcoal records from lake sediment cores were the only way to infer paleofire trends in this region before the 20th century. They revealed that biomass burning trends in Tropical South America were less pronounced than in other regions of the Americas, underlining the absence of a clear driver for biomass burning possibly due to the large diversity of climate, vegetation and topography in this region *(Power et al., 2012)*. Nevertheless, the last 2000 years showed an overall slight decrease in fire activity until around 1800 AD, followed by a strong increase in the 20th century *(Power et al., 2012)*. This is in contradiction with the "broken fire hockey stick" hypothesis *(Marlon et al., 2008)* suggesting a global decoupling since 1870 AD between the decreasing biomass burning trend and its main drivers, namely increasing temperature and population density, due to fire management and global expansion of intensive agriculture and grazing that fragmented the landscape. Composite charcoal records for Tropical South America display a great variability through the entire Holocene, with higher-than-present biomass burning levels in the mid-Holocene between 6500 and 4500 BP *(Marlon et al., 2013)*. However, charcoal records only reflect local to regional conditions and therefore have to be compiled while ice cores have the potential to integrate information over continental scales *(Kehrwald et al., 2013)*. Ice-core records from Antarctica have also shown their ability to give an insight into past biomass burning trends in the Southern Hemisphere, revealing elevated biomass burning activity around 8000 to 6000 BP in Southern America *(Arienzo et al., 2017)*, or confirming an overall agreement with the "broken fire hockey stick" hypothesis *(Wang et al., 2010)*. Given the remoteness of the Antarctic continent, limitations may arise from transport patterns, thus advocating for the use of ice-core records located closer to the source regions.

As the major moisture source in the tropical Andes is the Amazon Basin and ultimately the Atlantic Ocean *(Garreaud et al., 2003; Vuille et al., 2003)*, ice cores from tropical Andean glaciers could serve as potential archives of past biomass burning trends in the Amazon Basin and thus form the missing link between South American lake sediment charcoal records and Antarctic ice-core records, which could be helpful to better constrain fire models and historical fire databases *(van Marle et al., 2017b)*. However, the preservation of a biomass burning signal in tropical Andean ice cores has never been investigated extensively so far. *Bonnaveira (2004)* noted that an Amazonian biomass burning contribution was expressed in the concentrations of organic species (e.g. oxalate) at the end of the dry season (August–October) in aerosols collected at Plataforma Zongo, 40 km north of the Illimani site, but no paleofire reconstructions have been made in the Andes by means of ice cores. Nearby sedimentary charcoal records do show a biomass burning variability in the Bolivian Amazonian lowlands through the Holocene *(Brugger et al., 2016; Power et al., 2016)*, with enhanced burning during warmer/drier periods such as the early to mid-Holocene (approximately from 8000 to 5500 BP, *Baker et al., 2001)* and limited burning during colder/wetter periods such as the last deglaciation or the Little Ice Age.

Ice-core studies suggested that a variety of biomass burning proxies could be used to reconstruct paleofires. For instance, ammonium (NH_4^+) has been widely analyzed in polar ice cores from Greenland *(Fischer et al., 2015; Legrand et al., 2016)* and Antarctica *(Arienzo et al., 2017)*. Simple organic acids (formate, oxalate) were also considered, but they can experience post-depositional effects *(Legrand et al., 2016)*. However, the aforementioned compounds are not specific proxies as they also reflect continuous biogenic emissions from vegetation and soils in their background variations, while only peak values can be associated with biomass burning events *(Fischer et al., 2015)*. Black carbon (BC), produced by the incomplete combustion of biomass and fossil fuels *(Bond et al., 2013)*, has the advantage of being a specific proxy for biomass burning in preindustrial times, when no significant anthropogenic sources existed. Aerosol source apportionment studies in Amazonia have shown that recent BC emissions in this region originate only from biomass burning *(Artaxo et al., 1998)*. Several ice-core studies link preindustrial BC variations with biomass burning trends *(Arienzo et al., 2017; Osmont et al., 2018; Zennaro et al., 2014)*. However, an increasing anthropogenic BC contribution from fossil fuel combustion has been observed in ice cores from Greenland *(Keegan et al., 2014; McConnell et al., 2007; Sigl et al., 2013)* and the Alps *(Jenk et al., 2006; Lavanchy et al., 1999; Sigl et al., 2018)* since the second half of the 19th century, and from Eastern Europe *(Lim et al., 2017)* and Asia *(Kaspari et al., 2011; Wang et al., 2015)* in the last decades.

Here, we present the first Andean BC ice-core record, derived from the analysis of the Illimani 1999 (IL-99) ice core. When referring to our measurements using the laser-induced incandescence method, the term refractory black carbon (rBC) will be employed, following the recommendations of *Petzold et al. (2013)*. After discussing the seasonality of the rBC signal and the connections with regional climate parameters and biomass burning, we will present rBC long-term trends of the last millennium and through the Holocene, link them with climate variability and compare them to existing ice-core and lake sediment records.

5.2 Methods

5.2.1 Ice core and site characteristics

In June 1999, two ice cores were drilled at 6300 m a.s.l. on Nevado Illimani, Bolivia, on a glacier saddle between the summits of Pico Central and Pico Sur (16°39´ S, 67°47´ W, **Fig. 5.1**) by a joint French-Swiss team from the Institut de Recherche pour le Développement (IRD, France) and the Paul Scherrer Institut (PSI, Switzerland), using the Fast Electromechanical Lightweight Ice Coring System (FELICS, *Ginot et al., 2002a*). Bedrock was reached at 136.7 m depth (French core) and 138.7 m depth (Swiss core, this study). Low boreholes temperatures (<−7 °C) and very few ice lenses indicative of meltwater percolation ensured a good preservation of the chemical signal recorded in the ice core *(Kellerhals et al., 2010a)*. Further details can be found in *Knüsel et al. (2003)* and *Knüsel et al. (2005)*. *Bonnaveira (2004)* investigated post-depositional effects such as sublimation and wind scouring and showed that their influence on the preservation of ionic species remained limited compared to actual seasonal variations in concentration.

Fig. 5.1: Map showing the location of Nevado Illimani in Bolivia and the other sites and regions of interest in Bolivia and Brazil mentioned in the study (adapted from openstreetmap.org).

The climate of the Bolivian Altiplano is characterized by a wet season during the Austral summer (November–March) and a dry season during the Austral winter (April–October). Moisture mainly originates from the Amazon Basin, and ultimately from the Atlantic Ocean *(Garreaud et al., 2003; Vuille et al., 2003)*. Moreover, an interannual variability in precipitation is induced by El Niño Southern Oscillation (ENSO) processes. El Niño years tend to be drier on average as they inhibit moisture influx from the East whereas La Niña years are usually wetter *(Garreaud and Aceituno, 2001; Garreaud et al., 2003)*. The Illimani, located on the eastern margin of the Altiplano, can receive moisture influx also during the dry season, leading to a less pronounced seasonality with summer months (December–January–February,) representing only 50–60 % of the annual mean precipitation *(Garreaud et al., 2003)*. This trend is also reflected in the Illimani ice core record, compared to other Andean ice-core sites showing a more pronounced seasonality *(Ginot et al., 2002b)*. Similarly, the precipitation modulation by ENSO remains weaker at the Illimani site compared to the western side of the Andes *(Garreaud et al., 2003; Vuille et al., 2000)*.

Previous studies on the IL-99 ice core include the investigation of a potential impact of ENSO on the ionic records *(Knüsel et al., 2005)*, revealing elevated dust values during warm phases of ENSO, the use of thallium as a possible volcanic eruption tracer *(Kellerhals et al., 2010b)*, regional temperature reconstruction for the last 1600 years based on the NH_4^+ record *(Kellerhals et al., 2010a)*, the

historical reconstruction of regional silver production and recent leaded gasoline pollution derived from the lead record *(Eichler et al., 2015)*, and that of copper metallurgy inferred from the copper record *(Eichler et al., 2017)*, showing that earliest extensive copper metallurgy started in the Andes 2700 years ago.

5.2.2 Ice-core dating

Dating of the core was performed by using a multi-parameter approach combining annual layer counting of the electrical conductivity signal, reference horizons such as the 1963 AD nuclear fallout peak and volcanic eruptions (AD 1258, 1815, 1883, 1963, 1982, 1991), the ^{210}Pb decay *(Knüsel et al., 2003)*, and ^{14}C dating *(Kellerhals et al., 2010a)*. A continuous age-depth relationship was established by fitting a two-parameter glacier flow model through the reference horizons, except between the last five ^{14}C ages where linear interpolation was used due to the very strong layer thinning *(Kellerhals et al., 2010a)*, resulting in a bottom age of 13000 years BP and an overall accumulation rate of 0.58 m yr^{-1} weq (water equivalent). Dating uncertainty is estimated to be ±2 years in the vicinity of volcanic horizons and ±5 years otherwise back to 1800 AD, ±20 years for the time period 1250–1800 AD and ±110 years at the youngest ^{14}C age (1060–1280 BP, *Kellerhals et al., 2010a*).

5.2.3 Sampling and rBC analysis

The IL-99 ice core was cut for rBC analysis into 1.9 x 1.9 cm sections from the inner part of the core in a −20 °C cold room at PSI following clean protocols *(Eichler et al., 2000)*. Sampling resolution was 10 cm for the first 316 samples down to 33.15 m depth (spanning 1966–1999 AD) and 3–4 cm for the remaining 2754 samples below 33.15 m down to the bottom. A total of 3070 samples was obtained. 243 replicates from parallel ice-core sticks were cut from 12 different ice-core sections to check the reproducibility of our analyses. Furthermore, the section between 127.4 and 133 m depth (spanning roughly 0–2000 BC) was resampled at 3–7 cm resolution (121 samples) specifically due to poor ice-core quality (chips). Samples for the rBC analyses were collected in pre-cleaned 50 mL polypropylene tubes and stored at −20 °C.

The entire IL-99 ice core was analyzed for rBC at PSI between April and June 2017, following the method described by *Wendl et al. (2014)*. After melting the ice-core samples at room temperature and 25 min sonication in an ultrasonic bath, rBC was quantified using a Single Particle Soot Photometer (SP2, Droplet Measurement Technologies, USA, *Schwarz et al., 2006; Stephens et al., 2003*) coupled to an APEX-Q jet nebulizer (Elemental Scientific Inc., USA). Further analytical details regarding calibration, reproducibility and autosampling method can be found in *Osmont et al. (2018)*. Replicate samples for the IL-99 ice core showed good reproducibility (r = 0.65, p < 0.001, n = 243) in particular regarding rBC peak values and trends, while the resampled part in the period 0–2000 BC (121 samples) showed notable agreement with the original dataset, thus confirming the reliability of our rBC analysis.

5.3 Results and discussion

5.3.1 rBC seasonal variability in the Illimani ice core

The Illimani rBC record displays a strong seasonal variability, with high concentrations corresponding to the maximum of the dry season (June–October) and low concentrations during the wet season (November–March). In the IL-99 ice core, peak values typically range between 2 and 10 ng g^{-1}, with a high year-to-year variability and a maximum of 13.3 ng g^{-1} in 1996, while the wet season background

remains fairly constant, below 0.5 ng g^{-1} **(Fig. 5.2a)**. The observed rBC seasonality is similar to previous observations made on records of trace elements *(Correia et al., 2003)* and major ions *(Knüsel et al., 2005*; see e.g. NH$_4^+$ and Ca^{2+}, **Fig. 5.2b-c)** reflecting the seasonality in precipitation **(Fig. 5.2d)**. During the wet season, abundant precipitation occurs, which dilutes the chemical signal in the snow, whereas during the dry season, the little amount of precipitation leads to highly concentrated wet deposition and also enables dry deposition of dust particles *(Bonnaveira, 2004; Correia et al., 2003; De Angelis et al., 2003)*. The seasonal signal in the Illimani ice core is therefore mainly the result of transport to and deposition at the Illimani site combined with the fact that dust mobilization from the Altiplano *(Kellerhals et al., 2010a; Knüsel et al., 2005)* and biomass burning emissions in the Amazon Basin also peak during the dry season *(Mouillot and Field, 2005; Power et al., 2016)*.
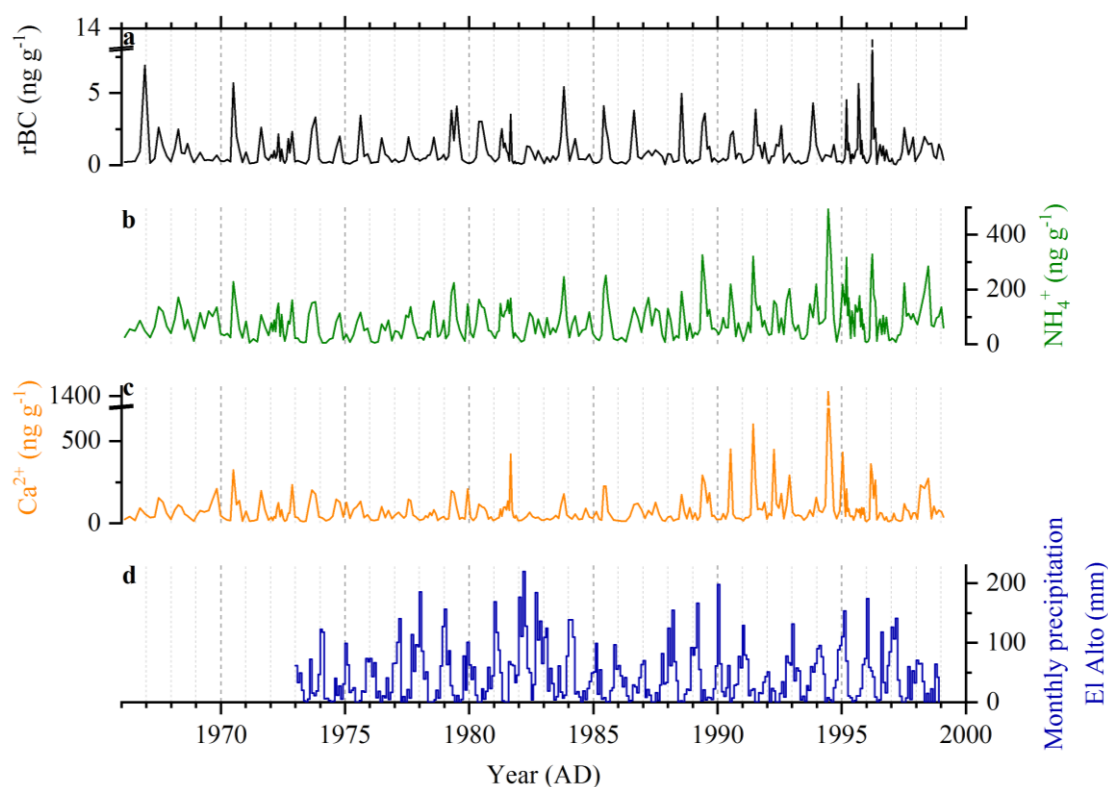

Fig. 5.2: Concentrations of a) rBC, b) ammonium and c) calcium in the upper 33.15 m of the IL-99 ice core (raw data). d) Monthly precipitation data from El Alto weather station, located 40 km west of Illimani, near the city of La Paz. Data is available on the website of the US National Climatic Data Center (NCDC) at the following address: *https://www7.ncdc.noaa.gov/CDO/cdoselect.cmd?datasetabbv=GSOD*.

5.3.2 Connection with climate parameters in South America during the 20th century

During the last century, rBC concentrations did not show an evident long-term trend, but decadal changes peaking in the 1900s, 1940s and 1960s **(Fig. 5.3a)**. These maxima are not in agreement with model-based BC emissions **(Fig. 5.3c)**. We extracted the time series of BC emissions from biomass burning for the 5x5° grid cell containing the Illimani site used in the Coupled Model Intercomparison Project Phase 6 (CMIP6) simulations *(van Marle et al., 2017b)* and compared it to the IL-99 rBC record for the time period 1900–2000 AD. Even if all the BC emissions recorded at Illimani are not expected to come solely from this grid cell, it is striking to note that estimated BC emissions remained perfectly constant until the start of satellite measurements in the 1980s, when the data coverage

107

greatly improved. Estimated BC emissions subsequently exhibited much more variability and increased by more than one order of magnitude until the late 1990s.

A direct relationship between the rBC record and biomass burning trends in the Amazon Basin before 1999 cannot be assessed due to the lack of accurate biomass burning statistics from Bolivia and Brazil, where the number of active fires is retrieved from satellite data starting only in 1998. In addition, data about the burned area remain scarce and are associated with larger uncertainties, despite their greater significance in terms of environmental impacts and aerosol emissions *(Montellano, 2012)*.
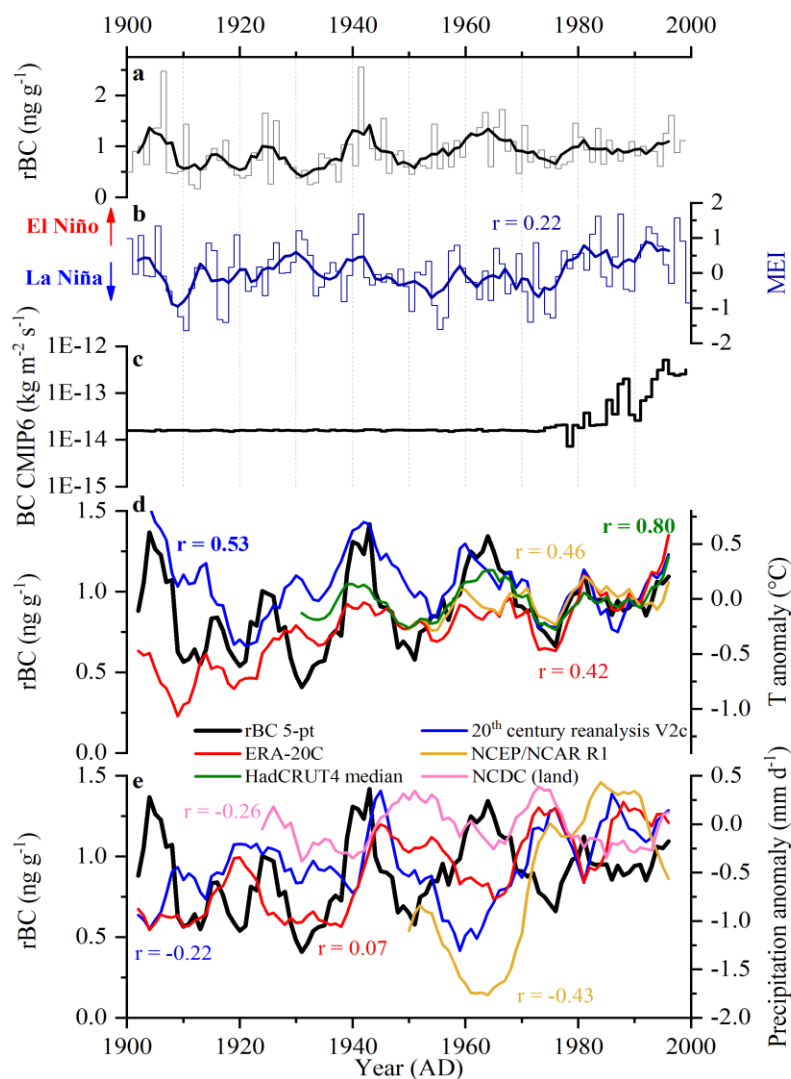

Fig. 5.3: Comparison of the IL-99 rBC record with South American climate parameters for the time period 1900–2000 AD. a) rBC record from the IL-99 ice core (thin lines: annual averages, thick lines: 5-year moving averages). b) Multivariate ENSO Index (MEI, thin lines: annual averages, thick lines: 5-year moving averages, *Wolter and Timlin, 1993, 1998, 2011*), a higher (lower) value standing for a stronger El Niño (La Niña) event, respectively. The Extended MEI is used before 1950. c) Annual BC emissions derived from the CMIP6 simulations for the 5x5° grid cell containing the Illimani site *(van Marle et al., 2017b)*. Comparison between the IL-99 rBC record and four d) temperature and e) precipitation datasets for the Amazon Basin (4 °N–16 °S and 51–76 °W). Data are 5-year moving averages and were extracted from the KNMI Climate Explorer. Anomalies are relative to the years 1971–2000. Pearson correlation coefficients between the IL-99 rBC record and the associated climate datasets were calculated based on 5-year moving averages and coefficients in bold are statistically significant.

For investigating major causes for rBC changes during the 20th century, we studied spatial and temporal correlations between the IL-99 rBC record and two important drivers of biomass burning activity, namely temperature and precipitation. Significant correlations ($p < 0.05$) between the IL-99 rBC record and re-analyzed temperature and precipitation from the NCEP/NCAR R1 dataset were found for areas in the Amazon Basin located East of the Illimani site, which are assumed to be the main source regions of the rBC deposited at Illimani **(Fig. 5.4)**. 5-year moving averages were used owing to the ice-core dating uncertainty which prevents detection of an annual connection with temperature and precipitation data. Positive correlations with temperature are highest along the arc of deforestation in Brazil and in regions of Eastern Bolivia (states of El Beni and Santa Cruz) and Western Brazil (state of Rondônia and Mato Grosso) where extensive fires occur during the dry season. Similarly, negative correlations with precipitation are highest along the Bolivian-Brazilian border, for the states of Santa Cruz and Mato Grosso. Comparisons between temperature/precipitation time series for the Amazon Basin (defined here as the region between 4 °N–16 °S and 76 °W–51 °W) and the IL-99 rBC record confirm that higher rBC concentrations are observed during warmer and drier periods, such as the 1900s, the 1940s and the 1960s **(Fig. 5.3d and 5.3e)**. Different temperature/precipitation datasets were used to highlight their strong variability, but the main conclusion remains unchanged. Depending on the used dataset, variations in temperature and precipitation account for 18–64 % and 1–18 % of the rBC variance, respectively.
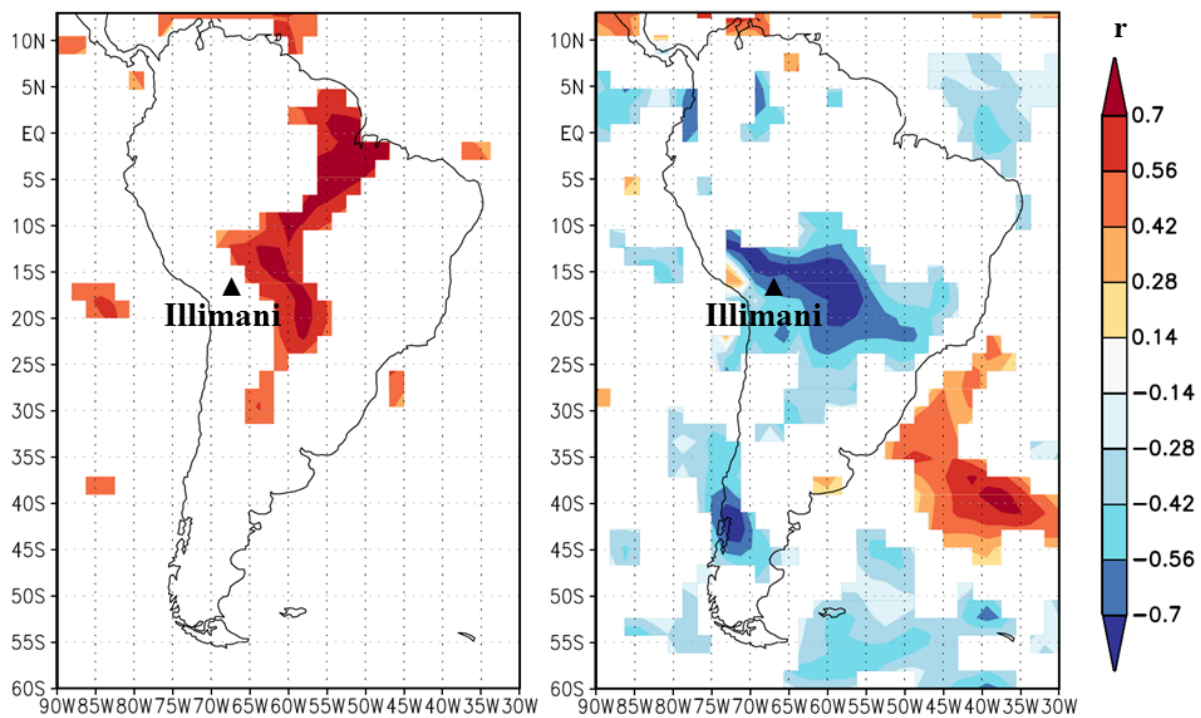

Fig. 5.4: Spatial correlation over South America between the IL-99 rBC record and re-analyzed temperature (left panel) and precipitation (right panel) data from the NCEP/NCAR R1 dataset for the time period 1948–1998, available on the KNMI Climate Explorer (*https://climexp.knmi.nl/start.cgi*). Data are annual averages smoothed with a 5-year running mean.

Potential connections between the IL-99 rBC record and the ENSO phenomenon were also investigated. In general, and similarly to the Altiplano, El Niño phases of ENSO induce drier and warmer conditions over the Amazon Basin, while La Niña phases are wetter and cooler *(Aceituno, 1988; Foley et al., 2002; Garreaud et al., 2009)*. The trend is more pronounced during the wet season *(Garreaud et al., 2009)*. However, this relationship weakens towards the western part of the Amazon

Basin *(Garreaud et al., 2009; Ronchail et al., 2002)* and becomes more complex on the Bolivian slopes between the Amazon Basin and the Altiplano as opposite effects can be observed depending on the altitude *(Ronchail and Gallaire, 2006)*. To determine whether ENSO can modulate rBC concentrations in the Illimani ice core, we compared the 20th-century IL-99 rBC record to the Multivariate ENSO Index (MEI, **Fig. 5.3b**) spanning 1950–2018 *(Wolter and Timlin, 1993, 1998)* and the Extended MEI reaching back to 1871 *(Wolter and Timlin, 2011)*. The low correlation coefficient between the rBC record and the MEI indicates no evident impact of ENSO. Interestingly, the highest two rBC annual values occurred during some of the most outstanding El Niño events (1905–1906 and 1941), but rBC values can also remain low during strong El Niño phases, for instance in 1929–1930. Conversely, rBC annual values are not necessarily low during intense La Niña phases, as seen in 1910, 1917 or 1954–1956. To comprehensively assess this relationship, we calculated the average rBC concentration for all the El Niño and La Niña years for the time period 1900–1998. Average rBC concentrations of 0.85 ± 0.44 ng g^{-1} for El Niño years (50 years in total) and 0.93 ± 0.42 ng g^{-1} for La Niña years (49 years in total) show that no significant difference is visible between the warm and cold phases of ENSO in the rBC record. Several hypotheses contribute to explain this lack of relationship despite drier conditions during El Niño years. First, it is well-known that the eastern side of the Andes is less influenced by ENSO modulation as the major moisture source is the Amazon Basin and not the Pacific Ocean, contrary to the western part of the Andes *(Garreaud et al., 2003; Vuille et al., 2000)*. Second, there is a difference in timing as the precipitation suppression induced by ENSO is more important during the wet season, whereas rBC emissions peak during the dry season due to biomass burning and limited but highly concentrated precipitation. Furthermore, if no precipitation occurs during the dry season owing to the El Niño phase of ENSO, (almost) no rBC will be deposited on the snow surface at the Illimani site as BC is preferentially removed from the atmosphere by wet deposition *(Cape et al., 2012; Ruppel et al., 2017)*. Lastly, as the moisture influx from the East tends to be reduced during El Niño years, the contribution from Eastern-origin rBC-enriched precipitation due to biomass burning in the Amazon Basin to the total amount of precipitation at Illimani becomes weaker.

5.3.3 rBC variability over the last 1000 years

In **Fig. 5.5a**, we present the IL-99 rBC long-term record for the last 1000 years. Higher rBC concentrations were observed between 1000 and 1300 AD (average $\pm$ 1σ unless otherwise stated: 0.94 ± 0.56 ng g^{-1}), in agreement with the temperature maximum corresponding to the Medieval Warm Period (MWP) in the Northern Hemisphere (NH) and also previously described in the IL-99 ammonium record by *Kellerhals et al. (2010a)*. Following the MWP, rBC concentrations slowly declined until they reached a minimum in the 18th century (average: 0.37 ± 0.34 ng g^{-1}) reflecting the Little Ice Age (LIA). The lowest rBC concentrations were recorded around 1730 AD, following the Maunder solar minimum. The LIA decline was interrupted by higher concentrations during the time periods 1460–1550 AD and 1630–1670 AD, potentially related to the apogee of the Inca Empire at the end of the 15th century and the Spanish colonization of Bolivia that started around 1535. Several cities were created on the Altiplano at that time (Sucre in 1538, Potosí in 1546 and La Paz in 1548). Mining activities rapidly took off and left an imprint on the IL-99 lead and copper records *(Eichler et al., 2015, 2017*, respectively). These time periods are also corroborated by the composite charcoal record for Tropical South America showing local maxima of fire activity (**Fig. 5.5e**; *Power et al., 2012*). Following the 1730 AD minimum, rBC concentrations started to rise until present time (average 1900–1999: 0.91 ± 1.23 ng g^{-1}). The IL-99 cerium record (**Fig. 5.5b**; *Eichler et al., 2015*), used as a dust deposition tracer, shows that the MWP was characterized by dustier and drier conditions which can indirectly explain the corresponding rBC peak as dry conditions favor biomass burning and lead to reduced but more concentrated wet deposition. Contrariwise, the LIA is generally marked by less

dry conditions, except the dusty period ~1600–1650 AD. The similar long-term variability of rBC and temperature **(Fig. 5.5a)** provides evidence that temperature is indeed a major driving force for changing biomass burning activity, in agreement with the results for the 20th century *(see section 5.3.2)*. Discrepancies between the two records, particularly between 1400 and 1700 AD when temperature anomalies were constantly negative while rBC concentrations displayed higher values during 1460–1550 AD and 1630–1670 AD, can most probably be related to an additional anthropogenic impact as discussed above. To summarize, rBC concentrations in the Illimani record tend to be lower during periods of colder/wetter climate and higher during periods of warmer/drier climate, suggesting that rBC could be used as an indirect temperature/moisture proxy through biomass burning variations.
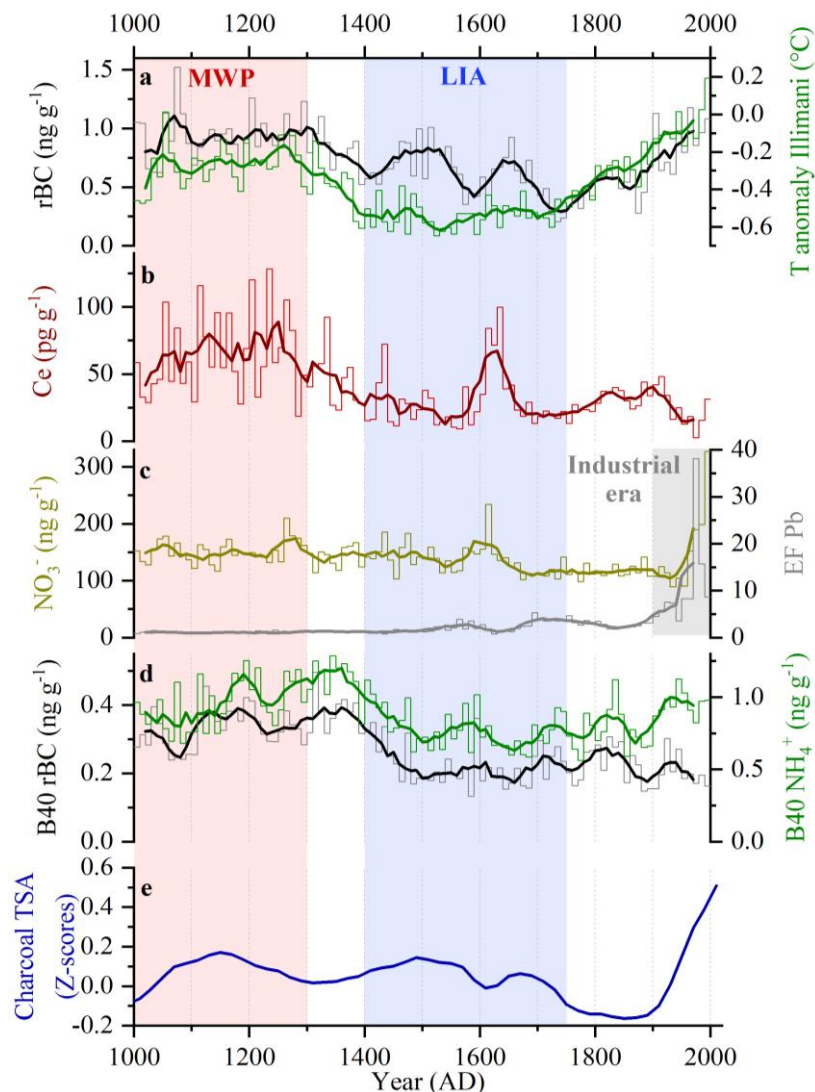

Fig. 5.5: Comparison for the time period 1000–2000 AD between a) IL-99 rBC record (left scale) and temperature anomalies (right scale) inferred from the ammonium IL-99 record *(Kellerhals et al., 2010a)*, b) IL-99 cerium record as a dust proxy *(Eichler et al., 2015)*, c) IL-99 nitrate (left scale) and lead enrichment factors (right scale) to illustrate 20th century anthropogenic impact *(Eichler et al., 2015)*, d) Antarctic B40 rBC (left scale) and ammonium (right scale) records *(Arienzo et al., 2017)* and e) composite charcoal record (Z-scores of transformed charcoal influx) for Tropical South America *(Power et al., 2012)*. Thin lines are 10-year averages and thick lines are 50-year moving averages, except for panel e where they represent 20-year averages. Timings of MWP (1000–1300 AD) and LIA (1400–1750 AD) are defined based on the IL-99 rBC and temperature records.

Comparable long-term trends were found in the B40 rBC and NH_4^+ ice-core records from Antarctica **(Fig. 5.5d)** with lower (higher) rBC and NH_4^+ concentrations during the LIA (MWP), respectively *(Arienzo et al., 2017)*. The authors of this study suggested South American biomass burning as the main source of Antarctic rBC and NH_4^+ throughout the Holocene, with little modification induced by long-range transport. However, some interesting differences can be noted. First, absolute rBC concentrations are lower in the Antarctic ice cores due to the remoteness from the main source regions. Second, while the timing of the MWP matches well between the two records, the transition towards the LIA was more abrupt in the B40 record, and the LIA signal displayed less variability in the Antarctic records compared to Illimani one. Third, while the B40 NH_4^+ record did show an increase since 1900 AD, no clear increasing trend was visible in the last 250 years in the Antarctic rBC record, contrary to Illimani, thus highlighting the importance of considering transport processes when discussing rBC records from the remote Antarctic regions. On the contrary, carbon monoxide (CO) ice-core records from Antarctica representative of Southern Hemisphere biomass burning follow a trend similar to the IL-99 rBC record, with a decreasing trend between 1300 and 1600 AD, a minimum in the 17th century and an increase for the time period 1700–1900 AD *(Wang et al., 2010)*. Divergences between rBC and CO Antarctic records might result from their different atmospheric lifetimes implying a different spatial representativeness. rBC has a relatively short atmospheric lifetime, from 3 to 10 days *(Bond et al., 2013)* while CO can remain in the atmosphere for weeks to months or even more than a year at the winter poles *(Holloway et al., 2000)*.

In rBC ice-core records from the Arctic and Europe, a predominant anthropogenic contribution starting in the second half of the 19th century due to rising fossil fuel emissions was observed *(Keegan et al., 2014; McConnell et al., 2007; Osmont et al., 2018; Sigl et al., 2013, 2018)*. At Illimani, rBC concentrations follow a long-term increasing trend since the 1730 AD minimum. It is therefore important to investigate to which extent climate variations and human activities influenced this increase. The IL-99 dust record **(Fig. 5.5b)** reveals that this increase was not driven by dustier and drier conditions leading to enhanced deposition as cerium concentrations remain low. On the contrary, temperatures likewise increase since 1720 AD, suggesting that the rBC increase is primarily driven by increasing temperatures responsible of enhanced biomass burning. The anthropogenic pollution pattern recorded in the IL-99 ice core by Pb and NO_3^- *(Eichler et al., 2015)* shows a dramatic increase only in second half of the 20th century, mainly due to emissions from traffic **(Fig. 5.5c)**. Since this strong rise is not visible in the rBC record of the past 50 years, we assume that anthropogenic BC emissions from fossil fuel combustion remain minor compared to biomass burning related BC emissions. Charcoal composite records for Tropical South America **(Fig. 5.5e)** also show a strong increase in fire activity during the 20th century, explained by enhanced of deforestation *(Power et al., 2012)*. Thus, we cannot exclude that, in the 20th century, a certain fraction of the biomass burning increase reflected by the rBC record does not only originate from rising temperatures but could be the result of the expansion of deforestation. However, a detailed assessment of the relative impact of those two factors cannot be obtained given the lack of accurate statistics before the satellite measurement era. The Food and Agriculture Organization (FAO) of the United Nations is monitoring forested areas since 1947 but many inconsistencies occurred in the first reports due to high uncertainties in estimating forested areas in remote regions and changing definitions and methodologies between the subsequent reports, thus making extensive comparison impossible *(Steininger et al., 2001)*.

5.3.4 Evidence of a Holocene Climatic Optimum dry period

The relationship between rBC concentrations and regional temperature/moisture variations extends further back in time through the entire Holocene. The bottommost part of the IL-99 ice core, between

11000 and 10000 BC, shows low concentrations of rBC **(Fig. 6.6a)** as well as low $\delta^{18}O$ values **(Fig. 6.6b)**, indicative of a cold and wet climate corresponding to the Younger Dryas (YD) cold period in the NH. Wet and cold conditions over the Bolivian Altiplano were suggested by an overflowing Lake Titicaca between 11000 and 9500 BC *(Baker et al., 2001)* and Late Glacial glacier advances in the Cordillera Real between 11000 and 9000 BC during the "Coipasa" humid phase *(Zech et al., 2007)*, showing that the Younger Dryas was not dry on a global scale despite increasing dustiness in Greenland ice-core records *(Mayewski et al., 1993)*. The establishment of warmer and drier conditions corresponding to the onset of the Holocene then occurred between 10000 and 9000 BC as evidenced by a pronounced increase (+5.5 ‰) in the $\delta^{18}O$ record *(Sigl et al., 2009)*, comparable to the +5.4 ‰ increase in the nearby Sajama ice core *(Thompson et al., 1998)*, followed by a stabilization around −16 ‰ between 9000 and 7000 BC.

Around 7000 BC, warm and dry conditions abruptly prevailed as indicated by a further increase in $\delta^{18}O$ (+2 ‰). These conditions that lasted until 3500 BC correspond to the Holocene Climatic Optimum (HCO). The HCO period is marked by the highest rBC concentrations of the whole 13000-year record (rBC average 7000–3500 BC: 2.97 ± 1.77 ng g^{-1}). Several other studies have already shown evidence of a dry HCO in Bolivia although timings might slightly differ between regions. The lowest Lake Titicaca level **(Fig. 6.6c)** occurred between 6000 and 3500 BC in a context of maximal aridity over the Bolivian Altiplano *(Baker et al., 2001)*. The charcoal record from Lake Titicaca **(Fig. 6.6d)** shows a broader maximum from 10000 to 1000 BC *(Paduano et al., 2003)*. Pollen data suggests a dry period lasting from 7000 to 1100 BC and peaking between 4000 and 2000 BC. Fire activity in the Bolivian lowlands, inferred from lake-sediment charcoal records, was high between 6100 and 3800 BC in the Llanos de Moxos **(Fig. 6.6d**, Lake Rogaguado, *Brugger et al., 2016)*, between 6000 and 5000 BC in the Chiquitano SDTF **(Fig. 6.6e**, Laguna La Gaiba, *Power et al., 2016)* and between 8000 and 4000 BC around Lake Santa Rosa **(Fig. 6.6e**, *Urrego, 2006)*. Composite charcoal records for tropical South America **(Fig. 6.6b)** show elevated biomass burning levels between 6000 and 2500 BC *(Marlon et al., 2013)*, but cover a much larger area which is not only representative of the Illimani source region. In the West Antarctic Ice Sheet Divide (WD) ice core, the highest rBC deposition occurred during the mid-Holocene from 6000 to 4000 BC **(Fig. 6.6c**, *Arienzo et al., 2017)*. The HCO maximum appears broader than in the IL-99 ice core, probably due to a larger catchment area and the influence of long-range transport processes.

Opposite hydroclimate variations have been detected in the northern South American tropics, as shown by the titanium and iron records from the Cariaco Basin, Venezuela *(Haug et al., 2001)*. Dry conditions prevailed during the YD while the HCO, dated between 8500 and 3400 BC, experienced the wettest conditions of the last 14000 years in this region. The Late Holocene was then characterized by a return to a drier climate. Similarly, wetter (drier) conditions were observed during the MWP (LIA), respectively. This anti-phasing between the northern and southern South American tropics has been best explained by latitudinal variations of the Intertropical Convergence Zone (ITCZ) *(Haug et al., 2001; Arienzo et al., 2017)*. During the HCO, in a context of a low Austral summer insolation due to orbital forcing, the ICTZ was shifted north, leading to more precipitation in the Cariaco region and to a weaker South American Summer Monsoon (SASM) responsible of drier conditions in the southern South American tropics, as evidenced in the Illimani record. Towards the Late Holocene, increasing (decreasing) insolation seasonality in the Southern (Northern) Hemisphere, respectively, may have resulted in a progressive southward shift of the ITCZ and a strengthening of the SASM, inducing wetter conditions over southern South American tropics but drier conditions in the northern South American tropics. A similar conclusion can be drawn for the LIA *(Arienzo et al., 2017)*.

Throughout the last 4000 years, rBC concentrations in the IL-99 ice core showed a much lower level **(Fig. 6.6a)**. Between 2250 BC and 100 AD, rBC concentrations remained low (average: 0.60 ± 0.37 ng g^{-1}) except a peak value of 1.55 ng g^{-1} around 300 BC. *Brugger et al. (2016)* also observed a minimum of burning in a lake sediment charcoal record from the Bolivian Amazonian lowlands around 2000 BP **(Fig. 6.6d)** in response to forest extension due to increased moisture availability. After 100 AD, rBC concentrations started to rise and remained higher for the time period 150–650 AD (average: 0.86 ± 0.32 ng g^{-1}) but declined again and stayed low between 750 and 1000 AD (average: 0.65 ± 0.41 ng g^{-1}).

In addition to the long-term trends described above, a particular event in the rBC IL-99 record is of special interest. Around 6000 BC, a dip in the δ^{18}O record **(Fig. 6.6b)** suggests an abrupt centennial-scale return to cooler and wetter conditions, potentially related to the NH 8.2 ka cold event detected in Greenland ice cores *(Alley et al., 1997; Thomas et al., 2007)*, and revealing that its impacts were also apparent in southern South American tropics and not only in the North Atlantic region. According to the current consensus, this cooling was caused by the Laurentide ice cap collapse that generated enormous freshwater fluxes into the North Atlantic Ocean *(Matero et al., 2017)*. A concurrent drop in the rBC concentration ~6000 BC **(Fig. 6.6a)** suggests that this climate anomaly also led to reduced levels of biomass burning.
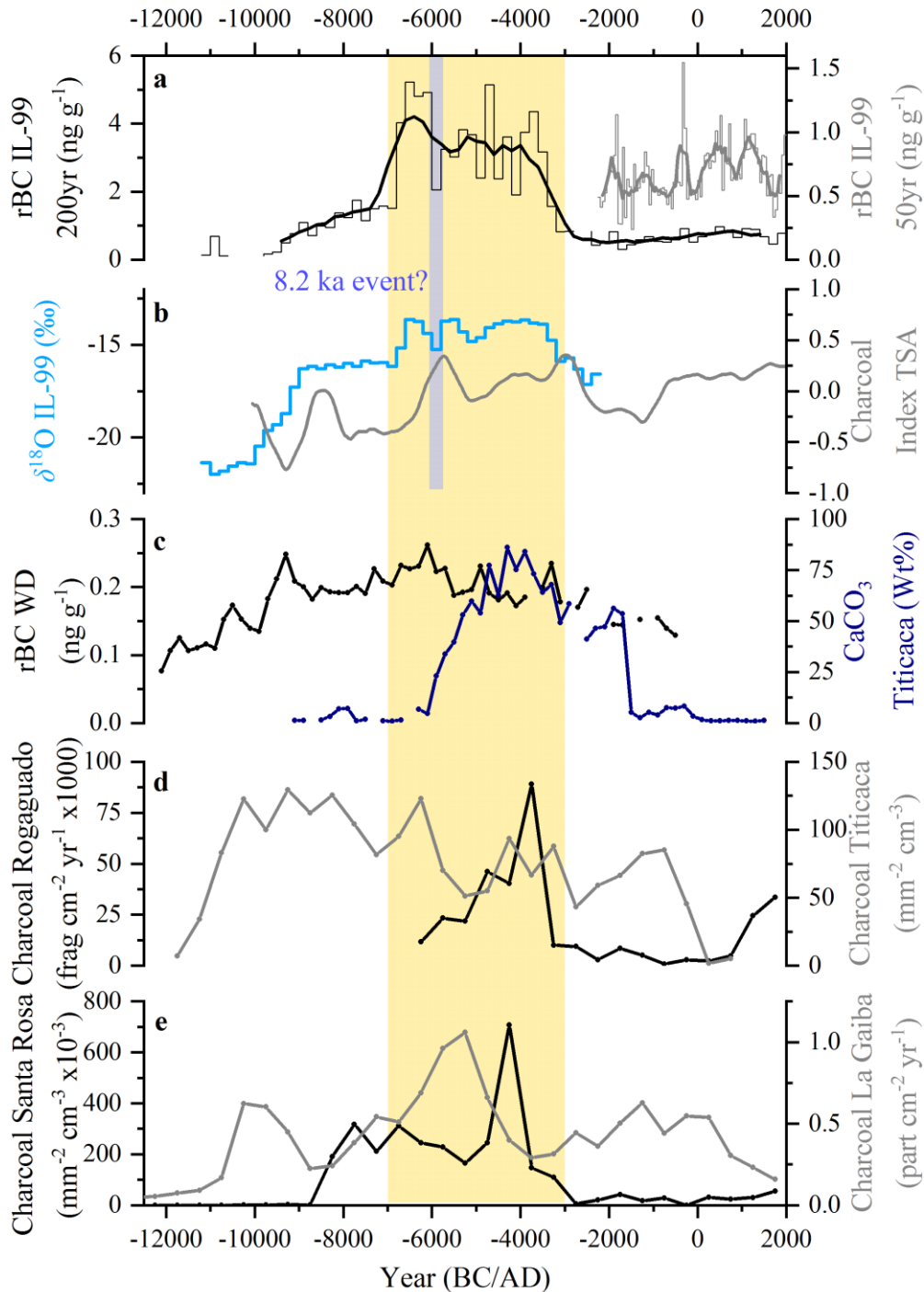
Fig. 5.6: Evidence of a dry period corresponding to the Holocene Climatic Optimum (HCO, yellow bar) in the IL-99 ice core and in other paleoclimatic reconstructions. a) IL-99 rBC record, 200-year averages (left scale) and 50-year averages (right scale). Thick lines are 5-point moving averages. The blue bar represents the cold/wet reversal potentially related to the 8.2 ka event. Gaps in the IL-99 rBC record are due to lack of available ice-core material due to previous samplings. b) IL-99 $\delta^{18}O$ record *(Sigl et al., 2009*, left scale) and composite charcoal record for Tropical South America (right scale, 20-year averages with a 500-year smoothing) *(Marlon et al., 2013)*. c) rBC record from the West Antarctic Ice Sheet Divide (WD) ice core, Antarctica *(Arienzo et al., 2017*, left scale) and calcium carbonate weight percent ($CaCO_3$ Wt%, right scale) recorded in a sediment core from Lake Titicaca as a proxy for lake-level variations, a higher percentage standing for a lower lake level induced by drier conditions *(Baker et al., 2001)*. Data are 200-year averages. d) Charcoal records from Lake Rogaguado *(Brugger et al., 2016*, left scale) and Lake Titicaca *(Paduano et al., 2003*, right scale). e) Charcoal records from Lake Santa Rosa *(Urrego, 2006*, left scale) and Laguna La Gaiba *(Power et al., 2016*, right scale). Data in panels d-e are 500-year averages.

5.4 Conclusions

Refractory black carbon (rBC) was analyzed in an ice core from Illimani (Bolivian Andes) spanning the entire Holocene back to the last deglaciation 13000 years ago. The high-resolution signal in the upper part of the ice cores revealed a strong seasonal pattern for rBC, with peak values during the dry season and low concentrations during the wet season as a result of the seasonality of emission sources and precipitation. Significant correlations were found between the 20th century rBC record and reanalyzed temperature/precipitation datasets from the Amazon Basin, particularly with regions located in Eastern Bolivia and Western Brazil experiencing high levels of biomass burning. The modulation of the seasonality by ENSO processes was shown to be weak due to the site location in the Eastern part of the Andes. The long-term rBC record behaves like an indirect regional temperature/moisture proxy through biomass burning variations, with low values during cold/wet periods such as the Younger Dryas and the Little Ice Age and higher concentrations during warm/dry periods such as the Holocene Climatic Optimum and the Medieval Warm Period. These findings are supported by an array of regional paleoclimate reconstructions and by Antarctic rBC ice-core records thought to represent South American biomass burning emissions, and are primarily controlled by insolation-driven latitudinal changes of the Intertropical Convergence Zone. Evidence of a cold/wet reversal induced by the 8.2 ka event was detected in the Illimani ice core. Our work confirms that most of the Northern Hemisphere climate variations throughout the Holocene also left an imprint in the tropical Andes and that opposite hydroclimate variations were observed between northern and southern South American tropics. Lastly, the rise in rBC concentrations since 1730 AD seems only driven by increased biomass burning levels due to higher temperatures and more intensive deforestation in the last decades but does not relate to fossil fuel rBC emissions. Therefore, the "broken fire hockey stick" trend was not observed in the Illimani record. Such ice-core records are of prime importance as the current global warming endangers the preservation of these glacial archives. Glaciers in the tropical Andes have retreated at a critical rate in the last 50 years *(Rabatel et al., 2013; Vuille et al., 2008)*, affecting drinking water supply for millions of people *(Bradley et al., 2006; Kaser et al., 2010; Vergara et al., 2007)* and creating new glacial lakes threatening local populations *(Carey, 2005, 2012)*.

Author contribution

D.O. sampled the Illimani ice cores, carried out SP2 measurements, analyzed the data and wrote the manuscript. Mi.S helped with ice cutting, rBC analyses and data interpretation. A.E. and T.M.J assisted with the data interpretation. Ma.S. designed and led the project and supervised the manuscript writing.

Competing interests

The authors declare that they have no conflict of interest.

Acknowledgements

References

Aceituno, P.: On the Functioning of the Southern Oscillation in the South American Sector. Part I: Surface Climate, *Monthly Weather Review*, 116, 505-524, 1988.

Alley, R. B., Mayewski, P. A., Sowers, T., Stuiver, M., Taylor, K. C., and Clark, P. U.: Holocene climatic instability: A prominent, widespread event 8200 yr ago, *Geology*, 25, 483–486, 1997.

Arienzo, M. M., McConnell, J. R., Murphy, L. N., Chellman, N., Das, S., Kipfstuhl, S., and Mulvaney, R.: Holocene black carbon in Antarctica paralleled Southern Hemisphere climate, *Journal of Geophysical Research: Atmospheres*, 122, 2017.

Artaxo, P., Fernandes, E. T., Martins, J. V., Yamasoe, M. A., Hobbs, P. V., Maenhaut, W., Longo, K. M., and Castanho, A. : Large-scale aerosol source apportionment in Amazonia, *Journal of Geophysical Research*, 103(D24), 31837–31847, 1998.

Baker, P. A., Seltzer, G. O., Fritz, S. C., Dunbar, R. B., Grove, M. J., Tapia, P. M., Cross, S. L., Rowe, H. D., and Broda, J.P.: The history of South American tropical precipitation for the past 25 000 years, *Science*, 291, 640–643, 2001.

Bond, T. C., Doherty, S. J., Fahey, D. W., Forster, P. M., Berntsen, T., DeAngelo, B. J., Flanner, M. G., Ghan, S., Karcher, B., Koch, D., Kinne, S., Kondo, Y., Quinn, P. K., Sarofim, M. C., Schultz, M. G., Schulz, M., Venkataraman, C., Zhang, H., Zhang, S., Bellouin, N., Guttikunda, S. K., Hopke, P. K., Jacobson, M. Z., Kaiser, J. W., Klimont, Z., Lohmann, U., Schwarz, J. P., Shindell, D., Storelvmo, T., Warren, S. G., and Zender, C. S.: Bounding the role of black carbon in the climate system: A scientific assessment, *Journal of Geophysical Research: Atmospheres*, 118, 5380–5552, 2013.

Bonnaveira, H.: Etude des phénomènes de dépôt et post-dépôt de la neige andine sur un site tropical d'altitude (Illimani-Bolivie-6340 m) en vue de l'interprétation d'une carotte de glace, Ph.D. Thesis, Université Joseph Fourier, Grenoble, France, 2004.

Bowman, D. M. J. S., Balch, J. K., Artaxo, P., Bond, W. J., Carlson, J. M., Cochrane, M. A., D'Antonio, C. M., DeFries, R. S., Doyle, J. C., Harrison, S. P., Johnston, F. H., Keeley, J. E., Krawchuk, M. A., Kull, C. A., Marston, J. B., Mortiz, M. A., Prentice, I. C., Roos, C. I., Scott, A. C., Swetnam, T. W., van der Werf, G. R., and Pyne, S. J.: Fire in the Earth System, *Science*, 324, 481–484, 2009.

Bowman, D. M. J. S., Balch, J., Artaxo, P., Bond, W. J., Cochrane, M. A., D'Antonio, C. M., DeFries, R., Johnston, F. H., Keeley, J. E., Krawchuk, M. A., Kull, C. A., Mack, M., Moritz, M. A., Pyne, S., Roos, C. I., Scott, A. C., Sodhi, N. S., and Swetnam, T. W.: The human dimension of fire regimes on Earth, *Journal of Biogeography*, 38, 2223–2236, 2011.

Bradley, R. S., Vuille, M., Diaz, H. F., and Vergara, W.: Threats to water supplies in the Tropical Andes, *Science*, 312, 1755–1756, 2006.

Brugger, S. O., Gobet, E., van Leeuwen, J. F. N., Ledru, M.-P., Colombaroli, D., van der Knaap, W. O., Lombardo, U., Escobar-Torrez, K., Finsinger, W., Rodrigues, L., Giesche, A., Zarate, M., Veit, H., and Tinner, W.: Long-term man-environment interactions in the Bolivian Amazon: 8000 years of vegetation dynamics, *Quaternary Science Reviews*, 132, 114–128, 2016.

Cape, J. N., Coyle, M., and Dumitrean, P.: The atmospheric lifetime of black carbon, *Atmospheric Environment*, 59, 256–263, 2012.

Carey, M.: Living and dying with glaciers: people's historical vulnerability to avalanches and outburst floods in Peru, *Global Planetary Change*, 47, 122–134, 2005.

Carey, M., Huggel, C., Bury, J., Portocarrero, C., and Haeberli, W.: An integrated socio-environmental framework for climate change adaptation and glacier hazard management: Lessons from Lake 513, Cordillera Blanca, Peru, *Climate Change*, 112, 733–767, 2012.

Chen, Y., Morton, D. C., Jin, Y., Collatz, G. J., Kasibhatla, P. S., van der Werf, G. R., DeFries, R. S., and Randerson, J. T.: Long-term trends and interannual variability of forest, savanna and agricultural fires in South America, *Carbon Management*, 4(6), 617–638, 2013.

Cochrane, M. A.: Fire science for rainforests, *Nature*, 421, 913–919, 2003.

Cochrane, M. A., Alencar, A., Schulze, M. D., Souza Jr., C. M., Nepstad, D. C., Lefebvre, P., and Davidson, E. A.: Positive feedbacks in the fire dynamic of closed canopy tropical forests, *Science*, 284, 1832–1835, 1999.

Correia, A., Freydier, R., Delmas, R. J., Simões, J. C., Taupin, J.-D., Dupré, B., and Artaxo, P.: Trace elements in South America aerosol during 20th century inferred from a Nevado Illimani ice core, Eastern Bolivian Andes (6350ma.s.l.), *Atmospheric Chemistry and Physics*, 3, 2143–2177, 2003.

De Angelis, M., Simões, J., Bonnaveira, H., Taupin, J.-D., and Delmas, R. J.: Volcanic eruptions recorded in the Illimani ice core (Bolivia): 1918-1998 and Tambora periods, *Atmospheric Chemistry and Physics*, 3, 1725–1741, 2003.

Eichler, A., Schwikowski, M., Gäggeler, H. W., Furrer, V., Synal, H.-A., Beer, J., Saurer, M., and Funk, M.: Glaciochemical dating of an ice core from upper Grenzgletscher (4200m a.s.l.), *Journal of Glaciology*, 46, 507–515, 2000.

Eichler, A., Gramlich, G., Kellerhals, T., Tobler, L., and Schwikowski, M.: Pb pollution from leaded gasoline in South America in the context of a 2000-year metallurgical history, *Science Advances*, 1, e1400196, 2015.

Eichler, A., Gramlich, G., Kellerhals, T., Tobler, L., Rehren, Th., and Schwikowski, M.: Ice-core evidence of earliest extensive copper metallurgy in the Andes 2700 years ago, *Scientific Reports*, 7, 41855, 2017.

Fischer, H., Schüpbach, S., Gfeller, G., Bigler, M., Rothlisberger, R., Erhardt, T., Stocker, T. F., Mulvaney, R., and Wolff, E.: Millennial changes in North American wildfire and soil activity over the last glacial cycle, *Nature Geoscience*, 8, 723–728, 2015.

Foley, J. A., Botta, A., and Coe, M. T.: El Niño-Southern oscillation and the climate, ecosystems and rivers of Amazonia, *Global Biogeochemical Cycles*, 16(4), 1132, 2002.

Garreaud, R. D. and Aceituno, P.: Interannual rainfall variability over the South American Altiplano, *Journal of Climate*, 14(12), 2779– 2789, 2001.

Garreaud, R., Vuille, M., and Clement, A. C.: The climate of the Altiplano: observed current conditions and mechanisms of past changes, *Palaeogeography, Palaeoclimatology, Palaeoecology*, 194, 5–22, 2003.

Garreaud, R. D., Vuille, M., Compagnucci, R., and Marengo, J.: Present-day South American climate, *Palaeogeography, Palaeoclimatology, Palaeoecology*, 281, 180-195, 2009.

Giglio, L., Randerson, J. T., and van der Werf, G. R.: Analysis of daily, monthly, and annual burned area using the fourth-generation global fire emissions database (GFED4), *Journal of Geophysical Research: Biogeosciences*, 118(1), 317–328, 2013.

Ginot, P., Stampfli, F., Stampfli, D., Schwikowski, M., and Gäggeler, H. W.: FELICS, a new ice core drilling system for high-altitude glaciers, *Memoirs of National Institute of Polar Research Special Issue*, 56, 38–48, 2002a.

Ginot, P., Schwikowski, M., Schotterer, U., Stichler, W., Gäggeler, H. W., Francou, B., Gallaire, R., and Pouyaud, B.: Potential for climate variability reconstruction from Andean glaciochemical records, *Annals of Glaciology*, 35, 443– 450, 2002b.

Haug, G. H., Hughen, K. A., Sigman, D. M., Peterson, L. C., and Röhl, U.: Southward Migration of the Intertropical Convergence Zone Through the Holocene, *Science*, 293, 1304–1308, 2001.

Holloway, T., Levy II, H., and Kasibhatla, P.: Global distribution of carbon monoxide, *Journal of Geophysical Research*, 105(D10), 12123–12147, 2000.

Jenk, T. M., Szidat, S., Schwikowski, M., Gaggeler, H. W., Brutsch, S., Wacker, L., Synal, H. A., and Saurer, M.: Radiocarbon analysis in an Alpine ice core: record of anthropogenic and biogenic contributions to carbonaceous aerosols in the past (1650-1940), *Atmospheric Chemistry and Physics*, 6, 5381–5390, 2006.

Kaser, G., Grosshauser, M., and Marzeion, B.: Contribution potential of glaciers to water availability in different climate regimes, *PNAS*, 107, 20223–20227, 2010.

Kaspari, S. D., Schwikowski, M., Gysel, M., Flanner, M. G., Kang, S., Hou, S., and Mayewski, P. A.: Recent Increase in Black Carbon Concentrations from a Mt. Everest Ice Core Spanning 1860–2000 AD, *Geophysical Research Letters*, 38, 2011.

Keegan, K. M., Albert, M. R., McConnell, J. R., and Baker, I.: Climate change and forest fires synergistically drive widespread melt events of the Greenland Ice Sheet, *PNAS*, 111, 7964–7967, 2014.

Kehrwald, N., Whitlock, C., Barbante, C., Brovkin, V., Daniau, A.-L., Kaplan, J. O., Marlon, J. R., Power, M. J., Thonicke, K., and van der Werf, G. R.: Fire research: linking past, present, and future data, *EOS*, 94(46), 421–422, 2013.

Kellerhals, T., Brütsch, S., Sigl, M., Knüsel, S., Gäggeler, H. W., and Schwikowski, M.: Ammonium concentration in ice cores: A new proxy for regional temperature reconstruction?, *Journal of Geophysical Research*, 115, D16123, 2010a.

Kellerhals, T., Tobler, L., Brütsch, S., Sigl, M., Wacker, L., Gäggeler, H. W., and Schwikowski, M.: Thallium as a tracer for preindustrial volcanic eruptions in an ice core record from Illimani, Bolivia, *Environmental Science and Technology*, 44, 888–893, 2010b.

Kloster, S., Mahowald, N. M., Randerson, J. T., Thornton, P. E., Hoffman, F. M., Levis, S., Lawrence, P. J., Feddema, J. J., Oleson, K. W., and Lawrence, D. M.: Fire dynamics during the 20th century simulated by the Community Land Model, *Biogeosciences*, 7, 1877–1902, 2010.

Knüsel, S., Ginot, P., Schotterer, U., Schwikowski, M., Gäggeler, H. W., Francou, B., Petit, J. R., Simões, J. C., and Taupin, J. D.: Dating of two nearby ice cores from the Illimani, Bolivia, *Journal of Geophysical Research*, 108(D6), 4181, 2003.

Knüsel, S., Brütsch, S., Henderson, K., Palmer, A. S., and Schwikowski, M.: ENSO signals of the 20th century in an ice core from Nevado Illimani, Bolivia, *Journal of Geophysical Research*, 110, D01102, 2005.

Lavanchy, V. M. H., Gäggeler, H. W., Schotterer, U., Schwikowski, M., and Baltensperger, U.: Historical record of carbonaceous particle concentrations from a European high-alpine glacier (Colle Gnifetti, Switzerland), *Journal of Geophysical Research*, 104(D17), 21227–21236, 1999.

Legrand, M., McConnell, J., Fischer, H., Wolff, E. W., Preunkert, S., Arienzo, M., Chellman, N., Leuenberger, D., Maselli, O., Place, P., Sigl, M., Schüpbach, S., and Flannigan, M.: Boreal fire records in Northern Hemisphere ice cores: a review, *Climate of the Past*, 12, 2033–2059, 2016.

Lim, S., Faïn, X., Ginot, P., Mikhalenko, V., Kutuzov, S., Paris, J.-D., Kozachek, A., and Laj, P.: Black carbon variability since preindustrial times in the eastern part of Europe reconstructed from Mt. Elbrus, Caucasus, ice cores, *Atmospheric Chemistry and Physics*, 17, 3489–3505, 2017.

Marlon, J. R., Bartlein, P. J., Carcaillet, C., Gavin, D. G., Harrison, S. P., Higuera, P. E., Joos, F., Power, M. J., and Prentice, I. C.: Climate and human influences on global biomass burning over the past two millennia, *Nature Geoscience*, 1(10), 697–702, 2008.

Marlon, J. R., Bartlein, P. J., Daniau, A.-L., Harrison, S. P., Maezumi, S. Y., Power, M. J., Tinner, W., and Vannière, B.: Global biomass burning: a synthesis and review of Holocene paleofire records and their controls, *Quaternary Science Reviews*, 65, 5–25, 2013.

Matero, I. S. O., Gregoire, L. J., Ivanovic, R. F., Tindall, J. C., and Haywood, A. M.: The 8.2 ka cooling event caused by Laurentide ice saddle collapse, *Earth and Planetary Science Letters*, 473, 205–214, 2017.

Mayewski, P. A., Meeker, L. D., Whitlow, S., Twickler, M. S., Morrison, M. C., Alley, R. B., Bloomfield, P., and Taylor, K.: The atmosphere during the Younger Dryas, *Science*, 261, 195–197, 1993.

McConnell, J. R., Edwards, R., Kok, G. L., Flanner, M. G., Zender, C. S., Saltzman, E. S., Banta, J. R., Pasteris, D. R., Carter, M. M., and Kahl, J. D. W.: 20th-century industrial black carbon emissions altered arctic climate forcing, *Science*, 317, 1381–1384, 2007.

Montellano, A. R.: Cartografía multitemporal de quemas e incendios forestales en Bolivia: Detección y validación post-incendio (Multitemporal mapping forest fires and burn in Bolivia: detection and post-fire validation), *Ecología en Bolivia*, 47(1), 53-71, 2012.

Mouillot, F. and Field, C.: Fire history and the global carbon budget: a $1° \times 1°$ fire history reconstruction for the 20th century, *Global Change Biology*, 11, 398–420, 2005.

Osmont, D., Wendl, I. A., Schmidely, L., Sigl, M., Vega, C. P., Isaksson, E., and Schwikowski, M.: An 800-year high-resolution black carbon ice core record from Lomonosovfonna, Svalbard, *Atmospheric Chemistry and Physics*, 18, 12777–12795, 2018.

Paduano, G. M., Bush, M. B., Baker, P. A., Fritz, S. C., and Seltzer, G. O.: A Vegetation and Fire History of Lake Titicaca since the Last Glacial Maximum, *Palaeogeography, Palaeoclimatology, Palaeoecology*, 194, 259–279, 2003.

Power, M. J., Mayle, F. E., Bartlein, P. J., Marlon, J. R., Anderson, R. S., Behling, H., Brown, K. J., Carcaillet, C., Colombaroli, D., Gavin, D. G., Hallett, D. J., Horn, S. P., Kennedy, L. M., Lane, C. S., Long, C. J., Moreno, P. I., Paitre, C., Robinson, G., Taylor, Z., and Walsh, M. K.: Climatic control of the biomass-burning decline in the Americas after AD 1500, *The Holocene*, 23, 3–13, 2012.

Power, M. J., Whitney, B. S., Mayle, F. E., Neves, D. M., de Boer, E. J., and Maclean, K. S.: Fire, climate and vegetation linkages in the Bolivian Chiquitano seasonally dry tropical forest, *Philosophical Transactions of the Royal Society B*, 371, 20150165, 2016.

Petzold, A., Ogren, J. A., Fiebig, M., Laj, P., Li, S. M., Baltensperger, U., Holzer-Popp, T., Kinne, S., Pappalardo, G., Sugimoto, N., Wehrli, C., Wiedensohler, A., and Zhang, X. Y.: Recommendations for reporting "black carbon" measurements, *Atmospheric Chemistry and Physics*, 13, 8365–8379, 2013.

Rabatel, A., Francou, B., Soruco, A., Gomez, J., Cáceres, B., Ceballos, J. L., Basantes, R., Vuille, M., Sicart, J.-E., Huggel, C., Scheel, M., Lejeune, Y., Arnaud, Y., Collet, M. ,Condom, T., Consoli, G., Favier, V., Jomelli, V., Galarraga, R., Ginot, P., Maisincho, L.,Mendoza, J., Ménégoz, M., Ramirez, E., Ribstein, P., Suarez, W., Villacis, M. and Wagnon, P.: Current state of glaciers in the tropical Andes: A multi-century perspective on glacier evolution and climate change, *The Cryosphere*, 7, 81–102, 2013.

Ronchail, J. and Gallaire, R.: ENSO and rainfall along the Zongo valley (Bolivia) from the Altiplano to the Amazon basin, *International Journal of Climatology*, 26, 1223–1236, 2006.

Ronchail, J., Cochonneau, G., Molinier, M., Guyot, J., Goretti De Miranda, A., Guimarães, V., and Oliveira, E.: Interannual rainfall variability in the Amazon basin and sea-surface temperatures in the equatorial Pacific and the tropical Atlantic Oceans, *International Journal of Climatology*, 22, 1663–1686, 2002.

Ruppel, M. M., Soares, J., Gallet, J.-C., Isaksson, E., Martma, T., Svensson, J., Kohler, J., Pedersen, C. A., Manninen, S., Korhola, A., and Ström, J.: Do contemporary (1980–2015) emissions determine the elemental carbon deposition trend at Holtedahlfonna glacier, Svalbard?, *Atmospheric Chemistry and Physics*, 17, 12779–12795, 2017.

Schultz, M. G., Heil, A., Hoelzemann, J. J., Spessa, A., Thonicke, K., Goldammer, J. G., Held, A. C., Pereira, J. M. C., and van het Bolscher, M.: Global wildland fire emissions from 1960 to 2000, *Global Biogeochemical Cycles*, 22, GB2002, 2008.

Schwarz, J. P., Gao, R. S., Fahey, D. W., Thomson, D. S., Watts, L. A., Wilson, J. C., Reeves, J. M., Darbeheshti, M., Baumgardner, D. G., Kok, G. L., Chung, S. H., Schulz, M., Hendricks, J., Lauer, A., Karcher, B., Slowik, J. G., Rosenlof, K. H., Thompson, T. L., Langford, A. O., Loewenstein, M., and Aikin, K. C.: Single-particle measurements of midlatitude black carbon and light-scattering aerosols from the boundary layer to the lower stratosphere, *Journal of Geophysical Research*, 111, D16207, 2006.

Sigl, M., Jenk, T. M., Kellerhals, T., Szidat, S., Gäggeler, H. W., Wacker, L., Synal, H.-A., Boutron, C., Barbante, C., Gabrieli, J., and Schwikowski, M.: Instruments and Methods Towards radiocarbon dating of ice cores, *Journal of Glaciology*, 55, 985–996, 2009.

Sigl, M., McConnell, J. R., Layman, L., Maselli, O., McGwire, K., Pasteris, D., Dahl-Jensen, D., Steffensen, J. P., Vinther, B., Edwards, R., Mulvaney, R., and Kipfstuhl, S.: A new bipolar ice core record of volcanism from WAIS Divide and NEEM and implications for climate forcing of the last 2000 years, *Journal of Geophysical Research: Atmospheres*, 118, 1151–1169, 2013.

Sigl, M., Abram, N. J., Gabrieli, J., Jenk, T. M., Osmont, D., and Schwikowski, M.: 19th century glacier retreat in the Alps preceded the emergence of industrial black carbon deposition on high-alpine glaciers, *The Cryosphere*, 12, 3311–3331, 2018.

Steininger, M. K, Tucker, C. J., Townshend, J. R. G., Killeen, T. J., Desch, A., Bell, V., and Ersts, P.: Tropical deforestation in the Bolivian Amazon, *Environmental Conservation*, 28(2), 127–134, 2001.

Stephens, M., Turner, N., and Sandberg, J.: Particle identification by laser-induced incandescence in a solid-state laser cavity, *Applied Optics*, 42, 3726–3736, 2003.

Thomas, E. R., Wolff, E. W., Mulvaney, R., Steffensen, J. P., Johnsen, S. J., Arrowsmith, C., White, J. W. C., Vaughn, B., and Popp, T.: The 8.2 ka event from Greenland ice cores, *Quaternary Science Reviews*, 26, 70–81, 2007.

Thompson, L. G., Davis, M. E., Mosley-Thompson, E., Sowers, T. A., Henderson, K. A., Zagorodnov, V. S., Lin, P.-N., Mikhalenko, V. N., Campen, R. K., Bolzan, J. F., Cole-Dai, J., and Francou, B.: A 25,000-year tropical climate history from Bolivian ice cores, *Science*, 282, 1858–1864, 1998.

Urrego, D. H.: Long-term vegetation and climate change in Western Amazonia, PhD Dissertation, Department of Biological Sciences, Florida Institute of Technology, Melbourne, USA, 278 pp, 2006.

van der Werf, G. R., Randerson, J. T., Giglio, L., Collatz, G. J., Mu, M., Kasibhatla, P. S., Morton, D. C., DeFries, R. S., Jin, Y., and van Leeuwen, T. T.: Global fire emissions and the contribution of deforestation, savanna, forest, agricultural, and peat fires (1997–2009), *Atmospheric Chemistry and Physics*, 10, 11707–11735, 2010.

van Marle, M. J. E., Field, R. D., van der Werf, G. R., Estrada de Wagt, I. A., Houghton, R. A., Rizzo, L. V., Artaxo , P., and Tsigaridis, K.: Fire and deforestation dynamics in Amazonia (1973–2014), *Global Biogeochemical Cycles*, 31, 24–38, 2017a.

van Marle, M. J. E., Kloster, S., Magi, B. I., Marlon, J. R., Daniau, A.-L., Field, R. D., Arneth, A., Forrest, M., Hantson, S., Kehrwald, N. M., Knorr, W., Lasslop, G., Li, F., Mangeon, S., Yue, C., Kaiser, J. W., and van der Werf, G. R.: Historic global biomass burning emissions from CMIP6 (BB4CMIP) based on merging satellite observations with proxies and fire models (1750–2015), *Geoscientific Model Development*, 10, 3329–3357, 2017b.

Vergara, W., Deeb, A. M., Valencia, A. M., Bradley, R. S., Francou, B., Zarzar, A., Grünwaldt, A., and Haeussling, S. M.: Economic impacts of rapid glacier retreat in the Andes, *Eos*, 88(25), 261–264, 2007.

Vuille, M., Bradley, R. S., and Keimig, F.: Interannual climate variability in the Central Andes and its relation to tropical Pacific and Atlantic forcing, *Journal of Geophysical Research*, 105(D10), 12447–12460, 2000.

Vuille, M., Bradley, R. S., Healy, R., Werner, M., Hardy, D. R., Thompson, L. G., and Keimig, F.: Modeling δ18O in precipitation over the tropical Americas: Part II. Simulation of the stable isotope signal in Andean ice cores, *Journal of Geophysical Research*, 108(D6), 4175, 2003.

Vuille, M., Francou, B., Wagnon, P., Juen, I., Kaser, G., Mark, B. G., and Bradley, R. S.: Climate change and tropical Andean glaciers: Past, present and future, *Earth-Science Reviews*, 89, 79–96, 2008.

Wang, M., Xu, B., Kaspari, S. D., Gleixner, G., Schwab, V. F., Zhao, H., Wang, H., and Yao, P.: Century-long record of black carbon in an ice core from the Eastern Pamirs: Estimated contributions from biomass burning, *Atmospheric Environment*, 115, 79–88, 2015.

Wang, Z., Chapellaz, J., Park, K., and Mak J. E.: Large variations in Southern Hemisphere biomass burning during the last 650 years, *Science*, 330, 1663–1666, 2010.

Wendl, I. A., Menking, J. A., Färber, R., Gysel, M., Kaspari, S. D., Laborde, M. J. G., and Schwikowski, M.: Optimized method for black carbon analysis in ice and snow using the Single Particle Soot Photometer, *Atmospheric Measurement Techniques*, 7, 2667–2681, 2014.

Wolter, K. and Timlin, M. S.: Monitoring ENSO in COADS with a seasonally adjusted principal component index. Proceedings of the 17th Climate Diagnostics Workshop, Norman, OK, NOAA/NMC/CAC, NSSL, Oklahoma Climate Survey, CIMMS and the School of Meteorology, University of Oklahoma: Norman, OK, 52–57, 1993.

Wolter, K. and Timlin, M. S.: Measuring the strength of ENSO events – how does 1997/98 rank?, *Weather*, 53, 315–324, 1998.

Wolter, K. and Timlin, M. S.: El Niño/Southern Oscillation behaviour since 1871 as diagnosed in an extended multivariate ENSO index (MEI.ext), *International Journal of Climatology*, 31, 1074–1087, 2011.

Zech, R., Kull, C., Kubik, P. W., and Veit, H.: LGM and Late Glacial glacier advances in the Cordillera Real and Cochabamba (Bolivia) deduced from 10Be surface exposure dating, *Climate of the Past*, 3(4), 623–635, 2007.

Zennaro, P., Kehrwald, N., McConnell, J. R., Schüpbach, S., Maselli, O. J., Marlon, J., Vallelonga,P., Leuenberger, D., Zangrando, R., Spolaor, A., Borrotti, M., Barbaro, E., Gambaro, A., and Barbante, C.: Fire in ice: two millennia of boreal forest fire history from the Greenland NEEM ice core, *Climate of the Past*, 10, 1905–1924, 2014.

Supplement

Here we present results from the Illimani 2015 shallow firn core (IL-15), with a particular focus on rBC. They were not combined with the rBC record from the IL-99 core because of an overall mismatch between the IL-99 and IL-15 rBC concentrations, the latter being around 1.7 times higher in average possibly due to the spatial variability between the two ice-core sites, despite their proximity.

S5.1 The Illimani 2015 firn core

To update the IL-99 ice core, a 25.7 m shallow firn core was extracted at the same site (16°38′58.57″ S, 67°47′03.57″ W) in June 2015 by a team from PSI. The IL-15 ice core was cut in a −20 °C cold room at PSI at 5–6 cm resolution, resulting in overall 487 samples. After sample melting and prior to rBC analysis, a 1 mL aliquot was taken for water stable isotope (δ^{18}O and δD) analysis by wavelength-scanned cavity ring down spectrometry (Picarro L2130-i, Picarro Inc., USA). Following rBC analysis, 13 ions (5 cations: NH_4^+, Ca^{2+}, Mg^{2+}, K^+ and Na^+; and 8 anions: CH_3COO^-, Cl^-, F^-, $HCOO^-$, $CH_3SO_3^-$, NO_3^-, $C_2O_4^{2-}$ and SO_4^{2-}) were quantified by ion chromatography (*850 Professional IC*, Metrohm, Switzerland). Dating of the IL-15 core was performed using well-resolved seasonal variations of rBC and Ca^{2+} (**Fig. S5.1**), attributing simultaneous minima of both compounds to 1st January of each year. Linear interpolation was made between two adjacent minima, thus neglecting the seasonal pattern of precipitation. The timescale of the IL-15 core was adjusted by wiggle matching to the top part of the IL-99 core using a 10 cm thick ice lens present in both records and corresponding to the warm year 1998 and three characteristic peaks in the rBC profile for the years 1995–1996. The IL-15 ice core thus spans the time period 1995–2015, corresponding to a net accumulation rate of 0.72 m weq yr^{-1}, higher than that of the IL-99 ice core.

An alternative method for dating of Andean ice cores was suggested by P. Ginot based on the variations of the δ^{18}O record. Two tie points were defined per year: minima were attributed to 1st of March of each year (wet season signal) while maxima were attributed to 1st of August (dry season signal). Linear interpolation was performed between those two tie points. Similar results were obtained with this method as the dating difference between the two methods did not exceed three months.

Compared to the IL-99 ice core, a similar pattern is observed in IL-15 and seasonality is even more pronounced due to the higher sampling resolution, resulting in peak values ranging from 4 to 18 ng g^{-1} (**Fig. S5.1a**). To identify common variability between the different chemical compounds in the IL-15 ice core, a principal component analysis (PCA) was performed on normalized annual values (**Table S5.1**). Four principal components (PC) were obtained. PC1, which accounts for 39 % of the total variance, has high loadings of sodium, potassium, magnesium, calcium, ammonium, chloride, nitrate and sulfate, representative of the regional dust input in the Illimani ice core from arid zones on the Altiplano. PC2 shows high loadings of rBC, ammonium, formate and oxalate, representing 29 % of the total variance. Ammonium and formate were previously attributed to biogenic emissions from Amazonian forests *(Kellerhals et al., 2010)* while oxalate peaks were observed in connection with biomass burning events *(Bonnaveira, 2004)*. However, rBC can only be emitted by combustion processes and therefore cannot be a proxy for biogenic emissions, thus suggesting that PC2 rather represents the biomass burning signal recorded in the Illimani ice core. *Kellerhals et al. (2010)* proposed that potassium and nitrate could be used as biomass burning tracers. However, here, their loadings in PC2 are low, particularly for potassium, suggesting that they are mainly related to the dust input, a fact already confirmed for potassium by *Bonnaveira (2004)*. PC3, accounting for 20 % of the total variance, contains a more mixed signal including oxalate, potassium and calcium, which

prevents us from assigning a clear aerosol source to it. Lastly, PC4 isolates acetate (12 % of the total variance), which is the only compound significantly affected by post-depositional processes, as revealed by the lack of seasonality of the signal, and whose chemical analysis is particularly prone to contamination. Therefore PC4 would quantify the impact of post-deposition on each compound.

Table S5.1: Results of the Principal Component Analysis (PCA) performed on the IL-15 log-transformed annual averages, after VARIMAX rotation. Values above 0.5 are in bold.

	PC1	PC2	PC3	PC4
Sodium	**0.66**	0.46	0.48	0.10
Potassium	**0.53**	0.11	**0.78**	0.20
Magnesium	**0.69**	0.49	0.34	0.22
Calcium	**0.64**	0.40	**0.57**	0.16
Chloride	**0.90**	0.19	0.03	0.32
Nitrate	**0.73**	0.44	0.18	− 0.34
Sulfate	**0.84**	− 0.06	0.34	0.08
Ammonium	**0.65**	**0.70**	0.18	− 0.06
rBC	0.25	**0.86**	0.05	0.27
Formate	0.05	**0.83**	0.47	0.05
Oxalate	0.13	**0.58**	**0.70**	0.12
Acetate	− 0.15	− 0.18	− 0.19	**− 0.93**
Variance explained (%)	38.5	29.0	20.4	12.1

To evaluate the relationship between the high-resolution rBC record and biomass burning trends in the Amazon Basin, we compared our data to biomass burning statistics from Bolivia and Brazil **(Fig. S5.1f)**. The states of El Beni and Santa Cruz in Bolivia, and Rondônia and Mato Grosso in Brazil are of particular interest given their proximity to the Illimani site and their important forest and savanna coverage. SDTFs cover a substantial part of the Bolivian state of Santa Cruz, while savannas are found along the states of Santa Cruz and El Beni (Bolivia), and Mato Grosso and Rondônia (Brazil) as well as further east in Brazil *(Chen et al., 2013)*. In August–September 2010, Bolivia experienced the worst forest and savanna fires of the last two decades due to the most severe drought of the last 30 years. A total of 4´343´156 ha burned in 2010 in this country, of which 25 % were forested areas and 75 % meadows and savannas areas, mainly in the states of El Beni (63 % of the 2010 national total, mainly meadows/savannas) and Santa Cruz (28 % of the 2010 national total, mainly forests) *(Montellano, 2012)*. The second year in terms of burned area was 2005, with a total of 3´693´820 ha. 2004 and 2007 were also critical years for the forest in the state of Santa Cruz *(Montellano, 2012)*. In Mato Grosso, the year 2004, followed by 2002, 2005 and 2007, were the years with most active fire counts. In Rondônia, 2004 and 2005 were also years with outstanding burning. The yearly peak of biomass burning in those regions usually occurs during the maximum of the dry season, between August and October *(Montellano, 2012)* and therefore overlaps with the dry season signal recorded in the Illimani ice core. In the IL-15 ice core, outstanding rBC peaks occurred in 2005, 2007, 2011 and 2013 **(Fig. S5.1a)**. However, the only years when extensive biomass burning seasons coincided with outstanding peaks in the IL-15 ice core were the years 2005 and 2007. Surprisingly, the year 2010 did not show remarkable rBC peaks in the IL-15 ice core. One possible explanation is that rBC could not be deposited on the snow surface due to the extremely dry conditions prevailing in August–September 2010 over the Bolivian Altiplano. Indeed, the meteorological station in El Alto airport, near La Paz and about 40 km far from Illimani, did only register 5 days of significant precipitation, with a total of 29.2 mm, for these two months **(Fig. S5.1d)**. As rBC is preferentially removed from the atmosphere
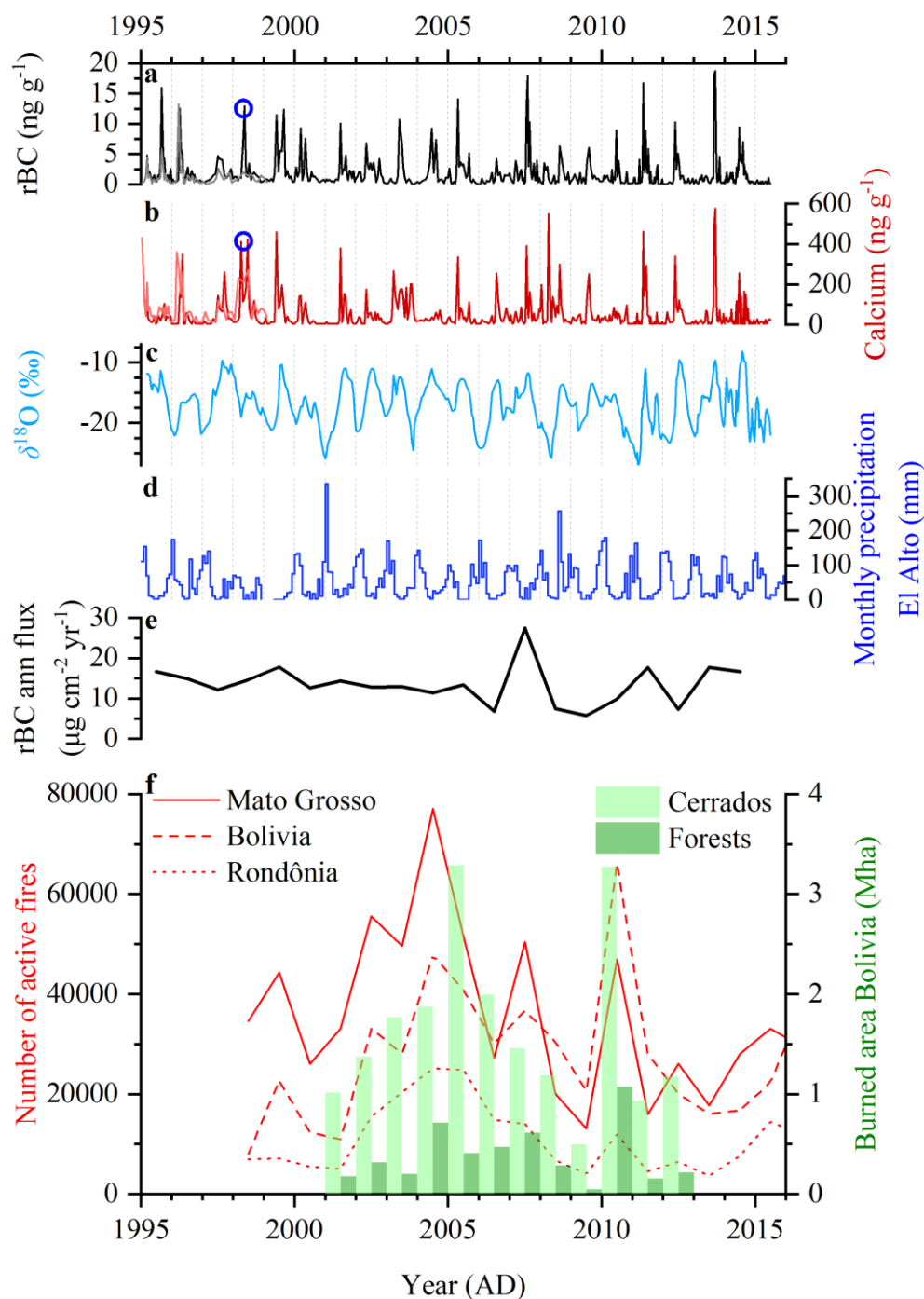
Fig. S5.1: Concentrations of a) rBC, b) calcium and c) $\delta^{18}O$ record in the IL-15 ice core (raw data). The blue circles represent the ice lens visible in both ice cores, corresponding to the year 1998 and used as a tie point (at a depth of 1.93 m in IL-99 and 22.48 m in IL-15). Lighter lines between 1995 and 1999 show the overlap with the IL-99 ice core (raw data). d) Monthly precipitation data from El Alto weather station, available on the website of the US National Climatic Data Center (NCDC) at the following address: *https://www7.ncdc.noaa.gov/CDO/cdoselect.cmd?datasetabbv=GSOD*. e) rBC annual fluxes from the IL-15 ice core, compared to f) biomass burning statistics from the Amazon Basin. The number of active fires is available on the website of the Brazilian Instituto Nacional de Pesquisas Espaciais (INPE) at the following address: *inpe.br/queimadas/portal*. Data of the burned area in Bolivia, split between *cerrados* and forests, is from *Montellano (2012)*.

by wet deposition *(Cape et al., 2012; Ruppel et al., 2017)*, it does not seem surprising that these fires, despite their massive extension, did not leave an imprint in the IL-15 ice core. As a consequence, on an annual basis, rBC variability in the Illimani ice core cannot systematically reflect the intensity of the biomass burning season in the Amazon Basin as it is controlled by precipitation at the drill site. A too dry Austral winter can prevent rBC from being deposited at Illimani (as in 2010), whereas a too wet Austral winter can dilute its signal in the snowpack, leading to low concentrations even during the dry season (as in 2008). Conversely, dry seasons with little biomass burning such as 2011 can also leave a strong imprint on the ice core record. Even annual rBC fluxes **(Fig. S5.1e)**, which take into account the precipitation pattern, do not reflect annual biomass burning statistics from the Amazon Basin. These discrepancies might also arise from unfavorable transport patterns, given the extreme difference in elevation between the Amazon Basin and the drill site (more than 6000 m).

S5.2 Principal Component Analysis on the Illimani 1999 ice core

A PCA was performed on 50-year averages for rBC and major ions for the time period 1550 BC–1999 AD **(Table S5.2)**. The results are in close agreement with those from the Illimani 2015 firn core **(Table S5.1)**. PC1 contains high loadings of calcium, magnesium, sodium, potassium, sulfate and chloride representative of the dust input signal. PC2 includes rBC, ammonium, formate and to a lesser extent, potassium, and is related to the biomass burning signal. PC3 is still representative of the post-deposition processes, but also includes oxalate in addition to acetate. PC4 only contains nitrate and could relate to the "nitric acid puzzle" discussed by *Knüsel et al. (2005)* and characterized by very high nitrate concentrations in some ice-core sections, potentially due to contamination. The diverging temporal PC trends **(Fig. S5.2)** also highlight the different sources of the species. While the dust input (PC1) remains fairly constant over the last 3500 years (except for a peak in 750 BC), the biomass burning contribution (PC2) shows a long-term increase modulated by climate variations, with minima (maxima) during cold/wet (warm/dry) periods, respectively, as already stated before. Conversely, PC3 shows higher (lower) values during cold/wet (warm/dry) periods. As acetate is anti-correlated with PC3 (negative sign), it means that post-deposition increases during warm/dry periods, which is consistent with the fact that those species will stay longer at the snow surface due to reduced precipitation and will therefore experience further re-volatilization. PC4 displays common features with PC3 but cannot be discussed in detail as part of it could stem from contamination processes.

Table S5.2: Results of the Principal Component Analysis (PCA) performed on the IL-99 50-year averages for the time period 1550 BC–1999 AD, after VARIMAX rotation. Values above 0.5 are in bold.

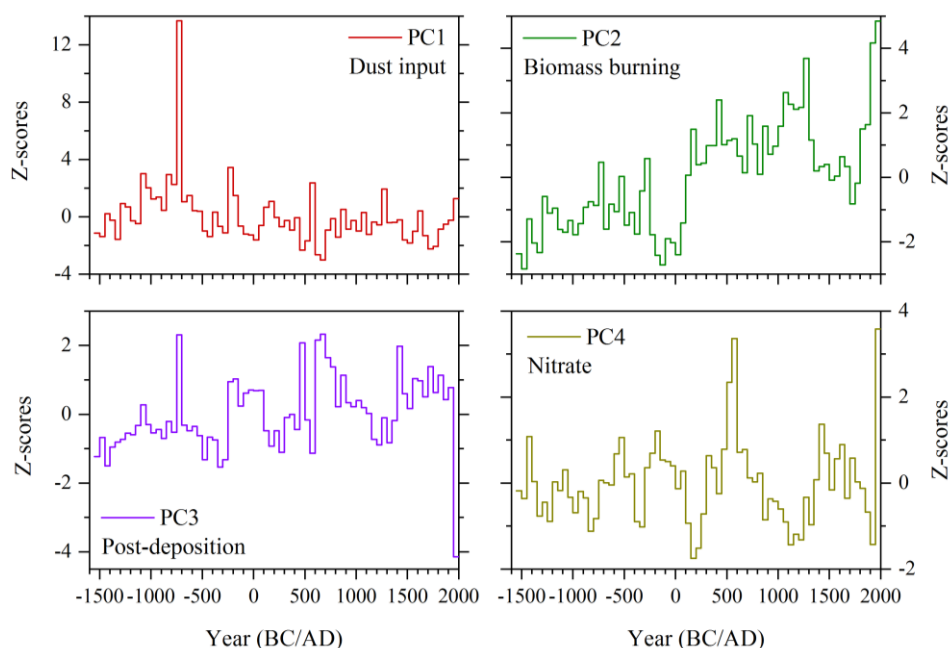|	PC1	PC2	PC3	PC4
Sodium	**0.85**	− 0.17	0.13	0.11
Potassium	**0.53**	**0.51**	0.35	0.02
Magnesium	**0.89**	− 0.12	0.26	− 0.07
Calcium	**0.90**	0.05	0.25	− 0.03
Chloride	**0.92**	− 0.11	− 0.04	0.23
Sulfate	**0.66**	0.42	− 0.31	0.16
rBC	− 0.17	**0.61**	− 0.04	0.09
Ammonium	0.10	**0.93**	0.01	0.19
Formate	− 0.12	**0.85**	− 0.32	− 0.13
Oxalate	0.49	− 0.32	**0.62**	− 0.21
Acetate	− 0.08	0.06	**− 0.82**	− 0.19
Nitrate	0.14	0.13	0.11	**0.94**
Variance explained (%)	44.5	27.3	16.4	11.9

Fig. S5.2: Temporal variations of the four Principal Components (PC) listed in **Table S5.2**.

References

Bonnaveira, H.: Etude des phénomènes de dépôt et post-dépôt de la neige andine sur un site tropical d'altitude (Illimani-Bolivie-6340 m) en vue de l'interprétation d'une carotte de glace, Ph.D. Thesis, Université Joseph Fourier, Grenoble, France, 2004.

Cape, J. N., Coyle, M., and Dumitrean, P.: The atmospheric lifetime of black carbon, *Atmospheric Environment*, 59, 256–263, 2012.

Chen, Y., Morton, D. C., Jin, Y., Collatz, G. J., Kasibhatla, P. S., van der Werf, G. R., DeFries, R. S., and Randerson, J. T.: Long-term trends and interannual variability of forest, savanna and agricultural fires in South America, *Carbon Management*, 4(6), 617–638, 2013.

Kellerhals, T., Brütsch, S., Sigl, M., Knüsel, S., Gäggeler, H. W., and Schwikowski, M.: Ammonium concentration in ice cores: A new proxy for regional temperature reconstruction?, *Journal of Geophysical Research*, 115, D16123, 2010.

Knüsel, S., Brütsch, S., Henderson, K., Palmer, A. S., and Schwikowski, M.: ENSO signals of the 20th century in an ice core from Nevado Illimani, Bolivia, *Journal of Geophysical Research*, 110, D01102, 2005.

Montellano, A. R.: Cartografía multitemporal de quemas e incendios forestales en Bolivia: Detección y validación post-incendio (Multitemporal mapping forest fires and burn in Bolivia: detection and post-fire validation), *Ecología en Bolivia*, 47(1), 53-71, 2012.

Ruppel, M. M., Soares, J., Gallet, J.-C., Isaksson, E., Martma, T., Svensson, J., Kohler, J., Pedersen, C. A., Manninen, S., Korhola, A., and Ström, J.: Do contemporary (1980–2015) emissions determine the elemental carbon deposition trend at Holtedahlfonna glacier, Svalbard?, *Atmospheric Chemistry and Physics*, 17, 12779–12795, 2017.

128

6 Main results from Colle Gnifetti and Tsambagarav ice cores

This chapter focuses on the other two rBC ice-core records of the project, namely Colle Gnifetti and Tsambagarav. The Colle Gnifetti industrial rBC record, spanning 1741–2015 AD, is presented in greater detail in *Sigl et al. (2018)* whose major findings are summarized in section 6.1.1 of this thesis. The Colle Gnifetti preindustrial and Tsambagarav rBC records will be the topic of upcoming papers. Here, we just give an overview of the main results from those two ice cores for sake of completeness with regard to the *PaleoFire* project.

6.1 Colle Gnifetti

6.1.1 Industrial BC not responsible of 19th-century glacier retreat in the Alps

Summary of: Sigl, M., Abram, N. J., Gabrieli, J., Jenk, T. M., Osmont, D., and Schwikowski, M.: 19th century glacier retreat in the Alps preceded the emergence of industrial black carbon deposition on high-alpine glaciers, *The Cryosphere*, 12, 3311–3331, 2018.

After reaching a maximum extent around 1850, most of the glaciers in the Alps started to rapidly retreat from the 1860s on, thus materializing the end of the Little Ice Age in this region *(Nussbaumer and Zumbühl, 2012; Zumbühl et al., 2008)*. Lower precipitation in autumn and higher temperatures in spring were commonly suggested to be the main drivers of this retreat *(Steiner et al., 2008; Zumbühl et al., 2008)*. However, an alternative study based on model simulations combined with the EC ice-core records from Colle Gnifetti *(Thevenon et al., 2009)* and Fiescherhorn *(Jenk et al., 2006)* claimed that industrial BC emissions from 1850 on could have been the main responsible of Alpine glacier retreat *(Painter et al., 2013)*. The basis of this hypothesis was that BC, once deposited on snow and ice surfaces, can trigger a strong snow-albedo feedback leading to increased snowmelt. However, this study was based on low resolution ice-core records using different analytical methods and low resolution measurements of glacier lengths, underlining the need of a high-resolution and reproducible BC Alpine ice-core record to test this hypothesis.

Here, we make use of the combined rBC records from the Colle Gnifetti 2003B and 2015 ice cores (respectively named CG03B and CG15) spanning 1741–2015 and of high resolution glacier length measurements from four glaciers from the Western Alps offering a high observation density already in the mid-19th century (Mer de Glace, Glacier des Bossons, Unterer and Oberer Grindelwaldgletscher). Time-of-emergence (ToE) analyses were performed following the methodology of *Abram et al. (2016)* to define the earliest time at which the rBC signal exceeds its natural variability, which corresponds to a signal-to-noise ratio higher than two.

rBC long-term trends are presented in **Fig. 6.1a**. During the preindustrial time period (1741–1850 AD), the rBC average concentration was 2 ng g^{-1} (with peak values above 4 ng g^{-1} excluded) and little variability can be observed. rBC concentrations started to increase in the last two decades of the 19th century before reaching a first maximum between 1910 and 1920 and a second one between 1933 and 1945. Lower values between 1921 and 1932 could be linked with the economic crisis between the two world wars when industrial production (and potentially rBC emissions) dropped. The average rBC concentration for the time period 1901-1950 was 7.2 ng g^{-1}, more than three times higher than the

preindustrial levels. After 1950, rBC concentrations remained high (average 1951–1993: 6.6 ng g^{-1}) and did only significantly decline in the 21st century, with concentrations around 5 ng g^{-1}.
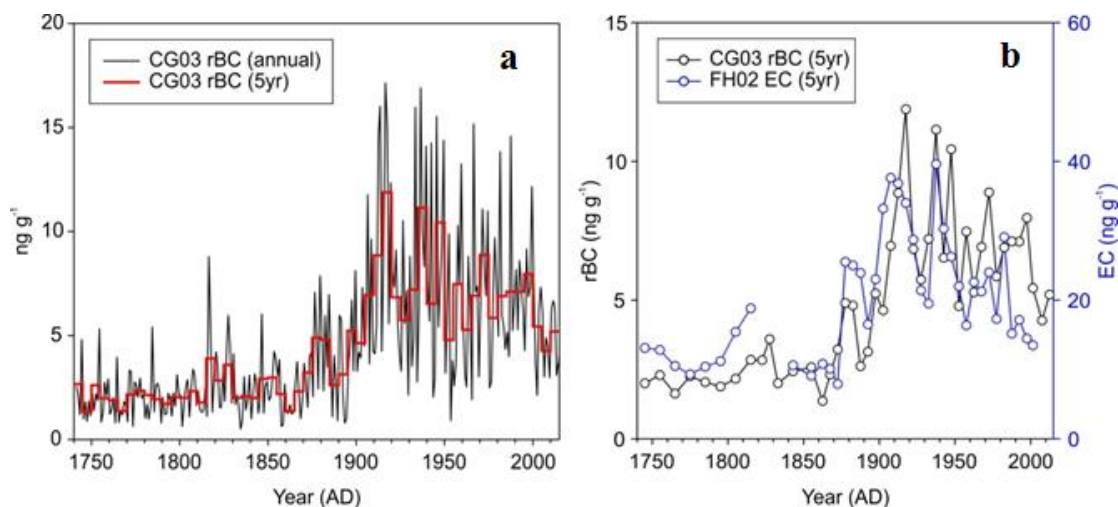

Fig. 6.1: a) Combined CG03B and CG15 rBC ice-core records and b) comparison between the Fiescherhorn (FH02) EC record and the CG rBC records averaged at the same resolution (adapted from *Sigl et al., 2018*).

In the preindustrial time period, the strong correlation between rBC and ammonium (R = 0.75, p < 0.0001, 11-year moving averages) indicates a common biomass burning source, although their natural or anthropogenic origin cannot be disentangled. In the first half of the 20th century, the anthropogenic origin of rBC is evidenced by a common variability between rBC and industrial pollution tracers typical of coal burning, such as sulfate, bismuth and lead. Correlations with the latter become weaker in the second half of the 20th century, thus pointing to a shift from coal-based to petroleum-based combustion sources.

rBC long-term trends in the CG records are supported by the FH02 EC ice-core record **(Fig. 6.1b)** derived from an ice core extracted 70 km north of the CG drill site, in the Bernese Alps *(Cao et al., to be submitted; Jenk et al., 2006)*. Despite large difference in absolute concentrations due to the different analytical methods used *(Lim et al., 2014; Sharma et al., 2017)*, relative variations are well reproduced (R = 0.71, p < 0.005), particularly the first increase in concentrations around 1875, the early-20th century maximum due to coal burning, the dip between the two world wars, the second maximum after Second World War and the slight decline in the last decades. On the contrary, rBC records from Greenland ice cores clearly differ from those from the Alps as they all show a similar pattern reflecting North American industrial emissions, with a unique maximum around 1910 and a strong decline in the 20th century with preindustrial values at the end of the 20th century *(Keegan et al., 2014; McConnell et al., 2007; Sigl et al., 2013)*.

An overall agreement is also observed between BC records from CG and FH02 and BC emissions inventories for both OECD Europe and the Western Alpine region (45–47 °N, 6–9 °E, **Fig. 6.2**, *Bond et al., 2007*). However, some interesting differences can be noted. First, ice-core reconstructions show that the linear increase visible in the inventories between 1850 and 1910 actually occurred in two subsequent steps. Second, BC inventories do not capture the drop between the two world wars. Third, ice-core reconstructions suggest a weaker decline in BC emissions in the second half of the 20th century compared to the trend in the inventories. These discrepancies highlight the fact that BC emission inventories still carry large uncertainties, especially in the earliest time period when data were lacking for Europe and were extrapolated based on USA datasets *(Bond et al., 2007)*. rBC ice-

core records such as the CG one are therefore of great interest as they could be helpful to better constrain BC emissions inventories which are then used as input parameters in coupled aerosol-climate models *(Lamarque et al., 2010; Lee et al., 2013; Shindell et al., 2013)*.
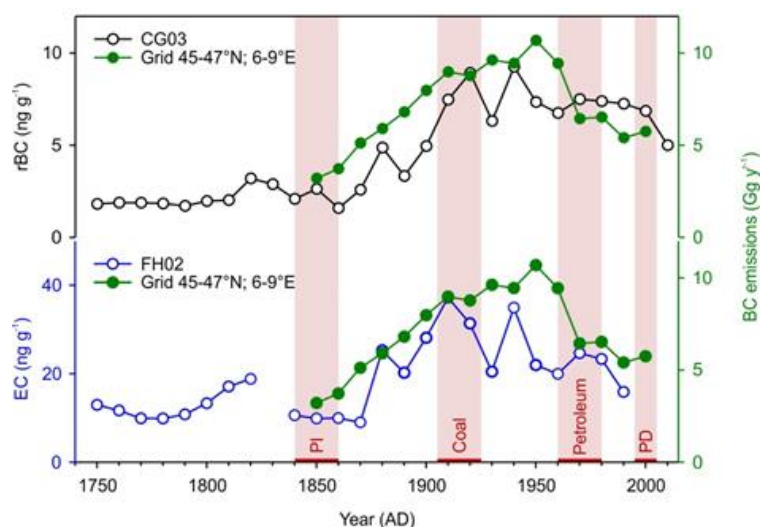

Fig. 6.2: Comparison between the CG rBC (upper panel) and FH02 EC (lower panel) records and BC emission inventories for the grid cells relative to the Western Alps *(Bond et al., 2007)*. PI = preindustrial, PD = present day. Figure adapted from *Sigl et al. (2018)*.

ToE analysis performed on the rBC CG03B record (with preindustrial biomass burning peaks excluded, **Fig. 6.3a**) identifies the year 1875 AD as the time at which rBC concentrations significantly increased above the preindustrial background, with a 5–95 % range spanning 1870–1882 AD **(Fig. 6.3c)**. A similar result (1876 AD, with a 5–95 % range spanning 1872–1876 AD) was given by another method, the Bayesian change point algorithm (**Fig. 6.3d**, *Ruggieri, 2013*). The year 1875 AD was therefore defined as the start of significant industrial BC deposition at the CG site. Interestingly, the stacked record of the four glacier length changes **(Fig. 6.3b)** reveals that at that time, those four glaciers had already experienced 82 % of their total 19th-century retreat (5–95 % range: 52–92 % of their total 19th-century retreat), which invalidates the hypothesis of *Painter et al. (2013)* as timing does not match between the high-resolution rBC and glacier length records. Most of the 19th-century glacier retreat took place between 1850 and 1875. Even if length reductions may vary for glaciers due to their different size and topography, a consistent trend was visible in all of them, with Bossons, Oberer Grindelwald, Mer de Glace and Unterer Grindelwald having experienced 100 %, 83 %, 79 % and 74 % of their cumulative 19th-century retreat in 1875, respectively **(Fig. 6.3e)**. Moreover, small glacier advances occurred around 1910–1920 when rBC concentrations were at their maximum (around 10 ng g^{-1}) which confirms the overall weak impact of rBC on Alpine glacier melting.

One possible explanation for the substantial post-1850 Alpine glacier retreat is that the first half of the 19th century was characterized by much colder conditions than average over Central Europe *(Brohan et al., 2012; Büntgen et al., 2011; Luterbacher et al., 2016)*, especially for summer surface air temperatures which have been shown to be important drivers of glacier mass balance *(Lüthi, 2014; Solomina et al., 2016*, **Fig. 6.4a**). This cooling could have been triggered by a series of large tropical volcanic eruptions from 1809 to 1835 (including the historic 1815 Tambora eruption) which injected billons of tons of aerosols in the atmosphere (*Sigl et al., 2015; Toohey and Sigl, 2017*, **Fig 6.4b**) and occurred simultaneously with the Dalton solar minimum (*Usoskin, 2013*). These conditions could have forced glaciers to advance beyond their natural variability range, leaving them in an unsteady

state. When the negative radiative forcing conditions stopped around 1850, temperatures started to increase and glaciers retreated back to the initial positions they had before this period of strong negative radiative forcing.
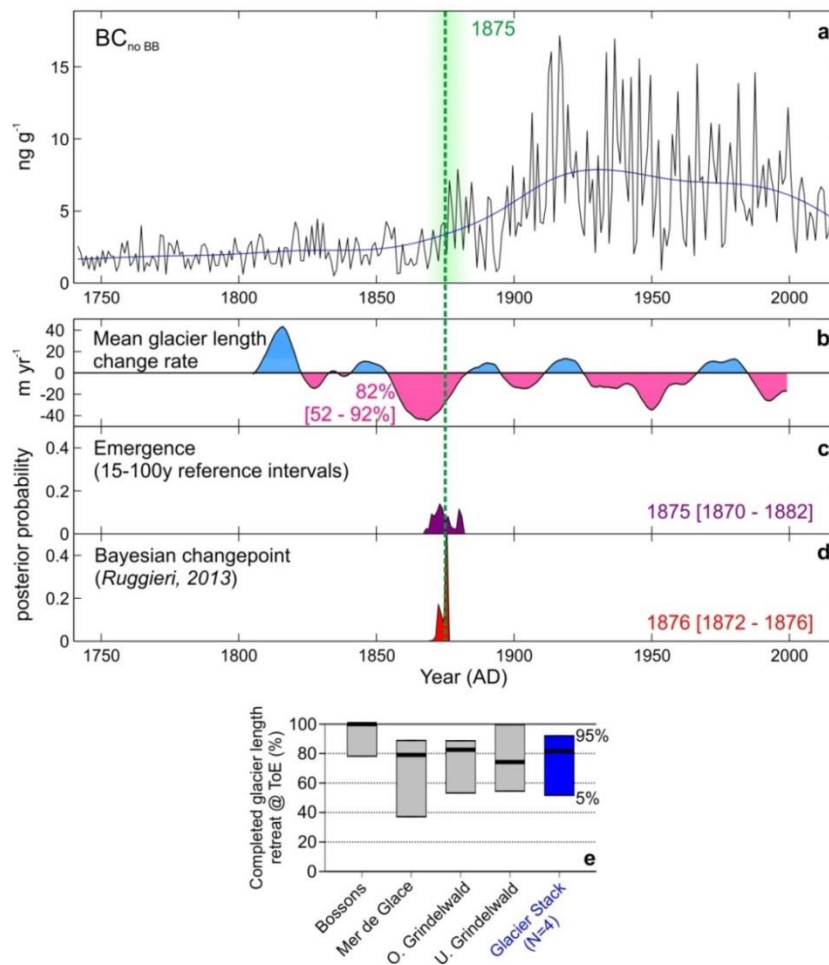

Fig. 6.3: a) Annual CG rBC record with biomass burning peaks excluded (BC$_{no\ BB}$, black) and 15-year filtered trend (blue). b) Mean glacier length change rate with an 11-year filter smooth for the combined four glacier records used in this study and mean value of the glacier retreat in 1875 with [5–95 % range]. c) ToE analysis and d) linear Bayesian change point algorithm showing the normalized distribution of the probabilities of the timing of emergence of industrial BC deposition associated with the median (panel c) and mode (panel d) values and [5–95 % range]. e) Completed 19th-century glacier retreat by 1875 for the four individual glaciers and the glacier stack. Black bars show the mean value and boxes represent the 5–95 % uncertainty range. Figure from *Sigl et al. (2018)*.
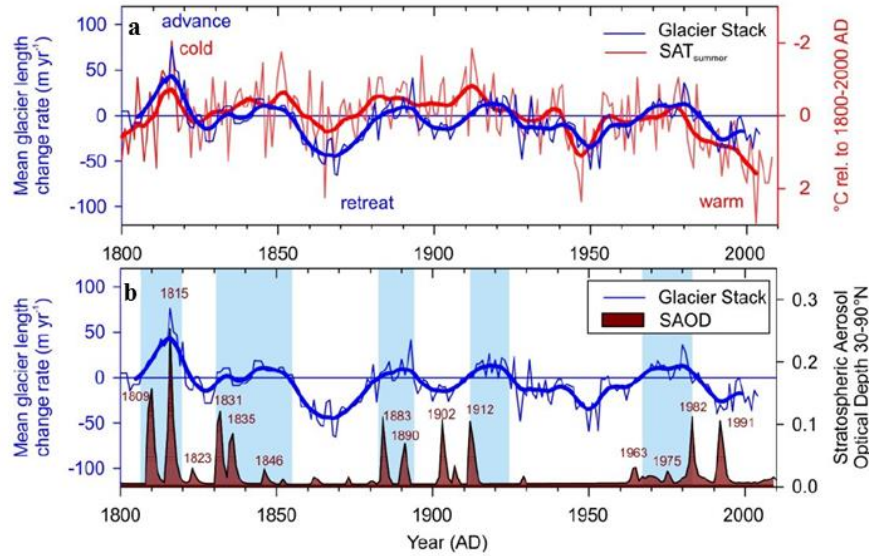
Fig. 6.4: a) Annual resolution and smoothed curve of the mean glacier length change rates for the four glaciers of study along with air temperature anomalies for the summer half year (SAT$_{summer}$) averaged at the same resolution for the Alpine region HISTALP station network *(Böhm et al., 2010)*. b) Glacier stack record (same as panel a) with stratospheric aerosol optical depth (SAOD) at 550 nm inferred from ice cores for the time period 1800–1850 *(Toohey and Sigl, 2017)* and from CMIP6 simulations otherwise *(Eyring et al., 2016)*. Figure adapted from *Sigl et al. (2018)*.

6.1.2 The preindustrial record

In this section we will focus on the time period 1039–1800 AD. The deepest 10 m of the core, spanning roughly 10000 BP–1000 BP, were not sampled due to poor ice quality (chips) and lack of available material. Moreover, the section between 1039 and 1253 AD was composed of brittle ice which could not be cut at high resolution. Annual resolution is not achieved before 1525 AD but as the resolution does not substantially decline until 1254 AD, missing years were linearly interpolated.

Three periods of lower concentrations are visible in the preindustrial rBC record **(Fig. 6.5)**, spanning roughly 1290–1330 AD, 1430–1490 AD and 1640–1730 AD. They are surrounded by periods of higher concentrations, except in the 18th century which shows the lowest centennial average (1.8 ng g^{-1}), in line with the coldest phase of the LIA recorded around 1700 AD *(Owens et al., 2017)*. rBC concentrations in the brittle ice section (average 1039–1253 AD: 2.6 ng g^{-1}) do not substantially differ from those observed in the following time period (average 1254–1400 AD: 2.7 ng g^{-1}).
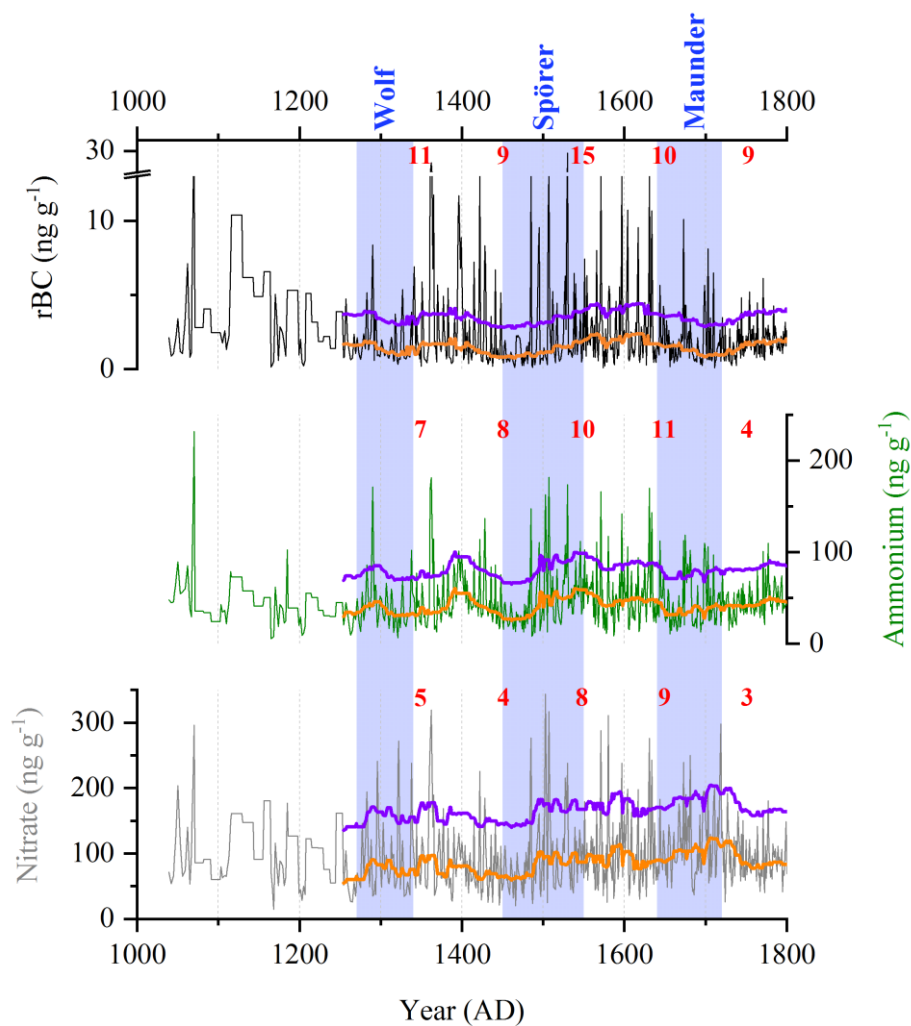
Fig. 6.5: rBC (upper panel), ammonium (middle panel) and nitrate (lower panel) annual concentrations in the CG03B ice core with 31-year moving medians (orange line), the fire threshold associated (purple line) and the number of years above the fire threshold per century corrected for neighboring outliers (red numbers above each chart). The section with brittle ice before 1254 AD was not considered for the outlier detection because of too low resolution. Blue bars show the periods of solar minima.

A correlation analysis was performed over the time period 1300–1799 AD to find common variability between major ions and rBC to highlight potential common sources **(Table 6.1)**. Two main groups could be distinguished: the dust-related compounds (sodium, potassium, magnesium, calcium, chloride and sulfate) and the biomass burning tracers (rBC, ammonium and nitrate). rBC (nitrate) displays the highest (lowest) peak-to-background ratio. Similar to the rBC record, ammonium presents lower concentrations around 1290–1350 AD and 1430–1490 AD. Nitrate concentrations are only reduced during 1410–1480 AD. Those three time periods are characterized by lower Northern Hemisphere temperatures *(Owens et al., 2017)* potentially inducing less biomass burning activity, and partially match minima of solar activity, namely the Wolf (1270–1340 AD), the Spörer (1450–1550 AD) and the Maunder (1640–1720 AD) solar minima *(Usoskin, 2013)* although direct causation between lower solar activity and colder temperatures cannot be established *(Owens et al., 2017)*. Transport and deposition processes seem to remain constant as the CG03B calcium record (not shown) does not present any clear trend over the same time period, therefore suggesting that rBC, ammonium and nitrate variations primarily record temperature-induced changes in biomass burning activity over Central Europe.

Table 6.1: Pearson correlation coefficients (r) between rBC and major ions in the CG03B ice core for the time period 1300–1799 AD performed on annual averages. Values above 0.5 are in bold. r is statistically significant if > 0.146 (n = 500, p = 0.001).

	Na^+	NH_4^+	K^+	Mg^{2+}	Ca^{2+}	Cl^-	NO_3^-	SO_4^{2-}	rBC
Na^+	1								
NH_4^+	0.44	1							
K^+	**0.65**	0.46	1						
Mg^{2+}	**0.79**	0.33	0.25	1					
Ca^{2+}	**0.75**	0.22	0.19	**0.95**	1				
Cl^-	**0.91**	**0.51**	**0.63**	**0.74**	**0.66**	1			
NO_3^-	0.42	**0.76**	0.38	0.30	0.24	0.44	1		
SO_4^{2-}	**0.77**	0.44	0.29	**0.91**	**0.90**	**0.78**	0.41	1	
rBC	0.28	**0.80**	0.45	0.19	0.08	0.37	**0.63**	0.29	1

Following the method presented by *Osmont et al. (2018)*, we performed a statistical counting of remarkable fire peaks in the CG03B rBC, ammonium and nitrate records, which confirmed the long-term trends showing reduced fire activity during the 18th century and enhanced fire activity in the 16th and 17th centuries. A significant peak match between the three fire proxies is observed. For instance, rBC and ammonium share 38 years with common peaks, representing 63 % (86 %) of the total rBC (ammonium) peaks. rBC and nitrate exhibit 26 common peaks, accounting for 43 % (76 %) of the total rBC (nitrate) peaks. Lastly, ammonium and nitrate have 29 peaks in common, representing 66 % (85 %) of the total ammonium (nitrate) peaks. Outstanding fire years, excluding years with simultaneous calcium peaks indicative of enhanced deposition due to the presence of mineral dust, are recorded in 1362, 1485, 1503–1507, 1530, 1571, 1597 and 1631. Interestingly, the year 1530, which shows the highest rBC concentration of the entire record (29.6 ng g^{-1}), could be associated with the 11-month historic megadrought which affected Europe in 1540 AD *(Wetter et al., 2014)*, as the discrepancy lies within the dating error of the ice core. The occurrence of extensive wildfires is supported by historical sources (chroniclers Biem in Cracow and Salat in Lucerne) mentioning that the sky was filled with smoke and the sunlight was dimmed.

6.1.3 Summary

The Colle Gnifetti 2003 and 2015 ice-core records enabled us to reconstruct past rBC variability over the last millennium. The rBC record presents a good correlation and peak-to-peak match with the ammonium and nitrate records, suggesting a potential common origin from biomass burning emissions. Those three records show lower concentrations and reduced peak occurrence during colder time periods such as the Wolf, Spörer and Maunder solar minima. The year 1875 can be considered as the time when rBC industrial emissions started to rise above the natural background. As most of the 19th-century Alpine glacier retreat took place between 1850 and 1875, rBC emissions at that time cannot be held responsible for having forced this retreat, which contradicts a previous study *(Painter et al., 2013)*. Anthropogenic rBC deposition at CG remained elevated throughout the 20th century and did only start to decrease in the last decades. The overall good agreement with the neighboring Fiescherhorn ice core and, to a lesser extent, with regional BC emission inventories, illustrates the ability of the CG ice core to accurately capture BC emission trends from Central Europe.

6.2 Tsambagarav

6.2.1 The paleofire record: 6000 years of fire dynamics in the Altai

Figure 6.6a presents the full rBC record from the Tsambagarav ice core. No major long-term trend is evident in the record except a period with much larger variability and higher concentrations in the oldest 1000 years (roughly 4800–3800 BC) corresponding to the lowest 2–3 m of the core. This trend at the bottom of the core is also present in the major ion **(Fig. 6.6b-d)** and isotope records **(Fig. 6.6e)** and could indicate more unstable climatic conditions during the transition from a wetter and warmer Holocene Climatic Optimum (HCO) to a drier and colder period spanning roughly the last five millennia until around 1750 AD, as inferred by accumulation reconstruction studies *(Herren et al., 2013)*. It has been shown that glaciers in the Mongolian Altai completely disappeared during the HCO and started to reform around 6000 years ago *(Herren et al., 2013)*. This reformation process might partially explain the greater variability in concentration towards the bottom of the ice core. Warmer, albeit wetter, conditions during the HCO might also be responsible of higher levels of biomass burning and therefore higher rBC emissions. It is also worth mentioning that the interpretation of the $\delta^{18}O$ remains difficult as it is influenced by both the temperature and moisture conditions *(Herren et al., 2013)*.

This transition from a wetter/warmer HCO to a subsequent drier/colder period can be primarily explained by insolation-driven latitudinal changes of the Intertropical Convergence Zone (ITCZ). As NH summer insolation decreased throughout the Holocene, the ITCZ was gradually shifted southwards and the NH summer monsoon systems were weakened, leading to a transition from wetter/warmer to drier/colder climatic conditions north of the Himalaya *(Wanner et al., 2011)*. We hypothesize that this transition was accompanied by a change from a monsoon-dominated climate regime to a Westerlies-dominated climate regime, thus bringing more stable conditions.

Using the Tsambagarav ice core, temperatures of the past 3200 years were reconstructed by *Herren (2013)* based on the concentration of biogenic species, namely ammonium and formate **(Fig. 6.6f)**. The underlining hypothesis is that higher emissions of ammonia and volatile organic compounds are produced by vegetation in periods of warmer temperatures and Tsambagarav is located downwind the huge Siberian taiga belt. The most pronounced feature corresponds to a period of elevated temperatures between 130 BC and 310 AD which can be associated with the Roman Warm Period (RWP). The recent temperature increase in the 20th century is also perceptible, but the origin of the increase in ammonium can be questioned as it could also stem from anthropogenic sources *(see section 6.2.2)*. Surprisingly, other characteristic periods such as the MWP and the LIA are barely visible as the record rather suggests a continuous period of negative temperature anomalies at that time. Similarly, climatic trends over the last 2000 years are not well pronounced in the rBC record **(Fig. 6.6a)**. Overall low rBC concentrations prevailed from 700 AD to 1850 AD, in line with the cold conditions evidenced by *Herren (2013)*. Contrary to the Colle Gnifetti ice core, no significant correlation is observed here between rBC and ammonium (r = 0.19, p = 0.05, entire record, 50-year averages), which suggests different sources, namely biogenic emissions for ammonium and biomass burning emissions for rBC.
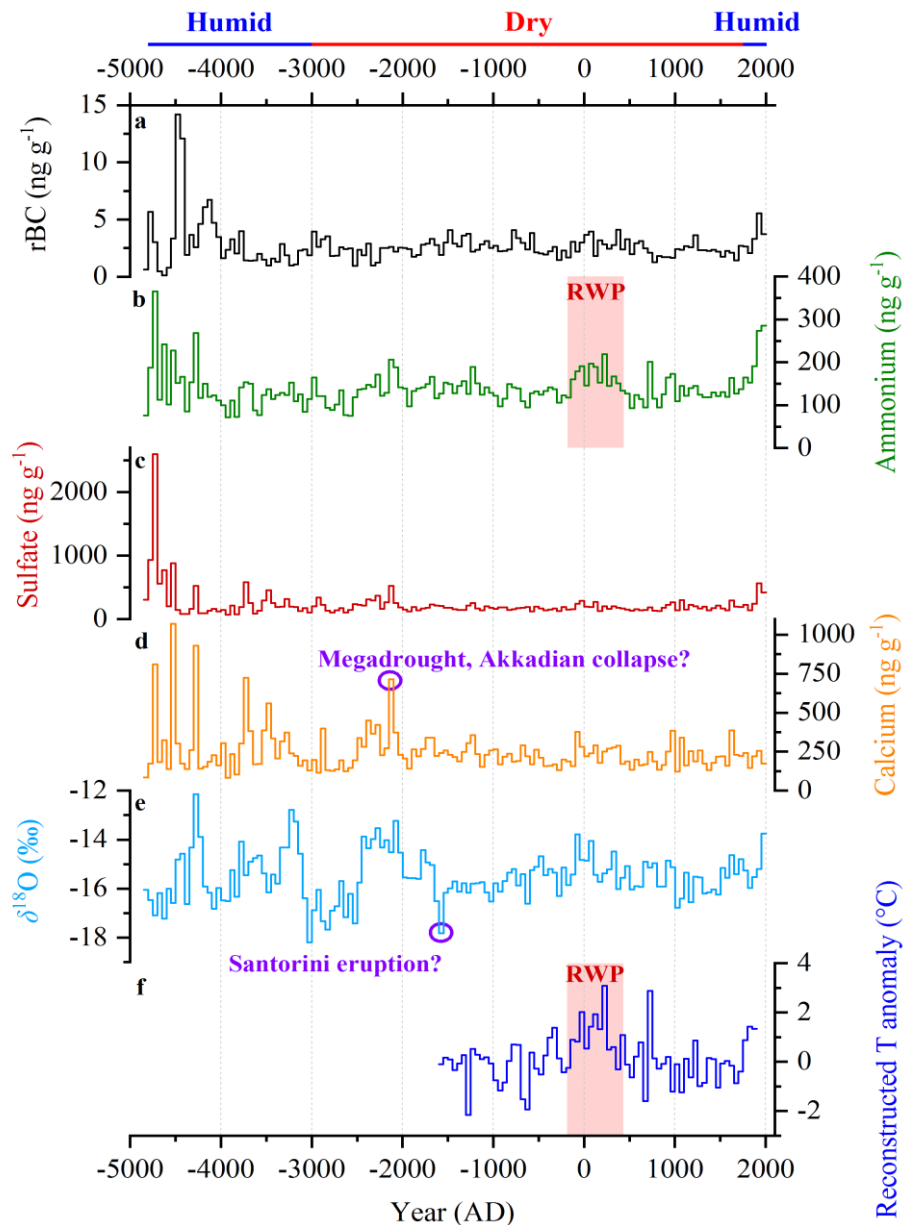
Fig 6.6: a) rBC, b) ammonium, c) sulfate, d) calcium and e) $\delta^{18}O$ records from the entire Tsambagarav ice core (for panels b to e, *Herren et al., 2013*). f) Reconstructed temperature anomalies for the last 3200 years based on the tracers for biogenic emissions, normalized to the period 1270–1930 AD *(Herren, 2013)*. All the data are 50-year averages. The red bar indicates the Roman Warm Period (RWP).

Annual resolution was achieved in the record back to 1582 AD, and extended by linear interpolation back to 1400 AD as the resolution did not significantly decrease until that time. The annual rBC record **(Fig. 6.7a)** shows periods of enhanced biomass burning from 1510 to 1550 AD, 1620 to 1680 AD and 1730 to 1790 AD, while the pronounced increase in the 20th century can be mainly attributed to industrial emissions *(see section 6.2.2)*. The time period 1620–1680 AD is in agreement with the charcoal record from Belukha ice core suggesting a period of very high fire activity in the Siberian Altai from 1600 to 1680 AD (**Fig. 6.7c**, *Eichler et al., 2011*) following an extremely dry period between 1540 and 1600 AD which triggered forest dieback and accumulation of dead biomass more susceptible to burning. Lowest rBC concentrations are recorded around 1670–1730 AD, during the Maunder minimum (1640–1720 AD) characterized by cold conditions in the area (**Fig. 6.7d**).
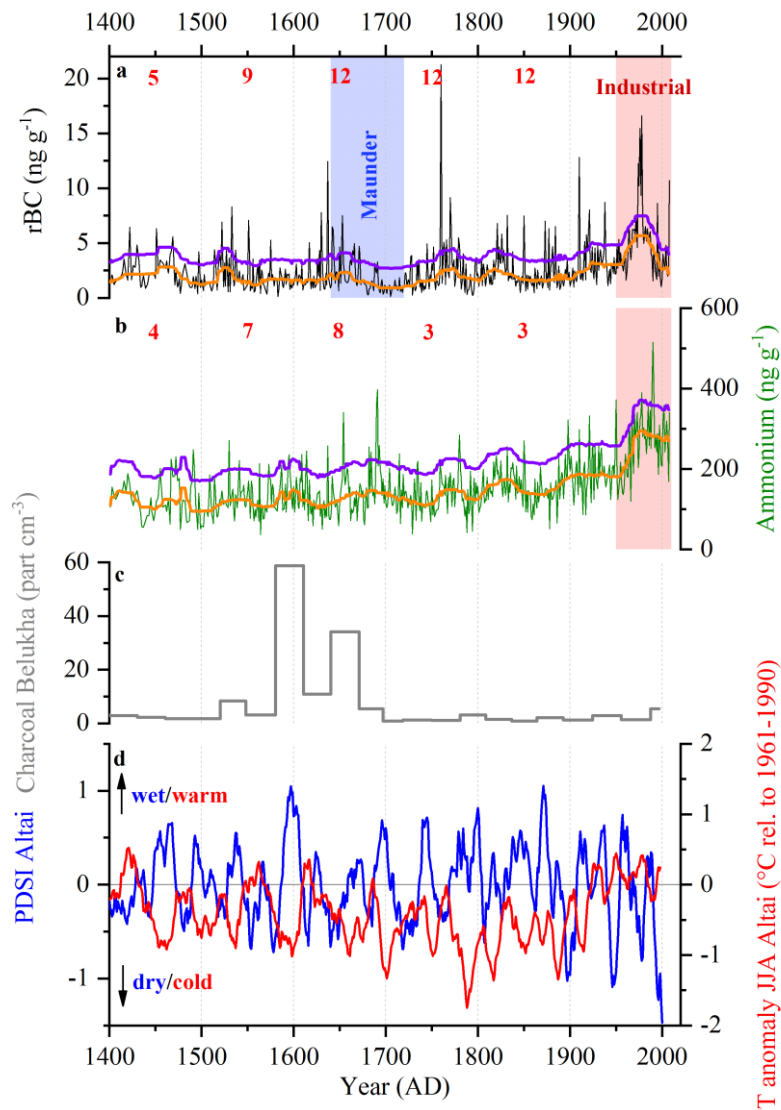
137

Fig. 6.7: a) rBC and b) ammonium *(Herren et al., 2013)* annual averages for the time period 1400-2009 AD in the Tsambagarav record. Orange lines are 31-year moving medians, purple lines correspond to the fire threshold associated and red numbers indicate the number of years with peaks above the fire threshold, corrected for neighboring outliers. c) Charcoal record from the Belukha ice core, raw data *(Eichler et al., 2011)*. d) Palmer Drought Severity Index (PDSI, left scale) for Southern Siberia (45–57.5 °N, 60–110 °E) including the Altai region *(Cook et al., 2010)* and summer (JJA) temperature anomalies relative to 1961–1990 AD (left scale) for the Altai region inferred from tree-ring reconstructions *(Büntgen et al., 2016)*. Data are 11-year moving averages.

Interestingly, the statistical counting of fire peaks based on the rBC record (for a description of the method, see *Osmont et al., 2018*) shows an increase in fire episodes with time, in contrast to temperature which exhibits a general decreasing trend until the coldest 19th century **(Fig. 6.7d)**. On the contrary, the ammonium record does not show such a trend but only a higher peak frequency in the 16th and 17th centuries **(Fig. 6.7b)**. Contrary to what is observed for the Colle Gnifetti ice core, little peak-to-peak correspondence is visible between the rBC and ammonium records, as only 18 % (36 %) of the rBC (ammonium) peaks occur in concert with ammonium (rBC) peaks. Moreover, the correlation coefficient between rBC and ammonium remains low (r = 0.31 for the preindustrial time period 1400-1899 AD, annual averages, p < 0.001). Both these long-term and peak discrepancies

138

underline that biogenic emissions are the major contributor to the ammonium budget at Tsambagarav and that the ammonium record cannot be convincingly associated with biomass burning emissions. Outstanding rBC peaks are visible in 1637 and 1760 AD in periods of regional cold and dry conditions **(Fig. 6.7d)**. A detailed time comparison between years with rBC peaks and major forest fires from Kazakhstan inferred from tree rings *(Mazarzhanova et al., 2017)* reveals that the rBC record from Tsambagarav is able to accurately capture biomass burning episodes from this region as all the large fires years described by *Mazarzhanova et al. (2017)* (1759, 1797, 1824, 1833, 1852 and 1871) match rBC peaks in the Tsambagarav record within ± 2 years owing to the dating uncertainty. This also indicates that areas located west of Tsambagarav are potential source regions, which is in line with the assumption that the current climate regime is dominated by Westerlies.

6.2.2 20th-century industrial BC emissions

In the 20th century, rBC **(Fig. 6.8a)** and ammonium background concentrations reached unprecedented levels since the HCO. Although the rise in ammonium might be partially driven by higher temperatures responsible of enhanced biogenic emissions *(Herren, 2013)*, this increase, starting from 1950 AD and peaking in the 1970s and 1980s, is also observed in the sulfate and nitrate records **(Fig. 6.8b-c)**, two well-known ice-core tracers for anthropogenic emissions. Anthropogenic sulfate primarily comes from SO_2 emissions produced by the combustion of fossil fuels *(Goto-Azuma and Koerner, 2001; McConnell et al., 2007; Schwikowski et al., 1999)* while nitrate mainly originates from NO_x emissions from traffic *(Eichler et al., 2011, 2015; Goto-Azuma and Koerner, 2001; Wendl et al., 2015)*. Ammonium can also be influenced by anthropogenic activities as it can stem from agriculture and livestock NH_3 emissions *(Wendl et al., 2015)*. Following this peak, rBC, sulfate, and to a lesser extent nitrate and ammonium, strongly declined in the late 1980s and 1990s back to early 20th century levels. This overall trend is also reproduced by industrial BC emission inventories for Eastern Europe and former USSR countries **(Fig. 6.8d***, Bond et al., 2007)*, suggesting those countries as probable source regions, with a maximum of emissions between 1950 and 1980 AD when the Soviet industrial production was at its maximum, followed by a dramatic decline caused by the USSR collapse and the sudden stop of many heavy industries. Nevertheless, the 20th-century increase starts earlier and appears smoother in the inventories than in the ice core, probably due to the linear extrapolation used in the emission inventories in the earliest times, for which reliable data is lacking.

6.2.3 Events of particular interest

Although speculative, some particular features recorded in the Tsambagarav ice core could potentially relate to well-documented historical or natural events. For instance, a clear calcium peak around 2100 BC could indicate severe drought conditions **(Fig. 6.6d)**. At the same time in Mesopotamia, the Akkadian empire collapsed in the context of a regional aridification *(Cullen et al., 2000)*. A local minimum in the $\delta^{18}O$ record around 1540 BC **(Fig. 6.6e)** suggests a sudden cooling, which could be related to a volcanic eruption, potentially that of Santorini, Greece, whose exact time is still debated. This cooling occurred in concert with the highest charcoal value recorded in the Tsambagarav ice core (29 particles cm^{-3}, *Brugger et al, in review*), indicative of a very high fire activity. More recently, a remarkable rBC peak (12.8 ng g^{-1}) was seen for the year 1910 AD **(Fig. 6.8a**, also slightly visible in the ammonium record). Forest fires triggered by the Tunguska event, a plausible meteoritic impact which occurred in June 1908 1500 km north of the Tsambagarav drill site, are a possible source, within dating uncertainties. In the Belukha ice core, a peak of nitrate in 1908 AD has been discussed as a potential evidence of the Tunguska event *(Olivier et al., 2006)*. Ammonium peaks were also observed in some of the Greenland ice cores for the year 1908 AD *(Legrand et al., 2016)*. Nevertheless, the authors concluded that those peaks were most probably related to forest fires in

North America and that the similarity in the year was just a coincidence as the burned area induced by the Tunguska event remained small (around 10 000 ha) compared to the average annual burned area over Siberia, amounting to millions of ha. Another outstanding rBC peak is visible for the year 1995 AD **(Fig. 6.8a)**. It is not accompanied by a sulfate peak, thus pointing to a biomass burning origin although no simultaneous charcoal peak can be seen, suggesting a non-local source. In Mongolia, the years 1996 and 1997 AD experienced historic fire seasons with a burned area around six times greater than on an average year **(Fig. 6.9)**. Per year, more than 10 Mha of forest and pasture burned during those two years *(IFFN, 2002)*, which represents around 7 % of the total country area.
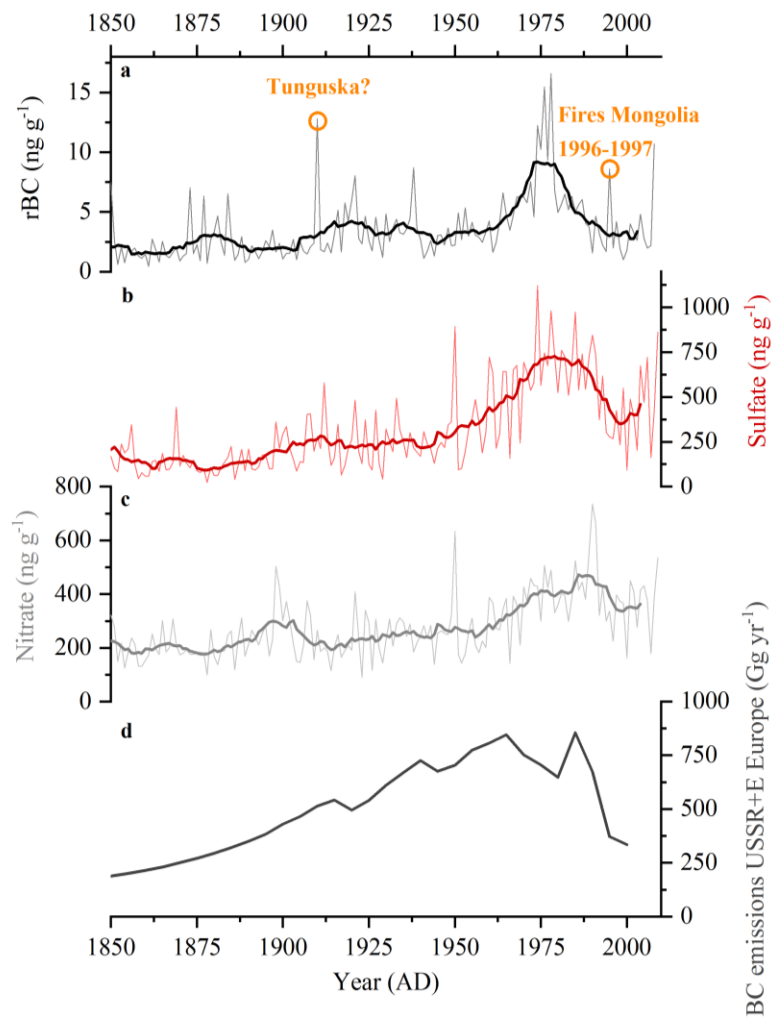

Fig. 6.8: a) rBC, b) sulfate and c) nitrate for the time period 1850-2009 AD in the Tsambagarav ice core. Thin lines are annual averages and thick lines, 11-year moving averages. Sulfate and nitrate data are from *Herren et al. (2013)*. d) Industrial BC emission estimates at 5-year resolution for Eastern Europe and former USSR countries *(Bond et al., 2007)*.
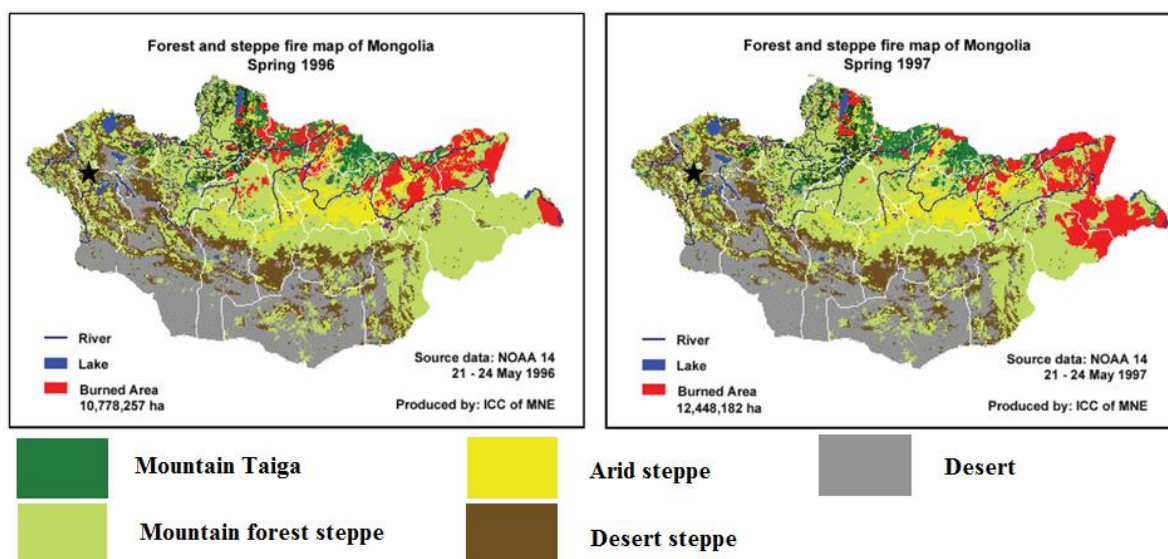
Figure 6.9: Map of Mongolia indicating the burned area (in red) for the years 1996 (left) and 1997 (right) (adapted from *IFFN, 2002*). The black star shows the Tsambagarav drill site.

6.2.4 Summary

The rBC record from the Tsambagarav ice core provides a detailed reconstruction of regional fire activity for the last 6000 years. A much larger variability was observed in the oldest 1000 years of the record, suggesting greater climate instability due to a predominant monsoon regime in the context of the Holocene Climatic Optimum, which subsequently shifted towards a Westerlies-dominated climate regime bringing more stable conditions due to latitudinal changes of the ITCZ. No long-term trend was obvious in the last 5000 years. The Roman Warm Period, clearly visible in the ammonium record and in the temperature reconstruction, was not outstanding in the rBC record. Only for the Maunder minimum could a clear rBC minimum be seen. The ammonium record seems to be solely related to biogenic emissions, as suggested by the weak agreement with the rBC record for both long-term trends and peak occurrence. The good agreement between the Tsambagarav rBC record and other regional fire reconstructions from Belukha and Kazakhstan as well as with particular biomass burning events (e.g. fire season 1996–1997) confirms that rBC can be used as a suitable proxy for regional paleofire reconstruction, except during the 20th century which was disturbed by industrial emissions from Eastern Europe and the USSR. In the future, connections with regional temperature, precipitation and climatic patterns such as the Pacific Decadal Oscillation, the Arctic Oscillation or the North Atlantic Oscillation need to be studied in greater detail to understand the driving forces of biomass burning in Mongolian forests and steppes.

References

Abram, N. J., McGregor, H. V., Tierney, J. E., Evans, M. N., McKay, N. P., Kaufman, D. S., and Consortium, P. K.: Early onset of industrial-era warming across the oceans and continents, *Nature*, 536, 411–418, 2016.

Böhm, R., Jones, P. D., Hiebl, J., Frank, D., Brunetti, M., and Maugeri, M.: The early instrumental warm-bias: a solution for long central European temperature series 1760-2007, *Climatic Change*, 101, 41–67, 2010.

Bond, T. C., Bhardwaj, E., Dong, R., Jogani, R., Jung, S. K., Roden, C., Streets, D. G., and Trautmann, N. M.: Historical emissions of black and organic carbon aerosol from energy-related combustion, 1850–2000, *Global Biogeochemical Cycles*, 21, 2007.

Brohan, P., Allan, R., Freeman, E., Wheeler, D., Wilkinson, C., and Williamson, F.: Constraining the temperature history of the past millennium using early instrumental observations, *Climate of the Past*, 8, 1551–1563, 2012.

Brugger, S. O., Gobet, E., Sigl, M., Osmont, D., Papina, T., Rudaya, N., Schwikowski, M., and Tinner, W.: Ice records provide new insights into climatic vulnerability of Central Asian forest and steppe communities, *Global and Planetary Change*, 2018, in review.

Büntgen, U., Tegel, W., Nicolussi, K., McCormick, M., Frank, D., Trouet, V., Kaplan, J. O., Herzig, F., Heussner, K. U., Wanner, H., Luterbacher, J., and Esper, J.: 2500 Years of European Climate Variability and Human Susceptibility, *Science*, 331, 578–582, 2011.

Büntgen, U., Myglan, V. S., Charpentier Ljungqvist, F., McCormick, M., Di Cosmo, N., Sigl, M., Jungclaus, J., Wagner, S., Krusic, P. J., Esper, J., Kaplan, J. O., de Vaan, M. A. C., Luterbacher, J., Wacker, L., Tegel, W., and Kirdyanov, A. V.: Cooling and societal change during the Late Antique Little Ice Age from 536 to around 660 AD, *Nature Geoscience*, 9, 231–236, 2016.

Cao, F., Zhang, Y.-L., Jenk, T. M., Wacker, L., Salazar, G., Szidat, S., and Schwikowski, M.: Enhancement of secondary biogenic secondary organic aerosol formation during the 20th century: insights from radiocarbon in particulate carbon from a high Alpine glacier, *to be submitted to Environmental Science and Technology*.

Cook, E. R., Anchukaitis, K. J., Buckley, B. M., D'Arrigo, R. D., Jacoby, G. C., and Wright, W. E.: Asian Monsoon Failure and Megadrought During the Last Millenium, *Science*, 328, 486–489, 2010.

Cullen, H. M., de Menocal, P. B., Hemming, S., Hemming, G., Brown, F. H., Guilderson, T., and Sirocko, F.: Climate change and the collapse of the Akkadian empire: evidence from the deep sea, *Geology*, 28(4), 379–382, 2000.

Eichler, A., Tinner, W., Brütsch, S., Olivier, S., Papina, T., and Schwikowski, M.: An ice-core based history of Siberian forest fires since AD 1250, *Quaternary Science Reviews*, 30, 1027–1034, 2011.

Eichler, A., Gramlich, G., Kellerhals, T., Tobler, L., and Schwikowski, M.: Pb pollution from leaded gasoline in South America in the context of a 2000-year metallurgical history, *Science Advances*, 1, e1400196, 2015.

Eyring, V., Bony, S., Meehl, G. A., Senior, C. A., Stevens, B., Stouffer, R. J., and Taylor, K. E.: Overview of the Coupled Model Intercomparison Project Phase 6 (CMIP6) experimental design and organization, *Geoscientific Model Development*, 9, 1937–1958, 2016.

Goto-Azuma, K. and Koerner, R. M.: Ice core studies of anthropogenic sulfate and nitrate trends in the Arctic, *Journal of Geophysical Research*, 106, 4959–4969, 2001.

Herren, P.-A.: Ice core based climate reconstruction from the Mongolian Altai, PhD thesis, University of Bern, 2013.

Herren, P.-A., Eichler, A., Machguth, H., Papina, T., Tobler, L., Zapf, A., and Schwikowski, M.: The onset of Neoglaciation 6000 years ago in western Mongolia revealed by an ice core from the Tsambagarav mountain range, *Quaternary Science Reviews*, 69, 59–69, 2013.

IFFN (International Forest Fire News), *Food and Agriculture Organization of the United Nations*, Report n°26, January 2002.

Jenk, T. M., Szidat, S., Schwikowski, M., Gaggeler, H. W., Brutsch, S., Wacker, L., Synal, H. A., and Saurer, M.: Radiocarbon analysis in an Alpine ice core: record of anthropogenic and biogenic contributions to carbonaceous aerosols in the past (1650-1940), *Atmospheric Chemistry and Physics*, 6, 5381–5390, 2006.

Keegan, K. M., Albert, M. R., McConnell, J. R., and Baker, I.: Climate change and forest fires synergistically drive widespread melt events of the Greenland Ice Sheet, *PNAS*, 111, 7964–7967, 2014.

Lamarque, J. F., Bond, T. C., Eyring, V., Granier, C., Heil, A., Klimont, Z., Lee, D., Liousse, C., Mieville, A., Owen, B., Schultz, M. G., Shindell, D., Smith, S. J., Stehfest, E., Van Aardenne, J., Cooper, O. R., Kainuma, M., Mahowald, N., McConnell, J. R., Naik, V., Riahi, K., and van Vuuren, D. P.: Historical (1850–2000) gridded anthropogenic and biomass burning emissions of reactive gases and aerosols: methodology and application, *Atmospheric Chemistry and Physics*, 10, 7017–7039, 2010.

Lee, Y. H., Lamarque, J. F., Flanner, M. G., Jiao, C., Shindell, D. T., Berntsen, T., Bisiaux, M. M., Cao, J., Collins, W. J., Curran, M., Edwards, R., Faluvegi, G., Ghan, S., Horowitz, L. W., McConnell, J. R., Ming, J., Myhre, G., Nagashima, T., Naik, V., Rumbold, S. T., Skeie, R. B., Sudo, K., Takemura, T., Thevenon, F., Xu, B., and Yoon, J. H.: Evaluation of preindustrial to present-day black carbon and its albedo forcing from Atmospheric Chemistry and Climate Model Intercomparison Project (ACCMIP), *Atmospheric Chemistry and Physics*, 13, 2607–2634, 2013b.

Legrand, M., McConnell, J., Fischer, H., Wolff, E. W., Preunkert, S., Arienzo, M., Chellman, N., Leuenberger, D., Maselli, O., Place, P., Sigl, M., Schüpbach, S., and Flannigan, M.: Boreal fire records in Northern Hemisphere ice cores: a review, *Climate of the Past*, 12, 2033–2059, 2016.

Lim, S., Fain, X., Zanatta, M., Cozic, J., Jaffrezo, J. L., Ginot, P., and Laj, P.: Refractory black carbon mass concentrations in snow and ice: method evaluation and inter-comparison with elemental carbon measurement, *Atmospheric Measurement Techniques*, 7, 3307–3324, 2014.

Luterbacher, J., Werner, J. P., Smerdon, J. E., Fernandez-Donado, L., Gonzalez-Rouco, F. J., Barriopedro, D., Ljungqvist, F. C., Büntgen, U., Zorita, E., Wagner, S., Esper, J., McCarroll, D., Toreti, A., Frank, D., Jungclaus, J. H., Barriendos, M., Bertolin, C., Bothe, O., Brazdil, R., Camuffo, D., Dobrovolny, P., Gagen, M., Garica-Bustamante, E., Ge, Q., Gomez-Navarro, J. J., Guiot, J., Hao, Z., Hegerl, G. C., Holmgren, K., Klimenko, V. V., Martin-Chivelet, J., Pfister, C., Roberts, N., Schindler, A., Schurer, A., Solomina, O., von Gunten, L., Wahl, E., Wanner, H., Wetter, O., Xoplaki, E., Yuan, N., Zanchettin, D., Zhang, H., and Zerefos, C.: European summer temperatures since Roman times, *Environmental Research Letters*, 11, 2016.

Lüthi, M. P.: Little Ice Age climate reconstruction from ensemble reanalysis of Alpine glacier fluctuations, *The Cryosphere*, 8, 639–650, 2014.

Mazarzhanova, K., Kopabayeva, A., Köse, N., and Akkemik, Ü.: The first forest fire history of the Burabai Region (Kazakhstan) from tree rings of pinus sylvestris, *Turkish Journal of Agriculture and Forestry*, 41, 165–174, 2017.

McConnell, J. R., Edwards, R., Kok, G. L., Flanner, M. G., Zender, C. S., Saltzman, E. S., Banta, J. R., Pasteris, D. R., Carter, M. M., and Kahl, J. D. W.: 20th-century industrial black carbon emissions altered arctic climate forcing, *Science*, 317, 1381–1384, 2007.

Nussbaumer, S. U. and Zumbühl, H. J.: The Little Ice Age history of the Glacier des Bossons (Mont Blanc massif, France): a new high-resolution glacier length curve based on historical documents, *Climatic Change*, 111, 301–334, 2012.

Olivier, S., Blaser, C., Brütsch, S., Frolova, N., Gäggeler, H. W., Henderson, K. A., Palmer, A. S., Papina, T., and Schwikowski, M.: Temporal variations of mineral dust, biogenic tracers, and anthropogenic species during the past two centuries from Belukha ice core, Siberian Altai, *Journal of Geophysical Research*, 111, D05309, 2006.

Osmont, D., Wendl, I. A., Schmidely, L., Sigl, M., Vega, C. P., Isaksson, E., and Schwikowski, M.: An 800-year high-resolution black carbon ice core record from Lomonosovfonna, Svalbard, *Atmospheric Chemistry and Physics*, 18, 12777–12795, 2018.

Owens, M. J., Lockwood, M., Hawkins, E., Usoskin, I., Jones, G. S., Barnard, L., Schurer, A., and Fasullo, J.: The Maunder minimum and the Little Ice Age: an update from recent reconstructions and climate simulations, *Journal of Space Weather and Space Climate*, 7, A33, 2017.

Painter, T. H., Flanner, M. G., Kaser, G., Marzeion, B., VanCuren, R. A., and Abdalati, W.: End of the Little Ice Age in the Alps forced by industrial black carbon, *PNAS*, 110, 15216–15221, 2013.

Ruggieri, E.: A Bayesian approach to detecting change points in climatic records, *International Journal of Climatology*, 33, 520–528, 2013.

Schwikowski, M., Döscher, A., Gäggeler, H. W., and Schotterer, U.: Anthropogenic versus natural sources of atmospheric sulphate from an Alpine ice core, *Tellus*, 51B, 938–951, 1999.

Sharma, S., Leaitch, W. R., Huang, L., Veber, D., Kolonjari, F., Zhang, W., Hanna, S. J., Bertram, A. K., and Ogren, J. A.: An evaluation of three methods for measuring black carbon in Alert, Canada, *Atmospheric Chemistry and Physics*, 17, 15225–15243, 2017.

Shindell, D. T., Lamarque, J. F., Schulz, M., Flanner, M., Jiao, C., Chin, M., Young, P. J., Lee, Y. H., Rotstayn, L., Mahowald, N., Milly, G., Faluvegi, G., Balkanski, Y., Collins, W. J., Conley, A. J., Dalsoren, S., Easter, R., Ghan, S., Horowitz, L., Liu, X., Myhre, G., Nagashima, T., Naik, V., Rumbold, S. T., Skeie, R., Sudo, K., Szopa, S., Takemura, T., Voulgarakis, A., Yoon, J. H., and Lo, F.: Radiative forcing in the ACCMIP historical and future climate simulations, *Atmospheric Chemistry and Physics*, 13, 2939–2974, 2013.

Sigl, M., McConnell, J. R., Layman, L., Maselli, O., McGwire, K., Pasteris, D., Dahl-Jensen, D., Steffensen, J. P., Vinther, B., Edwards, R., Mulvaney, R., and Kipfstuhl, S.: A new bipolar ice core record of volcanism from WAIS Divide and NEEM and implications for climate forcing of the last 2000 years, *Journal of Geophysical Research: Atmospheres*, 118, 1151–1169, 2013.

Sigl, M., Winstrup, M., McConnell, J. R., Welten, K. C., Plunkett, G., Ludlow, F., Buntgen, U., Caffee, M., Chellman, N., Dahl-Jensen, D., Fischer, H., Kipfstuhl, S., Kostick, C., Maselli, O. J., Mekhaldi, F., Mulvaney, R., Muscheler, R., Pasteris, D. R., Pilcher, J. R., Salzer, M., Schüpbach, S., Steffensen, J. P., Vinther, B. M., and Woodruff, T. E.: Timing and climate forcing of volcanic eruptions for the past 2,500 years, *Nature*, 523, 543–549, 2015.

Sigl, M., Abram, N. J., Gabrieli, J., Jenk, T. M., Osmont, D., and Schwikowski, M.: 19th century glacier retreat in the Alps preceded the emergence of industrial black carbon deposition on high-alpine glaciers, *The Cryosphere*, 12, 3311–3331, 2018.

Solomina, O. N., Bradley, R. S., Jomelli, V., Geirsdottir, A., Kaufman, D. S., Koch, J., McKay, N. P., Masiokas, M., Miller, G., Nesje, A., Nicolussi, K., Owen, L. A., Putnam, A. E., Wanner, H., Wiles, G., and Yang, B.: Glacier fluctuations during the past 2000 years, *Quaternary Science Reviews*, 149, 61–90, 2016.

Steiner, D., Pauling, A., Nussbaumer, S. U., Nesje, A., Luterbacher, J., Wanner, H., and Zumbuhl, H. J.: Sensitivity of European glaciers to precipitation and temperature - two case studies, *Climatic Change*, 90, 413–441, 2008.

Thevenon, F., Anselmetti, F. S., Bernasconi, S. M., and Schwikowski, M.: Mineral dust and elemental black carbon records from an Alpine ice core (Colle Gnifetti glacier) over the last millennium, *Journal of Geophysical Research: Atmospheres*, 114, 2009.

Toohey, M. and Sigl, M.: Volcanic stratospheric sulfur injections and aerosol optical depth from 500 BCE to 1900 CE, *Earth System Science Data*, 9, 809–831, 2017.

Usoskin, I. G.: A history of solar activity over millennia. , *Living Reviews in Solar Physics*, 10, 2013.

Wanner, H., Solomina, O., Grosjean, M., Ritz, S., and Jetel, M.: Structure and origin of Holocene cold events, *Quaternary Science Reviews*, 30, 3109–3123, 2011.

Wendl, I. A., Eichler, A., Isaksson, E., Martma, T., and Schwikowski, M.: 800-year ice-core record of nitrogen deposition in Svalbard linked to ocean productivity and biogenic emissions, *Atmospheric Chemistry and Physics*, 15, 7287–7300, 2015.

Wetter, O., Pfister, C., Werner, J. P., Zorita, E., Wagner, S., Seneviratne, S. I., Herget, J., Grünewald, U., Luterbacher, J., Alcoforado, M.-J., Barriendos, M., Bieber, U., Brázdil, R., Burmeister, K. H., Camenisch, C., Contino, A., Dobrovolný, P., Glaser, R., Himmelsbach, I., Kiss, A., Kotyza, O., Labbé, T., Limanówka, D., Litzenburger, L., Nordl, Ø., Pribyl, K., Retsö, D., Riemann, D., Rohr, C., Siegfried, W., Söderberg, J., and Spring, J.-L.: The year-long unprecedented European heat and drought of 1540 – a worst case, *Climatic Change*, 125, 349–363, 2014.

Zumbühl, H. J., Steiner, D., and Nussbaumer, S. U.: 19th century glacier representations and fluctuations in the central and western European Alps: An interdisciplinary approach, *Global Planetary Change*, 60, 42–57, 2008.

7 Biomass burning emissions observed at Jungfraujoch: a case study

Dimitri Osmont[1,2,3], Michael Sigl[1,3], Sandra Brugger[3,4], Willy Tinner[3,4],Helga Weber[3,5], Stefan Wunderle[3,5],Anina Gilgen[6], Ulrike Lohmann[6], Margit Schwikowski[1,2,3]

[1]Laboratory of Environmental Chemistry, Paul Scherrer Institut, 5232 Villigen, Switzerland
[2]Department of Chemistry and Biochemistry, University of Bern, 3012 Bern, Switzerland
[3]Oeschger Centre for Climate Change Research, University of Bern, 3012 Bern, Switzerland
[4]Institute of Plant Sciences, University of Bern, 3012 Bern, Switzerland
[5]Institute of Geography, University of Bern, 3012 Bern, Switzerland
[6]Institute for Atmospheric and Climate Science, ETH Zürich, 8092 Zürich, Switzerland

Manuscript in preparation

7.1 Introduction

Fires are an important component of the terrestrial environment as they influence vegetation cover and substantially contribute to the global carbon budget. Current global CO_2 emissions from fires, including landscape fires and biomass burning, represent around 50 % of the global CO_2 emissions produced by fossil fuel burning *(Bowman et al., 2009)*. Fires exert an influence on the climate system as they emit greenhouse gases and aerosols *(Andreae and Merlet, 2001)*. In the last two decades, the occurrence of devastating wildfires has increased in many regions of the world, leading to substantial socioeconomic and environmental consequences *(Moritz et al., 2014)*. In the context of global warming, fire activity is expected to increase in frequency, intensity, duration and extent in many regions of the globe *(Bowman et al., 2011; Keywood et al., 2011)*. To better understand the complex linkages between fires, climate and humans, and to more accurately predict the future evolution of fires in a warming climate, paleofire reconstructions are needed.

For this purpose, ice cores from polar and high-altitude glaciers can be used (see e.g. *Osmont et al., 2018; Zennaro et al., 2014*). Fires emit a wide range of chemical compounds, such as black carbon (BC) and charcoal, which can be transported over long distances, scavenged by precipitation and be deposited in the snowpack, where they will be archived. However, ice-core studies often focus only on paleofire trends but do not consider transport and deposition processes in detail. These processes can only be inferred from specific case studies implying detailed monitoring of the fire extent, the plume transport and the biomass burning tracer deposition and preservation in the snowpack, which is no longer possible for biomass burning events that occurred decades or centuries ago. It thus results that the footprint of the ice-cores sites regarding fires and their ability to preserve single biomass burning events remain largely unknown. Pioneer case studies have shown that elevated concentrations of ammonium, potassium and formate in Greenland atmosphere and snow could be directly related to forest fires in Canada *(Dibb et al., 1996)*.

Here, we focus on an outstanding fire event starting on 17th June 2017 in Portugal. On those days, this country was affected by a severe heat wave with temperatures higher than 40 °C. During a dry thunderstorm, lightning ignited the forest near Pedrógão Grande, in Central Portugal. The resulting fire rapidly spread out of control, killing 66 people and burning around 45000 ha, and was not entirely extinguished before 24th June. This event became the deadliest and most important forest fire Portugal ever experienced. A huge plume of smoke was emitted and transported towards the northeast direction. On 21st June, the MeteoSwiss automatic lidar in Payerne (Switzerland) detected a layer of smoke between 3000 and 5000 m a.s.l. corresponding to the arrival of the plume **(Fig. 7.1, left)**,

which intensified on 22nd June and whose origin was confirmed by atmospheric backward trajectory analysis **(Fig. 7.1, right)**. This layer of smoke became visible on 22nd June in the morning on the Jungfraujoch (JFJ) research station webcam **(Fig. 7.2)**, located at 3580 m a.s.l. in the Bernese Alps, and a peak in atmospheric equivalent black carbon (eBC) was detected by the Multi-Angle Absorption Photometer (MAAP, optical method for BC quantification, *Petzold and Schönlinner, 2004*) installed in the research station **(Fig. 7.3)**. Elevated values lasted until 25th June when the first snowfalls following the event occurred.
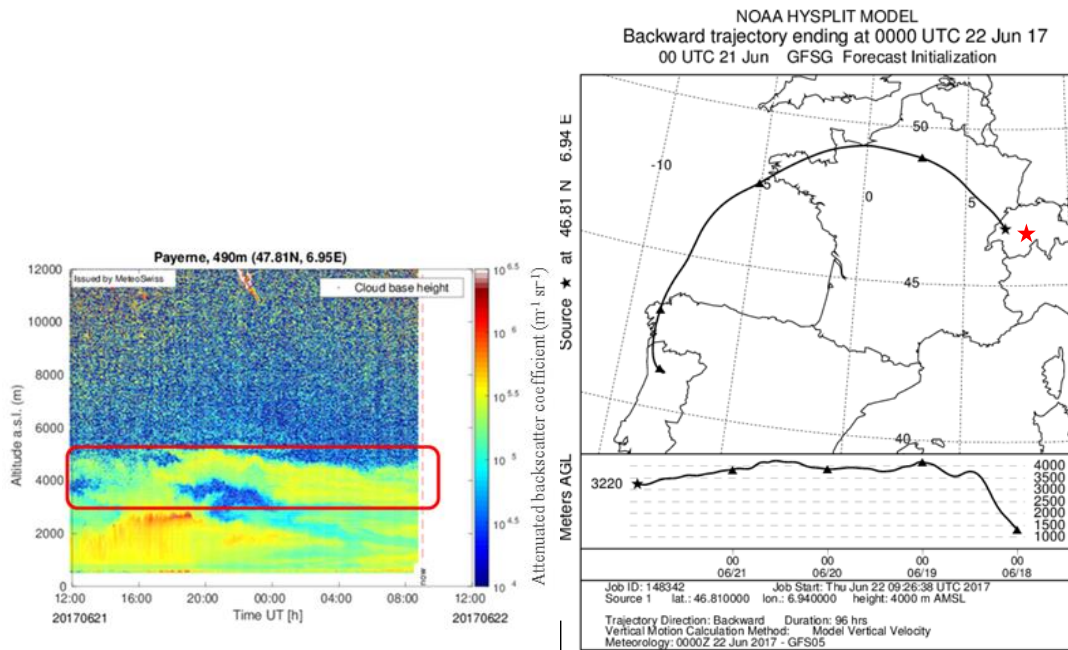
Fig 7.1: Lidar profile from the MeteoSwiss station in Payerne (left panel). The red rectangle shows the ash layer appearing on 21st June 2017 and getting more intense in the next hours. The pollution layer on the Swiss Plateau is visible below 2000 m. Atmospheric backward trajectory from Payerne (right panel) calculated by the Global Forecast System model (GFS) between 22nd June 00 UTC and 18th June 00 UTC, with the vertical profile shown below. The red star shows the location of the JFJ research station. Source: *http://www.meteosuisse.admin.ch/home.subpage.html/fr/data/blogs/2017/6/incendies-du-portugal-mesures-en-suisse.html.*
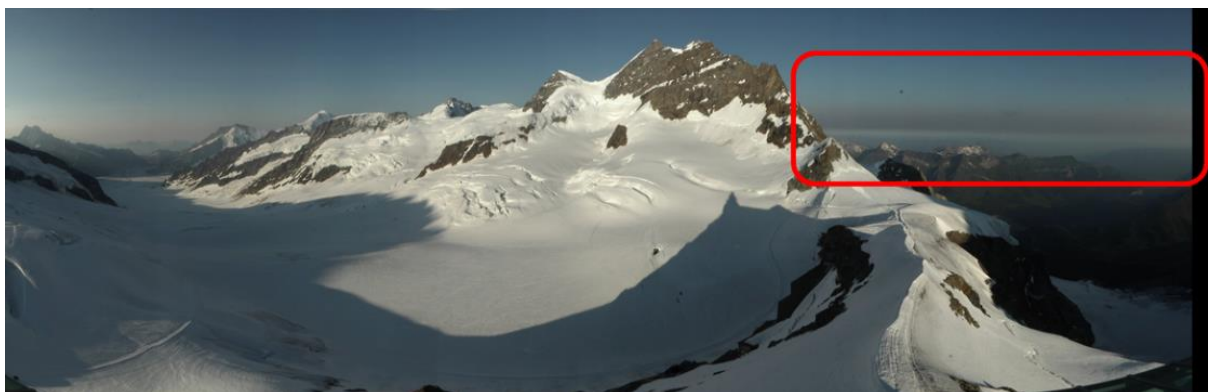

Fig. 7.2: View from the webcam of the JFJ research station, 3580 m a.s.l., Bernese Alps, Switzerland, in the morning of 22nd June 2017. The dark ash layer is clearly visible (red rectangle). Source: *http://www.meteosuisse.admin.ch/home.subpage.html/fr/data/blogs/2017/6/incendies-du-portugal-mesures-en-suisse.html.*

Following this interesting event, we collected a snowpit at the JFJ site in order to determine how this plume of smoke had been archived in the snowpack and which chemical imprint was left. We decided to wait for some precipitation to take into account wet deposition processes. Precipitation occurred on 25th, 26th, 28th and 29th June, so we planned the trip for 30th June.

7.2 Methods

7.2.1 Study site and meteorological conditions

The high-altitude research station Jungfraujoch (JFJ, 46°32´ N 7°59´ E) was founded in 1930 on the eponymous pass located between the summits of Jungfrau and Mönch, in the Bernese Alps, at an altitude of 3580 m a.s.l. in a high-alpine environment surrounded by glaciers and cliffs **(Fig. 7.4)**. The north side, facing the Swiss Plateau, consists of a steep ice fall while the relatively flat south side hosts a large glacier forming part of the Aletsch glacier. The JFJ site only partially lies within the free troposphere as it is frequently influenced by uplifted air from the planetary boundary layer (see e.g. *Bukowiecki et al., 2016*). Aerosol monitoring, which started there in the 1970s, provide continuous long-term atmospheric records of many parameters such as aerosol size distribution, number and mass concentrations, cloud condensation nuclei number concentration, light absorption coefficients and eBC concentration. In addition, a weather station from MeteoSwiss provides meteorological data (temperature, humidity, wind speed and direction, etc…). However, precipitation is not monitored at JFJ due to the difficulty of obtaining accurate data as most of the precipitation occurs in form of snow and in frequent association with strong winds. The closest precipitation data available comes from Lauterbrunnen (815 m a.s.l.), only 8 km apart but 2700 m below in the valley, which can lead to strong discrepancies between the two sites. Precipitation (rainfall) was recorded at Lauterbrunnen on 25th, 26th, 27th, 28th and 29th June, bringing 15.7, 17.1, 0.6, 18.8 and 21.8 mm of water, respectively. We used the JFJ webcam to determine whether snowfalls occurred at the same time at JFJ, which turned out to be true except on 27th June. We estimated the snowfall height by considering a density of 0.2 g cm^{-3} as observed in the fresh snow layer in the upper 10 cm of the snowpit **(Fig. 7.5b)**, thus giving snowfall heights of 7.9, 8.6, 9.4 and 10.9 cm for the days 25th, 26th, 28th and 29th June, respectively **(Fig. 7.3)**.
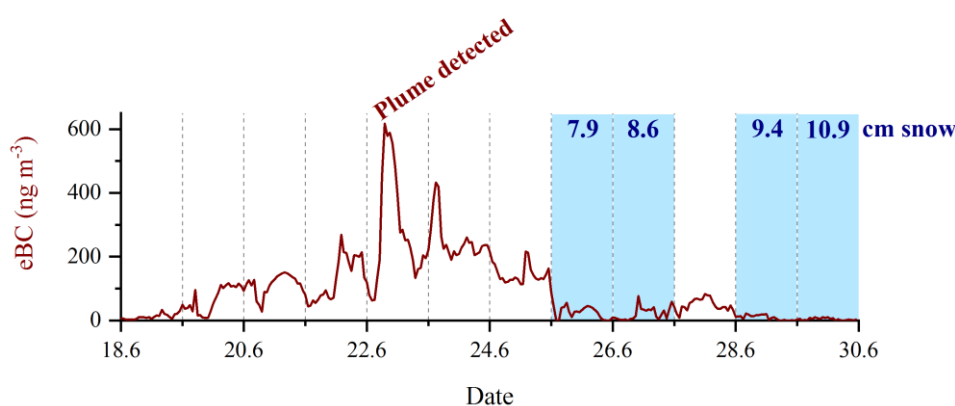

Fig. 7.3: Atmospheric equivalent black carbon (eBC) profile from the continuous MAAP measurements at JFJ showing the peak on 22nd June when the plume of smoke reached the site. Blue bars indicate days with significant snowfall, with the respective amount in cm.

Fig. 7.4: Topographic map of the JFJ site, with the location of the snowpit (red star). Source: *Federal Office of Topography, Swisstopo.*

7.2.2 Snowpit and sampling

The snowpit was collected on 30th June 2017, around 20 m off the prepared trail between JFJ and Mönchsjochhütte and 400 m east from the Jungfraujoch rock, at an altitude of 3460 m a.s.l. **(Fig. 7.4)**. Digging was stopped at 1.10 m depth when a massive ice layer was found, thus preventing us from going deeper. Density measurements were carried out on the spot for each layer by filling a stainless steel cylinder of known volume with snow and by weighing it. Following the stratigraphic study, 20 samples were collected at around 5 cm resolution by pushing pre-cleaned 50-mL polypropylene vials (Semadeni AG, Switzerland) in the snow wall **(Table 7.1)**. Ice layers were sampled specifically (if thick enough) to check the potential impact of melting on the chemical composition of the snowpack. 20 replicates samples were retrieved at the same resolution to test the reproducibility of the experiment. 6 pre-cleaned 1-L PETG jars (Semadeni AG, Switzerland) were also filled with snow for microscopic charcoal (> 10 μm) analysis, at 10 cm resolution between 20 and 80 cm depth.

Table 7.1: Sampling profile for rBC and major ions. Samples containing an ice layer are highlighted in blue.

Depth top (cm)	Depth bottom (cm)	Sample number	Ice layer (cm)
0	7	1	
7	14	2	
14	22	3	
22	27	4	
27	32	5	
32	37	6	
37	44	7	
44	50	8	
50	54	9	50–51
54	58	10	57–58
58	61	11	
61	67	12	
67	72	13	
72	76	14	
76	78	15	76–78
78	84	16	
84	90	17	
90	92	18	90–91
92	100	19	
100	110	20	

7.2.3 Analytical methods

Samples were stored in frozen state until analysis. 50-mL vials were melted and analyzed at PSI for rBC and major ions. rBC analysis followed the method described by *Wendl et al. (2014)*. After melting the samples at room temperature and 25 min sonication in an ultrasonic bath, rBC was quantified using a Single Particle Soot Photometer (SP2, Droplet Measurement Technologies, USA, *Schwarz et al., 2006; Stephens et al., 2003*) coupled to an APEX-Q jet nebulizer (Elemental Scientific Inc., USA). Further analytical details regarding calibration, reproducibility and autosampling method can be found in *Osmont et al. (2018)*. Samples were subsequently analyzed for 13 ions (5 cations: ammonium NH_4^+, calcium Ca^{2+}, magnesium Mg^{2+}, potassium K^+ and sodium Na^+; and 8 anions: acetate CH_3COO^-, chloride Cl^-, fluoride F^-, formate $HCOO^-$, methanesulfonate (MSA) $CH_3SO_3^-$, nitrate NO_3^-, oxalate $C_2O_4^{2-}$ and sulfate SO_4^{2-}) by ion chromatography (*850 Professional IC*, Metrohm, Switzerland). Charcoal samples were melted and treated according to *Brugger et al. (2018)* and *Brugger et al (in review)*. Briefly, a marker (a known number of *Lycopodium* spores) was added after melting to monitor the losses during the extraction process and charcoal particles were optically counted and corrected for the losses.

7.3 Results

7.3.1 Snowpit profile

The snowpit profile (**Fig. 7.5a**) clearly shows five layers with different grain size and density (**Fig. 7.5b**). Layer A, from 0 to 10 cm (d = 0.2 g cm^{-3}), is composed of fresh and very light powder snow corresponding to the 10.9 cm snowfall on 29th June. Layer B, from 10 to 22 cm (d = 0.37, g cm^{-3}) is made of light snow probably originating from the snowfall on 28th June (estimated height: 9.4 cm). Snow in layer C, from 22 to 50 cm (d = 0.54 g cm^{-3}), had already experienced some transformation as bigger (2–3 mm) round-shaped grains were observed and could relate to the snowfalls that occurred on 25th and 26th June (and even on 21st June, before the arrival of the biomass burning plume, with 2.3 cm estimated height), leading to a total estimated height of 18.8 cm. At that point, the estimated snowfall height does not match anymore with the actual height in the snowpit, thus pointing out the limits of our approach for the estimation of the precipitation. Below 50 cm depth, exact dating becomes impossible, but the frequent presence of ice layers and more compact snow indicates older snow which experienced warmer temperatures, in line with the heat wave which lasted until June 24th in Switzerland. Layer D, from 50 to 76 cm depth, is composed of denser and compact snow (d = 0.55 g cm^{-3}). Layer E, below 78 cm depth, is made of compact firn, although the density did not significantly change (d = 0.52 g cm^{-3}).

7.3.2 rBC and charcoal profiles

A remarkable peak with concentrations up to 9.8 ng g^{-1} is visible in the rBC profile (**Fig. 7.5c**) from 22 to 37 cm depth (samples 4 to 6), in the layer C corresponding to the first snowfalls recorded after the event. This suggests that atmospheric BC was scavenged by snow on 25th and 26th June, in agreement with a drop in atmospheric eBC concentration observed at the same time (**Fig. 7.3**). Wet deposition seems to be the preferential pathway as the peak is spread over the whole accumulated snow layer while dry deposition would rather create a thin and unique highly concentrated layer. Several studies have already indicated that rBC was preferentially scavenged from the atmosphere via wet deposition processes (*Cape et al., 2012; Ruppel et al., 2017*). As no precipitation occurred on 22th June when atmospheric rBC concentrations were peaking, we assume that the highest concentrations

were not archived in the snow and that only the atmospheric eBC fraction that remained in the atmosphere until 25th June was scavenged when snowfalls subsequently occurred. The uppermost two layers (A-B, samples 1 to 3) show very low rBC concentrations (average: 0.21 ng g^{-1}), in line with the clean atmospheric conditions which prevailed on 28th and 29th June with eBC concentrations below 10 ng m^{-3}. Below the rBC peak, from 37 to 110 cm depth, rBC concentrations, with an average of 2.02 ng g^{-1}, show some variability but no clear trend or peak. A very good agreement is obtained between the two series of replicate rBC samples (r = 0.90).

In general, the mode of the rBC mass size distribution **(Fig. 7.5c)** corresponds to particles with a rather large diameter (average of 306 nm and 291 nm for the two series of replicates), which suggests a predominant biomass burning origin, similarly to what *Lim et al. (2017)* observed in the summer layers of the Elbrus ice core, with a mean mass mode diameter of 290.8 nm. The mass size distribution remains fairly similar throughout the profile and does not display higher values in the samples containing rBC peak concentrations.

The impact of melting on the rBC profile remains unclear. Samples 9, 10, 15 and 18 specifically contain ice layers formed by refreezing of melt water. Only samples 9 and 15 show depleted rBC concentrations for both series of replicates compared to the neighboring samples. No impact was observed on the size distribution of the aforementioned samples, while a shift towards large particles can be expected due to the aggregation of rBC particles after melting and refreezing. However, given the small thickness of the ice layers (typically 1–2 cm), those samples might also contain surrounding snow and therefore might not be fully representative of melting conditions. Furthermore, the behavior of rBC particles during melting remains unclear as some studies indicate that rBC is preferentially enriched at the snow surface due to its low solubility in water *(Doherty et al., 2013)* while others suggest that rBC can also percolate through the snowpack *(Xu et al., 2012)*.

The charcoal profile **(Fig. 7.5d)** shows a concomitant peak between 30 and 40 cm depth, with values as high as 20 000 fragments L^{-1}. Compared to the rBC peak, the thinner charcoal peak could indicate that wet scavenging occurred more rapidly for charcoal due to its larger particle size (> 10 μm for charcoal, < 500 nm for rBC). As charcoal is a specific proxy for biomass burning, contrary to rBC which can also originate from fossil fuel combustion, it is evident that this common rBC-charcoal peak is associated with a biomass burning source. However, in the case of lake sediment studies, it is commonly admitted that charcoal particles mainly originate from regional sources (20–100 km, *Tinner and Hu, 2003*). A travel distance from Portugal to JFJ (around 1500 km) thus appears challenging. Given the extreme intensity of this fire, we hypothesize that charcoal particles could have been lifted up high enough in the atmosphere by convection in such a way that they were able to travel along a much longer distance than in case of a low-intensity fire. Moreover, transport patterns might differ between lake sediment studies, usually performed at low-elevations sites, and snowpit and ice-core studies from high altitude sites frequently lying within the free troposphere, which allows more long-range transport.
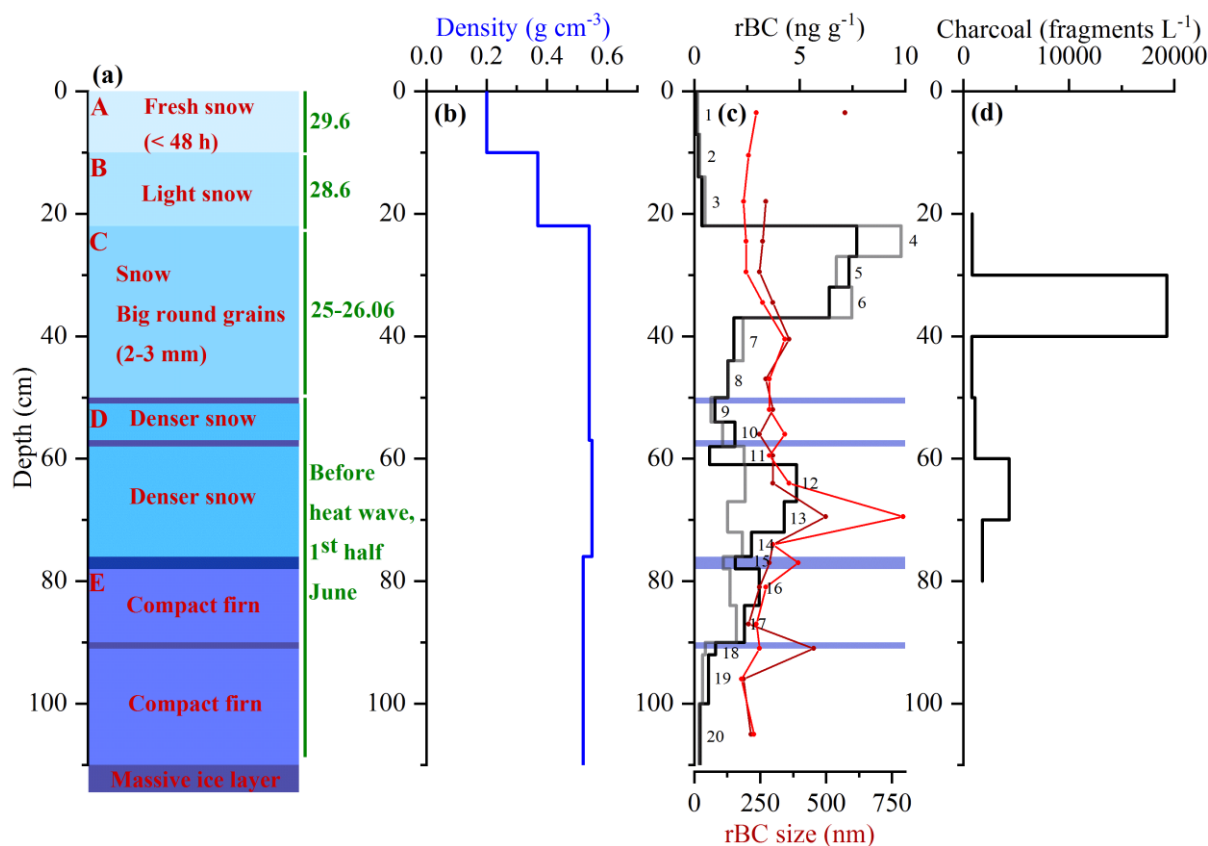
Fig. 7.5: a) Snowpit stratigraphy with ice lenses in dark blue. b) Density profile of the snowpit. c) rBC concentration profile (top scale) with the two series of replicates (black and grey) and sample number associated. Mode of the rBC mass size distribution (bottom scale) with the two series of replicates (dark red and red). Blue bars are ice lenses. d) Charcoal concentration profile.

7.3.3 Ionic profiles

Figure 7.6 presents the major ion profiles obtained from the JFJ snowpit. Due to very low concentrations constantly below 10 ng g^{-1}, the potassium, magnesium, fluoride, MSA and oxalate profiles are not shown nor discussed. Except for a few values, a good agreement is obtained between the two sets of replicates, particularly for ammonium and nitrate. The acetate profile appears less reproducible, which is not surprising given its sensitivity to contamination from ambient air *(Legrand and De Angelis, 1995)* and to post-depositional processes in the snowpack due to its volatile properties *(De Angelis and Legrand, 1995; Legrand et al., 2016)*. Due to the location of the JFJ site, low concentrations are obtained for ions related to sea salt (sodium, chloride) while elevated concentrations are found for ions related to biogenic emissions (ammonium, formate) and anthropogenic sources (agriculture for ammonium, traffic and agriculture for nitrate).

Surprisingly, other potential biomass burning proxies such as ammonium, formate or even nitrate do not display any significant enhancement of their concentrations from 22 to 37 cm depth, possibly due to the predominance of other emission sources, to different atmospheric lifetimes compared to rBC and to different sensitivities to wet deposition (different scavenging ratios). Only calcium shows a concomitant peak with rBC at this depth. One possible explanation is that snowfalls on 25th and 26th June were the first ones following the June 2017 heat wave in Switzerland. Dust concentrations might have been elevated during this dry and warm period and those subsequent snowfalls could have cleaned the atmosphere and led to wet deposition of dust-related ions such as calcium. Similarly to rBC, the impact of ice layers on the ionic records remains inconclusive as both enrichment (typically

sample 18) and depletion (typically sample 9) can be observed for each ion depending on the sample. Nevertheless, sodium, ammonium, formate and nitrate tend to show higher concentrations in the ice layers.
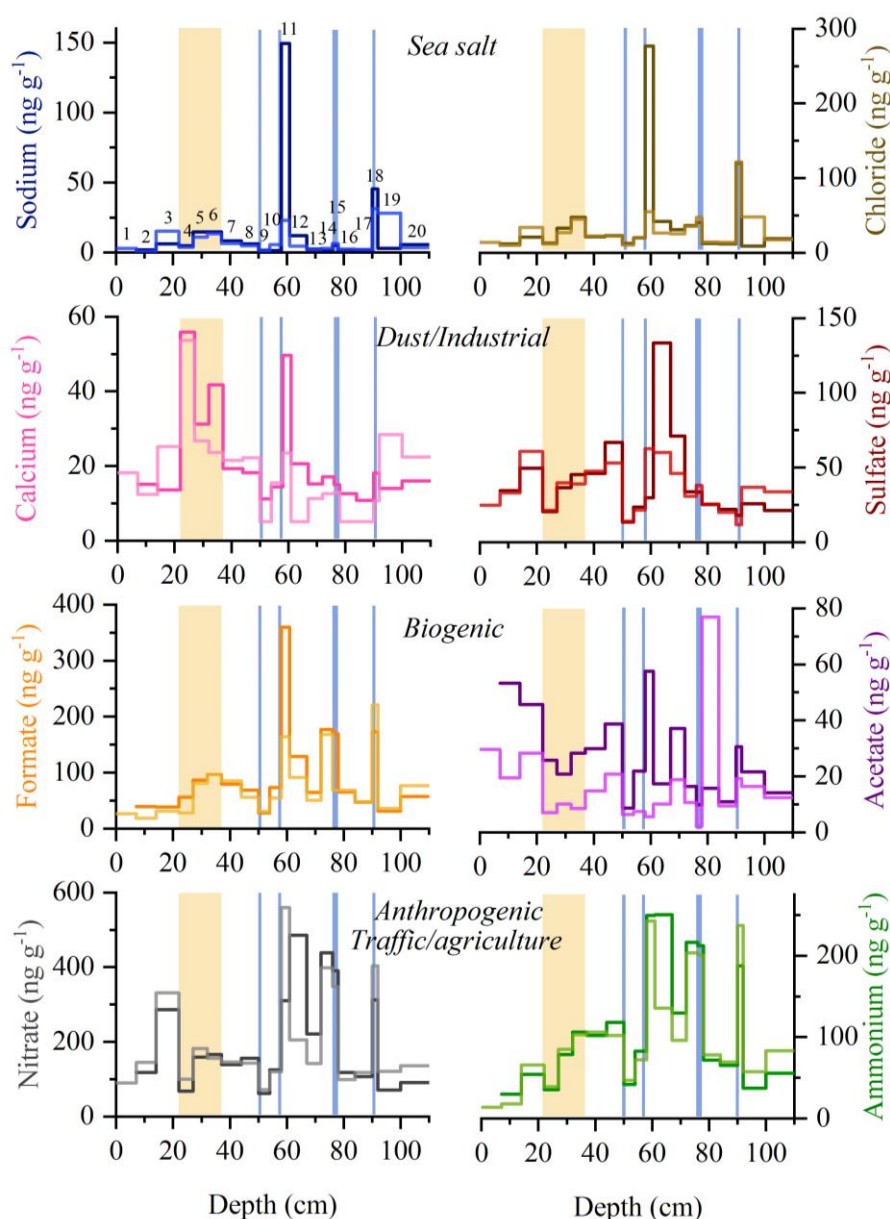

Fig. 7.6: Ionic records from the JFJ snowpit with the two sets of replicates (darker/lighter lines). The orange bar indicates the depth at which rBC and charcoal peaks are observed. Blue bars represent ice layers. Sample numbers are specified for sodium. Potential sources are indicated in the middle.

7.3.4 rBC scavenging ratios

rBC scavenging ratios W were calculated to determine the total scavenging of rBC from air to snow by snowfall, based on the following formula: $W = \rho C_s/C_a$, with ρ the air density in g m^{-3}, C_s the concentration of rBC in snow in ng g^{-1} and C_a the concentration of rBC in air in ng m^{-3} *(Schwikowski et al., 1995)*. Two different cases were considered, one with a high atmospheric rBC burden preceding the snowfalls on 25th and 26th June leading to the rBC peak in snow and the other with a low atmospheric rBC burden on 28th and 29th June associated with the very low rBC concentrations in snow recorded in layers A and B.

The air density had to be calculated for the JFJ site by using the ideal gas law. A small transformation gave the following formula: $\rho = PM/RT$, with P the atmospheric pressure at JFJ at the time of the snowfall (66000 Pa), M the molar mass of dry air (0.0290 kg mol^{-1}), R the ideal gas constant (8.314 J mol^{-1} K^{-1}) and T the temperature at JFJ at the time of the snowfall (273.15 K). We used temperature and pressure data from MeteoSwiss for the JFJ weather station. The calculated air density was therefore 843 g m^{-3}.

Scavenging ratios are presented in **Table 7.2**. As black carbon concentrations were obtained with two different methods, namely the MAAP for atmospheric BC (eBC, light absorption) and the SP2 for BC in snow (rBC, incandescence), both concentrations could not be directly compared as a different fraction of carbonaceous compounds was quantified. A division by a correction factor of 2.7 had to be used to adjust eBC values to rBC values, according to the comparison study of *Sharma et al. (2017)*, leading to scavenging ratios of 110 in the high BC burden case and 71 in the low BC burden case.

Table 7.2: Calculation of rBC scavenging ratios.

BC burden	C_a (ng m^{-3})	$C_{a\,corrected}$ (ng m^{-3})	C_s (ng g^{-1})	W
High	147.5 *Avg 24th June*	54.6	7.14 *Avg samples 4–6*	110
Low	6.8 *Avg 28th-29th June*	2.5	0.21 *Avg samples 1–3*	71

Few BC air-to-snow scavenging ratio values are available in the literature. **Table 7.3** lists some examples of values from previous works and shows that our scavenging ratios roughly lie within the previous estimations. Discrepancies can arise from the different locations implying different climatic conditions and also from the different methods used to quantify BC (light absorption, thermal-optical or incandescence). In our case, the calculation of rBC scavenging ratios is highly dependent on the choice of a conversion factor from eBC to rBC (2.7 here), and of a mass absorption coefficient (MAC) for converting the light absorption intensity given by the MAAP into an eBC concentration. A MAC of 10 m^2 g^{-1} was chosen here (λ = 637 nm), in line with previous studies, which suggested a median MAC of 10.2 ± 3.2 m^2 g^{-1} for JFJ *(Liu et al., 2010)* or 11.1 ± 0.2 m^2 g^{-1} in summer *(Cozic et al., 2008)*. Higher values (13.3 ± 3.0 m^2 g^{-1}) have also been reported in the case of eBC from a purely biomass burning origin *(Schwarz et al., 2008)*.

Table 7.3: Examples of BC scavenging ratios from air to snow available in the literature.

Location	W	BC type	Authors
Arctic	160	eBC	*Clarke and Noone, 1985*
Abisko, Sweden	97 ± 34	eBC	*Noone and Clarke, 1988*
Antarctica	150	eBC	*Warren and Clarke, 1990*
N-E China	140 ± 100	EC	*Wang et al., 2014*

7.3.5 Fire remote sensing and atmospheric transport

In the framework of the inter-disciplinary PaleoFire project, forest fires in Portugal were monitored by satellite using two products: Visible Infrared Imaging Radiometer Suite (VIIRS) for the active fires counts and fire radiative power and Moderate Resolution Imaging Spectroradiometer (MODIS) for

the burned area **(Fig. 7.7)**. The MODIS product showed that in total 446.5 km^2 of forest burned in the region of Pedrógão Grande from 17th to 22nd June 2017, mainly on 18th and 19th June 2017.
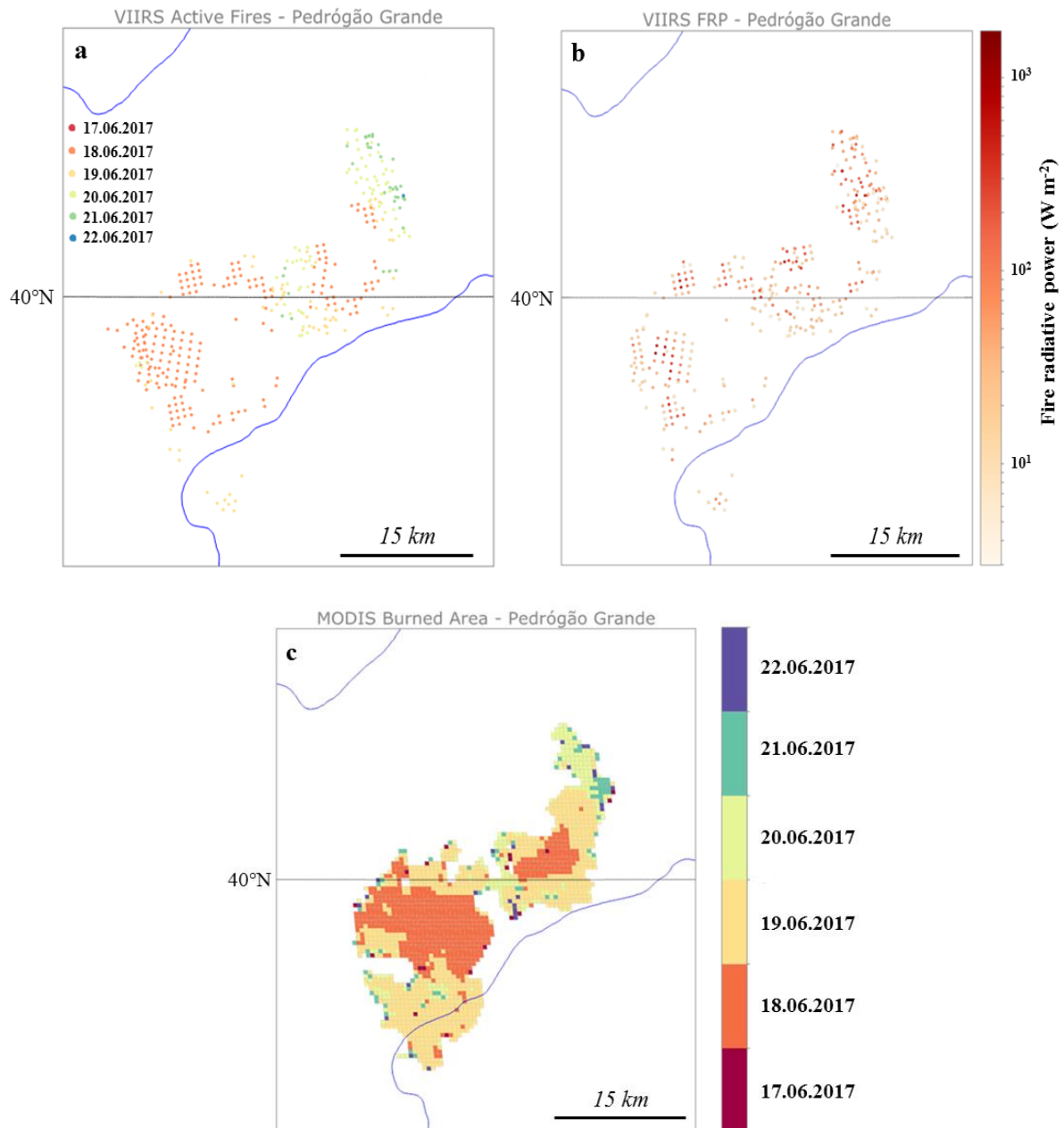

Fig. 7.7: a) Daily location of active fires and b) fire radiative power in the region of Pedrógão Grande from 17th to 22nd June 2017 monitored by VIIRS. c) MODIS burned area for the same region.

3-day air mass back-trajectory analyses performed from the JFJ site for 22nd and 23rd June when atmospheric eBC concentrations were at their maximum suggest Portugal as a likely source, especially for 23rd June **(Fig. 7.8)**, in line with our previous findings. Trajectories were computed with the Lagranto model *(Sprenger and Wernli, 2015)* on ERA-Interim reanalysis data, using the coordinates of JFJ as a starting point and 20 equidistant levels in pressure coordinates between 700 hPa and 200 hPa.
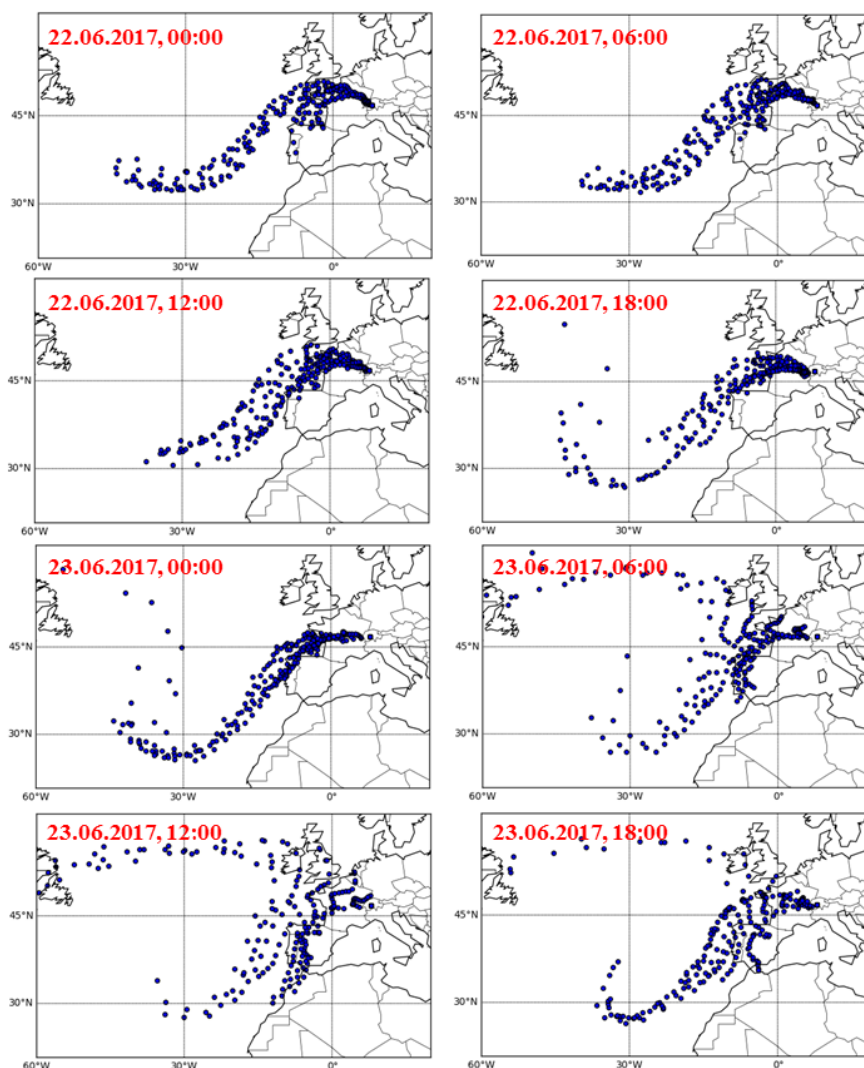
Fig 7.8: 3-day air mass back-trajectories performed every six hours from the JFJ site for the 22nd and 23rd June 2017.

7.4 Conclusions and outlook

This case study aimed at describing how biomass burning emissions from an outstanding fire event in Portugal in June 2017 were detected at the high-alpine site Jungfraujoch, Swiss Alps, in both the atmosphere and the snowpack. The resulting plume of smoke travelled for 4 days before reaching Switzerland, as shown by atmospheric back-trajectory analyses, and was responsible of a peak in atmospheric eBC observed at JFJ on 22nd June. Atmospheric eBC concentrations remained elevated until 25th June, when snowfall occurred. A snowpit study carried out at the same site showed that a peak in rBC and charcoal was observed in the corresponding snow layer. rBC seemed to be predominantly scavenged by wet deposition. We obtained scavenging ratios of 110 (71) in case of high (low) atmospheric eBC burden, in line with previous studies. Except for calcium, no concomitant peak was observed in the major ion profile, even for species usually related to biomass burning emissions (ammonium, formate). Ice layers in the snowpit were specifically sampled but the results remained inconclusive as both enrichment and depletion in rBC and major ions were observed in those layers.

156

In the future, using ECHAM-HAM global aerosol-climate simulations, fire emissions will be estimated and the transport to and deposition at JFJ will be quantitatively assessed to compare modelled with actual rBC concentrations. One possible option is also to combine these results with those from other case studies of fire emissions archived in high-alpine ice cores, such as the Ticino 1973 fires visible in the Colle Gnifetti ice core or the 1996–1997 Mongolian fires detected in the Tsambagarav ice core. Such case studies are of prime importance for paleofire reconstruction by means of ice cores as they help determine the footprint of an ice-core site using satellite data and transport modelling and allow looking in detail at transport and deposition processes of biomass burning tracers, with a main focus on rBC and charcoal in this case.

References

Andreae, M. O. and Merlet, P.: Emission of trace gases and aerosols from biomass burning, *Global Biogeochemical Cycles*, 15(4), 955–966, 2001.

Bowman, D. M. J. S., Balch, J. K., Artaxo, P., Bond, W. J., Carlson, J. M., Cochrane, M. A., D'Antonio, C. M., DeFries, R. S., Doyle, J. C., Harrison, S. P., Johnston, F. H., Keeley, J. E., Krawchuk, M. A., Kull, C. A., Marston, J. B., Moritz, M. A., Prentice, I. C., Roos, C. I., Scott, A. C., Swetnam , T. W., van der Werf, G. R., and Pyne, S. J.: Fire in the Earth System, *Science*, 324(5926), 481–484, 2009.

Bowman, D. M. J. S., Balch, J. K., Artaxo, P., Bond, W. J., Cochrane, M. A., D'Antonio, C. M., DeFries, R. S., Johnston, F. H., Keeley, J. E., Krawchuk, M. A., Kull, C. A., Mack, M., Moritz, M. A., Pyne, S. J., Roos, C. I., Scott, A. C., Sodhi, N. S., and Swetnam, T. W.: The human dimension of fire regimes on Earth, *Journal of Biogeography*, 38(12), 2223–2236, 2011.

Brugger, S. O., Gobet, E., Schanz, F. R., Heiri, O., Schwörer, C., Sigl, M., Schwikowski, M., and Tinner, W.: A quantitative comparison of microfossil extraction methods from ice cores, *Journal of Glaciology*, 64(245), 432–442, 2018.

Brugger, S. O., Gobet, E., Sigl, M., Osmont, D., Papina, T., Rudaya, N., Schwikowski, M., and Tinner, W.: Ice records provide new insights into climatic vulnerability of Central Asian forest and steppe communities, *Global and Planetary Change*, 2018, in review.

Bukowiecki, N., Weingartner, E., Gysel, M., Collaud Coen, M., Zieger, P., Herrmann, E., Steinbacher, M., Gäggeler, H. W., and Baltensperger, U.: A review of more than 20 years of aerosol observation at the high altitude research station Jungfraujoch, Switzerland (3580 m asl), *Aerosol and Air Quality Research*, 16, 764–788, 2016.

Cape, J. N., Coyle, M., and Dumitrean, P.: The atmospheric lifetime of black carbon, *Atmospheric Environment*, 59, 256–263, 2012.

Clarke, A. D. and Noone, K. J.: Soot in the Arctic snowpack: a cause for perturbations in radiative transfer, *Atmospheric Environment*, 19(12), 2045–2053, 1985.

Cozic, J., Verheggen, B., Weingartner, E., Crosier, J., Bower, K. N., Flynn, M., Coe, H., Henning, S., Steinbacher, M., Henne, S., Collaud Coen, M., Petzold, A., and Baltensperger, U.: Chemical composition of free tropospheric aerosol for PM1 and coarse mode at the high alpine site Jungfraujoch, *Atmospheric Chemistry and Physics*, 8, 407–423, 2008.

De Angelis, M. and Legrand, M.: Preliminary investigations of post depositional effects on HCl, HNO3, and organic acids in polar firn, in *Ice Core Studies of Global Biogeochemical Cycles*, edited by R.J. Delmas, NATO ASI Series I, 30, 336–381, 1995.

Dibb, J. E., Talbot, R. W., Whitlow, S. I., Shipham, M. C., Winterle, J., McConnell, J., and Bales, R.: Biomass burning signatures in the atmosphere and snow at Summit, Greenland: An event on 5 August 1994, *Atmospheric Environment*, 30(4), 553–561, 1996.

Doherty, S. J., Grenfell, T. C., Forsström, S., Hegg, D. L., Brandt, R. E., and Warren, S. G.: Observed vertical redistribution of black carbon and other insoluble light-absorbing particles in melting snow, *Journal of Geophysical Research: Atmospheres*, 118, 5553–5569, 2013.

Keywood, M., Kanakidou, M., Stohl, A., Dentener, F., Grassi, G., Meyer, C. P., Torseth, K., Edwards, D., Thompson, A. M., Lohmann, U., and Burrows, J.: Fire in the air: Biomass burning impacts in a changing climate, *Critical Reviews in Environmental Science and Technology*, 43(1), 40–83, 2011.

Legrand, M. and De Angelis, M: Origins and variations of light carboxylic acids in polar precipitation, *Journal of Geophysical Research*, 100, 1445–1462, 1995.

Legrand, M., McConnell, J., Fischer, H., Wolff, E. W., Preunkert, S., Arienzo, M., Chellman, N., Leuenberger, D., Maselli, O., Place, P., Sigl, M., Schüpbach, S., and Flannigan, M.: Boreal fire records in Northern Hemisphere ice cores: a review, *Climate of the Past*, 12, 2033–2059, 2016.

Lim, S., Faïn, X., Ginot, P., Mikhalenko, V., Kutuzov, S., Paris, J.-D., Kozachek, A., and Laj, P.: Black carbon variability since preindustrial times in the eastern part of Europe reconstructed from Mt. Elbrus, Caucasus, ice cores, *Atmospheric Chemistry and Physics*, 17, 3489–3505, 2017.

Liu, D., Flynn, M., Gysel, M., Targino, A., Crawford, I., Bower, K., Choularton, T., Jurányi, Z., Steinbacher, M., Hueglin, C., Curtius, J., Kampus, M., Petzold, A., Weingartner, E., Baltensperger, U., and Coe, H.: Single Particle Characterization of Black Carbon Aerosols at a Tropospheric Alpine Site in Switzerland, *Atmospheric Chemistry and Physics*, 10, 7389–7407, 2010.

Moritz, M. A., Batllori, E., Bradstock, R. A., Malcolm Gill, A., Handmer, J., Hessburg, P. F., Leonard, J., McCaffrey, S., Odion, D. C., Schoennagel, T., and Syphard, A. D.: Learning to coexist with wildfire, *Nature*, 515, 58–66, 2014.

Noone, K. J. and Clarke, A. D.: Soot scavenging measurements in Arctic snowfall, *Atmospheric Environment*, 22(12), 2773–2778, 1988.

Osmont, D., Wendl, I. A., Schmidely, L., Sigl, M., Vega, C. P., Isaksson, E., and Schwikowski, M.: An 800-year high-resolution black carbon ice core record from Lomonosovfonna, Svalbard, *Atmospheric Chemistry and Physics*, 18, 12777–12795, 2018.

Petzold, A. and Schönlinner, M.: Multi-angle absorption photometry – a new method for the measurement of aerosol light absorption and atmospheric black carbon, *Journal of Aerosol Science*, 35, 421–441, 2004.

Ruppel, M. M., Soares, J., Gallet, J.-C., Isaksson, E., Martma, T., Svensson, J., Kohler, J., Pedersen, C. A., Manninen, S., Korhola, A., and Ström, J.: Do contemporary (1980–2015) emissions determine the elemental carbon deposition trend at Holtedahlfonna glacier, Svalbard?, *Atmospheric Chemistry and Physics*, 17, 12779–12795, 2017.

Schwarz, J. P., Gao, R. S., Fahey, D. W., Thomson, D. S., Watts, L. A., Wilson, J. C., Reeves, J. M., Darbeheshti, M., Baumgardner, D. G., Kok, G. L., Chung, S. H., Schulz, M., Hendricks, J., Lauer, A., Karcher, B., Slowik, J. G., Rosenlof, K. H., Thompson, T. L., Langford, A. O., Loewenstein, M., and Aikin, K. C.: Single-particle measurements of midlatitude black carbon and light-scattering aerosols from the boundary layer to the lower stratosphere, *Journal of Geophysical Research*, 111, D16207, 2006.

Schwarz, J. P., Gao, R. S., Spackman, J. R., Watts, L. A., Thomson, D. S., Fahey, D. W., Ryerson, T. B., Peischl, J., Holloway, J. S., Trainer, M., Frost, G. J., Baynard, T., Lack, D. A., de Gouw, J. A., Warneke, C., and

Del Negro, L. A.: Measurement of the mixing state, mass, and optical size of individual black carbon particles in urban and biomass burning emissions, *Geophysical Research Letters*, 35, L13810, 2008.

Schwikowski, M., Seibert, P., Baltensperger, U., and Gäggeler, H. W.: A study of an outstanding Saharan dust event at the high-alpine site Jungfraujoch, Switzerland, *Atmospheric Environment*, 29(15), 1829–1842, 1995.

Sharma, S., Leaitch, W. R., Huang, L., Veber, D., Kolonjari, F., Zhang, W., Hanna, S. J., Bertram, A. K., and Ogren, J. A.: An evaluation of three methods for measuring black carbon in Alert, Canada, *Atmospheric Chemistry and Physics*, 17, 15225–15243, 2017.

Sprenger, M. and Wernli, H.: The LAGRANTO Lagrangian analysis tool – version 2.0, *Geoscientific Model Development*, 8, 2569–2586, 2015.

Stephens, M., Turner, N., and Sandberg, J.: Particle identification by laser-induced incandescence in a solid-state laser cavity, *Applied Optics*, 42, 3726–3736, 2003.

Tinner, W. and Hu, F. S.: Size parameters, size-class distribution and area-number relationship of microscopic charcoal: relevance for fire reconstruction, *The Holocene*, 13(4), 499–505, 2003.

Wang, Z. W., Gallet, J. C., Pedersen, C. A., Zhang, X. S., Ström, J., and Ci, Z. J.: Elemental carbon in snow at Changbai mountain, northeastern China: concentrations, scavenging ratios, and dry deposition velocities, *Atmospheric Chemistry and Physics*, 14, 629–640, 2014.

Warren, S. G. and Clarke, A. D.: Soot in the atmosphere and snow surface of Antarctica, *Journal of Geophysical Research*, 95(D2), 1811–1816, 1990.

Wendl, I. A., Menking, J. A., Färber, R., Gysel, M., Kaspari, S. D., Laborde, M. J. G., and Schwikowski, M.: Optimized method for black carbon analysis in ice and snow using the Single Particle Soot Photometer, *Atmospheric Measurement Techniques*, 7, 2667–2681, 2014.

Xu, B., Cao, J., Joswiak, D. R., Liu, X., Zhao, H., and He, J.: Post-depositional enrichment of black soot in snow-pack and accelerated melting of Tibetan glaciers, *Environmental Research Letters*, 7, 014022, 2012.

Zennaro, P., Kehrwald, N., McConnell, J. R., Schüpbach, S., Maselli, O. J., Marlon, J., Vallelonga,P., Leuenberger, D., Zangrando, R., Spolaor, A., Borrotti, M., Barbaro, E., Gambaro, A., and Barbante, C.: Fire in ice: two millennia of boreal forest fire history from the Greenland NEEM ice core, *Climate of the Past*, 10, 1905–1924, 2014.

8 Conclusion and Outlook

8.1 Conclusion

In the framework of this PhD thesis, rBC was analyzed in four ice cores from high-mountain glaciers, namely Lomonosovfonna, Illimani, Colle Gnifetti and Tsambagarav, allowing us to reconstruct regional to continental Holocene paleofire trends and more recent anthropogenic impacts (**Fig. 8.1**).

With the Lomonosovfonna ice core, 800 years of atmospheric rBC emissions could be reconstructed. No major long-term variations were detected in the paleofire record despite numerous single fire episodes. A multi-proxy comparison was carried out, showing that different trends were captured depending on the proxies due to their different sensitivities towards emission, transport, deposition and post-deposition processes. A predominant anthropogenic contribution was evidenced since 1860 in the rBC record, attributed to Eurasian emissions, with two maxima in the end of the 19th century and after the 2nd World War and a decline over the last decades. Multiple evidence of disturbance of the record by summer melting was also found.

In the Illimani record, Holocene biomass burning trends in the Amazon Basin could be derived from the rBC record. A high correlation was observed between rBC and reconstructed temperature. Paleofire variations showed elevated levels of biomass burning during warm/dry periods (HCO, MWP) and lower levels during cold/wet periods (last deglaciation LIA), in agreement with local lake-sediment charcoal records and remote Antarctic ice cores. rBC increasing trend since 1730 AD does not seem to be driven by anthropogenic emissions.

From the Colle Gnifetti ice core spanning the last millennium, two main findings were extracted. First, most of 19th-century Alpine glacier retreat took place before rBC levels started to rise around 1875 AD due to industrial emissions, thus contradicting a previous work by *Painter et al. (2013)*. Second, the paleofire reconstruction showed lower fire activity during colder time periods in line with minima of solar activity.

Lastly, the Tsambagarav ice core provided a detailed reconstruction of paleofire activity in Central Asia over the last 6000 years. Two main periods were identified, induced by latitudinal changes of the ITCZ: the oldest 1000 years of the core, with significantly higher fire activity suggesting a predominant Monsoon regime during the HCO, and the following 5000 years, showing lower fire activity in the context of a climate regime dominated by Westerlies. Industrial emissions from the former Soviet Union were also visible in the 2nd half of the 20th century.

By compiling the trends in the four ice-core records, four main conclusions can be highlighted:

- Maximum rBC concentrations were observed in the early- to mid-Holocene, during the HCO, suggesting a much higher fire activity than in the present day.
- In the last 1000 years, little variability in rBC concentrations was observed compared to the HCO. Generally, slightly higher (lower) concentrations were recorded during the MWP (LIA).
- In 3 out of the 4 cores, the recent increase in rBC concentrations is mainly attributed to anthropogenic emissions.
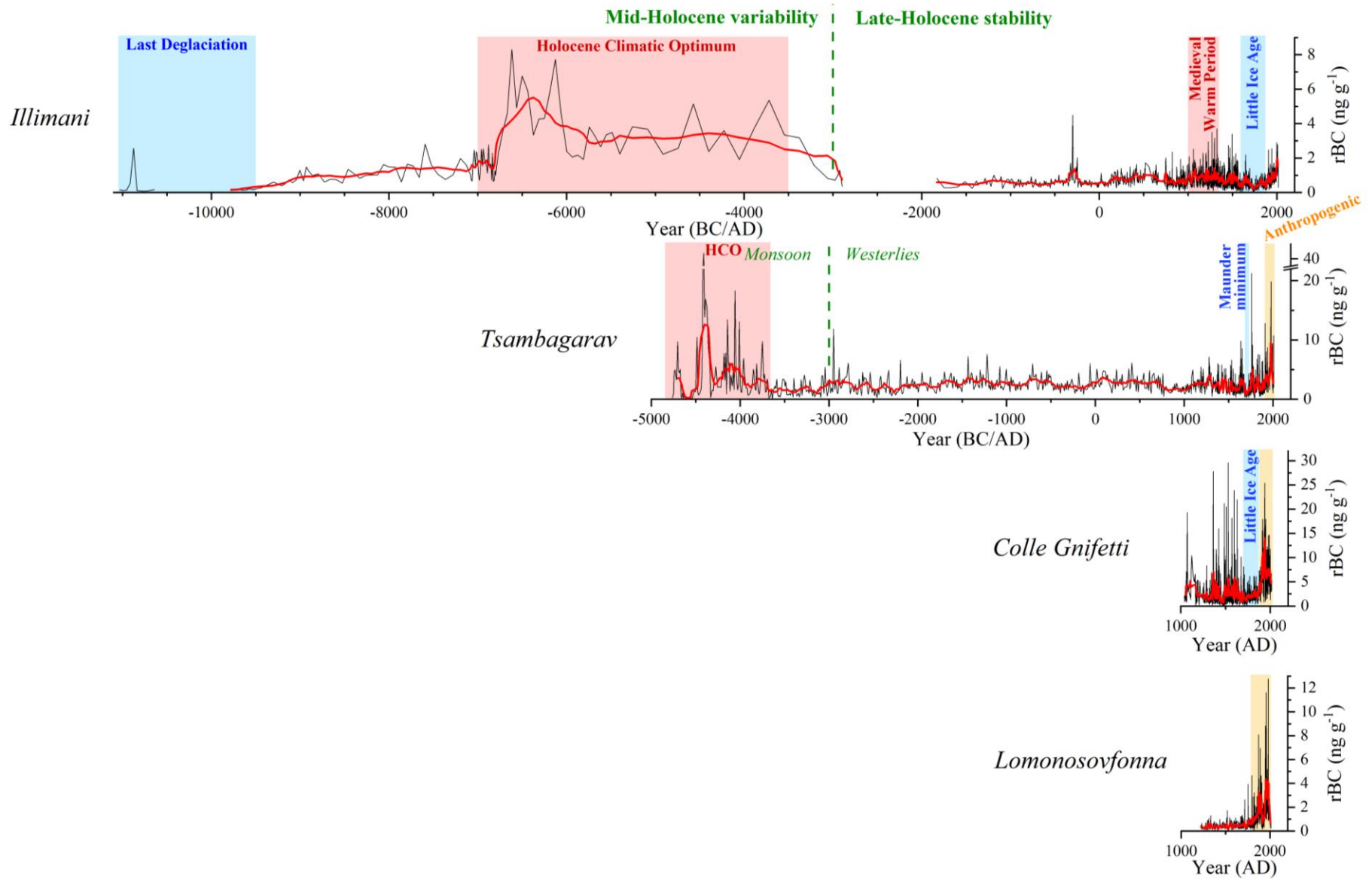- The BFHS hypothesis is not supported by our paleofire reconstructions *(see section 8.1.1)*.

Last Deglaciation

Mid-Holocene variability | Late-Holocene stability

Holocene Climatic Optimum

Medieval Warm Period

Little Ice Age

rBC (ng g⁻¹)

Illimani

Year (BC/AD)

Anthropogenic

HCO | *Monsoon* | *Westerlies*

Maunder minimum

rBC (ng g⁻¹)

Tsambagarav

Year (BC/AD)

Little Ice Age

rBC (ng g⁻¹)

Colle Gnifetti

Year (AD)

rBC (ng g⁻¹)

Lomonosovfonna

Year (AD)

161

Fig. 8.1 (previous page): rBC records from the four ice cores studied in the *PaleoFire* project. Black lines are annual averages (raw data in the deepest part due to lower resolution because of ice layer thinning). Red lines are 11-point moving averages. Note the different y-axis scales.

8.1.1 Is there any evidence of the "broken fire hockey stick" in our four ice cores?

In three out of the four ice cores of the project (Lomonosovfonna, Colle Gnifetti and Tsambagarav), recent rBC trends were dominated by anthropogenic emissions due to fossil fuel burning **(Fig. 8.2)**. A significant anthropogenic contribution was evidenced in Lomonosovfonna since the 1860s, in Colle Gnifetti since the 1870s and in Tsambagarav for the time period 1960–1990 due to USSR industrial emissions. It thus results that rBC cannot be used as a suitable biomass burning proxy for the last 150 years as the contribution from biomass burning emissions is overwhelmed by that of fossil fuels. Some contribution from forest fire episodes can still be identified (e.g. in 1994 in Lomonosovfonna, in 1996–1997 in Tsambagarav) but with these three records, we are not able to discuss the BFHS hypothesis (although it might be possible for Tsambagarav before 1950 as little anthropogenic influence is visible).

The Illimani rBC record is the only one that is not disturbed by anthropogenic emissions. Increasing rBC values since 1730 AD were suggested to originate from the increasing temperature trend observed in the Tropics since the end of the LIA, responsible of enhanced levels of biomass burning. The contribution from human-induced deforestation could have further contributed to this increase in the 20th century. However, with the Illimani record, no decrease in biomass burning activity could be observed for the 20th century, in contrast to the BFHS hypothesis, at least in the Tropics. Lake-sediment charcoal composite records from tropical South America show a similar trend with an unprecedented increase in the 20th century *(Power et al., 2012)*. Similarly, no decrease in rBC concentrations during the first half of the 20th century was observed in the Tsambagarav record, in contradiction with the BFHS hypothesis.

Charcoal records from the same ice cores, obtained in the framework of the *PaleoFire* project *(PhD thesis of S. Brugger, not shown here)*, do not support either the BFHS hypothesis. The charcoal record from Colle Gnifetti shows a raise of fire activity after 1750 AD linked to land-use changes, but no recent decline. The charcoal record from Tsambagarav suggests reduced fire activity since 1750 AD compared to the previous centuries and millennia, probably due to the decline of forests caused by more intensive grazing. Nevertheless, an increasing trend was observed in the 20th century, again in contradiction with the BFHS. In the Illimani ice core, charcoal concentrations are minimal in the 18th and 19th centuries before they start increasing in the 20th century, particularly in the most recent decades, which contradicts the BFHS hypothesis.

Our ice-core results from the *PaleoFire* project reveal that the BFHS trend was not observed in Europe, Central Asia and tropical South America. The BFHS trend might only result from the global compilation of hundreds of lake-sediment charcoal records but does not capture regional variability in paleofire activity, as highlighted by our work.
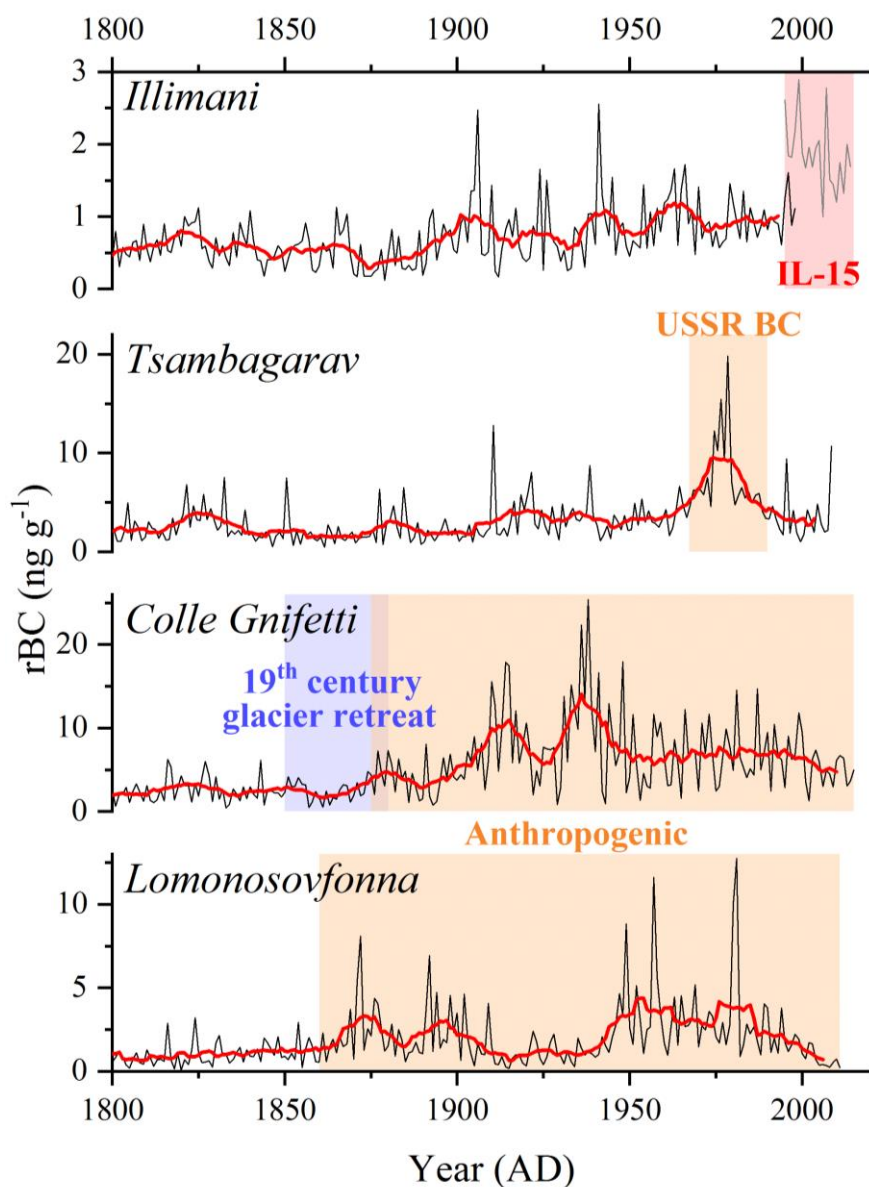
Fig. 8.2: rBC records of the four ice cores of the *PaleoFire* project since 1800 AD. Black lines are annual averages and red lines 11-year moving averages. Note the different y-axis scales and the rBC concentration mismatch between the IL-99 ice core and IL-15 firn core (red shading).

8.2 Outlook

Even if the main goal of the project, namely the analysis of rBC in the four ice cores, was reached, several directions remain to be explored to further improve the interpretation of the paleofire records. In addition to the publication of each of the four rBC records, we list in the following some ideas for potential future work. The progression is structured as follows: technical improvements, future analyses and unsolved scientific questions.

- Regarding technical improvements, the implementation of a flowmeter to monitor the liquid flow between the autosampler and the APEX-Q would be a valuable help to improve the quality of the analyses and replace the tedious flow measurements. Of course, this will not

solve clogging problems, but will ensure a better detection of them. From discussions with other research groups, two models could be considered (SENSIRION SLI-2000 and TruFlo sample monitor for ICP-MS Glass Expansion).

Further analyses could also be envisaged:

- The Lomonosovfonna ice core is the only one that has not been analyzed for charcoal. Despite expected low concentrations, such a record could be helpful to disentangle the origin of rBC and to study how charcoal compares with other biomass burning proxies and with the LF-97 charcoal record *(Hicks and Isaksson, 2006)*.
- All the cores of the project could be extensively investigated for specific molecular tracers of biomass burning such as levoglucosan, VA or *p*-HBA. In this respect, collaborations need to be developed with other research groups as our facilities at PSI do not allow for such analyses at the moment.
- The analysis of trace elements in the Lomonosovfonna and Tsambagarav ice cores, for which they are missing, could provide further indication of past climate variations and anthropogenic pollution.
- It would be very interesting to analyze rBC in the newly drilled ice core from Belukha (Siberian Altai) in 2018, in order to study how it compares with the Tsambagarav rBC record and to better understand paleofire activity in Central Asia.

Remaining scientific questions could be addressed by considering these ideas:

- **An exhaustive comparison of the discrepancies between the different biomass burning tracers:** In the framework of the synergies developed within the *PaleoFire* project, records of rBC, charcoal and other biomass burning tracers from the four ice cores could be combined. Similarly, records of rBC and other tracers of anthropogenic pollution since 1750 AD (e.g. SCPs, spheroidal carbonaceous particles, measured by S. Brugger in her PhD thesis along with charcoal particles) could be presented as indicators of early industrial and mining activities, especially for Colle Gnifetti and Tsambagarav ice cores. It would be particularly interesting to compare the differences between rBC, charcoal and SCPs. A special focus could be made on discussing the relevance of the BFHS hypothesis.
- **The determination of ice-core footprints and transport processes:** for this purpose, specific case studies need to be investigated in detail. A first attempt was made with the Portuguese fires recorded at Jungfraujoch *(chapter 7)*. Other case studies could be discussed, such as the Mongolian 1996–1997 fires archived in the Tsambagarav ice core and the 1973 Ticino fires visible in the Colle Gnifetti charcoal record. In the framework of the *PaleoFire* project, results from satellite data, atmospheric simulations and charcoal/rBC records could be combined to improve our understanding of transport and deposition processes.
- **The representativeness of rBC ice-core records:** rBC and major ion records from the IL-15 firn core could be combined with those from a firn core drilled in 2009 at the same location by scientists from the IRD *(P. Ginot)*. A special focus could be made on the identification of biomass burning events, by using accurate biomass burning statistics, aerosol optical depth (AOD) data from satellite measurements and high-resolution continuous eBC measurements by the MAAP based at Chacaltaya weather station (located around 45 km northwest of Illimani) since 2011. A discussion on the representativeness of rBC measurements from different cores could be considered, to try to explain the substantial differences in absolute rBC concentrations between the IL-99, IL-15 (twice as high as IL-99) and IL-09 (twice as

high as IL-15 despite comparable accumulation rates) ice cores. Performing an inter-comparison study between the two SP2 setups (PSI and LGGE Grenoble) might already help explain part of the discrepancy.

- **The effect of melting on the rBC records:** performing EC/OC measurements with the thermal-optical method for the four ice cores would also be of great interest for several reasons. First, inter-comparisons could be made with rBC measurements, given that such studies are very scarce for ice cores. Second, combining them with ^{14}C analysis of the EC and OC fractions would help apportion rBC sources (fossil vs biogenic). Third, it would be particularly interesting to see how periods with extensive melting, such as the 1920–1930s in the Lomonosovfonna ice core, would compare between EC and rBC. This would allow to confirm the existence of such melting events and to know whether EC methods are sensitive to melting or not.

References

Hicks, S. and Isaksson, E.: Assessing source areas of pollutants from studies of fly ash, charcoal and pollen from Svalbard snow and ice, *Journal of Geophysical Research*, 111, D02113, 2006.

Painter, T. H., Flanner, M. G., Kaser, G., Marzeion, B., VanCuren, R. A., and Abdalati, W.: End of the Little Ice Age in the Alps forced by industrial black carbon, *PNAS*, 110, 15216–15221, 2013.

Power, M. J., Mayle, F. E., Bartlein, P. J., Marlon, J. R., Anderson, R. S., Behling, H., Brown, K. J., Carcaillet, C., Colombaroli, D., Gavin, D. G., Hallett, D. J., Horn, S. P., Kennedy, L. M., Lane, C. S., Long, C. J., Moreno, P. I., Paitre, C., Robinson, G., Taylor, Z., and Walsh, M. K.: Climatic control of the biomass-burning decline in the Americas after AD 1500, *The Holocene*, 23, 3–13, 2012.

Appendix

SP2 operation instructions for ice cores with APEX-ASX520-SP2-setup

Updated by Dimitri Osmont (04/2018)

based on previous work by I. Wendl & L. Schmidely

Getting started

- Make sure SP2 valve is on filtered air and not on APEX.
- Press the ON button on the SP2 to start the computer. Login: ACRG. Pw: lch$2413.
- Turn on APEX by turning the red button down and the blue button up (see picture).
- Fix APEX drain tubes in peristaltic pump. **IMPORTANT otherwise liquid will reach the SP2.**
- Attach air tubing to nebulizer (already done normally) and turn on house air to 4 bar, Red-y should read 1.0 L/min when APEX is ready.
- As soon as the right temperatures are reached, all four lights on the front of the APEX will be on (light next to the red/blue buttons, see picture).
- Fill the water-supply container of the autosampler (AS) with ultrapure water (hereafter MQ).
- Empty the waste-water container of the AS (below the table).
- Make sure that silica gel in SP2 dryer connected to pump (sitting next to the window) is not completely consumed (e.g. part of it should still be dark purple). It gets light purple when wet. Otherwise, replace it.
- Turn AS on (button at the rear of the instrument) and attach the AS peristaltic pump (at the rear too). **Do it BEFORE starting the software otherwise bug.**
- Open the software SP2 4 on the PC (icon on desktop).
- Open a new logbook to keep track of the operations: click on the notepad icon in the menu of the PC, date and hours are inserted by pressing F5 on keyboard. Write everything which is relevant for the measurement (file number and ID, flows…).
- On Config tab -> Program, check and change data file path if necessary to: C:\Data\SP2\2018\SP2data (directory where files will be saved).
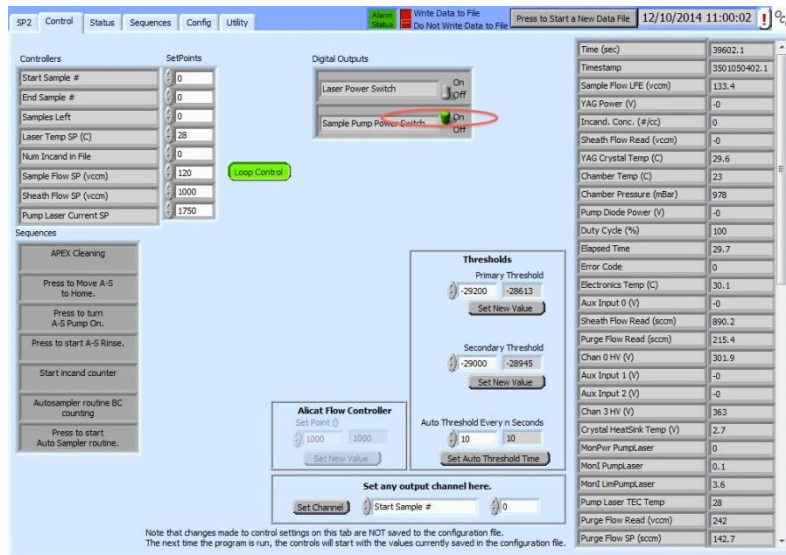
- Make sure the configuration file is "SP2 config for liquid_**new**" (configuration designed for this setup).

Remark: Configuration file is stored on the SP2 driver (file: 20140724132232)
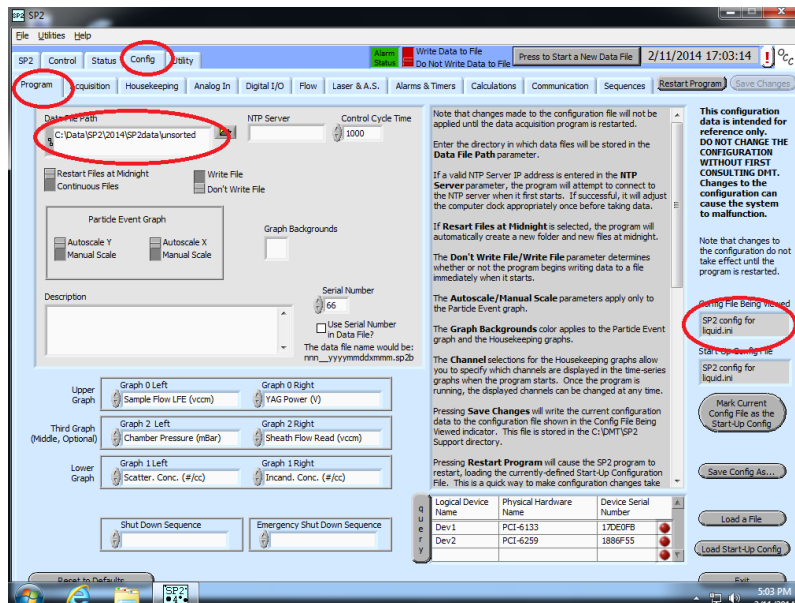
Screenshot 1: Location file path and configuration file.

- Go to Control tab and turn on the SP2 pump by clicking on the switch.

Screenshot 2: Switch for the pump.

- Look at Data Acquisition Program on the SP2 tab and wait till values below have settled (requires a few minutes):

-> Sheath Flow ~ 1000 vccm.

-> Sample Flow ~ 120 vccm.

-> Chamber Pressure between 940-1000 mbar.

Remark: All channels (sample flow, sheath flow, num in file, YAG power…) can be displayed in the SP2 tab on the right. Sample flow fluctuations should be ± 0.17 vccm (ideally), if the average flow is not centered around 120 vccm, if the flow exhibits much higher fluctuations, if the fluctuations are not stable over time (check for irregular noise of the pump) or if the flow keeps on increasing, turn pump off and contact Alexis Attwood from DMT for advice aattwood@dropletmeasurement.com

The window on the left displays single particle event. The height of the peak depends on the BC mass going through the laser.
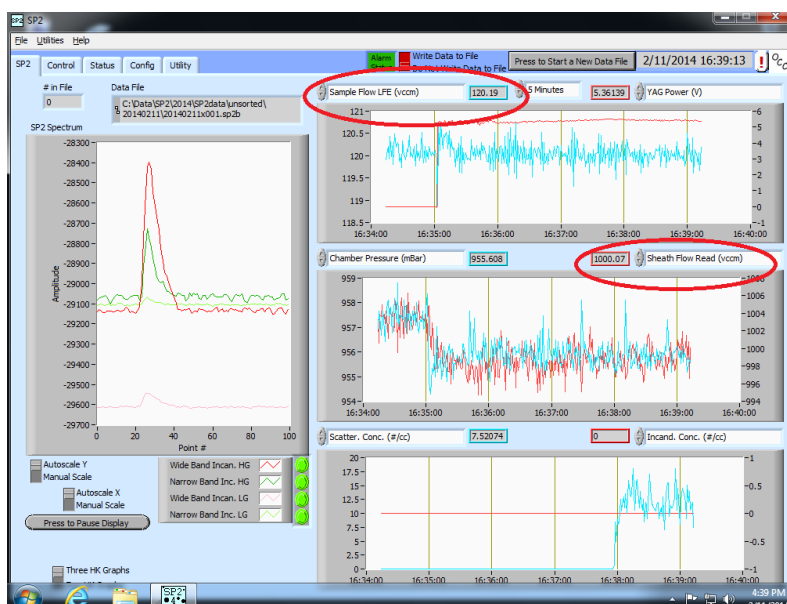
Screenshot 3: Monitoring channels with the SP2 tab.

- Leave the instrument for at least 2min on filtered air before turning on the laser.
- Go to control tab and turn on SP2 laser (same way as the pump). Chamber Pressure will drop slightly, if pressure drops or increases significantly **turn pump off** and contact Martin Gysel (tel. 4168).
- Check that YAG Power is between 3.5 and 5.5 V (definitively >>3.0 V) on the SP2 tab. As YAG power decreases (slightly) with time, it is necessary to increase it slightly by increasing the intensity of the laser current ("Pump Laser Current SP" in Control tab + do it every time the SP2 is switched on because this change can't be saved).
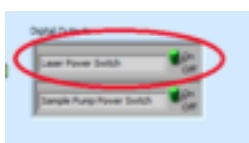
                    Screenshot 4: Laser and pump on.

168

- Perform an **APEX cleaning** and a **liquid flow control** before starting with the measurements (see below). It is essential **to disconnect SP2 from APEX** before cleaning with acid.

APEX cleaning (every day)

<u>Remark</u>: It's necessary to clean APEX regularly (once a day in case of regular measurements) when doing measurements to avoid clogging. The cleaning step is done automatically with an AS sequence which rinses the AS probe in MQ for 5 min., then in 3% HNO3 for 10 min. and again 5 min. in MQ. This is how to do it:

- SP2 should be on filtered air.
- **Disconnect** (if connected) the connection between APEX and the SP2. Close the outlet with a cap and connect exhaust tubing (long tube going to hood). Make sure SP2 valve is still on filtered air **(absolutely prevent acid from going into the SP2)**.
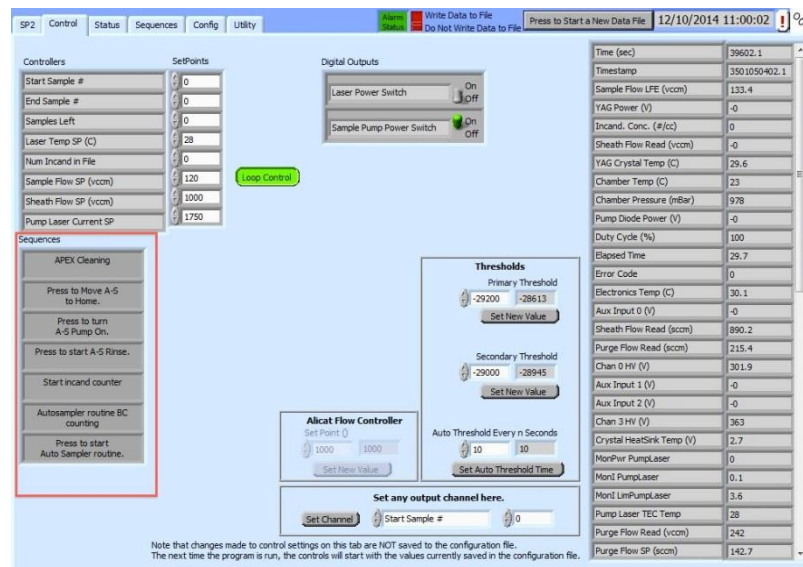
Screenshot 5: Sequences can be started from the control tab by clicking on the switch displayed in the red rectangle.

- Put a vial with 3% HNO3 in 1st position of the tray (**not higher concentration! Otherwise APEX and AS will be damaged!**).
- Check that "Start Sample" is at 0 and start the sequence called "APEX cleaning" on the control tab by clicking on the corresponding switch.
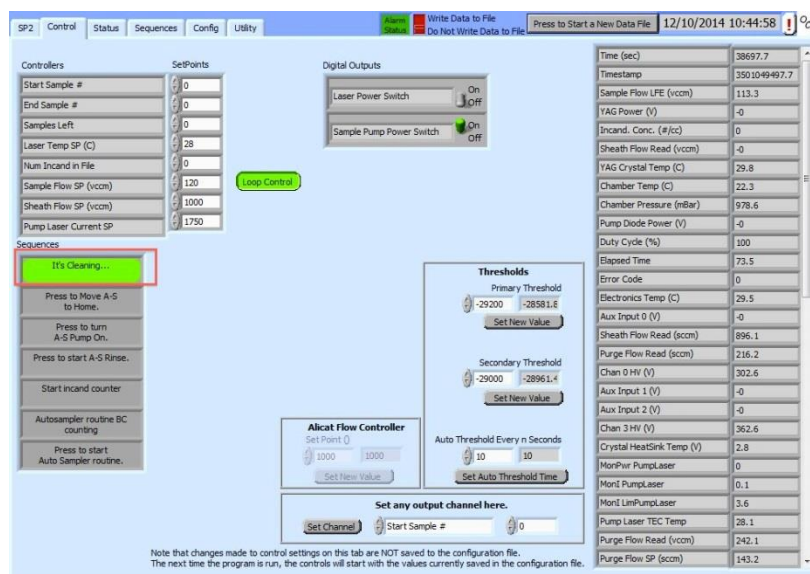
Screenshot 6: The green colour indicates that the sequence is currently running.

- Wait until the sequence is over (the switch won't be green anymore).
- Reconnect the tubing SP2-APEX and turn SP2 valve to APEX (this is associated with a short time fluctuation of the sample flow).

Liquid flow measurement (several times per day)

Remark: The liquid flow going from the AS to the nebulizer has to be measured every day before starting the measurements as we don't have a flowmeter so far. The flow should be more or less constant around 0.08 mL/min. It is important that this value doesn't change that much otherwise it will affect the amount of BC going into the machine and will lead to wrong results. In case the flow is too low, perform a second APEX cleaning. If it is not sufficient, sonicate the nebulizer **in MQ for a few minutes only**. In case the capillary is blocked, disconnect air tube from nebulizer, connect a syringe at the tip of the nebulizer and suck air from the capillary.

Below is described how the liquid flow is measured:

- Fill 2 vials with MQ.
- Weigh the first one, note the mass. Put it in the first position in the AS, and then put the other in the second position.
- In the Control tab, write "0" +Enter for Start Sample and "1" +Enter for End Sample.
- Start acquisition by clicking on the sequence button "AS routine BC counting" in the Control tab. Note the starting time.
- After 10-20 min, stop the sequence by clicking on "AS Home" and on the 3 sequence buttons which are green in order to deactivate them. Note the end time.

- Weigh again the first sample. The difference of mass for this certain amount of time will enable to calculate the liquid flow.

Measuring with AS

Remark: When using an AS sequence (other than "APEX Cleaning"), it's necessary to specify the number of vials involved. In the control tab set values for "Start sample" (position of the first vial), "End sample" (position of the last vial). "End sample" can be changed anytime during measurements. Leave "Sample left" to 0 as the program updates this value automatically. **The first position in the tray corresponds to 0 and not 1!!!** (see picture below).
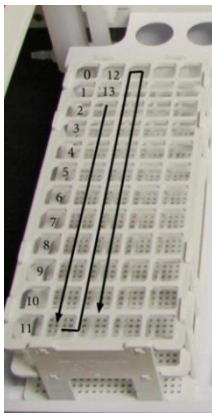
The sequence to use is called "Run Auto Sampler Min BC" ("AS routine BC counting" on the control tab). This personalized sequence increments sample based on a BC particle counting threshold assigned on the channel "num incand in file"). To look at the steps involved in this sequence go to Config -> Sequence and select "Run Auto Sampler Min BC".

- Melt the ice samples at room temperature.
- Once melted, sonicate them in the ultrasonic bath for 25 min without heating.
- Let them cool for a few minutes.
- Put them in the AS tray **(!! First position is 0 !!)**.
- Put a MQ vial at the end (for rinsing + blank measurement).
- Specify the value for "Start Sample" (0 + Enter) and "End Sample" (+Enter). "Samples Left" will be automatically calculated (keep it at 0+Enter).
- Check that all the signals and connections are OK.
- Start sequence "AS Routine BC Counting" on Control tab.
- Have a regular look at the measurements, go to Utility tab -> utilities menu -> housekeeping reader and load the current housekeeping file by clicking on the "Read a file" button.
- Perform an external calibration with AQ standards once a week (slope around 0.1 normally).
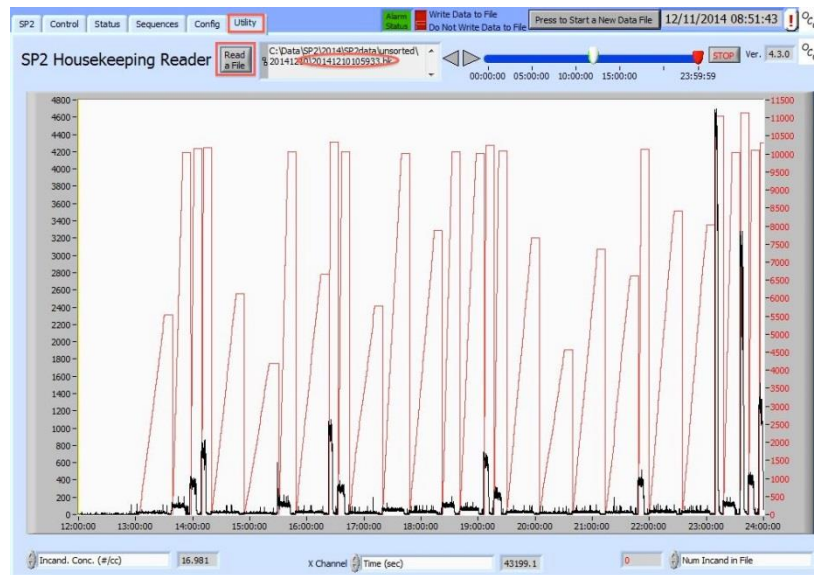
Screenshot 7: Utility tab with the housekeeping reader showing the "incand concentration" and "num incand" in file. Current housekeeping file is highlighted with the circle. In this case, not all samples have reached 10'000 particles.

Further details:

Set A-S tray to default -> Defines dimensions of the tray. When not using the default tray, one should specify here the number of rows and columns.

Set A-S depth -> Defines the sampling depth in the sample vial. Default value is set to 130 mm. However, with low volume samples it can be convenient to set a higher value.

Delay before writing -> Defines the time between the penetration of the probe in the sample and the start of the record. This is a little bit more than the time needed for the sample signal to reach the SP2. This has been experimentally set to 90 seconds. Once this delay is over the "Write data to file" switch on the top in the acquisition program will turn green indicating the results will be recorded from now on.
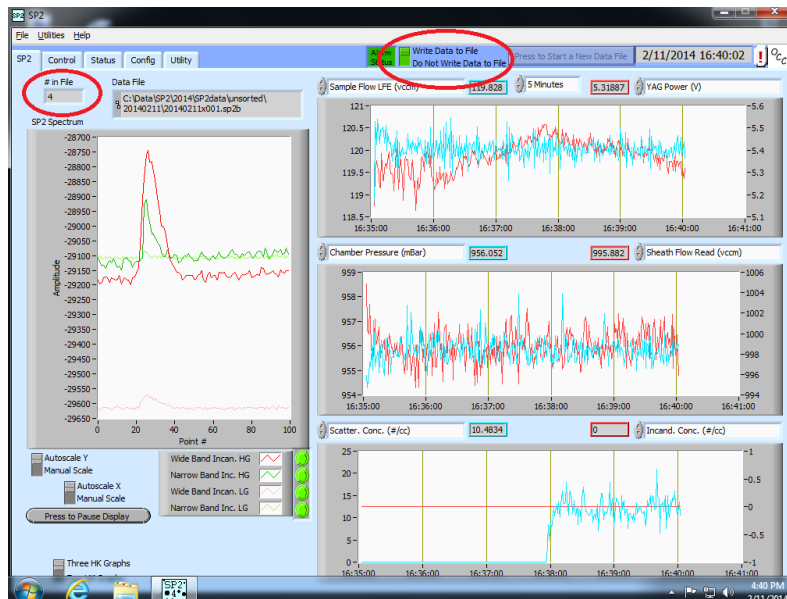
Screenshot 8: Green colour on the top indicates that files are currently being saved. The value on the top-left corner shows the total number of particles already recorded (this is always bigger than the number of incandescent particles recorded!).

Force exit if time too long -> Defines the maximum time during which a sample is measured. This has to be modified depending on the sample volume. An appropriate value is just smaller than the time needed to consume an entire sample (**probe should not pump too much air!!!**)

Acquiring -> Defines a threshold in term of particle counted. This value should be set to (or close to) 10'000 particles.

Always use ">" or "<" instead of "=" when defining condition associated to the different steps.
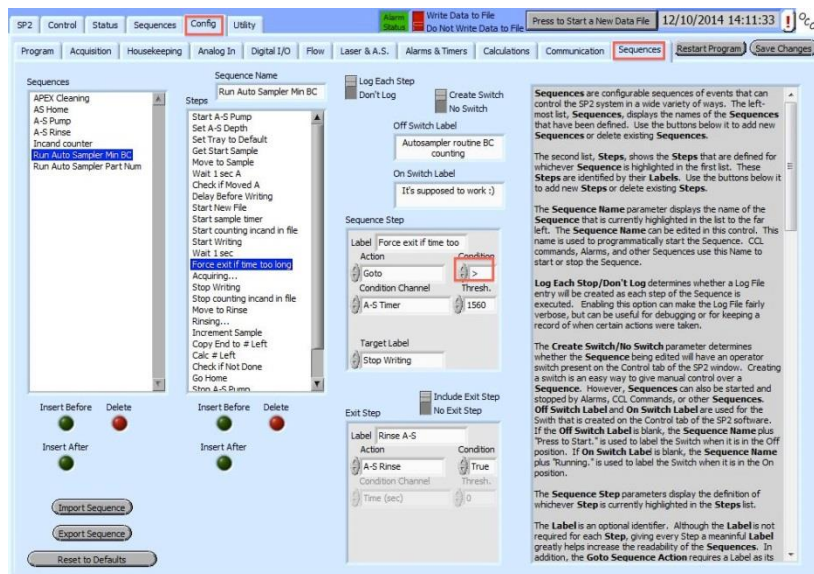
Screenshot 9: Sequence subtab displays all the sequences and allows the user to create, delete or modify steps of existing sequences.

The progress of a running sequence can be monitored anytime on the Sequences tab.
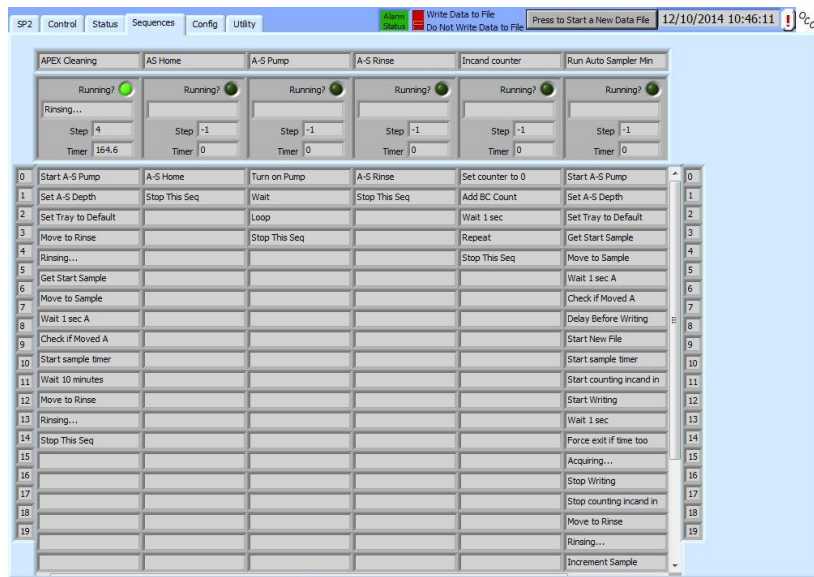
Screenshot 10: Sequence tab allows the user to monitor a sequence, to start or stop it.

Turn off SP2 (end of the week)

- Switch valve to filtered air and let instrument run like this for at least 2 minutes.
- Turn off laser.
- Turn SP2 pump off.
- Run another "APEX cleaning" sequence **(REMEMBER TO DISCONNECT SP2 FROM APEX AS DESCRIBED ABOVE!)**.
- Shut down acquisition program ("File" "Exit" button).
- Turn off AS, loosen its pump.
- Turn off cooling (APEX, blue button).
- 2-3 minutes later turn heating off (APEX, red button). Loosen peristaltic pump of APEX.
- Turn off house air.
- Empty waste container.

Back Up data

- Copy data from the local drive (C:\Data\SP2\2018\SP2data) to the SP2 drive:

  Logbooks -> I:\2018\Logbooks.

  SP2 files -> I:\2018\SP2 data (copy the whole folder).

- Do the PC updates from time to time as they are not automatically implemented.

Calibration with AQ standards (once or twice a week)

- Put a Parafilm cover on the stock solution.
- Sonicate the 2500 ppb stock for 25 min (without heating). Let it cool down.
- Pour a bit of the stock into a plastic beaker.

All the following standards are prepared by MASS in 50 mL PP vials so were always filled up to end up with an end weight of 50 g! It is crucial to <u>work exactly</u> (uncertainty only for the last figure of the weight).

Prepare a 100 ppb AQ stock solution

- Calculate dilution factor for 100 ppb stock solution.
- Weigh the empty vial, press Tara.
- Rinse pipette 3 times with MQ.
- Fill the vial with some MQ water and adjust to the desired mass with pipette (48g).
- Add the desired amount (2g) of stock solution with pipette (keep droplets on vial walls).

This stock is only shaken, NOT SONICATED again, but prepared freshly every time when preparing standards.

Prepare all the different standards

- Calculate the dilution factors.
  - Use 2500 ppb stock for 50, 20, 10 & 5 ppb.
  - Use 100 ppb stock for 2, 1, 0.5 and 0.1 ppb.
- Weigh empty vial, press Tara.
- Rinse pipette 3 times with MQ.
- Fill the vial with some MQ water, adjust with pipette.
- Add the desired amount of stock solution (or 100 ppb dilution), think of keeping droplets on walls.

Do not dilute from one standard to the other, but use the 2500 ppb & 100 ppb stock to create separate standards!

Before measuring

- All standards are sonicated for 25 min (without heating) prior measurement.

Preparation of the 2500 ppb stock solution (once a year)

It has been shown that the stock solution was stable over time (several months). Normally, preparing it once a year is sufficient, unless some unexpected decrease of the calibration slope is noticed.

- Optional: Check dry mass of AQ: put a certain mass in the oven, weigh before and after (dry mass is normally stable around 22.6-22.9%).
- Check weight of AQ glass bottle (with lid), if it lost mass since the last check: fill up to the last weight with MQ, MIX WELL!! (With spoon).
- Not completely fill 1 L glass volume flask with MilliQ (ultrapure water).
- Weigh AQ (the greasy stuff) on scale.
  NB! Mass depends on dry mass of AQ.

  - in Oct.2011: 22.611% of AQ is dry mass; 70.534% of dry AQ is EC => weighed in ~ 15.7 mg
  - in May 2013: 22.96% of AQ is dry mass; assumed that still 70.534% of dry AQ is EC => weighed in ~ 15.5 mg
- Fill the volume flask completely (assuming a density of the MilliQ of $1 g/cm^3$)
- Shake the whole mixture well.
- Write down (Excel sheet) the updates weight of the AQ bottle.

This stock is stored in this glass volume flask, but at ROOM TEMPERATURE not in the fridge!

Internal calibration

This has to be done no more than once a year or when the SP2 is moved (sent to DMT for example). To perform this (and further tasks as laser alignment), contact people from the Laboratory of Atmospheric Chemistry at PSI (Robin Modini).

# Drying the desiccant in the 1st cartridge (every day now!)

This has to be done when the purple balls inside the cartridge start to turn lighter. It usually happened every 3-4 months, but **now has to be done every day**. **Don't wait too much otherwise condensation will appear in the cartridge and even in the pipes!!**

- No need to turn the SP2 off if **ONLY** the 1st cartridge is replaced (before the pump). For the 2nd cartridge, located after the pump, the SP2 has to be turned off. Ideally, 1st cartridge should be replaced before 2nd cartridge gets wet.
- Cover the SP2 with kitchen paper so as to protect it.
- Open carefully the cartridge. Remove the spring, the metallic cap and the cotton piece.
- Pour the purple balls inside a crystallizer, and then transfer them to a glass plate so as to have a thin layer. **Be careful, the balls tend to jump everywhere!!**
- Leave the glass plate in the oven for a whole night (T°: 100°C max, ideally 80°C).
- When the desiccant is dry, remove it from the oven and pour it into the cartridge. Add the cotton piece on top, the metallic lid (pack down) and the spring. Close the cap.

- Check the connections (no leak).
- Check sample flow, it has to be stable and with low fluctuations around 120 vccm, otherwise it might be possible that there is a leak.

Data processing with Igor

- In the SP2 network drive (fs00) -> IGOR User Procedures, make a copy of "template_ice_cores.pxp" and open it.
- In the PSI toolkit, tab "Ice Cores", click on "prepare sample info waves".
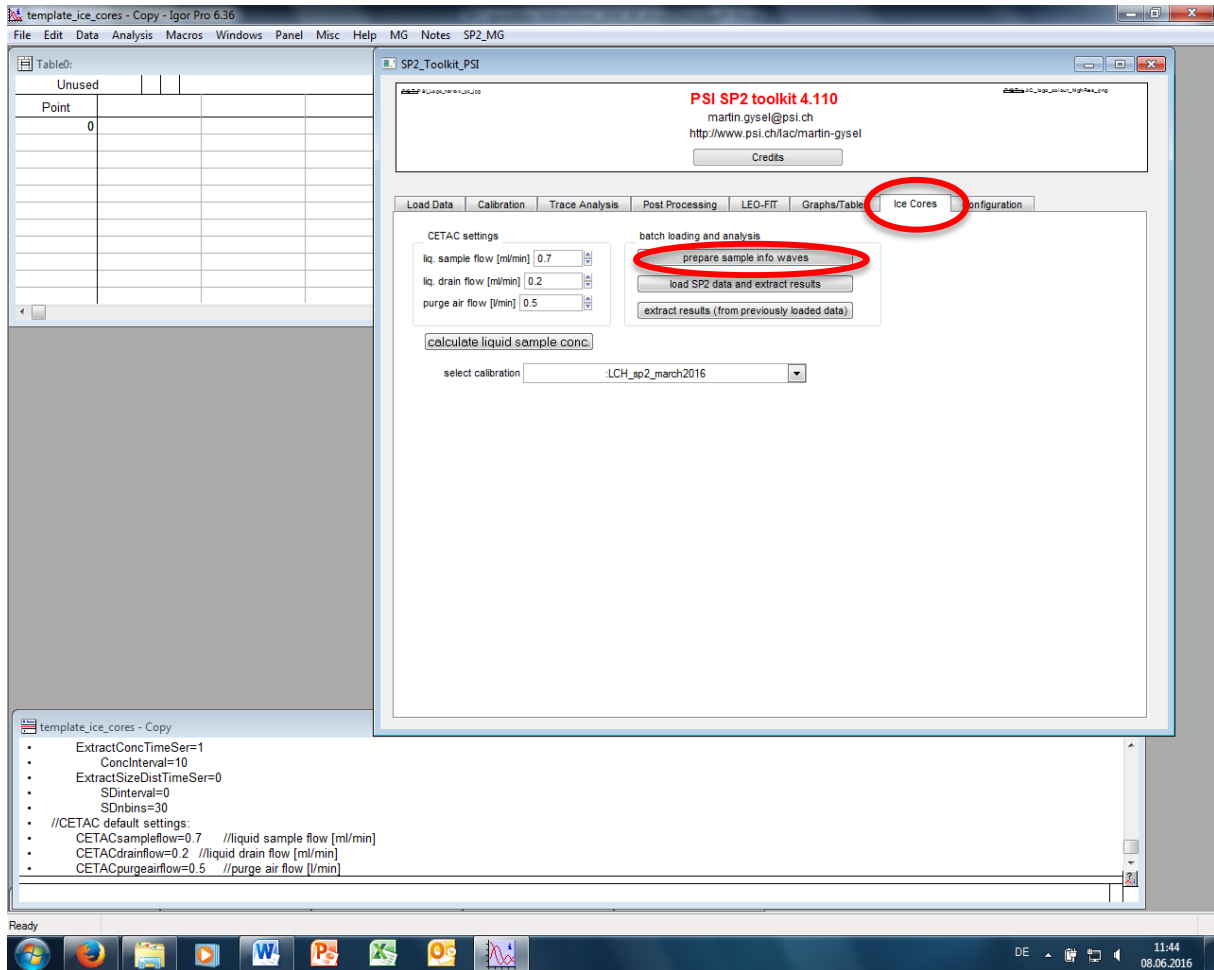
Screenshot 11: Igor homepage.

- A small window opens ("Target Folder and Number of Samples"). Replace the date YYYMMDD by the real date of your data and specify the number of samples you want to process. Click on "Continue".
- A table opens: fill it in with the date of the file, the file number and file ID (this info is available in the logbook). **Don't change the columns related to the flows**. *The best idea is to create an Excel template to fill this table more quickly by copy-paste because this table doesn't work like Excel (impossible to drag along a column).*
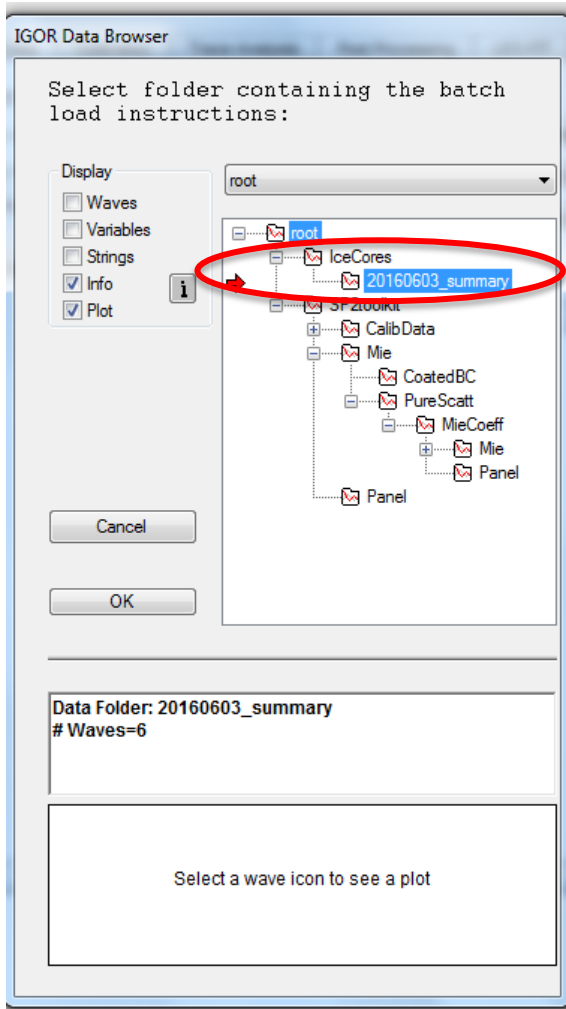
178
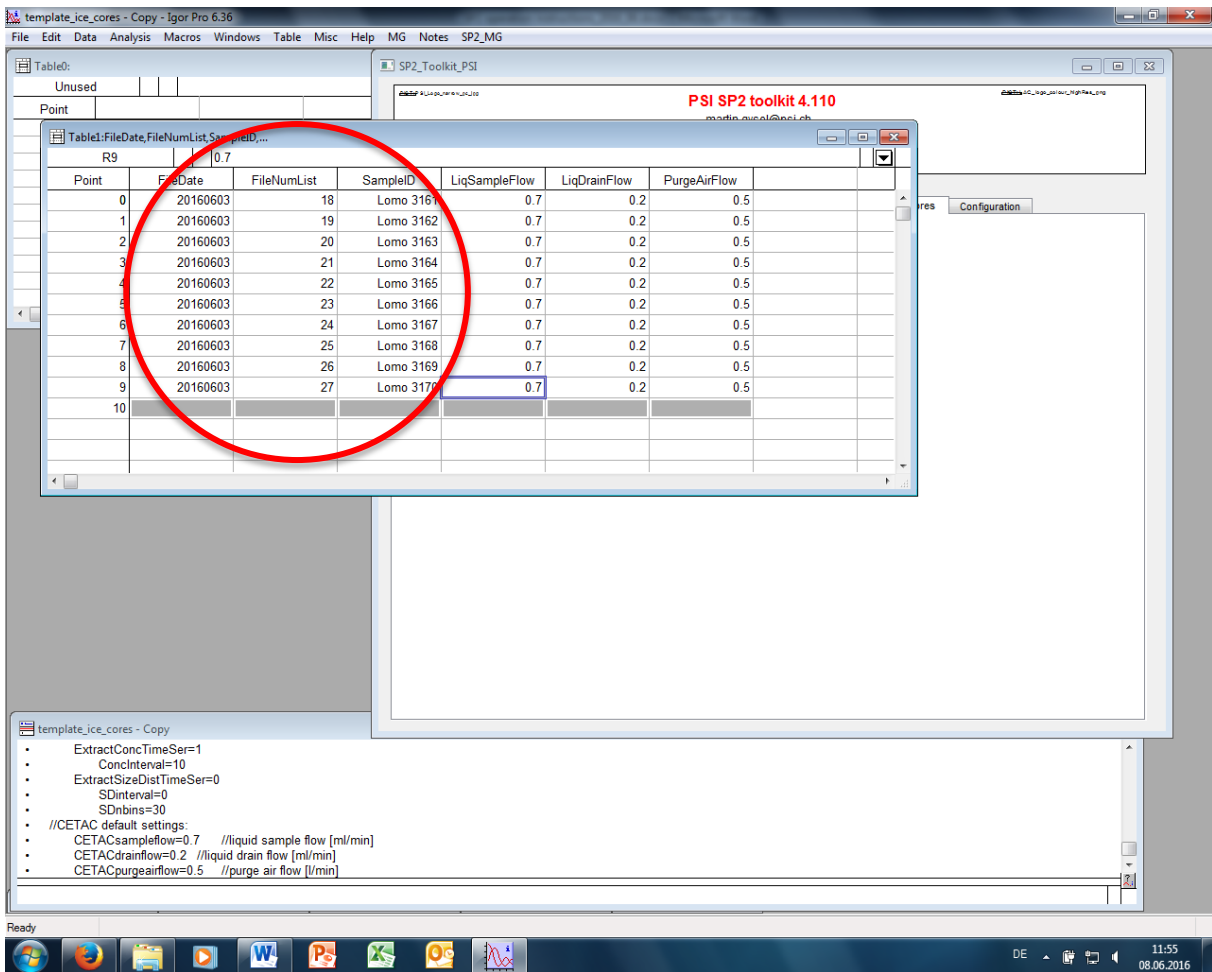
Screenshot 12: Igor table.

- Close this table. Click on save (not necessary to rename it).
- Back to the PSI Toolkit, click on "load SP2 data and extract results".
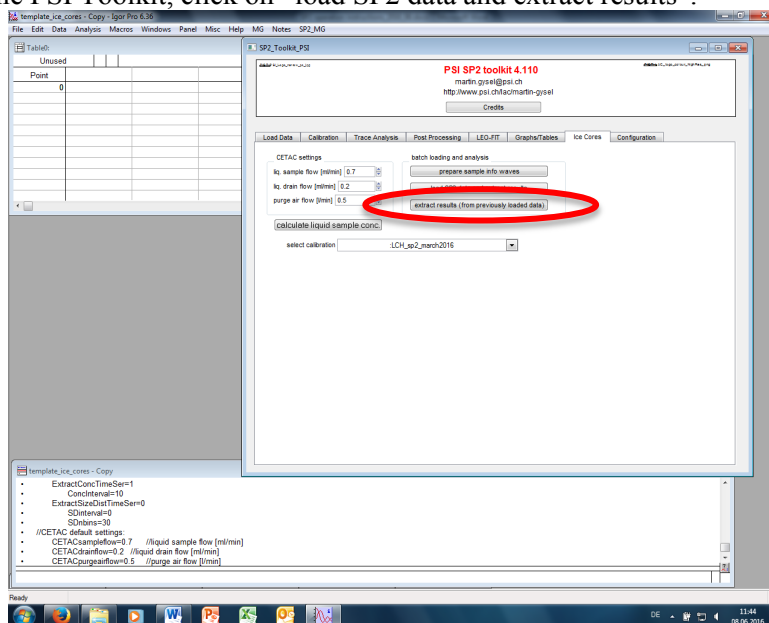
Screenshot 13: PSI toolkit.

- The "Igor Data Browser" window opens. In the menu, open the "IceCores" section by clicking on the "+". Select what is inside (YYYYMMDD_summary) and drag the red arrow in front of this line. Click on OK.

Screenshot 14: The Igor Data Browser.

- A window opens ("Select folder containing the SP2B raw data files") in order to specify the location of the data folder. Click on "Browse" and specify the correct data folder (called YYYYMMDD). Click on OK.
- Igor will carry out the calculations for each data file. This can take several minutes according to the size of the file. **Empty files will generate an error message and stop the process**.
- Once the calculation is completed, 3 windows open: one bar chart showing the values of the different channels, one graph showing the size distribution in the samples and one table with the raw data (the most interesting one).
- In this table ("IceCoreSummary_Table"), the interesting columns are "TimeDateAvg" and the 2 **BHNL** columns. "BHNL_LiquidSampleMassConc" shows the calculated concentration in the size detection range and "BHNL_LiqSampMassConcBlwCut" estimates the concentration which is below the size detection range.
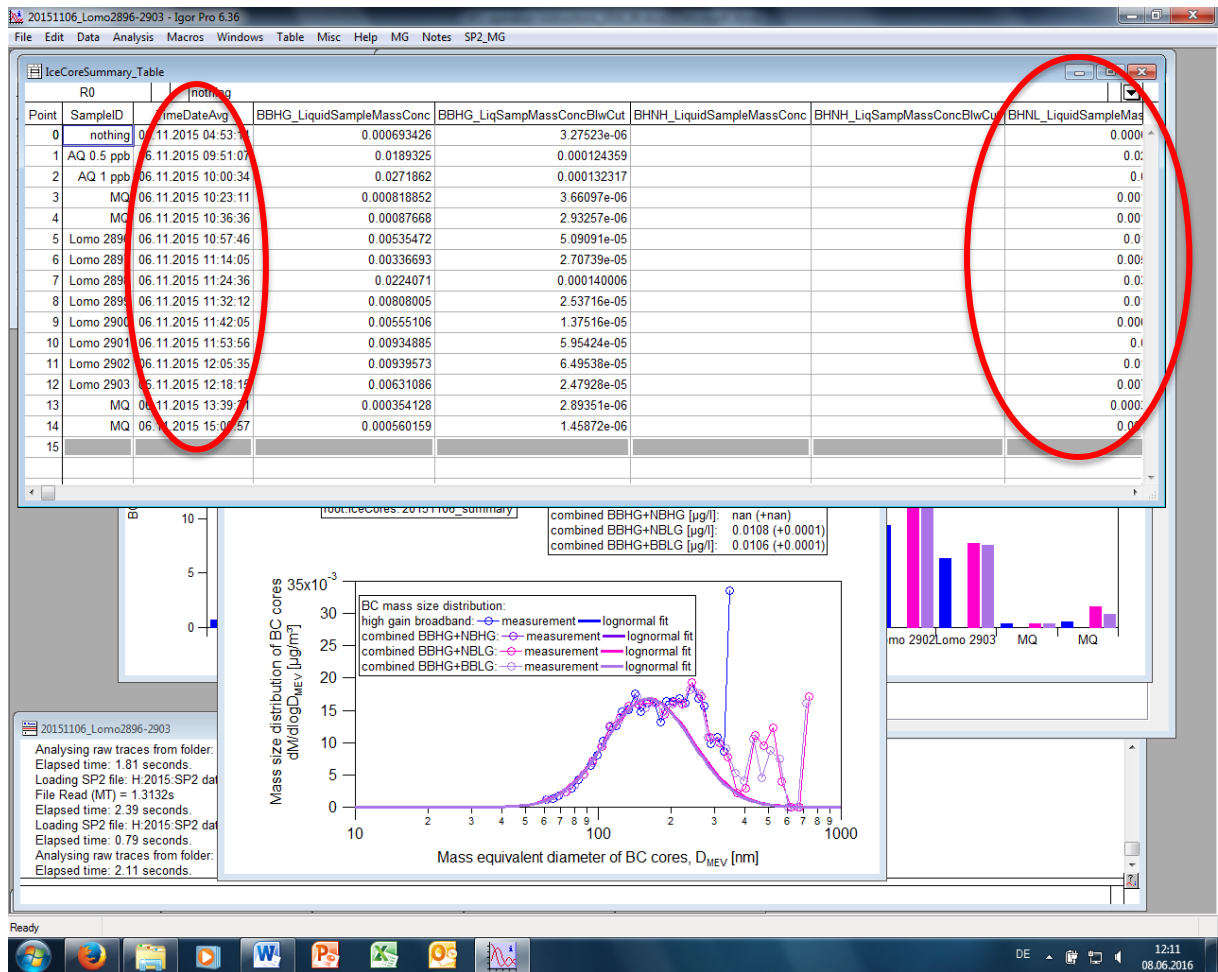
Screenshot 15: The results as displayed in Igor.

- Copy-paste the data in an Excel sheet. The following columns are needed: File number, Sample ID, Date and the 2 BHNL ones.
- In addition, some columns have to be created: Time start (end of the sonication), Time elapsed (for each sample after the end of the sonication), BHNL_sum (sum of the 2 BHNL columns -> real value), BC concentration (by applying the calibration equation obtained for the week) and BC **corrected** concentration, which is the data of interest. To get this, one needs to apply the following formula:

$$[BCcorr] = [BC] / (1 + (-0.017 * \text{time elapsed}).$$

- It's not necessary to save the Igor files as they are very heavy (hundreds of MB).
- Keep track of the daily values of the YAG power and the sample flow.
- Prepare an Excel sheet gathering all the weekly calibrations.

Acknowledgements

A PhD thesis is not a single-handed project. Without the assistance of many people, I would not have been able to complete such a work. Here I would like to thank the contribution from all those who made this project possible, from far and near.

My first thanks go of course to Margit Schwikowski, for giving me the opportunity to carry out this research project at PSI under good working conditions, and for guiding me through each step of this exciting adventure. I deeply appreciated her continuous support and commitment, her confidence in my abilities, her understanding and trust.

I am also very grateful to the entire LUC team for bringing such a nice and comfortable atmosphere. In particular, I would like to thank Michael Sigl for his supervision and assistance, and for having such an extensive ice-core database in mind; Anja Eichler for her contagious good mood and motivation as well as for her endless availability and the resulting fruitful discussions about data analysis and interpretation; Theo Jenk for his technical assistance and always relevant advice.

The office team, in particular Sven Avak, Johannes Schindler, Anna Dal Farra, Alexander Vogel, Jonas Stegmaier and Ling Fang (thank you for constantly feeding us with candies and for not logging off your computer!) also greatly contributed to make these almost four years as pleasant as possible. Other big thanks go to our secretary Doris Bühler for her perfect (Swiss) sense of organization, and to our lab technicians Silvia Köchli and Sabina Brütsch to whom I wish good luck with the moody SP2.

I would like to thank the other members of the Paleo Fire project, Willy Tinner, Sandra Brugger, Erika Gobet, Stefan Wunderle, Helga Weber, Ulrike Lohmann and Anina Gilgen, for the inspiring meetings and the nice meals in ZH or BE restaurants.

I am also very grateful to the students and technicians who temporarily visited us at PSI and helped me with the SP2 measurements, Loic Schmidely, Philipp Steffen, Stephanie Remke, Denis Alija, Sofia Schrekenbach and Susi Haselbeck. 15 000 samples is not a small thing, and I would have never been able to measure them without their continuous support and dedication.

I greatly appreciated the technical assistance from Susan Kaspari and the LAC team, namely Joel Corbin, Robin Modini, Jinfeng Yuan, Marco Zanatta and Ghislain Motos when problems arose with the SP2, and for supervising the internal calibrations.

I would like to thank my thesis committee, Michel Legrand for his careful review and relevant suggestions, and Willy Tinner for heading the commission with enthusiasm.

Many thanks go to my friends, Euphrasie, Benjamin, the two Maxime, Florian, Aurélia, Christophe, for keeping on visiting me, even abroad, and for sharing so many wonderful hikes together. Finally, I would like to deeply thank my family. Merci à toi Dominique pour ces précieux moments partagés en montagne. Et bien sûr, un immense merci à mes parents, Martine et Hervé, ainsi qu'à ma mamie, pour leur indéfectible soutien, dans les bons comme dans les mauvais moments, et pour leur confiance toujours renouvelée. Et bien évidemment merci à toi María pour le bout de chemin déjà parcouru ensemble. Puisse-t-il être encore long.

Declaration of consent

on the basis of Article 30 of the RSL Phil.-nat. 18

Name/First Name: Osmont Dimitri

Matriculation Number: 14-140-008

Study program: Chemistry and Molecular Sciences

Bachelor ☐   Master ☐   Dissertation ☑

Title of the thesis: Reconstruction of forest fires through chemical analysis of black carbon in ice cores from high-alpine glaciers

Supervisor: Prof. Dr. Margit Schwikowski

I declare herewith that this thesis is my own work and that I have not used any sources other than those stated. I have indicated the adoption of quotations as well as thoughts taken from other authors as such in the thesis. I am aware that the Senate pursuant to Article 36 paragraph 1 litera r of the University Act of 5 Septem¬ber, 1996 is authorized to revoke the title awarded on the basis of this thesis.

For the purposes of evaluation and verification of compli-ance with the declaration of originality and the regulations governing plagiarism, I hereby grant the University of Bern the right to process my personal data and to perform the acts of use this requires, in particular, to reproduce the written thesis and to store it permanently in a database, and to use said database, or to make said database available, to enable comparison with future theses submitted by others.

Villigen, 10.09.2018

Place/Date

Signature

Curriculum Vitae

Name: Dimitri Osmont
Birth date: 04.11.1992
Birth place: Rouen, France
Nationality: French

Education

2015–2018 **Ph.D. thesis in chemistry** at the Paul Scherrer Institute and the University of Bern, Switzerland.
Reconstruction of forest fires through chemical analysis of black carbon in ice cores from high-alpine glaciers.

2011–2014 **Engineering degree in chemistry**, equivalent to a Master, at ENSCR (Ecole Nationale Supérieure de Chimie de Rennes, France).
Specialization in Environment and Analysis.

2009–2011 **Cycle préparatoire Chem.I.St** (Chemistry International Studies), Ecole Nationale Supérieure de Chimie de Rennes, France

2009 **Baccalauréat scientifique**.
Major subjects: mathematics, physics, chemistry, earth and life sciences.

Professional experience

2016–2017
84h/year **Assistant in the laboratory course of Physical Chemistry** (2nd year of Bachelor in Chemistry, Biochemistry and Pharmacy) at the University of Bern.

2015–2018 **Supervision of several students (BsC, MsC) and one lab technician** in the frame of the PhD.

2014
6 months **Internship at Commissariat à l'Energie Atomique (CEA)**, Le Ripault, France.
Method development for the trace analysis of explosives in water by HPLC-MS.

2013
4 months **Internship at the Paul Scherrer Institute (PSI)**, Villigen, Switzerland.
Analysis of Black Carbon in an ice core from Svalbard by using a SP2.

2012
6 weeks **Internship at Laboratoire de Glaciologie et de Géophysique de l'Environnement (LGGE)**, University of Grenoble, France.
Isotopic analysis of nitrate in Antarctic snow by GC-IRMS.

Languages

French: mother tongue.
English: fluently written and spoken. Current working language. TOEIC 960/990 (2013).
Spanish: fluently written and spoken. Frequent stays in Spain.
German: basic notions.
Italian: basic notions.

Scientific publications

Osmont, D., Wendl, I. A., Schmidely, L., Sigl, M., Vega, C. P., Isaksson, E., and Schwikowski, M.: An 800-year high-resolution black carbon ice core record from Lomonosovfonna, Svalbard, *Atmospheric Chemistry and Physics*, 18, 12777–12795, 2018.

Osmont, D., Sigl, M., Eichler, A., Jenk, T. M., and Schwikowski, M.: A Holocene black carbon ice-core record of biomass burning in the Amazon Basin from Illimani, Bolivia, *Climate of the Past Discussions, 2018*, in review.

Sigl, M., Abram, N. J., Gabrieli, J., Jenk, T. M., Osmont, D., and Schwikowski, M.: 19th century glacier retreat in the Alps preceded the emergence of industrial black carbon deposition on high-alpine glaciers, *The Cryosphere*, 12, 3311–3331, 2018.

Brugger, S. O., Gobet, E., Sigl, M., Osmont, D., Papina, T., Rudaya, N., Schwikowski, M., and Tinner, W.: Ice records provide new insights into climatic vulnerability of Altai forest and steppe communities, *Global Change Biol.*, 2018, in press.

Contribution to scientific conferences and workshops

Jun. 2018   An Andean ice-core based Holocene biomass burning record of the Amazon Basin.
Polar 2018 SCAR/IASC Open Science Conference, 19–23 June 2018, Davos, Switzerland. *Oral presentation.*

Nov. 2016   The Black Carbon record from the Lomonosovfonna ice core as a proxy for past anthropogenic emissions and forest fires.
Early Human Impact Final Workshop, 24–25 November 2016, Venice, Italy. *Poster presentation.*

Nov. 2016   Towards the reconstruction of forest fires through chemical analysis of Black Carbon in ice cores from mountain glaciers.
14th Swiss Geoscience Meeting, 18–19 November 2015, Geneva, Switzerland. *Poster presentation.*

Sep. 2016   Reconstruction of forest fires through chemical analysis of black carbon in ice cores from high-alpine glaciers.
1st Year Graduate Student Symposium of the University of Bern, 12 September 2016, Bern, Switzerland. *Oral presentation.*

Aug. 2016   400 years of Black Carbon emissions recorded in the Lomonosovfonna ice core, Svalbard (Norway).
15th OCCR Swiss Climate Summer School, 28 August–2 September 2016, Grindelwald, Switzerland. *Poster presentation.*

Jan. 2016   350 years of Black Carbon emissions recorded in the Lomonosovfonna ice core, Svalbard.
24th European Research Course on Atmospheres, 6 January–4 February 2016, Grenoble, France. *Poster presentation.*

Nov. 2015   A 250-year Black Carbon record from the Lomonosovfonna ice core, Svalbard. 13th Swiss Geoscience Meeting, 20–21 November 2015, Basel, Switzerland. *Poster presentation. SEP award for best poster presentation.*

2015–2018   Several 1- or 2-day meetings within ProClim, OCCR and PSI.

Scientific field work

Jun. 2017	Jungfraujoch, Swiss Alps, snowpit study (1 day).
Aug. 2015	Glacier de la Plaine Morte, Swiss Alps, snow sampling (2 days).
Aug. 2015	Rhone glacier, Swiss Alps, ice sampling (1 day).